Methods in Molecular Biology™

VOLUME 166

Immunotoxin Methods and Protocols

Edited by

Walter A. Hall, MD

HUMANA PRESS

1

Development and Activities of the BR96-Doxorubicin Immunoconjugate

Ingegerd Hellström, Karl Erik Hellström, and Peter D. Senter

1. Introduction

1.1. Immunoconjugates for Tumor Targeting

The use of antibodies to selectively destroy tumors has attracted attention since Paul Ehrlich's dream about "magic bullets," and it gained support from the demonstration by Pressman in the 1950s that antibodies can be employed to deliver radioisotopes to tumors in rodents. The promise of this approach received a strong boost when Köhler and Milstein introduced monoclonal antibody (MAb) technology in the 1970s ***(1)***. However, the clinical success of unmodified MAbs or MAbs conjugated to drugs, radioisotopes, or toxins in the treatment of tumors has been modest so far. The primary exceptions are the use of MAbs targeting the HER2 growth factor receptor in breast carcinomas ***(2)*** and MAbs to treat B-cell lymphomas ***(3,4)***. Encouraging results have also been obtained when a MAb reacting with a differentiation antigen expressed on colorectal carcinomas was given to patients who were at high risk of tumor recurrence following primary surgery ***(5)***.

To target an anticancer drug to a tumor cell, one may chemically conjugate it to a MAb that is internalized upon binding to tumor antigen at the cell surface and releases the drug in the cytoplasm ***(6)***. Alternatively, one may use a MAb (or MAb fragment) that does not need to be internalized to target an enzyme that can convert an inactive prodrug into a cytotoxic drug at the tumor site ***(7)***.

This chapter will discuss chemically prepared immunoconjugates between the anticancer drug doxorubicin and MAbs to Lewis^y (Le^y). This antigen was chosen as a target because it is abundantly expressed at the surface of cells

From: *Methods in Molecular Biology, vol. 166: Immunotoxin Methods and Protocols*
Edited by: W. A. Hall © Humana Press Inc., Totowa, NJ

from most human carcinomas of the colon, breast, ovary, and lung (non–small cell), while it has low expression in normal tissues (except for epithelial cells in the gastrointestinal tract). The conjugates were constructed using MAbs that are internalized into cells following their binding to Le^y at the cell surface. While therapeutic efficacy of the one immunoconjugate of this type tested in man was modest at best, data from preclinical studies performed after the conjugate's clinical shortcomings became known leave us hopeful that targeting of doxorubicin or similar drugs to the Le^y antigen will find therapeutic utility.

1.2. Doxorubicin Chemistry

Doxorubicin and related anthracycline antibiotics have drawn widespread attention as the cytotoxic components of antibody-based drug delivery systems for a number of reasons. Doxorubicin, the most widely used member of the anthracycline family, has clinical activities that are very well understood. It can induce significant therapeutic responses in a broad array of human tumors such as breast carcinoma, lung cancer, sarcoma, lymphoma, leukemia, and neuroblastoma, and there is evidence that its antitumor activity increases with the intratumoral concentration of the drug ***(8,9)***. Theoretically, by selectively delivering doxorubicin to doxorubicin-sensitive tumors, it should be possible to maintain or improve the activity of the drug while minimizing its undesired toxic side effects, such as cardiomyopathy, gastrointestinal toxicity, and myelosuppression. Another advantage in using doxorubicin for targeted delivery is that the drug is available in large quantities, and there exists a large body of published work on its physical and chemical properties and the chemical reactions to which it can be subjected.

The functional groups in doxorubicin that have been used for conjugation to macromolecules are its carbonyl side chain and sugar amine (**Fig. 1**). A seminal study describing the preparation and activities of antibody–doxorubicin conjugates came from Michael Sela's laboratory before the advent of MAb technology ***(10)***. The drug was linked to polyclonal antibodies in three different ways: (1) carbodiimide coupling of the doxorubicin amine to antibody carboxyl groups, (2) oxidative cleavage of the carbohydrate moiety of doxorubicin with periodate followed by covalent coupling to antibody amino groups, (3) and glutaraldehyde crosslinking, presumably through the doxorubicin amino group. Selective elimination of antigen-positive cells was obtained with the periodate method ***(11)***, even though much of the activity of doxorubicin was lost when the carbohydrate was damaged.

This work set the stage for subsequent studies in which doxorubicin was linked to macromolecules, allowing the release of unmodified doxorubicin upon chemical hydrolysis of the labile bond. Hurwitz and coworkers ***(12)***

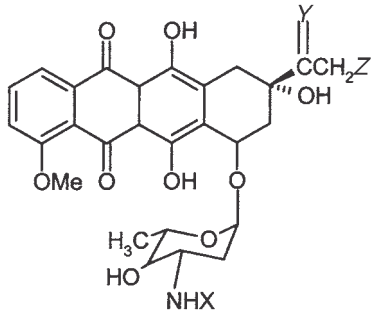

Compound	X	Y	Z
Doxorubicin	H	O	OH
Daunorubicin	H	O	H
Daunorubicin Hydrazone	H	=NNHCOR	H
cis-Aconityl-Daunorubicin	R, COOH, CO—	O	H

Fig. 1. Structures of doxorubicin, daunorubicin, and acid-labile daunorubicin adducts.

showed that reversible conjugates of daunorubicin, a closely related doxorubicin analog, could be formed by condensing the carbonyl group with macromolecular hydrazides. These molecules consisted of daunorubicin hydrazone derivatives that were hydrolytically unstable (**Fig. 1**).

Another method for the reversible attachment of doxorubicin to carrier molecules involves the formation of labile amides on the drug's carbohydrate amine. One of the first examples of such a labile amide was reported by Shen and Ryser ***(13)***, who described the development of a pH-sensitive *cis*-aconityl-daunomycin derivative (**Fig. 1**) that was attached to macromolecule carriers and was shown to be unstable under slightly acidic conditions. This work has been extended in several laboratories to include pH-sensitive doxorubicin and daunorubicin conjugates that were active against antigen-positive target cells ***(14–17)***. Taken together, these studies demonstrate that doxorubicin can be reversibly linked to macromolecular carriers with a significant retention in drug activity.

1.3. Design of Optimized Doxorubicin Linkers

The linkage of doxorubicin to MAb carriers should be stable until the conjugate reaches the tumor target, at which point the drug should be rapidly

released. Several studies have been directed towards the development of optimal pH-sensitive linkers for the attachment of doxorubicin to MAbs. By linking drugs to MAbs that are internalized following their binding to the tumor cell surface, it becomes possible to deliver drug molecules into the acidic environment of lysosomes and other intracellular vesicles ***(18–20)***. In addition, the pH of tumor masses is lower than that of surrounding tissues, which also facilitates drug release into the immediate environment of the neoplastic cells ***(17,21)***. Drug molecules that accumulate at the tumor site by this mechanism, as well as drug released subsequent to internalization of a conjugate by antigen-positive cells, may kill neighboring (e.g., neoplastic, endothelial) cells that lack the target antigen and thus further contribute to tumor destruction.

Kaneko and coworkers ***(22)*** explored several methods by which doxorubicin could be linked to MAbs through a carbonyl group in pH-sensitive manners. They used the 5E9 MAb, which binds to an antigen abundantly expressed by many lymphomas. The important feature of this MAb for tumor targeting is that it is rapidly internalized following its binding to the cell surface. A series of MAb–doxorubicin derivatives were prepared and tested for stability in neutral and acidic solutions. The linkers included hydrazones, semicarbazones, thiosemicarbazones, and hydrazine carboxylates. The hydrazone linker was shown to be acid labile but very stable at pH 7.4. Cytotoxicity assays established that 5E9–doxorubicin hydrazone conjugates were as active as free doxorubicin. The semicarbazone and thiosemicarbazone conjugates were stable under acidic conditions, and consequently were much less cytotoxic. The hydrazine carboxylate conjugate was unstable even at pH 7.4 and was therefore unsuitable for selective drug delivery. These studies indicated that conjugates containing the hydrazone linker between doxorubicin and an internalizing antibody have the requisite properties for selective tumor cell kill: stability at neutral pH, release of free drug under acidic conditions, and cytotoxic activities that are comparable to those of free doxorubicin ***(22)***. Antitumor activity of the conjugates was observed in athymic mice xenografted with antigen-expressing human lymphoma cells ***(19)***.

1.4. Formation of MAb-Doxorubicin Conjugates for Therapy of Carcinomas

Trail and coworkers ***(23)*** explored various strategies for attaching doxorubicin hydrazones to a different MAb, BR64, which recognizes Le^y on the surface of cells from a variety of carcinomas and, upon antigen binding, is rapidly internalized ***(24)***. BR64 was modified with the heterobifunctional crosslinking reagent SPDP, and doxorubicin hydrazone was then linked to the MAb through labile disulfide (BR64-SS-DOX) or through stable thioether (BR64-S-DOX) spacers. Both conjugates contained the same acid-sensitive hydrazone bond,

but the BR64-SS-DOX conjugate had a disulfide bond that could readily be cleaved by endogenous thiols. Thus, this particular conjugate contained two separate labile bonds. Pharmacokinetic studies in mice with subcutaneous Le^y-positive tumor xenografts established that BR64-S-DOX was more stable than BR64-SS-DOX in serum and led to higher intratumoral doxorubicin concentrations. Consistent with this was the finding that BR64-S-DOX was therapeutically superior to BR64-SS-DOX. When administered at 10 mg doxorubicin equivalents/kg (approx 500 mg conjugate/kg given at each of three occasions with 4 d intervals), BR64-S-DOX resulted in the regression of 100% of the tumors and had a 50% cure rate. At the same dose, BR64-SS-DOX was inactive. Systemic administration of doxorubicin and nonbinding control conjugates only led to slight delays in tumor outgrowth. This study demonstrated that pronounced therapeutic activities can be obtained with MAb–doxorubicin conjugates, and that the mode of drug attachment is a critical factor in achieving these effects.

The chemistry used to prepare BR64-S-DOX involved the introduction of thiols to the MAb via SPDP, a reagent that reacts with lysine residues. SPDP reacts in a relatively random manner, and the resulting MAb-drug conjugate consists of a binomial distribution of drug-to-antibody molar ratios. This particular conjugation chemistry gave low yields (<30%) when it was applied to BR96, a different anti-Le^y MAb, which was selected since it has higher tumor selectivity than BR64 and, like BR64, internalizes following binding to the cell surface ***(25)***. For this reason, Firestone and coworkers ***(26)*** established a procedure to generate MAb thiol groups by reducing disulfides with dithiothreitol, and combining the resulting reduced MAb with doxorubicin-6-maleimidocaproylhydrazone (**Fig. 2**). With both BR64 and BR96, the drug/MAb molecular ratios were approx 8, reflecting the presence of 4 interchain disulfides. Importantly, the resulting conjugates were easily prepared on multigram scales, the yields were quantitative, and antigen binding of the conjugates was completely preserved. A chimeric (mouse–human) version of BR96 was constructed ***(30)*** and used to prepare a conjugate, which was used for all tests in rodents, as well as for toxiology and for studies in man.

2. BR96-Doxorubicin

2.1. In Vivo Therapeutic Efficacy and Pharmacokinetics

Preclinical evaluation of the therapeutic effects of BR96-doxorubicin (BR96-DOX) was undertaken in athymic mice and rats with subcutaneous human tumor xenografts ***(27)***. Therapy was initiated when the tumors were well established and had a size of 50–100 mm^3. Treatment with BR96-DOX (100–500 mg/kg) given intraperitoneally resulted in regressions of the majority

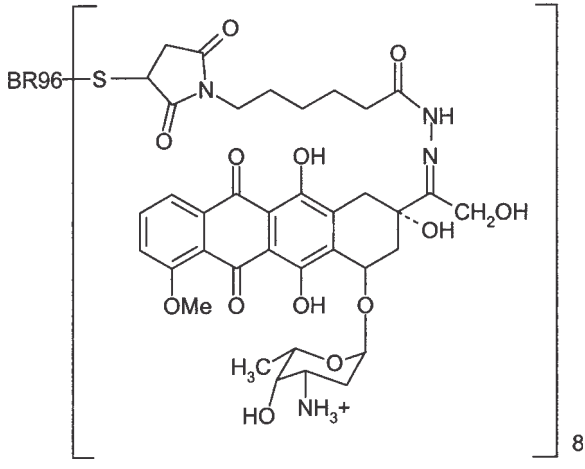

Fig. 2. Structure of BR96-doxorubicin.

of antigen-positive L2987 human lung adenocarcinomas and RCA colon carcinoma, with cures at the higher (≥200 mg/kg) doses (**Fig. 3**). The findings with colon carcinoma are of particular interest, as such tumors are resistant to doxorubicin given as an unconjugated drug. The effects were immunologically specific, since a nonbinding control conjugate was ineffective. It is noteworthy that BR96-DOX led to regressions and cures without any signs of toxicity, probably because it does not bind to any normal cells in athymic mice. Doxorubicin at the maximum tolerated dose (10 mg/kg/injection) had very little antitumor activity, and administration of "naked" BR96, alone or together with doxorubicin at its maximum tolerated dose, was not curative. BR96-DOX was also active in mouse xenograft models of human breast carcinomas, and in mice that had extensive disseminated disease (≥0.5 g of visible tumor burden at the onset of therapy) following intravenous inoculation approx 12 wk earlier with the L2987 human lung carcinoma *(27)*. In all these tumor models, the amount of conjugate needed to get high cure rates was at least 200 mg/kg/injection when injected 3 times, 4 d apart.

Rats display BR96 binding to epithelial cells in the esophagus, stomach, and intestine, and to the acinar cells of the pancreas *(27)*. This allowed studies to be undertaken in an animal model in which the expression of Le^y is similar to that in man. It was found that when athymic rats xenotransplanted with L2987 lung carcinoma were treated with BR96-DOX, 94% remained alive and tumor-free with no evidence of toxicity 150 d posttherapy. The maximum tolerated dose of doxorubicin led to a 25% cure rate.

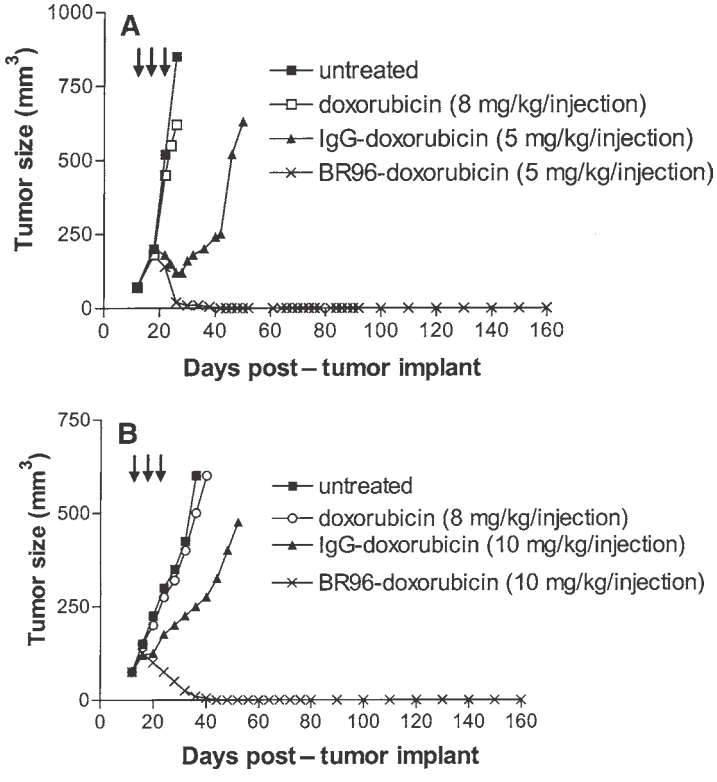

Fig. 3. Therapeutic activities of BR96-doxorubicin in athymic mice with **(A)** L2987 lung adenocarcinoma and **(B)** RCA colorectal carcinoma human-tumor xenografts. The tumors were implanted subcutaneously, and the animals were treated with intravenous doxorubicin or doxorubicin conjugates at the times indicated by the arrows. The conjugate doses were based on the drug component, and represent 246 and 176 mg MAb component/kg/injection for (A) and (B), respectively ***(27)***.

Experiments were subsequently performed in immunocompetent Brown Norway rats that carried subcutaneous or intrahepatic transplants of a chemically induced, syngeneic colon carcinoma, BN7005 ***(28)***. This tumor expresses Le^y at the cell surface and provides a model that is more similar to the human situation not only in that the target antigen is expressed in normal gastrointestinal epithelia (as it is in athymic rats), but also that the tumor is syngeneic and that the treated animals are immunocompetent. Cures of both subcutaneous and intrahepatic tumors were observed after treatment with BR96-DOX (≥100 mg/kg), while unconjugated doxorubicin at its maximum tolerated dose (or matching doses of a nonbinding IgG-DOX conjugate) were not active. An anticonjugate antibody response was induced in the rats, but this could be largely prevented

by giving the immunosuppressive drug deoxyspergualin. The therapeutic efficacy observed in the athymic and immunocompetent rat models implies that immunoconjugate binding to Le^y-positive normal tissues did not act as an "antigen sink" depriving tumors from available conjugate molecules.

Detailed pharmacokinetic studies were undertaken to gain insight into why BR96-DOX is so much more efficacious than systemically administered doxorubicin ***(29)***. Athymic mice with subcutaneous L2987 tumor xenografts were treated with maximum tolerated doses of doxorubicin or therapeutically effective doses of BR96–DOX, and the amount of free and conjugate-bound doxorubicin was measured in tumors and several normal tissues. It was found that the amount of free doxorubicin in the tumors of BR96–DOX treated mice greatly exceeded that of animals treated with unconjugated doxorubicin. After a single dose of BR96–DOX, the area under the curve of intratumoral unconjugated doxorubicin was more than four times that of animals that were treated systemically with doxorubicin. High levels of doxorubicin were maintained for several days following conjugate treatment. Importantly, the conjugate delivered less free doxorubicin to normal tissues, including the heart, compared to systemic doxorubicin treatment. The high intratumoral levels of doxorubicin in BR96–DOX treated mice probably accounts for the pronounced antitumor activities.

Toxicology studies were performed in dogs, which like humans and rats, express the Le^y antigen in epithelial cells from the gastrointestinal tract. They showed that BR96–DOX and unmodified MAb BR96 had the same dose-limiting toxicity (severe vomiting and bloody diarrhea) when given at doses greater than approx 400 mg/m^2, and there was evidence that this toxicity was mediated by complement. The immunoconjugate did not induce cardiomyopathy in a rat model and was therefore different from unconjugated doxorubicin.

2.2. Clinical Studies on BR96–DOX

Clinical evaluation was initiated in view of the encouraging preclinical findings. Two phase I trials were first performed in patients with advanced cancer, most of whom had carcinomas of the colon, breast, or ovary ***(31,32)***. In one trial, the patients received an intravenous infusion (over 24 h) of the conjugate every third week, while in the other trial the conjugate was given weekly over a short time span. Maximum tolerated doses were established as approx 700 mg/m^2 and 200 mg/m^2 conjugate per infusion (approx 18 and 5 mg/kg) for treatment every third week or each week, respectively. Two partial regressions (of breast and gastric carcinoma) and several tumor stabilizations were observed in the first (700 mg/m^2) trial. One of the problems that was identified in this study was that the circulating conjugate lost more than half of the attached drug molecules in 24–48 h, thereby limiting the length of time that active drug could be

delivered to tumors. A similar loss of drug molecules was seen in the rodent models, but this was compensated for by the more frequent administration of conjugate in those models.

A phase II trial was then performed in patients with metastatic breast carcinoma, administering the conjugate every third week at a dose of 700 mg/m^2 per injection. It demonstrated only one response in 14 patients, as compared with four responses in nine patients who received doxorubicin alone in a parallel control group ***(33)***. Importantly, two of four patients who initially received doxorubicin without responding had partial remissions following crossover into the BR96-DOX group ***(33)***. The reason for this is unknown and certainly worthy of further investigation.

The dose-limiting factor was gastrointestinal toxicity, particularly severe vomiting with hematemesis, which was commonly seen as the conjugate was being injected. Increases in serum amylase and lipase were also observed. Treatment with antiemetics (which were used except for the weekly phase I trial) increased the conjugate dose that could be given safely but did not allow doses above 700 mg/m^2 per injection. One patient who received unconjugated BR96 MAb displayed as much toxicity as patients receiving the corresponding dose of the conjugate, a finding reminiscent of the toxicology data in dogs. Gastrointestinal biopsies demonstrated conjugate binding to, and damage of, epithelial cells, most likely as a result of complement activation. The epithelial damage was reversible within approx 1 wk, and the increases of pancreatic enzymes were also reversible; there was no evidence that the toxicity increased as patients were retreated. No signs of cardiac toxicity were observed, and hematologic toxicities were significantly less with conjugate than with doxorubicin. Antibody responses to BR96-DOX were mild to moderate, with two of nine analyzed patients having more or equal to a 10-fold raise in titer ***(33)***. A limited number of tumor biopsies were obtained, and binding of BR96-DOX to the tumor cells was observed as well as uptake of doxorubicin ***(34)***.

The most likely reason for the lack of clinical efficacy of BR96-DOX is that gastrointestinal toxicity limited the doses to suboptimal levels. This becomes clear when one compares conjugate doses expressed as mg/kg body weight, which correlate well with the ensuing concentration in plasma. In mice and rats, the doses inducing tumor regressions, when given 3 times at 4 d apart, were at least 100 mg/kg body weight ***(34)***, i.e., approx 10 times greater than what could be safely given to man.

3. Future Studies

Since BR96-DOX failed in the clinical evaluation because of its binding to normal gastrointestinal tissues, an obvious goal would be to use a MAb with much higher tumor specificity. We are, however, skeptical about the existence

of such MAbs, except when a tumor expresses an antigen encoded by an oncogenic virus or has undergone a mutation that causes the abundant expression of a novel cell surface antigen (most likely, an infrequent event). This is in view of the fact that no MAbs to other truly specific antigens shared by tumor groups (and thus suitable for development towards products) have been found, in spite of tremendous efforts over the past 20 years. A more realistic approach may be to prepare immunoconjugates using MAbs to growth factor receptors known to play a key role in certain cancers, as is the case with MAbs to HER2 ***(2)***. Attachment of the appropriate drug may further increase their therapeutic efficacy, since the MAb may make tumor cells more sensitive to drug-induced apoptosis.

The data obtained from model studies performed in response to the clinical trials suggest a number of additional avenues for further investigation. These include both new clinical trials utilizing BR96-DOX, and the preparation of new conjugates that address some of the inherent limitations of BR96-DOX. Preclinical studies have shown that BR96-DOX synergizes with the anticancer drug Paclitaxel, when the two are administered together in athymic mice and rats that have been transplanted with antigen-positive human carcinomas. Tumor regressions and cures were observed at 20 mg/kg, i.e., at a dose that is within the range that can be given to patients ***(35)***. Either agent alone, or combinations of Paclitaxel with unmodified BR96 or doxorubicin, were not curative. It was also found that prolonged (over 2–3 wk) and more frequent (daily or every second day) administration of BR96-DOX induced regressions and cures of xenotransplanted human carcinomas in athymic mice also at doses expected to be tolerated in man (Trail et al., personal communication). Finally, preclinical studies have demonstrated that BR96-DOX is much more efficacious when used to treat micrometastases rather than bulky tumor masses (Trail et al., personal communication) into which penetration of many molecules, and particularly large ones, is known to be severely restricted ***(36)***. These findings are not surprising in view of the observation that unmodified MAb 17.1A, which is ineffective as a single agent against bulky tumors, has significant activity in high-risk patients with colon carcinoma following removal of macroscopically visible tumors ***(5)***.

Efforts are presently under way to develop new, more potent BR96–drug conjugates that will require greatly reduced doses to achieve antitumor activity. In developing such agents, a key requirement will be to design new linker chemistries that maintain the integrity of the MAb–drug conjugate until it reaches the tumor. Furthermore, the BR96 component can be genetically engineered so as not to cause toxicity through complement fixation. Such studies will provide a means to decreasing BR96-induced toxicity, and will greatly reduce the cost of therapy, since much lower conjugate doses will be used.

4. Conclusions

Chimeric (mouse–human) immunoconjugates have been made between doxorubicin and the anti-Le^y MAb BR96, which binds to the majority of cells within >70% of human carcinomas of the colon, breast, ovary, and lung (non–small cell) and can effectively treat xenotransplanted human carcinomas in athymic mice, if given at sufficiently high doses. They are also effective against human carcinomas transplanted into athymic rats, and against a transplanted rat colon carcinoma in immunocompetent, syngeneic rats. This is important since rats, like humans and dogs (but in contrast to mice), express the Le^y antigen in normal epithelial cells from the gastrointestinal tract.

A chimeric immunoconjugate between BR96 and doxorubicin (BR96-DOX) was evaluated in patients with metastatic carcinoma. Because of substantial gastrointestinal toxicity, the maximum tolerated dose (expressed as mg/kg body weight) was approx 10% of that needed for therapeutic efficacy in rodents, which may explain why the clinical effects observed were modest (a few partial regressions). The dose-limiting toxicity was mediated by the conjugate's protein part and was most likely caused by complement activation.

Subsequent preclinical studies were performed to address these issues. They showed that a combination of BR96-DOX with Paclitaxel induced regression of xenotransplanted human carcinomas in athymic mice and rats, also at immunoconjugate doses that are likely to be safe in man (approx ≤ 10mg/kg). More frequent administration of small (likely to be tolerated) conjugate doses provided another means to increase conjugate efficacy approx 10 times. Additional clinical trials, based on this information, are justified. Other approaches that need to be explored are replacement of doxorubicin with a more potent drug, preparation of conjugates that are more stable in vivo, and engineering of the BR96 molecule so that it cannot bind complement.

Acknowledgments

Part of the work on the targeting of anti-Le^y MAbs to carcinomas was performed at Bristol-Myers Squibb Pharmaceutical Research Institute (PRI) in Seattle, Washington, where the authors were then employed. Other parts of the work reviewed in this article were carried out at the Bristol-Myers Squibb PRI in Wallingford and Lawrenceville. Among former collaborators within the PRI, we would especially like to mention J. and U. Garrigues, H. Wan, P. Fell, and D. Yelton (manufacture, characterization, and genetic engineering of monoclonal antibodies); R. Firestone, D. Willner, G. Braslawsky, and T. Kaneko (design and preparation of immunoconjugates); P. Trail, A.-M. Casazza, and J. Brown (preclinical evaluation); J. Knipe (pharmacokinetic studies); C. Cimarusti (preclinical development of the BR96-DOX conjugate); N. Onetto,

W. Slichenmyer, and M. Birkhofer (clinical evaluation). Collaboration with H.O. Sjögren at the University of Lund, Sweden (testing of BR96-DOX in a syngeneic rat tumor model) is also acknowledged.

References

1. Hellström, I., Hellström, K. E., Siegall, C., and Trail, P. A. (1995) Immunoconjugates and immunotoxins for therapy of carcinomas, in *Ad. Pharmacol.* (August, J. T., Anders, M. W., Murad, F., and Coyle, J. T., eds.), Academic Press, San Diego, pp. 349–388.
2. Slamon, D., Leyland-Jones, B., Shak, S., Paton, V., Bajamonde, A., Fleming, T., et al. (1998) Addition of herceptin (humanized anti-HER2 antibody) to first line chemotherapy for HER2 overexpressing metastatic breast cancer (HER2+/MBC) markedly increases anticancer activity: a randomized, multinational controlled phase III trial. *Proc. of ASCO* (Abstract) **17,** 98A.
3. Kaminski, M., Zasadny, K., Francis, I., Milik, A., Ross, C., Moon, S., Crawford, et al. (1993) Radioimmunotherapy of B-cell lymphoma with ^{131}I anti-B1 (anti-CD20) antibody. *N. Engl. J. Med*. **329,** 459–465.
4. Press, O. W., Eary, J. F., Appelbaum, F. R., Martin, P. J., Badger, C. C., Nelp, W. B., et al. (1993) Radiolabeled-antibody therapy of B cell lymphoma with autologous bone marrow support. *N. Engl. J. Med.* **329,** 1219–1268.
5. Riethmüller, G., Schneider-Gadicke, E., Schlimok, G., Schmiegel, W., Raab, R., Hoffken, K., Gruber, R., Pechlmaier, H., Hirche, H., Piehlmayr, R., Buggisch, P., Witte, J., et al. (1994) Randomized trial of monoclonal antibody for adjuvant therapy of resected Dukes C colorectal carcinoma. *Lancet* **343,** 1177–1183.
6. Pietersz, G. A., Krauer, K., and McKenzie, I. F. (1994) The use of monoclonal antibody immunoconjugates in cancer therapy. *Adv. Exp. Med. Biol.* **353,** 169–179.
7. Senter, P. D., Wallace, P. M., Svensson, H. P., Vrudhula, V. M., Kerr, D. E., Hellström, I., et al. (1993) Generation of cytotoxic agents by targeted enzymes. *Bioconjugate Chem*. **4,** 3–9.
8. Carter, S. K. (1975) Adriamycin-a review. *J. Nat. Cancer Inst.* **55,** 1265–1274.
9. Young, R. C., Ozols, R. F., and Myers, C. E. (1981) The anthracycline antineoplastic drugs. *New Engl. J. Med.* **305,** 139–153.
10. Hurwitz, E., Levy, R., Maron, R., Wilchek, M., Arnon, R., and Sela, M. (1975) The covalent binding of daunomycin and adriamycin to antibodies, with retention of both drug and antibody activities. *Cancer Res.* **35,** 1175–1181.
11. Levy, R., Hurwitz, E., Maron, R., Arnon, R., and Sela, M. (1975) The specific cytotoxic effects of daunomycin conjugated to antitumor antibodies. *Cancer Res.* **35,** 1182–1186.
12. Hurwitz, E., Wilchek, M., and Pitha, J. (1980) Soluble macromolecules as carriers for daunorubicin. *J. Appl. Biochem.* **2,** 25–35.
13. Shen, W. C. and Ryser, H. J. (1981) Cis-aconityl spacer between daunomycin and macromolecular carriers: a model of pH-sensitive linkage releasing drug from a lysosomotropic conjugate. *Biochem. Biophys. Res. Commun.* **102,** 1048–1054.

14. Diener, E., Diner, U. E., Sinha, A., Xi, S., and Vergidis, R. (1986) Specific immunosuppression by immunotoxins containing daunomycin. *Science* **231,** 148–150.
15. Yang, H. Y. and Reisfeld, R. A. (1988) Doxorubicin conjugated with a monoclonal antibody directed to a human melanoma-associated proteoglycan suppresses the growth of established tumor xenografts in nude mice. *Proc. Natl. Acad. Sci.* **85,** 1189–1193.
16. Dillman, R. O., Johnson, D. E., Shawler, D. L., and Koziol, J. A. (1988) Superiority of an acid-labile daunorubicin-monoclonal antibody immunoconjugate compared to free drug. *Cancer Res.* **48,** 6097–6102.
17. Lavie, E., Hirschberg, D. L., Schreiber, G., Thor, K., Hill, L., Hellström, I., et al. (1991) Monoclonal antibody L6-daunomycin conjugates constructed to release free drug at the lower pH of tumor tissue. *Cancer Immunol. Immunother.* **33,** 223–230.
18. Poznansky, M. J. and Juliana, R. L. (1984) Biological approaches to the controlled delivery of drugs: a critical review. *Pharmacol. Rev.* **36,** 277–336.
19. Braslawsky, G. R., Edson, M. A., Pearce, W., Kaneko, T., and Greenfield, R. S. (1990) Antitumor activity of adriamycin (hydrazone-linked) immunoconjugates compared with free adriamycin and specificity of tumor cell killing. *Cancer Res.* **50,** 6608–6614.
20. Mattes, M. J., Griffiths, G. L., Diril, H., Goldenberg, D. M., Ong, G. L, and Shih, L. B. (1994) Processing of antibody-radioisotope conjugates after binding to the surface of tumor cells. *Cancer* **73,** 787–793.
21. Gerweck, L. E., and Seetharaman, K. (1996) Cellular pH gradient in tumor versus normal tissue: potential exploitation for the treatment of cancer. *Cancer Res.* **56,** 1194–1198.
22. Kaneko, T., Willner, D., Monkovic, I., Knipe, J. O., Braslawsky, G. R., Greenfield, R. S., and Vyas, D. M. (1991) New hydrazone derivatives of adriamycin and their immunoconjugates—a correlation between acid stability and cytotoxicity. *Bioconjug. Chem.* **2,** 133–141.
23. Trail, P. A., Willner, D., Knipe, J., Henderson, A. J., Lasch, S. J., Zockler, M. E., et al. (1997) Effect of linker variation on the stability, potency, and efficacy of carcinoma-reactive BR64–doxorubicin immunoconjugates. *Cancer Res.* **57,** 100–105.
24. Hellström, I., Garrigues, H. J., Garrigues, U., and Hellström, K. E. (1990) Highly tumor-reactive, internalizing, mouse monoclonal antibodies to Le^y related cell surface antigen. *Cancer Res.* **50,** 2183–2190.
25. Garrigues, J., Garrigues, U., Hellström, I., and Hellström, K. E. (1993) Le^y specific antibody with potent anti-tumor activity is internalized and degraded in lysosomes. *Am. J. Pathol.* **142,** 607–622.
26. Firestone, R. A., Willner, D., Hoffstead, S. J., King, H. D., Kaneko, T., Braslawsky, G. R., et al. (1996) Synthesis and antitumor activity of the immunoconjugate BR96-Dox. *J. Controlled Release* **39,** 251–259.
27. Trail, P. A., Willner, D., Lasch, S. J., Henderson, A. J., Hofstead, S., Casazza, A. M., et al. (1993) Cure of xenografted human carcinomas by BR96–doxorubicin immunoconjugates. *Science* **261,** 212–215.

28. Sjögren, H. O., Isaksson, M., Willner, D., Hellström, I., Hellström, K. E., and Trail, P. A. (1997) Antitumor activity of carcinoma-reactive BR96-doxorubicin conjugate against human carcinomas in athymic mice and rats and syngeneic rat carcinomas in immunocompetent rats. *Cancer Res*. **57,** 4530–4536.
29. Mosure, K. W., Henderson, A. J., Klunk, L. J., and Knipe, J. O. (1997) Disposition of conjugate-bound and free doxorubicin in tumor-bearing mice following administration of a BR96-doxorubicin immunoconjugate (BMS 182248) *Cancer Chemother. Pharmacol*. **40,** 251–258.
30. Yarnold, S. and Fell, H. P. (1994) Chimerization of anti-tumor antibodies via homologous recombination "conversion vectors." *Cancer Res.* **54,** 1–7.
31. Slichenmyer, W. J., Saleh, M. N., Bookman, M. A. et al (1996) Phase I studies of BR96 doxorubicin in patients with advanced solid tumors that express the Lewis Y antigen. *Anti-Cancer Treatment, Sixth International Congress* (Abstract) **95,** 6–9.
32. Saleh, M. N., LoBuglio, A. F., and Trail, P. A. (1998) Immunoconjugate therapy of solid tumors: studies with BR96-doxorubicin, in Basic and Clinical Oncology, vol. 15: *Monoclonal Antibody-Based Therapy of Cancer* (Grossbard, M., ed.), Marcel Dekker, New York, pp. 397–416.
33. Tolcher, A. W., Sugarman, S., Gelmon, K. A., Cohen, R., Saleh, M., Isaacs, C., et al. (1999) Randomized phase II study of BR96-doxorubicin conjugate in patients with metastatic breast cancer. *J. Clin. Oncol*. **17,** 478–484.
34. Trail, P. A., Slichenmyer, W. J., Birkhofer, M. J., Warner, G., Knipe, J., Willner, D., et al. (1996) BR96-doxorubicin immunoconjugate for treatment of patients with carcinoma. *Proc. Am. Assoc. Cancer Res.* (Abstract) **37,** 626.
35. Trail, P. A., Bianchi, A. B., Henderson, A. J., TrailSmith, M. D., Willner, D., Girit, E., et al. (1999a) Enhanced antitumor activity of paclitaxel in combinaiton with the anti-carcinoma immunoconjugate BR96–Dox Orubicin. *Clin. Cancer Res*. **5,** 3632–3638.
36. Jain, R. (1994) Barriers to drug delivery in solid tumors. *Sci. Am.* **271,** 58–65.

2

CD7-Specific Single Chain Fv Immunotoxins

Design and Expression

Christopher A. Pennell and Mary E. Pauza

1. Introduction

This chapter summarizes our experience with the design and expression of single-chain Fv (sFv) immunotoxins (sFv-IT) specific for CD7, a differentiation antigen found on human peripheral T and NK cells, and on subsets of committed myeloid and lymphoid progenitors in the bone marrow ***(1–4)***. In vitro studies have shown that CD7 participates in the activation and adhesion of mature T and NK cells, but the exact role it plays in the development and function of these cells in vivo remains obscure ***(5,6)***. A recent analysis of CD7-deficient mice revealed an association between resistance to endotoxin-induced shock and selective deficiencies of liver $NK1.1^+/CD3^+$ T-cell numbers and serum interferon-γ (IFN-γ) levels ***(7)***. These data suggest that CD7 participates in the development or migration of murine $NK1.1^+$ T-cells in the liver, and that reduced numbers of these cells results in decreased cytokine production elicited by bacterial lipopolysaccharides.

Regardless of its function, CD7 expression in disease has important clinical ramifications. It is one of the most useful markers for T-cell acute lymphoblastic leukemia (T-ALL), since most T-ALL cells are $CD7^+$ in >95% of cases ***(8–10)***. CD7 is expressed at high densities (approx 60,000 mol/cell) on T-cells and is rapidly internalized, even when bound by monovalent antibody fragments ***(11)***. It therefore makes an ideal target antigen for immunotoxin-mediated therapy of T-cell disease. This was evidenced in a recent phase I clinical trial of a CD7-specific immunotoxin called DA7 ***(12)***. DA7 was synthesized at the University of Minnesota by biochemically linking deglycosylated ricin toxin A-chain (RTA) to a CD7-specific monoclonal antibody ***(13)***. DA7 achieved

From: *Methods in Molecular Biology, vol. 166: Immunotoxin Methods and Protocols*
Edited by: W. A. Hall © Humana Press Inc., Totowa, NJ

objective clinical responses at its maximal tolerated dose despite being limited by instability and vascular toxicity.

Based on this trial, we reasoned that a recombinant sFv-IT derived from DA7 might have a larger "therapeutic window" due to enhanced stability and tissue penetration. Immunoglobulin sFv fragments consist of heavy- and light-chain variable regions (V_H and V_L) linked by small, flexible peptides; as such, sFv fragments retain the specificity of the antibodies from which they are derived ***(14,15)***. The major advantages of recombinant sFv-IT over biochemically synthesized immunotoxins are that the former are homogenous, genetically modifiable, have enhanced tissue penetration, and the site and manner in which the sFv and toxin moieties are joined can be exactly controlled.

To construct the *sFv* genes, we first used a commercial kit (RPAS; Amersham Pharmacia Biotech) to clone the V_H and kappa light chain variable (V_κ) region genes expressed by several CD7-specific hybridomas by reverse-transcriptase polymerase chain reaction (RT-PCR; ***11***). One of these was 3A1e, the hybridoma used to produce the antibody moiety in DA7. A carboxy-terminal cysteine residue was genetically added to each sFv fragment. This provided an exact site for the sFv to be disulfide-linked to RTA to yield an sFv-IT.

For reasons that remain unclear, we were unable to obtain a functional 3A1e sFv fragment following denaturation and refolding of the protein when it was expressed as an insoluble inclusion body. Because we successfully refolded the other sFv fragments, we suspected that the 3A1e sFv was "disulfide restricted" (i.e., a protein prone to inappropriate disulfide bond formation during refolding in a redox buffer; ***16,17***). To circumvent this and other problems inherent to protein refolding, we switched to expressing all sFv fragments solubly in bacteria and yeast ***(11,18,19)***. We found that the yields of soluble and functional sFv fragments were approx 100-fold greater in yeast than in bacteria; therefore, we routinely used the yeast system for sFv expression ***(18,19)***. The methods presented below include sFv cloning and assembly, sFv expression in yeast, and construction and purification of the sFv–RTA conjugates.

2. Materials

2.1. sFv Cloning

1. 3A1a, 3A1d, 3A1e, and 3A1f are murine hybridomas that secrete cross-blocking antibodies specific for human CD7 ***(20,21)***. 3A1d, e, and f hybridomas were generously provided by Dr. Barton Haynes' laboratory (Duke University). 3A1a was purchased from the American Type Culture Collection (ATCC; Rockville, MD). The *E. coli* bacterial strain INVαF' was purchased from Invitrogen (Carlsbad, CA).
2. Dulbecco's minimal essential medium supplemented with 10% fetal bovine serum, 50 U of penicillin G, and 50 µg/mL streptomycin sulfate (all were purchased from Celox, Hopkins, MN).

3. FastTrack mRNA isolation kit (Invitrogen); diethyl pyrocarbonate (DEPC; Sigma; St. Louis, MO).
4. Random hexamer primers for first-strand cDNA synthesis (Boehringer Mannheim; Indianapolis, IN); dithiothreitol (DTT; Pierce; Rockford, IL); deoxynucleotide triphosphates (dNTPs; Boehringer Mannheim); 5X first-strand cDNA buffer (250 m*M* Tris-HCl (pH 8.3), 15 m*M* $MgCl_2$, 375 m*M* KCl; BRL Life Technologies; Gaithersburg, MD); Moloney murine leukemia virus reverse transcriptase (BRL Life Technologies) and recombinant RNasin (Promega Corp.; Madison, WI)
5. RPAS mouse scFv module (Amersham Pharmacia Biotech) kit contains oligonucleotide primers specific for the conserved 5' and 3' ends of immunoglobulin *V* genes, as well as primers that link a pair of amplified V_H and V_κ genes together to construct an sFv. The 5' and 3' primers anneal to conserved nucleotides that encode the amino-terminal portion of the first framework (FR) region and the *J*-gene–encoded carboxy-terminal portion of the fourth FR region, respectively. The sequences of these oligonucleotides are proprietary but can be gleaned from work published by Winter and colleagues ***(22)***. The two complementary linker primers that join a V_H and V_κ gene pair encode the flexible $(Gly_4\text{-}Ser)_3$ peptide commonly used in sFv constructs ***(16)***. The $(Gly_4\text{-}Ser)_3$ codons are flanked by nucleotides designed to anneal to the 3' ends of J_H genes and the 5' ends of V_κ genes. Correctly assembled V_H–linker–V_κ constructs are amplified by splice overlap extension using 5' V_H and 3' V_κ primers modified to include *Sfi*I and *Not*I restriction endonuclease sites, respectively.
6. All oligonucleotide primers were synthesized by Oligos Etc. (Bethel, ME) and were ordered at their 50 n*M* scale as "primer grade" (i.e., the oligonucleotides underwent organic extraction, precipitation, and two vacuum desiccation steps to remove small contaminants). The lyophilized oligonucleotides were dissolved to a final concentration of 500 pmol/μL in TE (10 m*M* Tris-HCl, pH 8.0, 1 m*M* EDTA), aliquoted (10 μL), and stored at –85˚C. Single aliquots of each primer were stored at 4˚C and the required amount was diluted to 5 pmol/μL in TE just prior to use.
7. Cloned *Pfu* polymerase and 10X *Pfu* buffer (100 m*M* KCl, 100 m*M* $[NH_4]_2SO_4$, 200 m*M* Tris-HCl [pH 8.75], 20 m*M* $MgSO_4$, 1% Triton X-100, 1 mg/mL bovine serum albumin) (Stratagene; La Jolla, CA); *Taq* polymerase in buffer B and 10X reaction buffer without $MgCl_2$ (500 m*M* KCl, 100 m*M* Tris-HCl [pH 9.0] and 1% Triton X-100; Promega; Madison, WI). The enzymes were stored at –20˚C in a Stratacooler II benchtop cooler (Stratagene).
8. Agarose (BRL Life Technologies); 6X loading dye (0.25% bromophenol blue, 30% glycerol in water); 0.5X TBE running buffer (for 5X TBE, add 54 g Tris-base, 27.5 g boric acid, 20 mL 0.5 *M* EDTA [pH 8.0], and distilled water to bring to 1 L final volume); ethidium bromide (10 mg/mL in distilled water); 100 bp ladder (BRL Life Technologies).
9. Qiagen II gel extraction kit (Qiagen; Valencia, CA); PRISM sequencing kit (PE Applied Biosystems, Foster City, CA).
10. Vectors: pCRII and pPIC9K (Invitrogen).

2.2. sFv Expression

1. GS115 *his4*-deficient *Pichia pastoris* strain (Invitrogen).
2. Electroporator and 0.2 cm electroporation cuvets (Eppendorf; Madison, WI).
3. Recipes for the following solutions can be downloaded as a PDF file from Invitrogen (http://www.invitrogen.com/manuals.html): YPD (1% yeast extract, 2% peptone, 2% dextrose); BMMY (1% yeast extract, 2% peptone, 100 m*M* potassium phosphate [pH 6.0], 1.34% yeast nitrogen base, 4×10^{-5}% biotin, 0.5% methanol); MM and MD agar plates (1.5% agar, 1.34% yeast nitrogen base, 4×10^{-5}% biotin, and either 0.5% methanol or 2% dextrose, respectively).
4. BA85 0.45 μm nitrocellulose filters, 82 mm diameter (Schleicher & Schuell; Keene, NH); Whatman 3MM chromatography paper cut in 82 mm diameter circles (Whatman; Clifton, NJ); Penta-His tag mouse monoclonal antibody (Qiagen); goat antimouse immunoglobulin–horseradish peroxidase (HRP) conjugate (Promega); ECL kit (Amersham Pharmacia Biotech); TBS (20 m*M* Tris-HCl [pH 7.5], 137 m*M* NaCl) TBST (TBS with 0.1% Tween-20), solution A (TBST with 10% w/v nonfat dry milk).
5. Laemmli minigel apparatus and power supply for SDS-PAGE; GelCode blue stain reagent (Pierce).
6. Centricon-3 and -10 concentrators (Millipore; Bedford, MA).

2.3. sFv-RTA Conjugate Formation and Purification

1. Deglycosylated RTA (Inland Laboratories; Austin, TX); SPDP, DTT, 5-5'-dithiobis-(2-nitrobenzoic acid) (DTNB/Ellman's reagent) (Pierce).
2. 5-mL Chelating–high trap, PD-10, Superdex 75 HR10/30 columns (Amersham Pharmacia Biotech).

3. Methods

3.1. V Gene Amplification and sFv Assembly

1. Culture the CD7-specific hybridomas in tissue culture medium at 37˚C in a humidified atmosphere containing 5% CO_2. The cells should be at a density of $0.5–1 \times 10^6$ cells/mL and >90% viable, as determined by trypan blue exclusion when harvested for mRNA isolation. Always wear gloves (and change frequently) in this and subsequent steps to prevent contamination of nucleic acid preparations.
2. Centrifuge 100 mL of cells for 5 min at 1000*g* and decant the supernatant. To purify mRNA from a pellet of $0.5–1 \times 10^8$ hybridoma cells, use the mRNA isolation kit exactly according to the manufacturer's protocol. Resuspend the purified mRNA in DEPC-treated distilled water (*see* **Note 1**) and store in aliquots at –85˚C. To minimize sample cross-contamination, use positive displacement pipets or pipet tips with aerosol blocks for all subsequent manipulations. Use each tip once.
3. Use RT-PCR to amplify the expressed *V* genes by initially synthesizing first-strand cDNA as follows. In a sterile 1.5-mL Eppendorf tube, combine 5 μg mRNA with 0.5 μg random hexamer primers, 10 m*M* DTT, 0.5 m*M* of dNTP, 20 μL of

5X first-strand cDNA buffer, and bring to a final volume of 100 µL with DEPC-treated water (all reagents should be prepared and diluted in DEPC-treated water). Include a negative control that contains DEPC-treated water in place of the mRNA. Place the tubes in heating block filled with water preheated to 68°C. Allow the mRNA to denature at 68°C for 10 min, then remove the block with the tubes from the heating element and place it on the bench top. Once the block has cooled to 37°C, add 4 U Moloney murine leukemia virus reverse transcriptase and 0.8 U recombinant RNasin to each tube. Place the tubes in a 37°C water bath for 1 h to allow for first-strand cDNA synthesis.

4. The V_H and V_κ genes are individually amplified from separate cDNA aliquots using the 5' and 3' V_H and V_κ primer sets supplied in the RPAS kit according to the manufacture's directions. (What follows are our adaptations of these directions. If we followed the directions exactly, then this is noted.) Add 33 µL from the first-strand cDNA synthesis tube, 2 µL of the V_κ light-chain primer mix, and 64 µL of sterile distilled water. To a second tube, add 33 µL from the first-strand cDNA synthesis tube, 2 µL each of V_H primers 1 and 2, and 62 µL of sterile distilled water. For negative controls, substitute 33 µL from the water control tube for the cDNA mix added to each primer pair. Overlay each sample with 100 µL mineral oil, tightly close the tubes, and place them in a thermal cycler. Denature the cDNA by heating at 95°C for 5 min, then add 1 µL of *Pfu* polymerase beneath the mineral oil using a fresh pipet tip every time. Amplify the *V* genes for 30 cycles as follows: 94°C for 1 min, 55°C for 2 min, and 72°C for 3 min.
5. To determine if the amplifications were successful, add 5 µL of each reaction mix to 5 µL of 0.5X TBE buffer and 2 µL of 6X agarose gel-loading dye. Prepare a 1.5% agarose gel in 0.5X TBE buffer with 0.5 µg/mL ethidium bromide (added after the agarose is melted and cooled and before the gel is poured). Submerge the gel in a horizontal electrophoresis box containing 0.5X TBE. Load each sample into a separate well and load an additional well with a molecular weight marker (such as a 100 bp ladder). Apply a constant voltage between 50–100 V until the bromophenol blue dye front has migrated about two-thirds the length of the gel. Place the gel on a UV light box to visualize the ethidium bromide-stained DNA fragments. Expect to see bands of approx 340 and 325 bp resulting from the V_H and V_κ primer sets, respectively. No bands should be visible in the negative control lanes. Clone the amplified V_H and V_κ genes into pCRII and transform *E. coli* strain INVFα' according to the manufacturer's protocol. Pool all recombinant (white) colonies from an individual *V* gene transformation and sequence using an automated DNA sequencer.
6. To construct an *sF*v gene, the V_H and V_κ genes amplified from a given hybridoma are linked in a second PCR. The amplified *V* genes are gel purified by first adding 85 µL of each PCR mix to 18 µL of the 6X agarose gel loading dye, and then by loading the samples on a 1% agarose gel. Prepare the gel in 0.5X TBE buffer with 0.5 µg/mL ethidium bromide as described above. To make wells large enough to hold approx 100 µL, use a small piece of autoclave tape to join 3–4 teeth on the comb prior to inserting it into the molten agarose. Electrophorese the DNA as

previously described, but place a cardboard box over the gel box to minimize light-induced nicking of DNA in the presence of ethidium bromide. Visualize the ethidium bromide-stained DNA fragments using a hand-held long-wave UV light source, again to minimize DNA damage. Excise each DNA fragment by cutting it out of the gel with a separate razor blade. Remove excess gel from around the DNA fragment and then dice the gel slice into small pieces prior to extraction. Extract DNA using the gel extraction kit according to its protocol.

7. Determine the amount of each gel-purified PCR product relative to the linker–primer DNA supplied in the RPAS kit. The goal is to add equimolar amounts of the two PCR products and linker–primer DNA in a second PCR. Mix 5 μL of each PCR mix with 1 μL 6X agarose gel-loading dye. Mix 1 μL of the linker–primer DNA with 1 μL 6X agarose gel-loading dye and 4 μL distilled water. Run the three samples on a 1.5% agarose gel as described earlier. For equimolar concentrations, the ethidium bromide staining intensity of the two PCR products should be equivalent and about 3–4 times greater than the linker–primer DNA. Adjust the concentrations of the PCR products accordingly before proceeding to the next step.
8. The sFv assembly and fill-in reactions are performed as described by the manufacturer. Briefly, equimolar amounts of the amplified *V* gene PCR products and the linker–primer DNA (1–3 μL) are added to 2.5 μL 10X reaction buffer without $MgCl_2$, 12.5 μL dNTP mix (each at 2 m*M*), 4 μL 25 m*M* $MgCl_2$, 1 μL *Taq* polymerase (*see* **Note 2**), and sterile distilled water to a final volume of 25 μL. Overlay with 25 μL mineral oil, place in a thermocycler, and run seven cycles at: 94°C for 1 min, 63°C for 4 min. This procedure should append the linker–primer to the 3' and 5' ends of the amplified V_H and V_κ genes, respectively.
9. To link the modified V_H and V_κ genes and simultaneously append 5' and 3' restriction endonuclease sites, add the following components beneath the mineral oil to the 25 μL assembly mix: 13 μL sterile distilled water, 2.5 μL 10X reaction buffer without $MgCl_2$, 5 μL dNTP mix (each at 2 m*M*), 1 μL *Taq* polymerase, 1.5 μL 25 m*M* $MgCl_2$, and 2 μL restriction-site primer mix (these primers contain *Sfi*I or *Not*I restriction sites and anneal to the 5' end of the V_H [*Sfi*I site] and/or the 3' end of the V_κ gene [*Not*I site]). Overlay with an additional 25 μL mineral oil, place in a thermocycler, and run 30 cycles at: 94°C for 1 min, 55°C for 2 min, and 72°C for 2 min.
10. Analyze the reactions by 1.5% agarose gel electrophoresis as described above. A band of approx 750 bp is expected, along with some heavy- and light-chain monomers.
11. Clone the PCR products into the pCRII vector and transform *E. coli* strain INVFα' (*see* **Note 3**). Pool all recombinant (white) colonies from an individual transformation, isolate plasmid DNA, and digest with *Sfi*I and *Not*I. DNA fragments of the size predicted for full-length *sFv* genes (approx 750 bp) are gel purified (see above), ligated to the pCANTAB 5E phagemid vector, and used to transform *E. coli* strain HB2151 as described in the RPAS manual.
12. Directly sequence the *sFv* genes in at least three 3 clones derived from a given hybridoma to identify ones that lack *Taq* polymerase-induced mutations. These

mutations are identified by comparing the *sFv V*-gene sequences to the originally amplified *V*-gene sequences (as previously discussed). First, amplify 0.5 μg of plasmid DNA from each clone using 25 p*M* of each S1 and R2 primer in a buffer containing 1.5 m*M* $MgCl_2$, 2.5 U *Taq* DNA polymerase, 100 m*M* Tris-HCl (pH 8.3) and 500 m*M* KCl. The S1 and R2 primers anneal to pCANTAB 5E vector-encoded nucleotides that flank the sFv insert. Incubate the reaction mixtures at 94°C for 5 min, then add 10 μL dNTPs (at 2 m*M* each). Amplify the mixtures for 1 min at 94°C, 2 min at 55°C, and 2 min at 72°C for 30 cycles. An additional extension time of 10 min at 72°C completes the amplification reaction. Gel purify the approx 875 bp product for direct sequencing. Sequencing is performed using the S1 and R2 primers and 50–100 ng of gel-purified DNA with the PRISM sequencing kit according to the manufacturer's directions.

3.2. sFv Expression and Purification

1. The pCANTAB 5E vector encodes a leader sequence upstream of the sFv cloning site. This theoretically allows for the transport of the sFv fragment to the periplasmic space, where it can be isolated as a soluble protein. However, only two of the four sFv- pCANTAB 5E constructs (3A1e and 3A1f) were exported to the periplasm upon induction. The other two (3A1a and 3A1d) were expressed insolubly in the cytoplasm. Because of this and the consistently low yields (in the range of 200 μg/L) of purified sFv fragments from the periplasm, we suggest modifying the sFv constructs to allow for their expression as secreted proteins by the yeast *P. pastoris.* For example, we modified the 3A1f sFv by adding a cysteine residue followed by six histidines at the carboxy terminus. The cysteine provided a free thiol for disulfide conjugation to RTA, while the histidine tag allowed for identification with a specific monoclonal antibody and purification via immobilized metal-cation affinity chromatography. The modifications were made in one step by PCR amplification (30 cycles: 1 min at 95°C, 1.5 min at 55°C, 2 min at 74°C) from pCANTAB 5E-3A1f sFv template DNA using the primers 5'-CCGGAATTCATGGCCCAGGTCCAGCTGCAG-3' and 5'-CCGGAATTCCCGGGCGGCCGCTCAGTGGTGGTGGTGGTGGTGACACCG TTTGATTTCCAACTTTGTCCC-3'. The amplified 3A1fcysHis_6 sFv fragment was cloned into pCRII, sequenced, and subcloned into a *P. pastoris* expression vector, pPIC9, as an *Eco*RI/*Not*I restriction fragment.
2. pPIC9 is designed to integrate into the yeast genome via homologous recombination following transformation. To facilitate homologous recombination, the plasmid DNA is linearized prior to electroporation. Linearization with *Bgl*II allows the endogenous *AOX1* gene in the GS115 genome to be replaced with the *3A1fcysHis_6* and plasmid-encoded histidinol dehydrogenase *(HIS4)* genes upon homologous recombination. Prepare electrocompetent *P. pastoris* by inoculating 5 mL YPD in a 50 mL conical tube with frozen stock GS115 cells and incubating at 30°C overnight with vigorous shaking (220–250 rpm). Inoculate 500 mL of fresh YPD medium in a 2 L flask with 0.1–0.5 mL of the overnight culture. Cover the opening at the top of the flask loosely with sterile aluminum foil. Incubate at

Table 1

Electroporator	Charging voltage (V)	Capacitance (μF)	Resistance (Ω)
Invitrogen Electroporator II	1500	50	200
Bio-Rad Gene Pulser	1500	25	200
Eppendorf 2510	1500	10	600

30˚C with vigorous shaking until the OD_{600} = 1.3–1.5 (this typically takes an overnight incubation [12–15 h]). Centrifuge the cells at 1500*g* for 5 min at 4˚C. Suspend the cell pellet in 500 mL of ice-cold, sterile water. Recentrifuge and resuspend the cell pellet in 250 mL of ice-cold, sterile water. Centrifuge the cells again, then resuspend the cell pellet in 20 mL of ice-cold, sterile 1 *M* sorbitol. Centrifuge the cells once more and resuspend cell pellet in 0.5–1 mL of ice-cold, sterile 1 *M* sorbitol for a final volume of approx 3–4 mL (accounting for the volume of the cell pellet). Electrocompetent cells can be aliquoted and stored at –80˚C for up to 6 mo.

3. Mix 80 μL of ice-cold electrocompetent cells with 1–3 μg of plasmid DNA linearized with Bgl II. Transfer the DNA and cell mix to an ice-cold 0.2 cm electroporation cuvet and incubate on ice for 5 min. Wipe the outside of the cuvet with a Kimwipe to remove moisture and place the cuvet in the electroporation unit. Pulse the cells according to the parameters for yeast (*S. cerevisiae*) suggested by the manufacturer of the specific electroporation device being used (**Table 1**). Using a 0.2 cm cuvet, these parameters generate a pulse length of approx 5 msec with a field strength of approx 7500 V/cm (*see* **Note 4**). Immediately after electroporation, add 1 mL ice-cold, sterile 1 *M* sorbitol to the cells in the cuvet. Transfer the cells to a sterile microcentrifuge tube. Spread 200–600 mL aliquots on MD plates. Incubate the plates at 30˚C until colonies appear (this takes at least 2 d; 3–4 d is not unusual).
4. To screen for clones secreting sFvcysHis$_6$ proteins, probe colony lifts with an anti-His tag antibody as follows. Replica plate His^+ clones from the transformation plates by using sterile toothpicks first to streak isolated clones onto an MM plate and then onto the corresponding positions on an MD plate (*see* **Note 5**). Incubate 2–3 d at 30°C. Store the master MD plates at 4°C. Place a BA85 nitrocellulose filter over the colonies on the MM plate using gloved hands to grasp the opposite edges of the filter, bend the edges upwards, and touch the bottom of the filter to the plate. Gently lower the edges of the filter so that the filter wets from the center outwards. On top of this filter, place three circular pieces of Whatman 3MM chromatography paper cut to about 80 mm in diameter. Add several paper towels and weigh down the blotting pile with a 150 mL empty beaker. Incubate at 30°C for 1–3 h. Remove the nitrocellulose filter with forceps and wash in TBS (20 m*M* Tris–base, 137 m*M* NaCl, pH 7.6) to remove adherent yeast. Use 50 mL/wash and wash three times for 5 min each at room temperature with

constant shaking. Add positive controls by spotting 100 ng of each protein diluted in TBST on the filter. The positive controls are any purified His-tagged protein and the secondary goat antimouse–HRP conjugate (see below). After two minutes, block the filter with 3% BSA/TBS overnight at 4°C or for 2 h at 37°C. Incubate the filter with mouse anti-Penta-His tag antibody diluted 1:1000 in 3% BSA/TBS at room temperature with constant shaking for 1 h. Wash once for 15 min followed by three 5-min washes in TBST (50 mL/wash) with constant shaking at room temperature. Incubate membrane with goat antimouse immunoglobulin-HRP diluted 1:10,000 in solution A at room temperature with constant shaking for 1 h. Wash as above. Leave the filter in its final wash and go to the dark room. Pour off the final wash from the filter. Pipet 1 mL each of ECL developing reagents 1 and 2 onto the filter (use the same container in which the filter was washed). Incubate for 1 min. Place the filter in a film cassette, smooth some plastic wrap on top of the filter, turn the lights off, and place a piece of XAR-5 film (Kodak) on top of the plastic. Close the cassette, expose for 30–60 s initially, and develop the film. If there are no initial results, try a longer exposure time. The ECL mix should be effective for up to half an hour.

5. Select several positive clones to analyze their time course of protein secretion. Grow clones expressing the sFvcysHis$_6$ fragments in 100 mL of YPD medium in a sterile 1 L flask for 2 d at 30°C in a shaking (250 rpm) incubator. Centrifuge cells (10 min at 3000*g*), resuspend in 10 mL of BMMY in a sterile 100 mL flask (with foil loosely covering the top), and incubate for another 5 d at 30°C in a shaking (250 rpm) incubator. Take 500 µL aliquots of culture supernatants daily, store at –20°C, and examine after 5 d by reducing SDS-PAGE to determine the optimal time for expression. For SDS-PAGE, combine 5 µL 4X SDS loading dye, 1 µL 2-mercaptoethanol, and 14 µL of culture supernatant in a 1.5 mL centrifugation tube. Cap tightly and place in boiling water for 2–3 min. Cool on ice and quick-spin in an Eppendorf centrifuge to recover condensate. Load samples in wells of a 15% polyacrylamide Laemmli gel. Electrophorese for 40 min at a constant 200 V. Remove the gel from its glass plates and wash three times (200 mL per wash for 5 min at room temperature with agitation) to remove excess SDS. Stain proteins by adding just enough GelCode to cover the gel. Agitate gently at room temperature for 1 h, remove the GelCode, and destain with distilled water for at least 1 h at room temperature. Bands at about 28 kDa should be visible in the induced supernatants.
6. For large-scale expression, grow clones in 1 L of YPD medium in sterile 2 L baffle flasks (with foil covering their openings) for 3 d at 30°C in a shaking (250 rpm) incubator. Centrifuge cells (10 min at 3000*g*), resuspend in 50 mL of BMMY in a sterile 500 mL flask (with foil covering the opening), and incubate for the optimal number of days (e.g., 4 d) at 30°C in a shaking (250 rpm) incubator (*see* **Note 6**). Harvest the supernatants following centrifugation (10 min at 3000*g*). Clarify supernatants by centrifuging at 12,000*g* at 4°C for 20 min.
7. To purify the sFvcysHis$_6$ fragments, dialyze clarified supernatants from the induced culture against 50 m*M* sodium phosphate (pH 7.0) plus 100 m*M* NaCl. Filter

dialysates through a 0.8 μm filter syringe, followed by a 0.45 μm filter syringe, and run over a prepacked Chelating-High Trap 5 mL column using FPLC (*see* **Note 7**). Prior to loading sFv samples, wash the column with 25 mL distilled water (2 mL/min), activate it with 6 mL 100 m*M* $ZnCl_2$, and wash it again with 25 mL distilled water (2 mL/min) followed by 30 mL dialysis buffer (2 mL/min). Run dialysate over the column at 1 mL/min and save the flow through. Wash the column with 30 mL dialysis buffer (2 mL/min) and then elute bound fragments with a linear gradient of 0–100% 300 m*M* imidazole at 1 mL/min for 35 min. Collect 1 mL fractions and pool those fractions that absorb light at 280 nm. Determine the purified protein concentration with Coomassie Plus protein assay reagent (Pierce) using BSA as the standard.

3.3. sFv–RTA Conjugate Formation and Purification

1. Dilute the dgRTA chain to 0.5–1.0 mg/mL with PBS, 1 m*M* EDTA, pH 7.2, and reduce with 1–2 m*M* DTT for 1 h at room temperature. Remove excess DTT from the reduced dgRTA by gel filtration with a PD-10 column following the manufacturer's protocol.
2. Derivatize the reduced dgRTA (RTA-TNB) by adding DTNB (Ellman's reagent) for 1 h at room temperature. Derivatization prevents dgRTA homodimerization in subsequent steps. Use PD-10 gel filtration to remove excess DTNB from the RTA-TNB.
3. Concentrate each affinity-purified sFvcysHis_6 sample to 250–500 μg/mL using Centricon-3 concentrators and mildly reduce with 1–2 m*M* DTT for 1 h at room temperature. This does not reduce the intrachain disulfide bonds in the immunoglobulin domains, but it does yield free thiols at the carboxy-terminal cysteines. Remove excess DTT from the reduced sFvcysHis_6 fragments by gel filtration with a PD-10 column following the manufacturer's protocol, and mix the reduced sFvcysHis_6 with the RTA-TNB at a 1:1 molar ratio. Incubate the mixture for 1 h at room temperature and then overnight at 4°C. Purify conjugated protein (approx 58 kDa) by size-exclusion chromatography using a Superdex 75 HR 10/30 column and FPLC apparatus. Collect 1 mL fractions in PBS. Pool fractions that contain protein corresponding to approx 58–60 kDa. Concentrate protein with Centricon-10 concentrators, analyze by 10% nonreducing SDS-PAGE (do not add 2-mercaptoethanol to the sample), and determine the concentration, all as described above.

4. Notes

1. To prepare DEPC-treated water, add 500 mL of distilled water to a baked Pyrex bottle (250°C for 4 h). Add 0.5 mL DEPC and swirl to disperse. Cover with a sterile bottle cap and incubate for at least 12 h at 37°C. Autoclave to inactivate DEPC.
2. We initially tried to use the high-fidelity *Pfu* polymerase for sFv assembly but were unsuccessful despite repeated attempts under varying experimental conditions. Therefore, we used *Taq* polymerase for this step and had uniform success.

3. The RPAS manual recommends purifying the assembled sFv DNA, incubating it directly with *Sfi*I and *Not*I restriction endonucleases, and cloning the digested fragment into pCANTAB 5E. We found this step problematic because of the inability to monitor the efficiency of digestion. Therefore, we first cloned the amplified sFv constructs into pCRII. This linearized vector has single T-nucleotide 5' and 3' overhangs, allowing for the easy ligation of *Taq*-amplified DNA (due to the terminal transferase activity of *Taq,* and its inherent preference for adding single A nucleotides to 3' OH groups). The clones were pooled, digested with *Not*I and *Sfi*I, and the doubly digested DNA fragments were gel purified and ligated to pCANTAB 5E.
4. After a 90 min incubation at 37°C, inactivate *Bgl*II by heating the sample at 68°C for 10 min. It is important to ethanol-precipitate the DNA and wash it several times in 70% ethanol to remove salt prior to electroporation. Residual salt in the DNA preparation leads to high conductance (pulse lengths ≤ 2–3 ms) and poor transformation efficiencies due to excessive cell death.
5. These plates are overlaid on a template that has two 80 mm diameter circles divided into 52 numbered squares of equivalent size. A clone is first streaked diagonally across one square on the MM plate and then across the same numbered square on the MD plate.
6. Optimal protein expression requires good aeration, and therefore Invitrogen suggests the use of sterile cotton or gauze to plug the flasks. We and our colleagues have noted that these porous materials allow strong and unpleasant odors from the cultures to permeate the work area, and so we loosely cover our baffled flasks with sterile foil. This reduces the odor without adversely affecting protein yields.
7. All solutions used for FPLC are passed through 0.45 μm filters to prevent clogging the columns.

Acknowledgments

Chris Pennell's research is supported by grants from the National Institutes of Health (CA-59510) and the Minnesota Medical Foundation.

References

1. Barcena, A., Muench, M. O., Roncarolo, M. G., and Spits, H. (1995) Tracing the expression of CD7 and other antigens during T- and myeloid-cell differentiation in the human fetal liver and thymus. *Leuk. Lymphoma* **17,** 1–11.
2. Nakase, K., Kita, K., Sekine, T., Otsuji, A., Shirakawa, S., Tsuji, K., et al. (1993) CD7, CD4 and myeloid antigen-positive acute lymphoblastic leukemia. *Internat. J. Hematol.* **59,** 41–46.
3. Del Poeta, G., Stasi, R., Venditti, A., Cox, C., Aronica, G., Masi, M., et al. (1995) CD7 expression in acute myeloid leukemia. *Leuk. Lymphoma* **17,** 111–119.
4. Nimgaonkar, M. T., Roscoe, R. A., Persichetti, J., Rybka, W. B., and Winkelstein, A. (1995) A unique population of $CD34^+$ cells in cord blood. *Stem Cells* **13,** 158–166.

5. Shimizu, Y., van Seventer, G. A., Ennis, E., Newman, W., Horgan, K. J., and Shaw, S. (1992) Crosslinking of the T cell-specific accessory molecules CD7 and CD28 modulates T cell adhesion. *J. Exp. Med.* **175,** 577–582.
6. Chan, A. S., Mobley, J. L., Fields, G. B., and Shimizu, Y. (1997) CD7-mediated regulation of integrin adhesiveness on human T cells involves tyrosine phosphorylation-dependent activation of phosphatidylinositol 3-kinase. *J. Immunol.* **159,** 934–942.
7. Sempowski, G. D., Lee, D. M., Scearce, R. M., Patel, D. D., and Haynes, B. F. (1999) Resistance of CD7-deficient mice to lipopolysaccharide-induced shock syndromes. *J. Exp. Med.* **189,** 1011–1016.
8. Haynes, B. F., Denning, S. M., Singer, K. H., and Kurtzberg, J. (1989) Ontogeny of T-cell precursors: a model for the initial stages of human T-cell development. *Immunol. Today* **10,** 87–91.
9. Janossy, G., Coustan-Smith, E., and Campana, D. (1989) The reliability of cytoplasmic CD3 and CD22 antigen expression in the immunodiagnosis of acute leukemia: a study of 500 cases. *Leukemia* **3,** 170–181.
10. Janossy, G., Campana, D., Burnett, A., Coustan-Smith, E., Timms, A., Bekassy, A. N., et al. (1988) Autologous bone marrow transplantation in acute lymphoblastic leukemia—preclinical immunologic studies. *Leukemia* **2,** 485–495.
11. Pauza, M. E., Doumbia, S. O., and Pennell, C. A. (1997) Construction and characterization of human CD7-specific single-chain Fv immunotoxins. *J. Immunol.* **158,** 3259–3269.
12. Frankel, A. E., Laver, J. H., Willingham, M. C., Burns, L. J., Kersey, J. H., and Vallera, D. A. (1997) Therapy of patients with T-cell lymphomas and leukemias using an anti-CD7 monoclonal antibody ricin A chain immunotoxin. *Leuk. Lymphoma* **26,** 287–298.
13. Vallera, D. A., Burns, L. J., Frankel, A. E., Sicheneder, A. R., Gunther, R., Gajl-Peczalska, K., et al. (1996) Laboratory preparation of a deglycosylated ricin toxin A chain containing immunotoxin directed against a CD7 T lineage differentiation antigen for phase I human clinical studies involving T cell malignancies. *J. Immunol. Methods* **197,** 69–83.
14. Huston, J. S., Levinson, D., Mudgett-Hunter, M., Tai, M.-S., Novotny, J., Margolies, M. N., et al. (1988) Protein engineering of antibody binding sites: recovery of specific activity in an anti-digoxin single-chain Fv analogue produced in *Escherichia coli. Proc. Natl. Acad. Sci. USA* **85,** 5879–5883.
15. Bird, R. E., Hardman, K. D., Jacobson, J. W., Johnson, S., Kaufman, B. M., Lee, S.-M., et al. (1988) Single-chain antigen-binding proteins. *Science* **242,** 1038–1041.
16. Huston, J. S., McCartney, J., Tai, M. S., Mottola-Hartshorn, C., Jin, D., Warren, F., et al. (1993) Medical applications of single-chain antibodies. *Internat. Rev. Immunol.***10,** 195–217.
17. Huston, J. S., Mudgett-Hunter, M., Tai, M. S., McCartney, J., Warren, F., Haber, E., et al. (1991) Protein engineering of single-chain Fv analogs and fusion proteins. *Methods Enzymol.* **203,** 46–88.

18. Eldin, P., Pauza, M. E., Hieda, Y., Lin, G., Murtaugh, M. P., Pentel, P. R., et al. (1997) High-level secretion of two antibody single chain Fv fragments by *Pichia pastoris. J. Immunol. Methods* **201,** 67–75.
19. Pennell, C. A. and Eldin, P. (1998) In vitro production of recombinant antibody fragments in *Pichia pastoris. Res. Immunol.* **149,** 599–603.
20. Palker, T. J., Scearce, R. M., Hensley, L. L., Ho, W., and Haynes, B. F. (1984) Comparison of the CD7 (3A1) group of T cell workshop antibodies, in *Leukocyte Typing II, Vol. I.* (Rheinherz, E. L., ed.), Springer-Verlag, New York, pp. 303–313.
21. Amlot, P. and Cammisuli, S. (1990) CD7 monoclonal antibodies, in *Therapeutic monoclonal antibodies* (Borrebaeck, C. A. K. and Larrick, J. W., eds.), Stockton Press, New York, pp. 287–302.
22. Orlandi, R., Gussow, D. H., Jones, P. T., and Winter, G. (1989) Cloning immunoglobulin variable domains for expression by the polymerase chain reaction. *Proc. Natl. Acad. Sci. USA* **86,** 3833–3837.

3

Recombinant Fusion Toxins Directed Against the Human Granulocyte-Macrophage Colony Stimulating Factor (GM-CSF) Receptor

Yu Shao, Berta E. Warman, and John P. Perentesis

1. Introduction

1.1 Acute Myeloid Leukemia

Acute myeloid leukemia (AML) has an annual incidence of 2.4 cases per 100,000 persons and is the most common form of acute leukemia in adults ***(1,2)***. AML is a model for drug-resistant human cancers, and current therapies for AML possess a narrow therapeutic margin. The use of high-dose and intensive chemotherapy regimens produces remission in the majority of patients with AML; however, most cases subsequently relapse and eventually succumb to chemotherapy-refractory disease ***(3,4)***. Attempts to further increase chemotherapy dose intensity in AML treatment regimens often result in an increased incidence of therapy-related morbidity and mortality.

1.2. Chemotherapy Drug Resistance in AML

Multiple mechanisms contribute to the emergence of drug-resistance in AML and include the multidrug-resistance (MDR) phenotype and resistance to chemotherapy-induced apoptotic cell death. The MDR phenotype results from overexpression of members of the family of energy-dependent ABC transmembrane transporter pumps. It is characterized by the efflux of multiple hydrophobic cytotoxins, including the anthracyclines, epipodophyllotoxins, vinca alkaloids, and others, with disparate mechanisms of action ***(5–7)***. In AML, the MDR phenotype can be generated in vitro by overexpresson of the *MDR1* and the *MRP* genes, which encode P-glycoprotein (P-gp) and the multidrug resistance protein, respectively ***(8–12)***. P-gp expression in AML blasts from patients

From: *Methods in Molecular Biology, vol. 166: Immunotoxin Methods and Protocols*
Edited by: W. A. Hall © Humana Press Inc., Totowa, NJ

has been associated with poor outcomes, including higher rates of refractory disease in newly diagnosed patients, shorter remission duration, and increased frequency of relapse ***(13–19)***. A superior response to chemotherapy and survival have been observed in AML patients whose blasts possess inversion in chromosome 16 that deletes the *MRP* gene ***(20)***, though other mechanisms may also contribute to this favorable outcome ***(21)***. Overexpression of *MRP* alone does not appear to be a major cause of *de novo* drug resistance in most other newly diagnosed patients ***(22,23)***, although increased expression has been observed in cases of relapsed AML ***(24,25)***. Overexpression of another gene isolated from MDR cell lines, the lung resistance protein (*LRP*) gene, has also been associated with poor outcome in some studies ***(26,27)***.

Failure to activate apoptotic cell death mechanisms after chemotherapy-induced genotoxic damage may be another important factor contributing to chemotherapy drug resistance in AML ***(28,29)***. Apoptosis is the result of activation of a downstream pathway mediating leukemic blast cell death resulting from DNA and cellular damage from chemotherapy. Ionizing radiation and chemotherapeutic drugs have been shown to inflict cellular damage, including cytochrome c release ***(30–32)***, that activates caspases ***(33,34)*** leading to the apoptotic cell death of leukemia cells. The p53 tumor suppressor protein appears to play a central role in cellular detection of DNA damage, activation of cell cycle arrest pathways, and the induction of apoptosis ***(35,36)***. Inactivation of p53 and defective induction of apoptosis have been associated with treatment resistance and relapse ***(37)***. Leukemias with *p53* mutations are associated with a poor response to therapy and short survival ***(38,39)***. Similarly, expression of the antiapoptotic *BCL-2* gene has been associated with refractory disease and relapse in AML ***(40–42)***.

Immunotoxins and recombinant fusion toxins target catalytic protein toxins to malignant cells with high specificity. These catalytic protein toxins generally possess a unique mechanism of action and are not substrates for MDR transmembrane pumps. They also may overcome resistance to apoptosis and exhibit considerable potential for treating drug-resistant cancers ***(43–47)***. We have demonstrated that a targeted catalytic toxin can be the basis of an effective strategy to treat drug-resistant myeloid leukemia cells ***(48–51)***.

1.3. Growth Factor Receptor-Targeted Toxins for AML Therapy

The aberrant expression of hematopoietic growth factors, including granulocyte-macrophage colony-stimulating factor (GM-CSF) and its high-affinity receptor, have been postulated to play central roles in AML leukemogenesis ***(52–55)***. GM-CSF receptor expression has been identified on the leukemic blasts from the majority of patients with AML ***(56–59)***. In in vitro assays, GM-CSF has been observed to be the major growth factor responsible for the

direct autonomous growth of AML blasts ***(60,61)***. Autonomous growth related to GM-CSF autocrine or paracrine production and secretion has been identified in blast samples from a majority of patients with AML ***(62)*** and has been associated with therapy-refractory disease and inferior survival ***(63,64)***. Dysregulated autocrine growth factor pathways have been similarly observed in a variety of other human cancers.

The entry into the cytoplasm of a single molecule of diphtheria toxin (DT) is lethal to mammalian cells as a consequence of the catalytic inactivation of protein synthesis ***(65)***. DT catalyzes the ADP ribosylation and inactivation of protein synthesis elongation factor 2 (EF-2) at a specific posttranslationally modified histidine residue known as diphthamide ***(66)***. EF-2 is an essential GTPase that is required for the translocation of ribosome along RNA during protein synthesis. The ADP ribosylation of EF-2 by DT is irreversible under physiologic conditions.

There are several potential advantages to using genetically engineered DT in targeted therapies for drug-resistant human cancers. Cytotoxicity mediated through protein synthesis inhibition may serve as an efficient and complementary mechanism for cell killing when used in conjunction with other conventional chemotherapies that generally act by inflicting DNA damage. In addition, structure–function relationships of DT have been well elucidated through molecular, genetic, biochemical, and X-ray crystallographic analyses, allowing for rational drug design using genetic engineering. These studies have revealed that DT possesses functionally distinct structural domains corresponding to (a) a region of ADP ribosyltransferase catalytic activity (C domain), (b) a region of membrane translocation activity (T domain), and (c) a unique receptor-binding moiety (R domain) ***(66)***.

Successful genetic engineering of DT to target human malignancies expressing high-affinity cytokine and growth factor receptors in vivo was first conducted by Murphy and coworkers ***(67–72)***. Their prototype recombinant DT–interleukin-2 fusion toxin (DAB_{486}IL-2) was shown to specifically bind only to cells expressing the high-affinity receptor for interleukin-2 (IL-2) with subsequent induction of rapid receptor-mediated endocytosis and cell killing by protein synthesis inhibition. The DT–IL-2 recombinant fusion toxin has been refined to reduce molecular size and susceptibility to proteolysis. The IL-2 domain has also been effectively substituted with other ligands, resulting in the efficient and specific targeting of cytokine and growth hormone receptors found on other human malignancies ***(73–76)***. The design, production, and clinical use of DAB_{486}IL-2 and its successor, DAB_{389}IL-2, have served as a paradigm for the development of other DT-based recombinant fusion toxins.

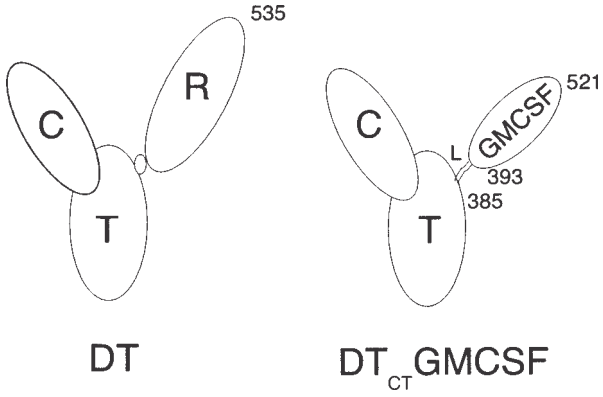

Fig. 1. The structural organization of diphtheria toxin (DT) and comparison to the recombinant fusion toxin DT_{CT}GMCSF.

Employing the solved crystal structure of DT *(77,78)* and GM-CSF *(79,80)*, we have used genetic engineering to construct a novel fusion toxin, DT_{CT}GMCSF, to redirect the lethal action of DT to the high-affinity GM-CSF-receptor found on AML blasts (*see* **Note 1**). In DT_{CT}GMCSF, the C and T domains of DT are preserved, but the native receptor-binding domain of DT that mediates its indiscriminate binding to human cells is genetically replaced with human GM-CSF (**Fig. 1**). The construction of the expression vector pET11d:DT_{CT}GMCSF was accomplished as outlined in **Fig. 2**. The coding sequence of mature human GM-CSF was contained in a 392-bp *Nco*I–*Bam*HI DNA fragment that was cloned between the *Nco*I and *Bam*HI sites of plasmid pET11d downstream of the T7 promoter to produce pET11d:GMCSF. In parallel, the gene encoding the DT fragment A was engineered by PCR mutagenesis to obtain an *Nco*I gene cassette that encoded 385 amino-terminal residues of DT, including the entire C domain and the contiguous proximal portion of the T domain. The C and T domain gene cassette (DT_{CT}) was fused to the gene that encodes the mature form of GM-CSF. This gene fusion lacks the entire coding sequence for the native DT binding domain. To ensure that the N-terminal helices of GM-CSF would be available for participation in high-affinity receptor binding, a synthetic DNA sequence encoding a short Ser-$(Gly)_4$-Ser-Met intervening linker was inserted at a DT hinge site separating DT and GM-CSF. Production of DT_{CT}GMCSF was achieved through high-efficiency expression in *E. coli* followed by serial purification through antidiphtheria toxin affinity chromatography, anion exchange chromatography, and extensive dialysis (*see* **Fig. 3**).

The methods and procedures described in this chapter describe the rationale, design, and production of the DT_{CT}GMCSF fusion toxin. This conceptual

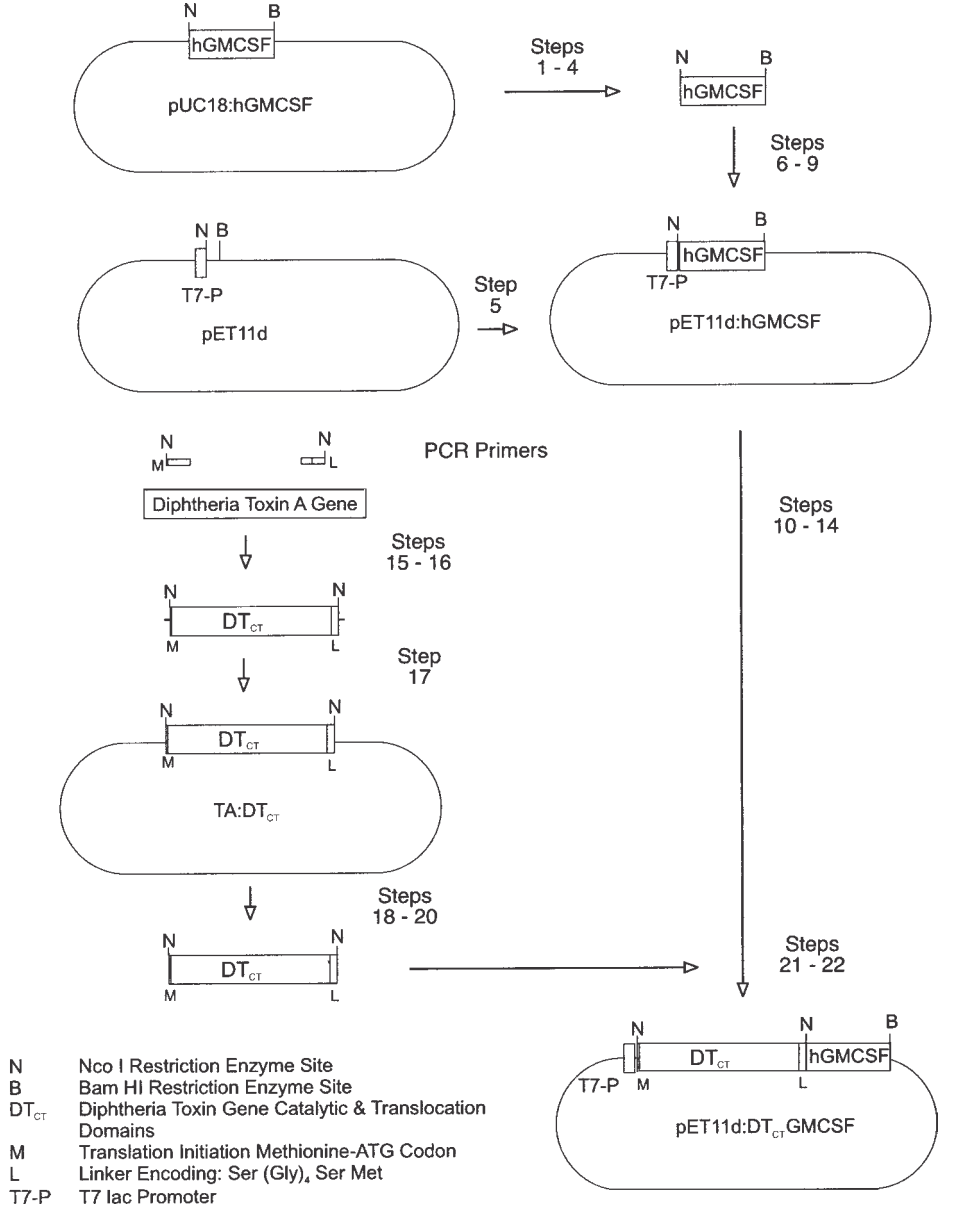

Fig. 2. DNA cloning methods for the production of the recombinant fusion toxin DT_{CT}GMCSF. Steps as noted in **Subheading 3.1.**

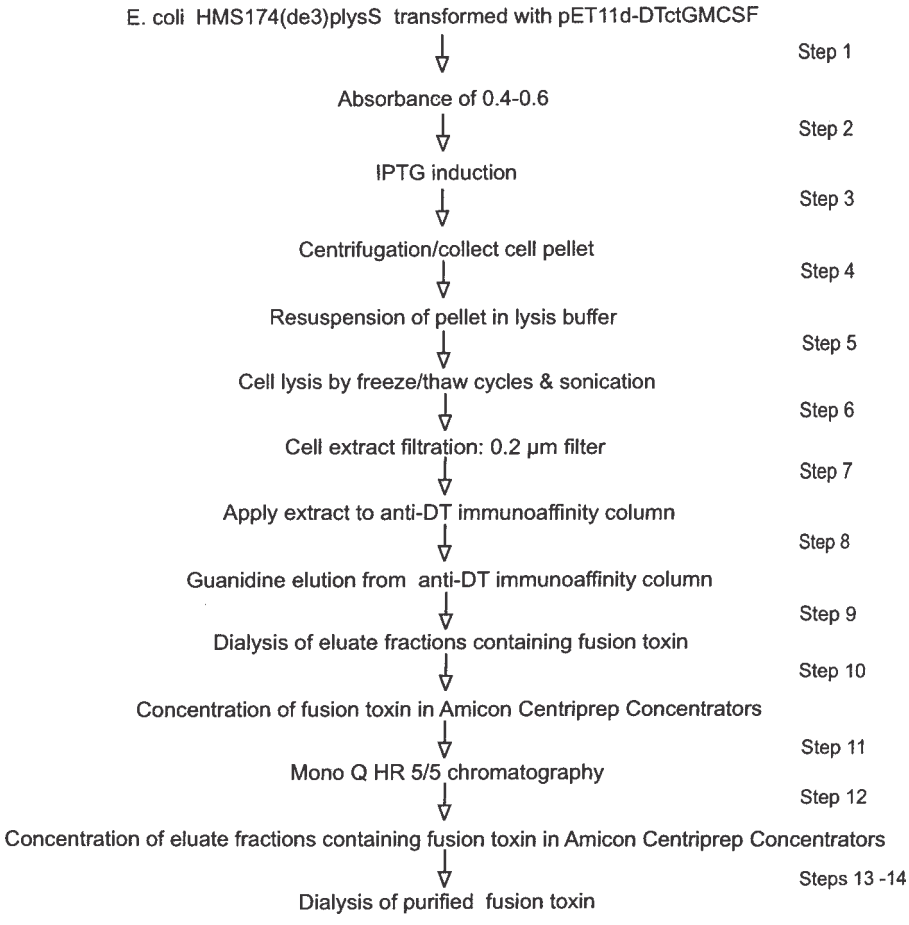

Fig. 3. Expression and purification methods for $DT_{CT}GMCSF$. Steps as noted in **Subheading 3.2.2.**

approach can be applied generally to the construction of fusion toxins incorporating other ligands or toxins (*see* **Note 2**).

2. Materials

2.1. Nucleic Acids and DNA Cloning

1. Oligonucleotide primers are synthesized with an Applied Biosystems 394 DNA synthesizer or equivalent.
2. Synthetic cDNA encoding human GM-CSF using *E. coli* codon preferences (R & D Systems, Minneapolis, MN) (*see* **Note 3**).
3. PCR mutagenesis 5' primer (5'-GCCATGGGCGCTGATGATGTTGTTGATTC-3'), and 3' primer (5'-GCCATGGAGCCACCTCCACCCGATTTATGCCCCGGA GAATACGC-3').

4. *E. coli* cloning strain BL21, cloning vector pET11d (Novagen, Madison, WI)
5. Wizard DNA purification resin (Promega, Madison, WI).
6. CircumVent thermal cycling reagents (New England Biolabs, Beverly, MA).
7. Restriction endonucleases, *Taq* DNA polymerase, and T4 DNA ligase can be procured from BRL-Life Technologies (Gaithersburg, MD), Promega, New England Biolabs, or Perkin-Elmer (Norwalk, CT).
8. Low melting point agarose (Life Technologies, Grand Island, NY).
9. TA cloning kit (Invitrogen, Carlsbad, CA).
10. Speed-Vac (Savant, Farmingdale, NY).

2.2. Production of the Recombinant Fusion Toxin

1. *E. coli* HMS174(de3)plysS (Novagen, Madison, WI).
2. Luria-Bertani (LB) broth, carbenicillin, and isopropyl-β-D-thiogalactopyranoside (IPTG) (Life Technologies, Grand Island, NY).
3. Potassium phosphate, EDTA, sodium chloride, Tris-HCl, Tween 20, guanidine hydrochloride (Sigma, St. Louis, MO).
4. Sonifier 250 (VWR Scientific, Philadelphia, PA).
5. 0.2 μm Amicon filter, 30 kD Amicon exclusion filter (Millipore, Bedford, MA).
6. 12 kD exclusion-dialysis tubing (Sigma, St. Louis, MO).
7. Microprotein assay kit (Bio-Rad Laboratories, Hercules, CA).
8. Mono Q HR 5/5 chromatography column (Pharmacia, Piscataway, NJ).
9. Affinica antibody orientation kit (Schleicher and Schuell, Keene, NH).

2.3. Biochemical Characterization of the Recombinant Fusion Toxin

1. SDS-PAGE peptide electrophoresis kit, including complete reagent system for the separation of proteins (10–20% Tris-Tricine Ready Gel with premixed running and sample buffers, and prestained Kaleidoscope molecular weight SDS-PAGE standards) (Biorad Laboratories, Hercules, CA).
2. SDS-PAGE Mini-Protean II gel electrophoresis apparatus and Mini Trans-Blot Electrophoretic Transfer Cell blot transfer equipment, Coomassie brilliant blue R-250, 0.5-micron nitrocellulose membranes, and premixed running buffers (Biorad Laboratories, Hercules, CA).
3. Goat antihuman GM-CSF antibodies and human GM-CSF (R & D Systems, Minneapolis, MN).
4. Horseradish peroxidase conjugated rabbit antigoat antibodies (Calbiochem, La Jolla, CA).
5. Diphtheria toxin, Tris-HCl, dithiothreitol, EDTA, trichloracetic acid (Sigma, St. Louis, MO).
6. Reticulocyte lysate (Promega, Madison, WI).
7. (Adenylate-^{32}P)NAD^{+}(Dupont-NEN, Boston, MA).
8. Vacuum filter/microfiltration units (25 mm) (Fisher Scientific, Hanover Park, IL).
9. Econo-Safe liquid scintillation fluid or equivalent (RPI, Mount Prospect, FL).

2.4. Characterization of the In Vitro Activity of the Fusion Toxin

2.4.1. Leukemia Cell Lines and Culture Supplies

1. Human acute promyelocytic leukemia cell line HL-60, monocytic leukemia cell line THP-1, mixed lineage leukemia cell line MV4–11, mixed lineage acute leukemia cell line RS4;11, leukemia cell line K562, and pre-B leukemia cell line NALM-6 (American Type Culture Collection, Rockville, MD).
2. Roswell Park Memorial Institute (RPMI) culture medium, fetal bovine serum, bovine serum albumin (BSA), aqueous streptomycin, aqueous penicillin (Life Technologies, Grand Island, NY).
3. Human GM-CSF (R & D Systems, Minneapolis, MN).
4. 2-Mercaptoethanol (Sigma, St. Louis, MO).

2.4.2. Cytotoxicity Assays

1. 96-well V-bottom and 96-well flat-bottom microtiter plates (Fisher Scientific, Hanover Park, IL).
2. Modified Eagle Medium (MEM) ^{3}H-leucine (L-[4,5-^{3}H]) (DuPont-NEN, Boston, MA).
3. KOH, PBS, isobutanol, SDS, and trichloroacetic acid (Sigma, St. Louis, MO).
4. Cell harvester (Cambridge Technology Inc.).
5. Beckman LS7000 scintillation counter or equivalent.
6. 3-(4,5-dimethylthiazol-2-yl)-2,5-diphenyltetrazolium bromide (MTT) assay kit.
7. Bio-Rad ELISA reader or equivalent.

2.5. GM-CSF Receptor α-Chain Expression Assay

1. Micro-FastTrack mRNA isolation kit (Invitrogen, San Diego, CA).
2. Internal primer set for the human GM-CSF receptor α-chain (5' primer: 5'-AG AAATCGGATCTGCGAACAGTGGCACC-3'; 3' primer: 5'-TCCAGGTACG ACAGCTTCTGATAGGTCC-3') (Clontech Laboratories, Palo Alto, CA).
3. Positive control human β-actin primer sets and RT-PCR kit (Stratagene, La Jolla, CA).

3. Methods

3.1. Nucleic Acids and DNA Cloning (see also Fig. 2)

1. Use 10 U each of the restriction enzymes *Nco*I and *Bam*HI to completely digest the restriction enzyme sites in the human GM-CSF coding sequence gene cassette in plasmid pUC18. Use the reaction buffer supplied with the enzymes in a total reaction volume of 100 µL with a 2 h incubation at 37°C. Stop the reaction and precipitate the DNA by placing on ice and adding 0.1 vol of 10 *M* ammonium acetate and 2.5 vol of 95% ethanol. Store samples until analysis at –20°C (*see* **Notes 3** and **4**).
2. Collect the precipitated DNA by centrifugation at 5000*g* at 4°C. Wash the pelleted DNA with a gentle rinse of 70% ethanol followed by a gentle rinse of 95% ethanol. Allow samples to completely air-dry or use a Speed-Vac.

3. Prepare a 0.8% low melting point agarose gel. Use it to analyze the efficiency of the reaction and to separate the *Nco*I–*Bam*HI *GM-CSF* gene cassette (392 bp) from its parent vector (5638 bp) by electrophoresis.
4. Excise the agarose gel fragment containing the *Nco*I–*Bam*HI *GM-CSF* gene cassette and purify using the Wizard DNA purification resin. Store the DNA at 4°C.
5. Use 10 U each of the restriction enzymes *Nco*I and *Bam*HI to completely digest the pET11d vector restriction enzyme sites with a 2 h incubation at 37°C. Stop the reaction and precipitate the DNA as outlined above (*see* **Note 5**).
6. Ligate 1 μg of the purified *Nco*I–*Bam*HI *GM-CSF* gene cassette into 250 ng of the *Nco*I–*Bam*HI linearized pET11d cloning vector to produce the pET11d:GMCSF vector. Incubate with 1–2 U of T4 DNA ligase at 16°C for 16 h in a total reaction volume of 10 μL containing 50 m*M* Tris-HCl (pH 7.6), 10 m*M* $MgCl_2$, 1 m*M* ATP, 1 m*M* DTT, 5% (w/v) polyethylene glycol-8000.
7. Transform the ligation mix into competent *E. coli* BL21.
8. Extract and purify plasmid DNA from candidate pET11d:GMCSF clones using the Wizard DNA purification resin mini-prep kit.
9. Identify clones with the successful insertion of the *GM-CSF* gene cassette into plasmid pET11d by incubation of DNA from candidate pET11d:GMCSF clones with 10 U each of the restriction enzymes *Bam*HI and *Nco*I. Stop the reaction and precipitate the DNA as outlined above. Analyze clones by electrophoresis on an 0.8% agarose gel.
10. Use 10 U of *Nco*I to digest and linearize the pET11d:GMCSF vector by conducting the incubation at 37°C for 2 h.
11. Analyze the efficiency of the *Nco*I digestion on a 0.8% low melting point agarose gel to identify optimal yield and separation of the *Nco*I single-cut linearized pET11d:GMCSF vector
12. Dephosphorylate the 5'-phosphorylated termini of the *Nco*I-linearized pET11d:GMCSF vector by treating for 10 min at 37°C with calf intestinal alkaline phosphatase, followed by heat inactivation at 75°C for 10 min. Precipitate the DNA as outlined above.
13. Separate the *Nco*I single-cut, linearized pET11d:GMCSF vector from the uncut (i.e., supercoiled and nicked-circle) forms of the parent vector by electrophoresis on an 0.8% low melting point agarose gel. Include a sample of the parent pET11d:GMCSF vector that had not been treated with restriction enzymes as a control to identify supercoiled and nicked-circle forms of the vector.
14. Excise the *Nco*I single cut linearized pET11d:GMCSF vector from the agarose and purify using the Wizard DNA purification resin.
15. PCR is employed for mutagenesis of the DT fragment *A* gene to provide coding sequences for a translation initiation ATG codon, a 7-residue linker segment for fusion with the *GM-CSF* gene, and convenient flanking *Nco*I restriction enzyme sites for cloning. This engineered fragment of the *DT* gene is termed "DT_{CT}" because it contains the DT catalytic and translocation domains. PCR mutagenesis primers include a 5' primer (5'-GCCATGGGCGCTGATGATGTTGTTGATTC-3')

introducing an *Nco*I restriction enzyme site and ATG codon, and a 3' primer (5'-GCCATGGAGCCACCTCCACCCGATTTATGCCCCGGAGAATACGC-3') that incorporates sequences encoding a linker domain for steric spacing of the *GM-CSF* gene and an *Nco*I restriction enzyme site. PCR mutagenesis reactions of the DT fragment A gene contains 150 nmole of each primer, 0.1 m*M* deoxynucleotide triphosphates, 2.5 U of *Taq* polymerase, 20 m*M* Tris-HCl (pH 8.4), 150 m*M* NaCl, 50 m*M* KCl, and 2 m*M* $MgCl_2$ in a 50 μL total reaction. PCR amplification conditions include 35 cycles of 1 min at 95°C, 1 min at 60°C, and 1 min at 72°C, with a final extension step of 10 min at 72°C (*see* **Note 3**).

16. Analyze the yield and fidelity of a 10 μL aliquot of the PCR-mutagenized DT_{CT} reaction on 0.8% agarose gel.
17. Ligate and clone the PCR-mutagenized DT_{CT} reaction samples into the TA vector using the TA cloning kit to produce the vector TA–DT_{CT}. Use the cloning techniques, plasmid DNA isolation, restriction enzyme digestion, and gel analysis methods described above to identify clones with successful insertion of the DT_{CT} gene cassette into the TA vector.
18. Use 10 U of *Nco*I to completely digest the TA–DT_{CT} vector with a 2 h incubation at 37°C. Stop the reaction and precipitate the DNA as previously outlined.
19. Prepare a 0.8% low melting point agarose gel. Use it to separate the *Nco*I DT_{CT} gene cassette (1182 bp) from the TA vector (3.9 kbp) by electrophoresis.
20. Excise the *Nco*I DT_{CT} gene cassette from the agarose and purify using the Wizard DNA purification resin.
21. Construct the expression plasmid pET11d:DT_{CT}GMCSF by cloning the intact DAB *Nco*I gene cassette into the *Nco*I site of pET11d:GMCSF. Use the cloning techniques, plasmid DNA isolation, restriction enzyme digestion, and gel analysis methods described above to identify clones with successful insertion of the DT_{CT} gene cassette into the pET11d:GMCSF vector.
22. DNA sequencing of the DT_{CT}GMCSF insert (1576 bp) should be conducted on candidate pET11d:DT_{CT}GMCSF plasmid clones to insure correct orientation of the insert fragments and fidelity of sequence. Use the AmpliCycle sequencing kit with the reaction conditions specified by the manufacturer.

3.2. Production of the Recombinant Fusion Toxin

3.2.1. Construction of Antidiphtheria Toxin Immunoaffinity Column

1. Polyvalent anti-DT antibodies are prepared in goats by Bethyl Laboratories (Montgomery, TX) using diphtheria-tetanus toxoid (Wyeth-Ayerst Laboratories, Philadelphia, PA) or diphtheria toxoid purified pool (Connaught, Swiftwater, PA) as the immunizing antigen. Optimal antibody titer is generally obtained after two immunizations.
2. The immunoaffinity column is prepared with the Affinica antibody orientation kit using goat diphtheria antitoxin and following the instructions provided by the manufacturer.

3.2.2. Expression and Purification of the Recombinant Fusion Toxin (see also ***Fig. 3***)

All manipulations of *E. coli* bearing intact recombinant fusion toxin were performed under modified biosafety level 3 (BL3) containment practices.

1. *E. coli* HMS174(de3)plysS is transformed with pET11d:DT_{CT}GMCSF and grown at 37°C in 1 L LB medium with carbenicillin (50 μg/mL) to an absorbance (600Å) of 0.4–0.6 OD.
2. Expression of the fusion gene is induced by the addition of IPTG to a final concentration of 0.5 m*M* with 1 h of induction (*see* **Note 6**).
3. The bacterial cells are collected by centrifugation at 500*g*.
4. The cell pellet is resuspended in 50 m*M* potassium phosphate, 10 m*M* EDTA, 750 m*M* NaCl, and 0.1% Tween 20 (pH 8.0) in 20 mL vol.
5. Lysis of the cells is achieved by freezing in a dry ice/ethanol bath followed by thawing and sonication. Optimal methods for sonication using a Sonifer 250 include a constant cycle setting with two 1 min sonication pulses separated by 1 min. Sonication is conducted in a 50 mL conical tube on ice. This procedure may require optimization if other sonication equipment is employed (*see* **Note 7**).
6. The soluble extract is filtered through a 0.2 μm filter.
7. The soluble extract is applied to a 20 mL antidiphtheria toxin immunoaffinity column prepared as previously outlined. After loading of the soluble extract, the column is washed with 5 vol of PBS solution.
8. Bound proteins are eluted from the immunoaffinity column with 4 *M* guanidine hydrochloride, 100 m*M* potassium phosphate, and 0.1% Tween 20 (pH 7.2).
9. Eluate fractions containing the fusion toxin (approx 25 mL) are dialyzed exhaustively using 12 kD exclusion dialysis tubing in 2 L of 20 m*M* Tris-HCl and 150 m*M* NaCl (pH 7.5) with 5 buffer changes over 18 h.
10. The dialyzed fusion toxin is concentrated 8–10-fold using 30 kD Amicon exclusion filters in Amicon centriprep concentrators.
11. The dialyzed and concentrated fusion toxin is applied onto a Mono Q HR 5/5 chromatography column and eluted at a flow rate of 1 mL/min over 35 min with a linear gradient of NaCl (150–500 m*M* in 20 m*M* Tris-HCl [pH 7.5]).
12. The purified and dialyzed fusion toxin is concentrated 10–20-fold in a 30 kD Amicon exclusion filter in Amicon centriprep concentrators.
13. The concentrated fusion toxin is dialyzed in 2 L PBS with 5 buffer changes over 18 h.
14. Protein concentration is determined by the Bio-Rad protein assay. Approximately 1–10 μg of purified DT_{CT}GMCSF protein can be obtained from 100 mL pilot cultures (*see* **Note 8**).

3.3. Biochemical Characterization of Recombinant DT_{CT}GMCSF

3.3.1. PAGE and Western Blot Analyses

1. SDS-PAGE analysis of the purified fusion toxin is conducted using a 10–20% Tris-Tricine Ready Gel in a Mini-Protean II gel apparatus. The electrophoresis is

run at 200 V for 45 min. This procedure is useful in monitoring each step of fusion toxin production and purification.

2. Each gel lane should be loaded with approx 10–15 μg of the fusion toxin preparation; control lanes with native human GM-CSF and DT should also be employed.
3. Three identical SDS-PAGE gels should be prepared—one gel employed for SDS-PAGE electrophoresis and staining with Coomassie brilliant blue R-250 (to identify and analyze total proteins and relative purification of the fusion toxin), and two sister gels employed for SDS-PAGE electrophoresis and subsequent Western protein immunoblotting (to analyze GM-CSF and DT immunoreactive proteins).
4. For western protein immunoblotting, electrophoretic blotting of the Ready Gel to 0.45 micron nitrocellulose membranes is conducted in a Mini Trans-Blot cell with cooling by the self-contained Bio-Ice unit. The electrophoresis transfer is run at 100 V for 60 min.
5. The transferred Western protein immunoblot membranes are incubated in 50 mL of 1% milk for 30 min at 37°C, then incubated with primary antibodies at a dilution of 1:5000 (the GM-CSF immunoblot is incubated with goat antihuman GM-CSF, and the DT immunoblot is incubated with goat anti-DT). The primary antibody incubation is conducted for 30 min at room temperature.
6. The membranes are washed three times at room temperature with 1% milk/0.1% Tween 20.
7. The membranes are then incubated in 50 mL of 1% milk with secondary antibodies (rabbit antigoat covalently linked to horseradish peroxidase) at a 1:10,000 dilution.
8. The membranes are washed three times at room temperature with 1% milk/0.1% Tween 20.
9. Suspend the membranes in 50 mL of PBS buffer and 10 mg of DAB (3,3'-diamionbenzidine) followed by 250 μL of hydrogen peroxide.
10. The reaction is stopped at optimal development by washing the membranes three times with 50–100 mL of cold water. Excessive reaction times result in high nonspecific background staining.

3.3.2. Measurement of ADP Ribosyltransferase Catalytic Activity

1. ADP ribosyltransferase catalytic activity of the recombinant toxin is determined by measuring fusion toxin incorporation of (adenylate-^{32}P)NAD$^+$ into the EF-2 of reticulocyte lysates and comparison of activity with a reference standard of native diphtheria toxin.
2. Approximately 300 ng of DT_{CT}GMCSF is incubated at 37°C in a reaction mixture containing 20 m*M* Tris-HCl (pH 7.5), 50 m*M* dithiothreitol, 1 m*M* EDTA, and 2.5 μ*M* (adenylate-^{32}P)NAD$^+$ (approx 1×10^6 cpm).
3. Reference reactions with standard amounts of native DT containing 200 ng of nicked DT is incubated at 37°C for 15 min in a 50 μL reaction mixture containing 20 m*M* Tris-HCl (pH 7.5), 50 m*M* dithiothreitol, 1 m*M* EDTA, and 2.5 μ*M* (adenylate-^{32}P)NAD$^+$ (approx 1×10^6 cpm).
4. The reaction is terminated by adding 50 μL of 20% cold trichloroacetic acid.

5. The insoluble protein is collected by vacuum filtration onto 0.45 micron nitrocellulose filters and rinsed twice with 5% cold trichloroacetic acid.
6. The filters are dried and placed in scintillation counter vials, and approx 1 mL of 95% Econo-Safe scintillation fluid is added.
7. Radioisotope incorporation into protein is measured in a Beckman LS7000 scintillation counter.

3.4. Characterization of the In Vitro Activity of Fusion Toxin

3.4.1. Cell Lines and Culture Conditions

1. GM-CSF receptor-bearing human leukemia cell lines useful for analysis include the human acute promyelocytic leukemia cell line HL-60 and the human monocytic leukemia cell line THP-1.
2. A GM-CSF receptor-negative control leukemia cell line suitable for study is K562.
3. HL-60 cells can be maintained in IMDM, 10% fetal bovine serum and 50 U/mL penicillin, and 50 μg/mL streptomycin.
4. THP-1 and K562 cells were maintained in RPMI medium, 10% fetal bovine serum, 50 U/mL penicillin, 50 μg/mL streptomycin, and 5×10^{-5}M 2-mercaptoethanol (for THP-1 cells only).

3.4.2. Cytotoxicity Assays

1. Seed 1×10^5 cells/well into 96-well V-bottom microtiter plates containing leucine-free RPMI medium.
2. Add DT or DT_{CT}GMCSF at a range of concentrations, including 0.01 ng/mL, 0.05 ng/mL, 0.1 ng/mL, 0.5 ng/mL, 1.0 ng/mL, 5.0 ng/mL, 10 ng/mL, and 50 ng/mL. A no-toxin control should also be assayed. Each reaction should be conducted in triplicate and incubated at 37°C for 48 h. Experiments should be repeated on at least three separate occasions.
3. MEM ^{3}H-leucine (L-[4,5–^{3}H]) is then added to a final concentration of 1 μCi/well with a 4 h pulse incubation.
4. Cells are then lysed with 40 μL of 6 *M* KOH and the insoluble protein is precipitated with 70 μL of 20% trichloroacetic acid.
5. A PH.D. cell harvester is used to collect the insoluble protein on glass fiber filters.
6. The filters are dried and placed in Econo-Safe scintillation fluid in scintillation counter vials.
7. Radioisotope incorporation into protein is measured in a Beckman LS7000 scintillation counter.
8. The percentage protein synthesis inhibition can be calculated by subtraction of the background incorporation and subsequent comparison of maximal incorporation (in the no-toxin control sample) with measured incorporation at each DT and DT_{CT}GMCSF experimental point.
9. Cytotoxicity can also be measured by MTT assays. For MTT assays, cells are seeded into 96-well flat-bottom microtiter plates at a final concentration of 5×10^4

cells/well and incubated at 37°C in a humidified incubator under a 5% CO_2 atmosphere for 16–24 h.

10. Dilutions of the DT_{CT}GMCSF fusion toxin in PBS with 1% BSA (*see* concentrations in **step 2**) or dilutions (e.g., 0.01 ng/mL, 0.05 ng/mL, 0.1 ng/mL, 0.5 ng/mL, 1.0 ng/mL, 5.0 ng/mL, 10 ng/mL, and 50 ng/mL) of vincristine in PBS/0.2% BSA or doxorubicin in PBS/0.2% normal saline are added to each well, and the incubation is continued for an additional 72–96 h. Each reaction should be conducted in triplicate and experiments should be repeated on at least three separate occasions.
11. MTT is then added to a final concentration of 0.75 mg/mL with 4 h of further incubation at 37°C.
12. The dye is then solubilized with 50% isobutanol/10% SDS.
13. Cell viability is determined by measure of absorption (595Å) using a Bio-Rad ELISA reader.
14. The cytotoxicity can be calculated by subtraction of the background absorption and subsequent comparison of maximal absorption (in the no-toxin control sample) with measured absorption at each DT_{CT}GMCSF and chemotherapy experimental point (*see* **Note 9**).

3.5. GM-CSF Receptor α-Chain Expression Assay

1. Individual leukemia cell lines for testing should be analyzed for GM-CSF receptor α-chain expression by the use of reverse-transcriptase PCR methodology to produce cellular cDNA, followed by the use of gene-specific oligonucleotide primers for amplification and analysis of receptor expression.
2. Poly(A)$^+$ RNA should be isolated directly from approx 10^5 cells after detergent lysis with an oligo(dT) cellulose-affinity resin using the Micro-FastTrack mRNA isolation kit.
3. Approximately 100 ng of poly(A)$^+$ RNA should be used with random hexamer oligonucleotide primers and Moloney murine leukemia virus reverse transcriptase for first strand cDNA synthesis.
4. An internal primer set for the human GM-CSF receptor α-chain obtained from Clontech Laboratories was used to amplify a 682-bp PCR fragment between nucleotides 69 and 749 of the receptor cDNA coding sequence.
5. PCR reactions for amplification of human GM-CSF receptor α-chain contain 150 nmol of each primer, 0.1 m*M* deoxynucleotide triphosphates, 2.5 U of *Taq* polymerase, 20 m*M* Tris-HCl (pH 8.4), 150 m*M* NaCl, 50 m*M* KCl, and 2 m*M* $MgCl_2$ in a 50 μL reaction. PCR amplification conditions include 35 cycles of 1 min at 95°C, 1 min at 60°C, and 1 min at 72°C, with a final extension step of 10 min at 72°C.
6. Control experiments should be conducted with each set of PCR amplification experiments and include positive controls using human β-actin primer sets and negative controls lacking template DNA.
7. PCR reactions for amplification of human β-actin contain 150 nmol of each primer, 0.1 m*M* deoxynucleotide triphosphates, 2.5 U of *Taq* polymerase, 20 m*M*

Tris-HCl (pH 8.4), 150 m*M* NaCl, 50 m*M* KCl, and 2 m*M* $MgCl_2$ in a 50 µL reaction. PCR amplification conditions include 35 cycles of 1 min at 95°C, 1 min at 60°C, and 1 min at 72°C, with a final extension step of 10 min at 72°C.

4. Notes

1. Biochemical, genetic, and X-ray crystallographic analyses have yielded important information regarding structure–function relationships in DT, and have provided the basis for the rational drug design of DT_{CT}GMCSF. These principles can be applied to the design and production of other DT-based fusion toxins incorporating other ligands. The DT structure contains three separate regions including:
   a. An amino-terminal domain that contains the ADP-ribosyltransferase catalytic site ("C" domain),
   b. A domain found in the middle of the toxin that facilitates the transmembrane translocation ("T" domain) of the C domain across membranes, and
   c. A carboxyl-terminal domain that mediates receptor binding ("R" domain) and results in receptor-mediated endocytosis.

   Of particular relevance to the construction of recombinant fusion toxins, these studies have identified a small "flexible" peptide loop that separates the receptor-binding domain from the catalytic and transmembrane domains of DT. This flexible loop is located in amino acid residues 380–386 and permits the entire 15-kDa receptor-binding domain to rotate as a unit by 180°, with atomic movement of up to 65 Å. Our studies suggest that genetically engineered ligand fusions with the DT catalytic and translocation domains in the region of this natural flexible loop provides improved recombinant fusion-toxin binding and production. We have also included a synthetic DNA sequence encoding a short Ser-$(Gly)_4$-Ser-Met intervening linker inserted at the DT hinge site separating the DT and GM-CSF moieties to ensure that the N-terminal helices of GM-CSF would be available for participation in high-affinity receptor binding. It would be reasonable to consider the incorporation of this linker in fusion-toxin constructions with other ligands.
2. Studies of the crystal structure of GM-CSF reveal that it is a member of the four-helix bundle family of cytokines and defined critical domains that are essential for high-affinity binding to its receptor, which is preserved in the construction of DT_{CT}GMCSF. Similar considerations should be applied to the use of other ligands in the construction of recombinant fusion toxins with DT.
3. A synthetic DT_{CT} gene segment can be easily constructed by obtaining the published gene sequence (Genbank Accession K01722). This can also be obtained from the National Center for Biotechnology Information website at www.ncbi.nlm.nih.gov. Construction of a synthetic DT_{CT} allows for the use of optimal codon preference for the bacterial expression host (e.g., *E. coli* in the experiments outlined in this chapter). The use of optimal codon preferences may have a potential significant advantage in augmenting expression of the fusion toxin when compared with the use of a copy of the DT fragment *A* gene using its native sequence from *Corynebacterium diphtheriae*. Similar considerations can be applied to the construction

of a synthetic human *GM-CSF* cDNA gene. The human GM-CSF cDNA sequence is also available from the National Center for Biotechnology Information website. The construction of synthetic genes with optimal codon preferences is also an important consideration in the use of other microorganisms (e.g., baculovirus) as expression hosts.

4. The reaction conditions for restriction endonuclease treatment and PCR reactions are given as a general guideline but may regard optimization for specific preparations of oligonucleotides and templates. Various PCR optimization kits are available (e.g., Stratagene, Palo Alto, CA) and can be successfully used for this purpose.
5. It may be difficult to achieve complete digestion at the *Nco*I and *Bam*HI restriction sites of the pET11d vector. This results in a high frequency of plasmid re-ligations (i.e., closure without inserts) in subsequent cloning steps and a high background transformation rate. The 5'-phosphorylated termini of the *Nco*I- and *Bam*HI-cut pET11d vector can be dephosphorylated by treating for 10 min at 37°C with calf intestinal alkaline phosphatase, followed by heat inactivation at 75°C for 10 min. Precipitate the DNA as outlined under **Subheading 3.**
6. Because the level of recombinant protein expression may vary based upon the ligand that is fused with DT, it is useful to consider ancillary methods for optimizing protein production. Different *E. coli* clones may have varying efficiency in the production of fusion toxin. High expression clones can by identified by screening a dozen 10 mL pilot cultures of independent clones of *E. coli* HMS174(de3)plysS transformed with pET11d:DT_{CT}GMCSF (or other recombinant fusion-toxin expression vector). Analysis of expression can be conducted by collection of cells by centrifugation at the end of induction and relative quantitation of protein production by Western blot as described earlier. In a similar manner, it is fruitful to compare varying fusion-toxin expression conditions by varying the IPTG induction times (e.g., 15, 30, 45, 60, 90, 120, 150 min), temperature (e.g., 24°C, 30°C, 37°C), and cell density at the time of induction (e.g., absorbance (600Å) of 0.5, 1.0, 1.5).
7. The expression of some fusion toxins is greatest in insoluble cellular fractions. In this circumstance, fusion toxin can be recovered by inclusion-body isolation and protein recovery and renaturation procedures. In their pioneering work developing fusion toxins with *Pseudomonas* exotoxin A, Pastan, FitzGerald and Kreitman ***(44,81)*** have developed and refined methods for the production and purification of fusion toxins from bacterial inclusion bodies, and these methods can also be applied to DT-based fusions ***(82)***.
8. Some fusion toxins have optimal purification with other column chromatography purification methods, or some investigators may not wish to employ an immunoaffinity chromatography step. In those circumstances, one should consider filtration of a soluble preparation of the fusion toxin (or a refolded and resolubilized inclusion-body fraction) through a 0.2 μm filter. The protein can then be loaded onto a Q-sepharose column and eluted with 0.3 *M* NaCl in 20 m*M* Tris-HCl (pH 7.8). The eluted protein is diluted five times with 20 m*M* Tris-HCl, then

loaded onto a Q-sepharose column again and eluted with a linear salt gradient from 0.06–0.4 *M* NaCl in 20 m*M* Tris-HCl (pH 7.8). Final size-exclusion purification is conducted using a TSK-gel G2000 column.

9. As a final consideration, the methods and procedures in this chapter are intended as a general guideline for the design, construction, and production of recombinant fusion toxins. While we have used GM-CSF as the ligand for these studies, alternative ligands may be appropriate for targeting autocrine cytokine pathways in other malignant disorders. Similarly, consideration should also be made for the use of protein toxins other than DT ***(43)***. The use of DT as a cytotoxic effector moiety in fusion toxins has multiple advantages as outlined above (*see* **Subheading 1.3.**). However, it has been suggested that the possible in vivo immunologic clearance of DT-based fusion toxins in the face of universal pediatric DT immunization programs is a consideration that may favor the choice of other toxins for fusion proteins. The demonstrated clinical activity of IL-2 fusion toxins with DT underscores the observation that adults apparently may not form neutralizing antibody responses to the DT moiety of fusion toxins. This is consistent with studies indicating that only approximately half of the adult population possesses DT antitoxin titers that are below protective levels ***(83,84)***. However, contemporary immunization programs for children in the United States may potentially produce high-titer anti-DT antibodies. The currently recommended series of 5–6 DT immunizations results in extremely high and effective antitoxin titers for almost all infants and children ***(83,84)***. In addition, the immunogenic CRM-197 mutant of DT is commonly employed as a carrier protein in other conjugated vaccines. For example, the new and recently licensed heptavalent pneumococcal vaccine conjugated to CRM-197 is recommended for universal administration to all U.S. children under 2 yr of age in a series of four immunizations. It is possible that individuals who have received these multiple series of highly immunogenic vaccines may form antibody titers and specificities that result in efficient clearance of DT-based fusion toxins. Clinical studies of DT-based fusions should incorporate the sequential measurement of anti-DT antibody titers and have these observations integrated with comprehensive pharmacology profiles.

References

1. Sandler, D. P. (1987) Epidemiology of acute myelogenous leukemia. *Sem. Oncol.* **14,** 359–364.
2. Kosary, C. L., Ries, L. A. G., Miller, B. A., Hankey, B. F., Edwards, B. K., eds. (1995) SEER cancer statistics review, 1973–1992: tables and graphs. Bethesda, MD: National Cancer Institute (NIH Publication No. 96-2789).
3. Rohatiner, A. and Lister, T. A. (1996) Acute myelogenous leukemia in adults, in *Leukemia, 6th ed.* (Henderson, E. S., Lister, T. A., and Greaves, M. F., eds.), Philadelphia, W. B. Saunders, pp. 479–508.
4. Löwenberg, B., Downing, J. R., and Burnett, A. (1999) Acute myeloid leukemia. *N. Engl. J. Med.* **341,** 1051–1062.

5. Löwenberg, B. and Sonneveld, P. (1998) Resistance to chemotherapy in acute leukemia. *Curr. Opin. Oncol.* **10,** 31–35.
6. Chan, H. S., DeBoer, G., Thorner, P. S., Haddad, G., Gallie, B. L., and Ling, V. (1994) Multidrug resistance. Clinical opportunities in diagnosis and circumvention. *Hematology-Oncology Clin. North Am.* **8,** 383–410.
7. Arceci, R. J. (1993) Clinical significance of P-glycoprotein in multidrug resistance malignancies. *Blood* **81,** 2215–2222.
8. Marsh, W., Sicheri, D., and Center, M. S. (1986) Isolation and characterization of adriamycin-resistant HL-60 cells which are not defective in the initial intracellular accumulation of drug. *Cancer Res.* **46,** 4053–4057.
9. Licht, T., Pastan, I., Gottesman, M., and Herrmann, F. (1994) P-glycoprotein-mediated multidrug resistance in normal and neoplastic hematopoietic cells. *Ann. Hematol.* **69,** 159–171.
10. Endicott, J. A. and Ling, V. (1989) The biochemistry of P-glycoprotein-mediated multidrug resistance. *Ann. Rev. Biochem.* **58,** 137–171.
11. Bhalla, K., Hindenburg, A., Taub, R. N., and Grant, S. (1985) Isolation and characterization of an anthracycline-resistant human leukemic cell line. *Cancer Res.* **45,** 3657–3662.
12. Cole, S. P., Bhardwaj, G., Gerlach, J. H., Mackie, J. E., Grant, C. E., Almquist, K. C., et al. (1992) Overexpression of a transporter gene in a multidrug-resistant human lung cancer cell line. *Science* **258,** 1650–1654.
13. Campos, L., Guyotat, D., Archimbaud, E., Calmard-Oriol, P., Tsuruo, T., Troncy, J., et al. (1992) Clinical significance of multidrug resistance P-glycoprotein expression on acute non-lymphoblastic leukemia cells at diagnosis. *Blood* **79,** 473–476.
14. Musto, P., Melillo, L., Lombardi, G., Matera, R., di Giorgio, G., and Carotenuto, M. (1991) High risk of early resistant relapse for leukaemic patients with presence of multidrug resistance associated P-glycoprotein positive cells in complete remission. *Br. J. Haematol.* **77,** 50–53.
15. Pirker, R., Wallner, J., Geissler, K., Linkesch, W., Haas, O. A., Bettelheim, P., et al. (1991) MDR1 gene expression and treatment outcome in acute myeloid leukemia. *J. Natl. Cancer Inst.* **83,** 708–712.
16. Marie, J. P., Zittoun, R., and Sikic, B.I. (1991) Multidrug resistance (mdr1) gene expression in adult acute leukemias: correlations with treatment outcome and in vitro drug sensitivity. *Blood* **78,** 586–592.
17. Sato, H., Gottesman, M. M., Goldstein, L. J., Pastan, I., Block, A. M., Sandberg, A. A., et al. (1990) Expression of the multidrug resistance gene in myeloid leukemias. *Leuk. Res.* **14,** 11–21.
18. Sato, H., Preisler, H., Day, R., Raza, A., Larson, R., Browman, G., Goldberg, J., et al. (1990) MDR1 transcript levels as an indication of resistant disease in acute myelogenous leukaemia. *Br. J. Haematol.* **75,** 340–345.
19. Zöchbauer, S., Gsur, A., Brunner, R., Kyrle, P. A., Lechner, K., and Pirker, R. (1994) P-glycoprotein expression as unfavorable prognostic factor in acute myeloid leukemia. *Leukemia* **8,** 974–977.

20. Kuss, B. J., Deeley, R. G., Cole, S. P. C., Willman, C. L., Kopecky, K. J., Wolman, S. R., et al. (1994) Deletion of gene for multidrug resistance in acute myeloid leukemia with inversion in chromosome 16: Prognostic implications. *Lancet* **343,** 1531–1534.
21. Zöchbauer, S., Haas, O. A., Schwarzinger, I., Lechner, K., and Pirker, R. (1994) Multidrug resistance in acute myeloid leukemia with inversion in chromosome 16 or FAB M4Eo subtype. *Lancet* **344,** 894.
22. Filipits, M., Suchomel, R. W., Zöchbauer, S., Brunner, R., Lechner, K., and Pirker, R. (1997) Multidrug resistance-associated protein (MRP) in acute myeloid leukemia: No impact on treatment outcome. *Clin. Cancer Res.* **3,** 1419–1425.
23. Leith, C. P., Kopecky, K. J., Chen, I-.M., Eijdems, L., Slovak, M. L., McConnell, T. S., et al. (1999) Frequency and clinical significance of the expression of the multidrug resistance proteins MDR1/P-glycoprotein, MRP1, and LRP in acute myeloid leukemia. A Southwest Oncology Group study. *Blood* **94,** 1086–1099.
24. Schneider, E., Cowan, K. H., Bader, H., Toomey, S., Schwartz, G. N., Karp, J. E., et al. (1995) Increased expression of the multidrug resistance-associated protein gene in relapsed acute leukemia. *Blood* **85,** 186–192.
25. Slapak, C. A., Mizunuma, N., and Kufe, D. W. (1994) Expression of the multidrug resistance associated protein and P-glycoprotein in doxorubicin-selected human myeloid leukemia cells. *Blood* **84,** 3113- 3121.
26. Filipits, M., Pohl, G., Stranzl, T., Suchomel, R. W., Scheper, R. J., Jager, U., et al. (1998) Expression of the lung resistance protein predicts poor outcome in de novo acute myeloid leukemia. *Blood* **91,** 1508–1513.
27. List, A. F., Spier, C. S., Grogan, T. M., Johnson, C., Roe, D. J., Greer, J. P., et al. (1996) Overexpression of the major vault transporter protein lung-resistance protein predicts treatment outcome in acute myeloid leukemia. *Blood* **87,** 2464–2469.
28. Wickremasinghe, R. G. and Hoffbrand, A. V. (1999) Biochemical and genetic control of apoptosis: Relevance to normal hematopoiesis and hematological malignancies. *Blood* **93,** 3587–3600.
29. Fisher, D. E. (1994) Apoptosis in cancer therapy: Crossing the threshold. *Cell* **78,** 539–542.
30. Yang, J., Liu, X., Bhalla, K., Kim, C. N., Ibrado, A. M., Cai, J., et al. (1997) Prevention of apoptosis by *bcl*-2: Release of cytochrome c from mitochondria blocked. *Science* **275,** 1129–1132.
31. Kluck, R. M., Bossy-Wetzel, E., Green, D. R., and Newmeyer, D. D. (1997) The release of cytochrome c from mitochondria: A primary site for *bcl*-2 regulation of apoptosis. *Science* **275,** 1132–1136.
32. Vander Heiden, M. G., Chandel, N. S., Williamson, E. K., Schumacker, P. T., and Thompson, C. B. (1997) *Bcl-XL* regulates the membrane potential and volume homeostasis of mitochondria. *Cell* **91,** 627–635.
33. Datta, R., Banach, D., Kojima, H., Talanian, R. V., Alnemri, E. S., Wong, W. W., et al. (1996) Activation of the CPP32 protease in apoptosis induced by 1—D arabinofuranosylcytosine and other DNA-damaging agents. *Blood* **88,** 1936–1943.

34. Belosillo, B., Dalmau, M., Colomer, D., and Gil, J. (1997) Involvement of CED-3/ICE proteases in the apoptosis of B-chronic lymphocytic leukemia cells. *Blood* **89,** 3378–3384.
35. Vogelstein, B. and Kinzler, K. W. (1992) P53 function and dysfunction. *Cell* **70,** 523–526.
36. Harris, C. C. and Hollstein, M. (1993) Clinical implications of the p53 tumor-suppressor gene. *N. Engl. J. Med.* **329,** 1318–1327.
37. Lowe, S. W., Bodis, S., McClatchey, A., Remington, L., Ruley, H. E., Fisher, D. E., et al. (1994) p53 status and the efficacy of cancer therapy in vivo. *Science* **266,** 807–810.
38. Wattel, E., Preudhomme, C., Hecquet, B., Vanrumbeke, M., Quesnel, B., Dervitte, I., et al. (1994) P53 mutations are associated with resistance to chemotherapy and short survival in hematologic malignancies. *Blood* **84,** 3148–3157.
39. Newcomb, E. W. (1995) P53 gene mutations in lymphoid diseases and their possible relevance to drug resistance. *Leuk. Lymphoma* **17,** 211–221.
40. Campos, L., Rouault, J. P., Sabido, O., Oriol, P., Roubi, N., Vasselon, C., et al. (1993) High expression of *bcl*-2 protein in acute myeloid leukemia cells is associated with poor response to chemotherapy. *Blood* **81,** 3091–3096.
41. Maung, Z. T., MacLean, F. R., Reid, M. M., Pearson, A. D. J., Proctor, S. J., Hamilton, P. J., et al. (1994) The relationship between *bcl*-2 expression and response to chemotherapy in acute leukaemia. *Br. J. Haematol.* **88,** 105–109.
42. Banker, D. E., Groudine, M., Norwood, T., and Appelbaum, F. R. (1997) Measurement of spontaneous and therapeutic agent-induced apoptosis with *bcl*-2 protein expression in acute myeloid leukemia. *Blood* **89,** 243–255.
43. Perentesis, J. P. and Kersey J. H. (1996) Biologic therapy of leukemia, in *Leukemia, 6th ed.,* (Henderson, E. S., Lister, T. A., Greaves, M. F., eds.), W. B. Saunders, London, pp. 354–388.
44. Kreitman, R. J. (1999) Immunotoxins in cancer therapy. *Curr. Opin. Immunol.* **11,** 570–578.
45. Weiner, L. M. (1999) An overview of monoclonal antibody therapy of cancer. *Semin. Oncology* **26,** 41–50.
46. Multani P. S. and Grossbard M. L. (1998) Monoclonal antibody-based therapies for hematologic malignancies. *J. Clin. Oncol.* **16,** 3691–3710.
47. Jurcic, J. G., Scheinberg, D. A., and Houghton, A. N. (1997) Monoclonal antibody therapy of cancer. *Cancer Chemother. Biol. Resp. Modifiers.* **17,** 195–216.
48. Bendel, A. E., Shao, Y., Davies, S. M., Warman, B. E., Yang, C. H., Waddick, K. G., et al. (1997) A recombinant fusion toxin targeted to the granulocyte-macrophage colony-stimulating factor receptor. *Leuk. Lymphoma* **25,** 257–270.
49. Perentesis, J. P., Waddick, K. G., Bendel, A., Shao, Y., Warman, B., Chandan-Langlie, M., et al. (1997) Induction of apoptosis in multidrug-resistant and radiation-resistant acute myeloid leukemia cells by a recombinant fusion toxin targeted to the granulocyte-macrophage colony-stimulating factor (GMCSF) receptor. *Clin. Cancer Res.* **3,** 347–355.
50. Perentesis, J. P., Bendel, A. E., Shao, Y., Warman, B. E., Davies, S. M., Yang, C. H., et al. (1997) Granulocyte-macrophage colony-stimulating factor receptor

targeted therapy of chemotherapy and radiation-resistant human myeloid leukemias. *Leuk. Lymphoma* **25,** 247–256.
51. Perentesis. J. P., Gunther, R., Waurzyniak, B., Yanishevski, Y., Eki, O., Messenger, Y., et al. (1997) In vivo biotherapy of HL-60 myeloid leukemia with a genetically engineered recombinant fusion toxin directed against the GMCSF receptor. *Clin. Cancer Res.* **3,** 2217–2227.
52. Young, D. C. and Griffin, J. D. (1988) Autocrine secretion of GM-CSF in acute myeloblastic leukemia. *Blood* **68,** 1178–1181.
53. Cheng, G. Y. M., Kelleher, C. A., Miyauchi, J., Wang, C., Wong, G., Clark, S. C., Met al. (1988) Structure and expression of genes of GM-CSF and G-CSF in blast cells from patients with acute myeloblastic leukemia. *Blood* **71,** 204–208.
54. Murohashi, I., Tonda, S., Susuki, T., Nazata, K., Yamashita, Y., and Nara, N. (1989) Autocrine growth mechanisms of the progenitors of blast cells in acute myeloblastic leukemia. *Blood* **74,** 35–41.
55. Russell, N. H. (1992) Autocrine growth factors and leukaemic haemopoiesis. *Blood Rev.* **6,** 149–156.
56. Budel, L. M., Touw, I.P., Delwel, R., Clark, S. C., and Lowenberg, B. (1989) Interleukin-3 and granulocyte-monocyte colony-stimulating factor receptors on human acute myelocytic leukemia cells and relationship to the proliferative response. *Blood* **74,** 565–571.
57. Park, L. S., Waldron, P. E., Friend, D., Sassenfeld, H. M., Price, V., Anderson, D., et al. (1989) Interleukin-3, GM-CSF, and G-CSF receptor expression on cell lines and primary leukemia cells: Receptor heterogeneity and relationship to growth factor responsiveness. *Blood* **74,** 56–65.
58. Onetto-Pothier, N., Aumont, N., Haman, A., Park, L., Clark, S. C., De Lean, A., et al. (1990) IL-3 inhibits the binding of GM-CSF to AML blasts, but the two cytokines act synergistically in supporting blast proliferation. *Leukemia* **4,** 329–336.
59. Onetto-Pothier, N., Aumont, N., Haman, A., Bigras, C., Wong, G. G., Clark, S. C., et al. (1990) Characterization of granulocyte-macrophage colony-stimulating factor receptor on the blast cells of acute myeloblastic leukemia. *Blood* **75,** 59–66.
60. Bradbury, D., Rogers, S., Kozlowski, R., Bowen, G., Reilly, I. A. G., and Russell, N. H. (1990) Interleukin-1 is one factor which regulates autocrine production of GM-CSF by the blast cells of acute myeloblastic leukaemia. *Br. J. Haematol.* **76,** 488–493.
61. Bradbury, D., Rogers, S., Reilly, I. A. G., Kozlowski, R., and Russell, N. H. (1992) Role of autocrine and paracrine production of granulocyte-macrophage colony-stimulating factor and interleukin-1–beta in the autonomous growth of acute myeloblastic leukemia cells—Studies using purified CD34–postive cells. *Leukemia* **6,** 562–566.
62. Rogers, S. Y., Bradbury, D., Kozlowski, R., and Russell, N. H. (1994) Evidence for internal autocrine regulation of growth in acute myeloblastic leukemia cells. *Exp. Hematol.* **22,** 593–598.

63. Löwenberg, B., van Putten, W. L. J., Touw, I. P., Delwel, R., and Santini, V. (1993) Autonomous growth determines prognosis in adult acute myeloid leukemia. *N. Engl. J. Med.* **328,** 614–619.
64. Hunter, A. E., Rogers, S. Y., Roberts, I. A. G., Barrett, A. J., and Russell, N. (1993) Autonomous growth of blast cells is associated with reduced survival in acute myeloblastic leukemia. *Blood* **82,** 899–903.
65. Yamaizumi, J., Mekada, E., Uchida, T., and Okada, Y. (1978) One molecule of diphtheria toxin fragment A introduced into a cell can kill the cell. *Cell* **15,** 245–250.
66. Perentesis, J. P., Miller, S. P., and Bodley, J. W. (1992) Protein toxin inhibitors of protein synthesis. *Biofactors* **3,** 173–184.
67. Williams, D. P., Parker, K., Bacha, P., Bishai, W., Borowski, M., Genbauffe, F., et al. (1987) Diphtheria toxin receptor binding domain substitution with interleukin-2: Genetic construction and properties of a diphtheria toxin-related interleukin-2 fusion protein. *Protein Engineering* **1,** 493–498.
68. LeMaistre, C. F., Meneghetti, C., Rosenblum, M., Reuben, J., Parker, K., Shaw, J., et al. (1992) Phase I trial of an interleukin-2 (IL-2) fusion toxin (DAB486IL-2) in hematologic malignancies expressing the IL-2 receptor. *Blood* **79,** 2547–2554.
69. LeMaistre, C. F., Craig, F. E., Meneghetti, C., McMullin, B., Parker, K., Reuben, J., et al. (1993) Phase I trial of a 90-minute infusion of the fusion toxin DAB486IL-2 in hematologic cancers. *Cancer Res.* **53,** 3930–3934.
70. Waters, C. A., Schimke, P. A., Snider, C. E., Strom, T. B., and Murphy, J. R. (1990) Receptor binding requirements for entry of a diphtheria toxin-related interleukin 2 fusion protein into cells. *Eur. J. Immunol.* **20,** 785–791.
71. Bacha, P., Williams, D. P., Waters, C., Murphy, J. R., and Strom, T. B. (1988) Interleukin-2 receptor cytotoxicity: Interleukin-2 receptor mediated action of a diphtheria toxin-related interleuin-2 fusion protein. *J. Exp. Med.* **167,** 612–622.
72. Perentesis, J. P., Genbauffe, F. S., Veldman, S. A., Galeotti, C. L., Livingston, D. M., Bodley, J. W., et al. (1988) Expression of diphtheria toxin fragment A and hormone-toxin fusion proteins in toxin-resistant yeast mutants. *Proc. Natl. Acad. Sci. USA* **85,** 8386–8390.
73. Jean, L. F. and Murphy, J. R. (1991) Diphtheria toxin receptor-binding domain substitution with interleukin 6. Genetic construction and interleukin 6 receptor-specific action of a diphtheria toxin-related interleukin 6 fusion protein, *Protein Engineering* **4,** 989–994.
74. Lakkis, F., Steele, A., Pacheco-Silva, A., Rubin-Kelley, V., Strom, T. B., and Murphy, J. R. (1991) Interleukin 4 receptor targeted cytotoxicity: Genetic construction and in vivo immunosuppresive activity of a diphtheria toxin-related murine interleukin 4 fusion protein. *Eur. J. Immunol.* **21,** 2253–2258.
75. Shaw, J. P., Akiyoshi, D. E., Arrigo, D. A., Rhoad, A. E., Sullivan, B., Thomas, J., et al. (1991) Cytotoxic properties of DAB486EGF and DAB389EGF, epidermal growth factor (EGF) receptor-targeted fusion toxins. *J. Biol. Chem.* **266,** 21,118–21,124.
76. Woodworth, T. G. and J. C. Nichols. (1993) Recombinant fusion toxins—A new class of targeted biologic therapeutics. *Cancer Treat. Res.* **68,** 145–160.

77. Choe, S., Bennett, M. J., Fujii, G., Curmi, P. M. G., Kantafdjieff, K. A., Collier, R. J., and Eisenberg, D. (1992) The crystal structure of diphtheria toxin. *Nature* **357,** 216–222.
78. Bennett, M. J., Choe, S., and Eisenberg, D. (1994) Domain swapping: Entangling alliances between proteins. *Proc. Natl. Acad. Sci. USA* **91,** 3127–3131.
79. Diederichs, K., Boone, T., and Karplus, P. A. (1991) Novel fold and putative receptor binding site of granulocyte-macrophage colony-stimulating factor. *Science* **254,** 1779–1782.
80. Walter, M. R., Cook, W. J., Ealick, S. E., Nagabhushan, T. L., Trotta, P. P., and Bugg, C. E. (1992) Three-dimensional structure of recombinant human granulocyte-macrophage colony-stimulating factor. *J. Mol. Biol.* **224,** 1075–1085.
81. Buchner, J., Pastan, I., and Brinkmann, U. (1992) A method for increasing the yield of properly folded recombinant fusion proteins: Single chain immunotoxins from renaturation of bacterial inclusion bodies. *Anal. Biochem.* **205,** 263–270.
82. Chan, C-.H., Blazar, B. B., Eide, C. R., Kreitman, R. J., and Vallera, D. A. (1995) A murine cytokine fusion toxin specifically targeting the murine granulocyte-macrophage colony-stimulating factor (GM-CSF) receptor on normal committed bone marrow progenitor cells and GM-CSF-dependent tumor cells. *Blood* **86,** 2732–2740.
83. Mastroeni, I., Patti, A. M., Santi, A. L., Vesci, N., Bocchini, S., Bagnod, S., et al. (1998) Diphtheria antitoxin levels in the 14–30-year age groups in Italy. *Eur. J. Epi.* **14,** 683–686.
84. Nicolay, U., Girgsdies, O. E., Banzhoff, A., Hundt, E., and Jilg, W. (1999) Diphtheria booster vaccination: One or two injections? *Vaccine* **17,** 2223–2228.

4

Synthesis of Monensin Derivatives and Their Effect on the Activity of Ricin A-Chain Immunotoxins

Marco Colombatti and Franco Dosio

1. Introduction

Cell-specific cytotoxic heteroconjugates are made by linking bacterial toxins (e.g., diphtheria toxin, *Pseudomonas* exotoxin A) or plant toxins (e.g., ricin, abrin) to monoclonal antibody (MAb)/ligands that bind target antigens or receptors at the cell surface ***(1–3)***. Toxins used for the synthesis of cytotoxic heteroconjugates are formed by two subunits: the A-chain, an enzyme that inhibits protein synthesis in the target cell; and the B-chain, able to bind ubiquitous cell surface structures and to help A-chain translocation to the cytosol ***(4,5)***. Naturally occurring A-chain–like toxins (ribosome-inactivating proteins, or RIPs) have also been used as toxic components of cell-selective conjugates ***(6,7)***. Unlike intact toxin conjugates, ricin toxin-A-chain (RTA) or RIP conjugates show high target-cell specificity but variable cytotoxicity, often too low to be of appreciable therapeutic value, particularly in solid tumor treatment ***(1)***. The cytotoxic activity of RTA conjugates can be potentiated in vitro by lysosomotropic amines (e.g., NH_4Cl, chloroquine, methylamine, amantadine), ionophores (e.g., monensin, nigericin, lasalocid), or lysosomal enzyme inhibitors (e.g., leupeptin, pepstatin) ***(8–13)***.

Monensin is a carboxylic ionophore regulating Na^+–H^+ exchange across the cell membrane ***(14)***. It potentiates the cytotoxic effect of immunotoxins (IT) directed against different cell surface structures and enters the cell by different pathways ***(8,9)***. Several other properties make monensin a potential candidate for the enhancement of RTA-IT in vivo. It potentiates RTA-IT at nanomolar concentrations in cell lines of different histotypes ***(8,9)***, and it can be delivered in vivo encapsulated in liposomes or crosslinked to carrier proteins (e.g., human serum albumin, HSA) to decrease its clearance rate ***(13,15)***. Unlike other potentiators (e.g., NH_4Cl), monensin action is not limited by intracellular or extracellular

From: *Methods in Molecular Biology, vol. 166: Immunotoxin Methods and Protocols*
Edited by: W. A. Hall

pH ***(16)*** and may also exert its functions in the low pH areas of a growing tumor mass. Also, large amounts of monensin can be tolerated in vivo in animals following intravenous or intraperitoneal inoculation ***(13,15,17,18)***.

The mechanism of potentiation of toxic conjugates by monensin has not yet been fully elucidated. Monensin affects cells in many ways, apparently as a consequence of profound changes in the cytoplasmic Na^+/K^+ balance ***(19)***. However, it must be noted that at the low concentrations of monensin yielding substantial potentiation of RTA-IT (i.e., 50 n*M*), monensin seems unable to alter the pH of intracellular compartments ***(18)***. A possible explanation of the RTA-IT enhancing properties of monensin might thus reside in its lipophilic character.

In an effort to obtain new RTA-IT-enhancers with high activity, and to investigate the possible correlation between the structure of monensin and its potentiating activity, we synthesized and assayed seven structural analogs: two compounds with an increased negative polarity (sulfate and phosphate group); one with an ionizable positive charge (dimethylamino group); three compounds with more lipophilic groups (a rigid phenyl group; and two long-chain structures of 28 carbon atoms with varying flexibility) and for comparison, we also prepared a methyl ester derivative of monensin to reduce the polarity of its carboxyl group. Two cell surface structures of human leukemia cells were taken as the targets of RTA-IT: CD5 (expressed by T-cells) and the transferrin receptor (expressed by all proliferating cells).

In the present chapter, we will describe the synthesis of monensin–protein conjugates and the production of monensin analogs endowed with different lipophilic properties. The technical aspects concerning the crosslinkage of HSA and monensin will be described in greater detail.

2. Materials

2.1. Chemicals

All chemicals were of reagent grade and were obtained from either Aldrich Chemicals or Bracco-Merck (Milan, Italy).

1. Monensin was purchased from Fluka Chemical Co. (Milan, Italy).
2. ^1H NMR spectra were recorded on a Jeol EX-400.
3. Mass spectra were obtained on a VC Analytical 7070 EQHP spectrometer.
4. IR were recorded on a Perkin-Elmer 781.
5. Microanalyses performed on an elemental analyser 1106 (Carlo Erba Instrumentation) were within ± 0.4% of theoretical values.

2.2. Crosslinkers

The following crosslinkers were used in our studies.

1. SAMSA (*S*-acetylmercaptosuccinic anhydride) from Sigma (St. Louis, MO).
2. SPDP (*N*-succinimidyl 3-[2-pyridyl-dithio] propionate) from Pierce (Milan, Italy).

3. SATA (*N*-succinimidyl-S-thioacetate) synthesized as described by Duncan et al. ***(20)***.
4. SIA (*N*-succinimidyl-iodoacetic acid) synthesized as described by Higgins et al. ***(21)***.

2.3. Biologicals

1. Jurkat, a human $CD5^+$ T-lymphoblastoid cell line, was used. Jurkat cells are maintained by serial passage in RPMI 1640 + 10% fetal bovine serum (Seromed, Berlin, Germany) and gentamicin at 37°C in 5% CO_2 in a humidified atmosphere.
2. HSA was received from Behring (Scoppito, Italy).
3. Human transferrin (Tfn) was purchased from Miles (Milan, Italy).
4. RTA was donated by Dr. P. Casellas (Sanofi Recherche, Montpellier, France).
5. Protease was purchased from Sigma (St. Louis, MO).

3. Methods

3.1. Synthesis of Immunotoxins

Two types of ITs are used in these studies.

1. RTA was linked to human Tfn by a disulfide bridge ***(22)***. RTA (fourfold molar excess over Tfn) was reduced with 100 m*M* DTT for 2 h at room temperature in 200–300 μL PBS total volume. This was followed by gel filtration on a Sephadex G-25 column and mixing with MAb (800 μg in 125 μL PBS) or Tfn (2 mg in 360 μL PBS) previously derivatized with a sevenfold molar excess of SPDP at 2.6 mg/mL in 95% ethanol, which introduced about 3 sulfhydryl groups per molecule. Tfn–RTA conjugates were purified by gel filtration on a TSK3000 SW HPLC column (Beckman) equilibrated in 0.1 *M* phosphate buffer (PB), pH 6.9, and run at 0.5 ml/min. Tfn–toxin conjugates were a mixture of conjugates of different stoichiometry that showed an average molecular weight of 1:1 to 1:3 molar conjugates. These were separated from unconjugated Tfn and toxin.
2. ST.1 $(Fab)_2$-RTA (a conjugate of the $(Fab)_2$ fragment of MAb ST1 and RTA, henceforth designated ST1-RTA for brevity) to the CD5 differentiation antigen on human cells was supplied by Dr. P. Casellas. ST1-RTA contained an average of two molecules of RTA per molecule of antibody.

3.2. Production of Disulfide-Crosslinked Protein–Monensin Conjugates

The synthesis of disulfide- and thioether-linked HSA–monensin conjugates is schematized in **Fig. 1**.

1. HSA is coupled to monensin via a disulfide bridge.
2. HSA 5 mg/mL in PB are reacted with a 25 molar excess SPDP to introduce 20 sulfhydryl groups/HSA molecule (*see* **Note 1**).
3. Following 30 min incubation at room temperature, unreacted SPDP is eliminated by dialysis against PB (at least 400 vol PB), and the number of sulfhydryl groups introduced is evaluated spectrophotometrically ***(23)*** (*see* **Note 2**).

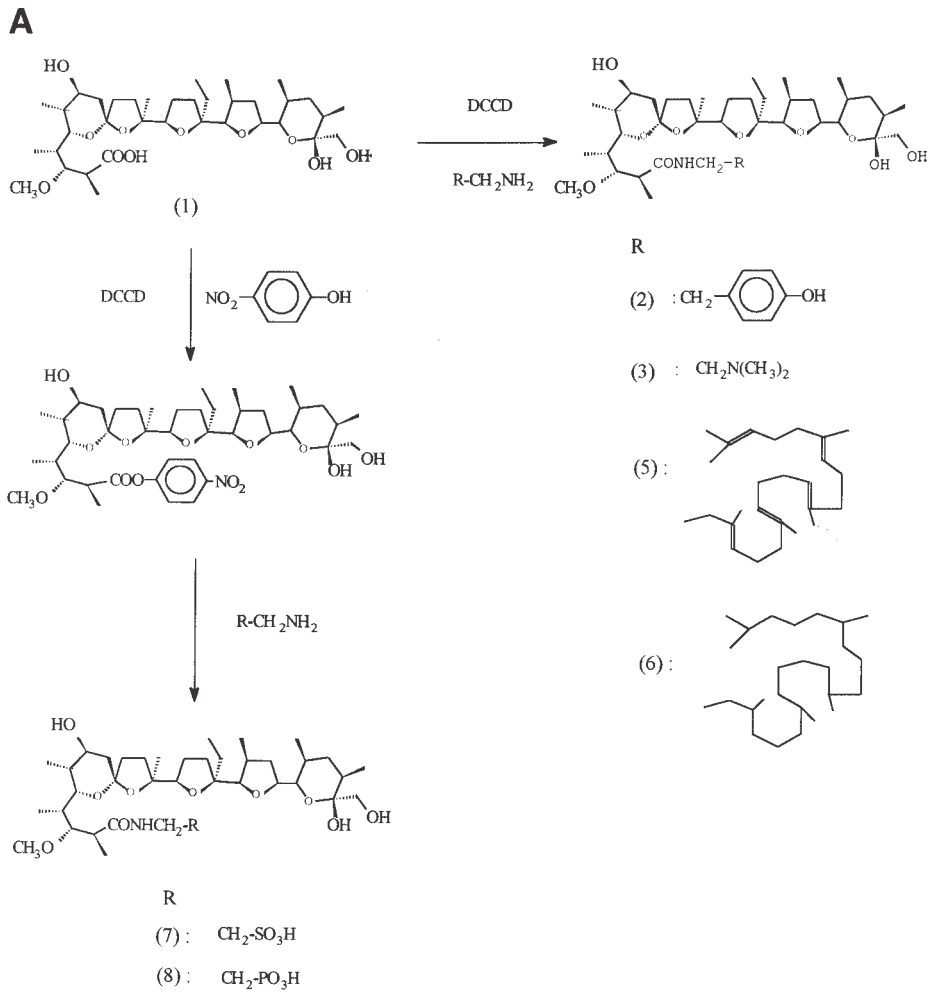

Fig. 1. Synthetic route to monensin amide derivatives. **(A)** Monensin (1) was condensed with primary amino compounds in the presence of DCCD to provide monensin tyramide (2), dimethylaminoethyl amide (3), squalane amide (5), and squalene amide (5). Alternatively, to provide monensin taurine amide (7) or monensin ciliatin amide (8), monensin acid was first condensed with 4-nitro-phenol in the presence of DCCD, and the 4-nitro-phenolate derivative then reacted with the amino compound. **(B)** *(opposite page)* Synthetic route to monensin methyl ester derivative (4). Monensin sodium salt was reacted with methyl iodide and 1,8-diazabicyclo[5.4.0]undecene.

B

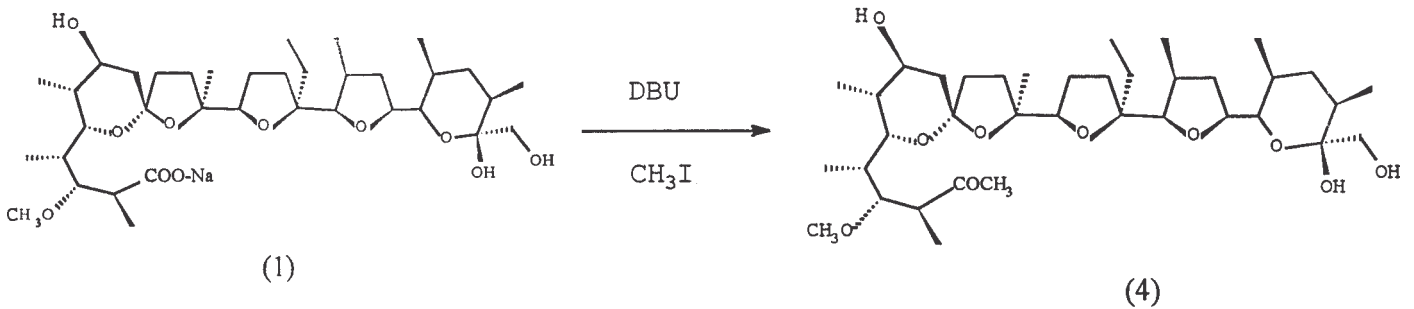

(1) (4)

4. Monensin 300 mg in anhydrous chloroform (40 mL) are first reacted with 80 mg of the bifunctional crosslinker SAMSA for 1 h at room temperature to introduce one protected thiol group/monensin molecule (*see* **Note 3**).
5. The reaction mixture is dried under vacuum at 37°C. Evaporation yields a yellowish oily material that is dissolved in ethyl acetate.
6. After this, derivatized monensin is separated from unreacted SAMSA by extraction with ethyl acetate/water (1:2). The extraction procedure is repeated 5–7 times to ensure that all traces of unreacted crosslinker are eliminated.
7. The solution containing derivatized monensin (upper layer of the ethyl acetate/water mixture) is placed in a glass flask, and anhydrous Na_2SO_4 is added.
8. The mixture is then incubated for 1 h at room temperature, salt crystals are filtered off with a glass-synthesized Buckner filter, and the derivatized monensin solution is placed in a glass flask.
9. Ethyl acetate is then eliminated by vacuum evaporation. After ethyl acetate is evaporated, monensin–SAMSA is resolubilized in 1 mL ether.
10. Measurement of derivatized monensin content can be carried out at this stage by taking 100 μL monensin–SAMSA in ether, drying it up under an N_2 flow, and resuspending it in 2 mL methanol before running the vanillin assay (***24***; *see* **Note 4**).
11. After determination of the total activated monensin content, the stock solution of monensin–SAMSA is dried under N_2 and then mixed with HSA-SPDP in a 3:1 molar excess (with respect to sulfhydryl groups introduced into HSA) and incubated for 1 h at room temperature in the presence of 1.0 *M* NH_2OH to allow conjugate formation.
12. HSA–monensin conjugates are then separated from uncoupled monensin by dialysis against 400 vol of PB (two changes).
13. The monensin:HSA ratio is calculated by measuring HSA and monensin concentrations in the conjugates. HSA is determined by the Lowry method ***(25)***. Monensin concentration is determined with the vanillin method modified for quantitative colorimetric measurements ***(24)***.

3.3. Production of Thioether Crosslinked Protein–Monensin Conjugates

1. HSA 100 mg (5 mg/mL in PB) are reacted with a 30-fold molar excess of SIA crosslinker ***(26)*** by adding 8 mg SIA in 1 mL dimethylformamide, followed by a 30 min incubation at room temperature.
2. Unreacted SIA is eliminated by dialysis against 400 vol PB.
3. Monensin 150 mg in chloroform (20 mL) are first reacted with 80 mg of the bifunctional crosslinker SAMSA (1:2 molar ratio) for 1 h at room temperature to introduce one protected thiol group per monensin molecule.
4. The reaction mixture is dried under vacuum and dissolved in 20 mL ethyl acetate. Unreacted SAMSA is separated from derivatized monensin by extraction with ethyl acetate. The ethyl acetate is then evaporated under vacuum, and monensin–SAMSA resolubilized in 20 mL ether.

5. Monensin–SAMSA is then dried under N_2, mixed with HSA–SIA in a 3:1 molar excess, and incubated for 1 h at room temperature in the presence of 1.0 *M* hydroxylamine to allow conjugate formation.
6. HSA–monensin conjugates are then separated from uncoupled monensin by dialysis against 400 vol PB.
7. The monensin:HSA ratio is calculated by measuring the HSA and monensin concentration in the conjugates. HSA is determined by the Lowry method ***(25)***. Monensin concentration can be determined with the vanillin method modified for quantitative colorimetric measurements, as mentioned in **Subheading 3.2.** (*see* **Note 4**).
8. To estimate the monensin:HSA ratio, thioether-crosslinked conjugates must first be treated with 10 mg/mL protease for 24 h at 37°C.
9. Monensin is then isolated by four sequential chloroform extractions, and the extracts treated as described for the standard curve. By this method, four monensin molecules can be reproducibly crosslinked per HSA molecule in several different HSA-SIA–monensin batches.

3.4. Production of Monensin Analogs

All synthesized analogs are characterized by ^{1}H-NMR, fast-atom–bombardment mass spectrometry (FAB-MS), and IR. The synthetic route to monensin amide derivatives is illustrated in **Fig. 2**.

3.4.1. Squalene Amine:(4E,8E,12E,l6F)-4,8,13,17,21-Pentamethyl-4,8,12,16,20-Docosapentaenylamine

1. NH_3 (approx 5 mL) is liquefied at –80°C, and anhydrous methanol (10 mL) previously cooled at –50°C is added with continuous stirring.
2. A solution of HCl in anhydrous methanol is subsequently added in drops up to pH 6.0. During this addition, a white precipitate forms.
3. $NaBH_3CN$ (314 mg, 5 mmol) is then added, followed by 1,1',2-Tris-nor-squalene aldehyde (1.92 g, 5 mmol) prepared as described by Ceruti et al. ***(27)***.
4. The reaction mixture is allowed to reach –25°C and left for 12 h at this temperature. It is then extracted with diethyl ether (100 mL) after addition of water (100 mL), dried over anhydrous sodium sulphate, and evaporated to dryness under vacuum.
5. The resulting oil is purified by flash chromatography using diethyl ether/light petroleum 70:30, diethyl ether, and finally diethyl ether/methanol (95:5) to give squalene amine (482 mg, 25% yield).

3.4.2. Squalane Amine: 4,8,13,17,21-Pentamethyldocosylamine

1. Palladium adsorbed on activated carbon (Merck) (10% Pd, 15 mg) is added to absolute ethanol (100 mL) with stirring, and the suspension is then placed under H_2 atmosphere.
2. Squalene amine (250 mg, 0.65 mmol) is added and left for 24 h under H_2 atmosphere with stirring.
3. The suspension is filtered to remove the catalyst and then concentrated under vacuum. The crude product is purified by flash chromatography with diethyl ether

A

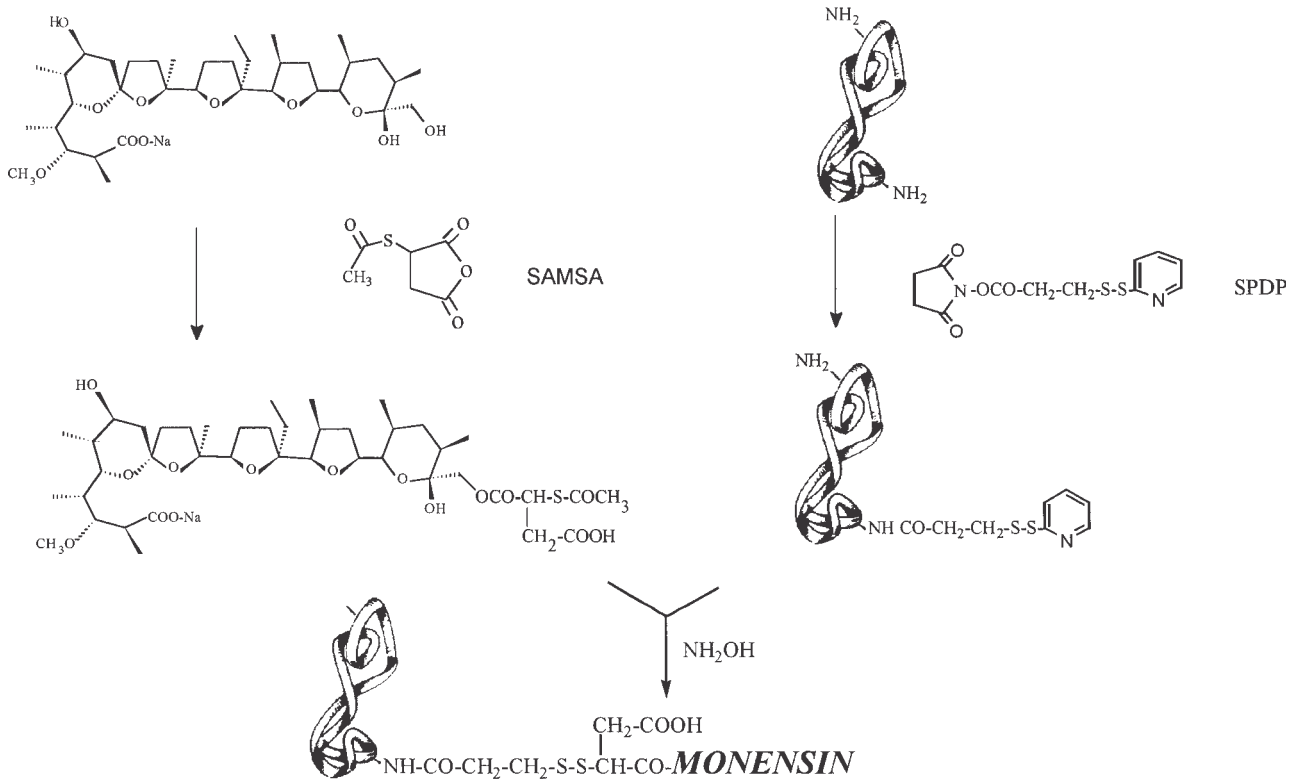
HO
COO-Na
CH3O
OH
OH
NH2
NH2
SAMSA
SPDP
N-OCO-CH2-CH2-S-S
OCO-CH-S-COCH3
CH2-COOH
NH CO-CH2-CH2-S-S
NH2OH
NH-CO-CH2-CH2-S-S-CH-CO-MONENSIN

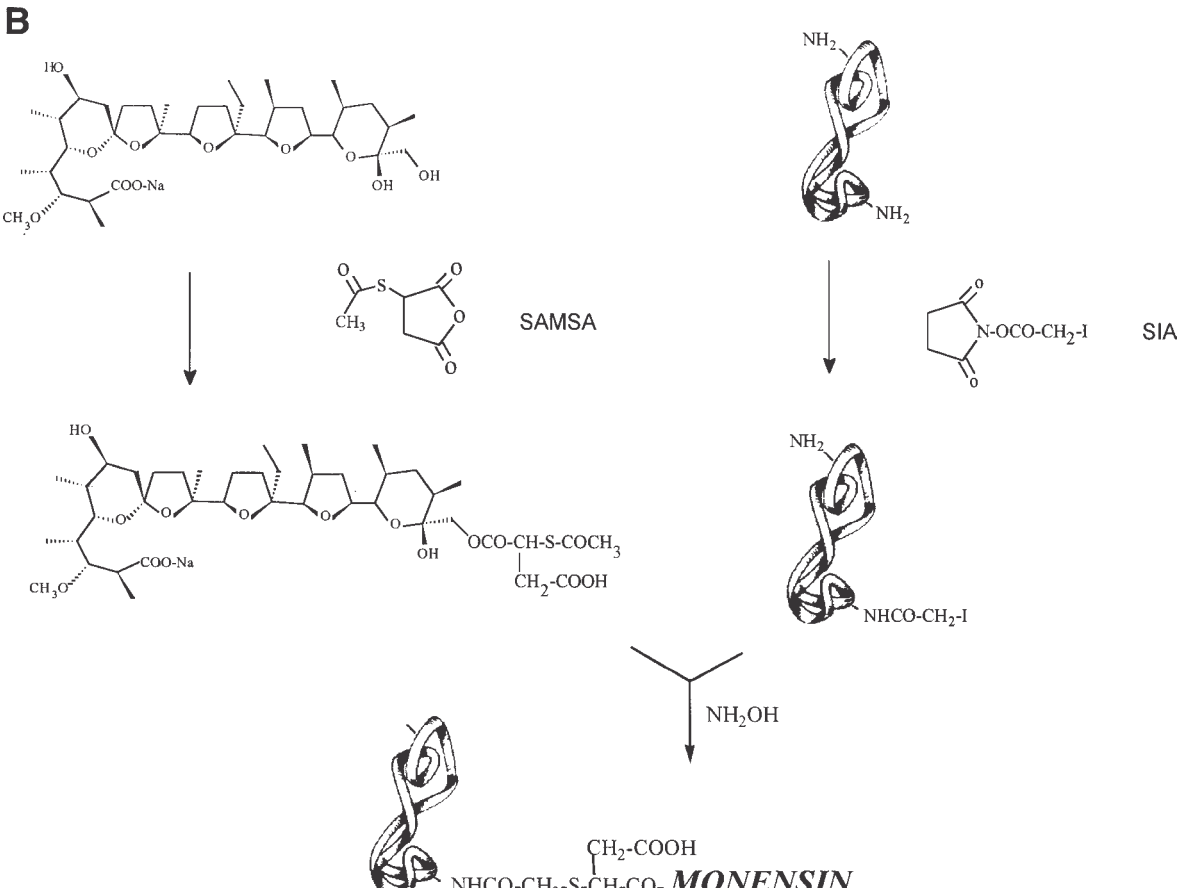

Fig. 2. Schematic representation of the synthesis of disulfide- **(A)** and thioether-linked **(B)** HSA–monensin conjugates.

and then diethyl ether/methanol 95:5 to remove impurities, and finally with methanol to give 236 mg (92% yield) as a colorless viscous oil.

3.4.3. Monensin Acid (Compound 1, see ***Fig. 1***)

1. Sodium monensin is dissolved in hot methanol and the solution filtered.
2. Monensin is then precipitated by adding water to the cooled methanolic solution. This purification step is repeated twice.
3. The white salt obtained is then dried under vacuum (yield 83–87%), dissolved in distilled chloroform, and stirred vigorously for 1 h at room temperature with a layer of aqueous perchloric acid (1 *M*) to convert the sodium salt into the acid form of monensin.
4. The chloroform layer is washed with distilled water until the washings are neutral, and then evaporated to dryness.
5. The obtained crystals are dried under vacuum and stored at –20°C.
6. To synthesize the reactive intermediate monensin 4-nitrophenolate, 500 mg of monensin acid (0.745 mmol) is dissolved in 10 mL of freshly prepared dry tetrahydrofuran (THF) and maintained at 5°C. 4-nitrophenol (160 mg, 1.15 mmol) and dicyclohexylcarboclimide (DCCD) (250 mg, 1.2 mmol) dissolved in 3 mL of THF are added, and the reaction maintained at 5°C for 24 h.
7. The precipitated dicyclohexylurea is removed by centrifugation, and the reaction mixture purified by flash chromatography (2 × 20 cm SiO_2; Merck) using ethyl acetate/methylene chloride 15:85 and then 30:70.
8. The fractions containing monensin 4-nitrophenolate are collected and dried under vacuum to obtain 450 mg of white crystalline product (yield 76%, Retardation factor (Rf) = 0.38 in EtOAc-CH_2CI_2 [30:70]).

3.4.4. Monensin Methyl Ester (Compound 4)

To synthesize this compound, the procedure described by Tohda et al. ***(28)*** is followed using methyl iodide and 1,8-diazabicyclo-[5,4,0]-undecene (**Fig. 2**). The tyramide (compound 2), *N*,*N*-dimethylaminoethylamide (compound 3), squalene amide (compound 5), and squalane amide (compound 6) derivatives of monensin are prepared using essentially the same procedure as in **Fig. 1**.

3.4.5. Monensin Amide Compounds

1. Monensin acid (200 mg, 0.3 mmol) is stirred at 5°C for 30 min in 2 mL of dry dimethylformamide (DMF) or THF. DCCD (64 mg, 0.31 mmol) is then added.
2. After being stirred for 1 h, the reaction is treated with 0.4 mmol of the corresponding amine: tyramine, *N*,*N*-dimethylethylenediamine, squalene, and squalane amine dissolved in 1 mL of dry DMF.
3. Stirring is continued at 5°C for 24 h. The mixture is then evaporated under vacuum and the residue suspended in ethyl acetate and filtered off. To remove all the precipitated dicyclohexylurea, this step must be repeated three times.
4. The crude product is then purified by flash chromatography on 230–400 mesh silica gel.

3.4.6. Monensin Tyramide (Compound 2)

Elution mixture: methylene chloride/ethyl acetate 85:15 and 5:95 to give 170 mg of pure 2 (Rf = 0.28 in CH_2CI_2–MeOH [90:10]).

3.4.7. Monensin Dimethytaminoethylamide (Compound 3)

Reaction solvent THF: Elution mixture ethyl acetate/methanol/ammonia 97.5:2:0.5 and 96:3:1 to give 167 mg of pure 3 (Rf = 0.22 in EtOAc-MeOH–NH_3 [70:28:0.2]).

3.4.8. Monensin Squalene Amide (Compound 5)

Elution mixture: CH_2Cl/MeOH 99:1 and 96:4 to give 150 mg of pure 5 (Rf = 0.58 in CH_2Cl–MeOH [90:10]).

3.4.9. Monensin Squalane Amide (Compound 6)

Elution mixture: methylene chloride/methanol 99:1 and 96:4 to give 110 mg of pure 6 (Rf = 0.68 in CH_2CI_2–MeOH [90:10]).

3.4.10. Monensin Taurine Amide (Compound 7)

1. To a solution of 400 mg monensin 4-nitrophenolate (0.5 mmol) in 5 mL of dry pyridine, add 160 mg taurine (2-aminoethanesulfonic acid, 1.28 mmol), previously dissolved in 2.3 mL of distilled water.
2. The solution is vigorously stirred for 48 h at room temperature.
3. After evaporation under vacuum, the unreacted taurine is filtered off in ethyl acetate, and the crude product purified by flash chromatography using methylene chloride/ethyl acetate (95:5) and then methylene chloride/ethyl acetate/methanol (55:30:15).
4. The white powder is then crystallized from acetone/ethyl acetate to give 383 mg of pure 7. Melting point 161–162°C. (Rf = 0.08 in CH_2Cl_2–MeOH [90:10]).

3.4.11. Monensin Ciliatine Amide (Compound 8)

1. To a solution of 400 mg of monensin 4-nitrophenolate (0.5 mmol) in 10 mL of dry pyridine, add 160 mg ciliatine (2-aminoethylphosphonic acid, 1.28 mmol) previously dissolved in 4.5 mL of distilled water.
2. The solution is vigorously stirred for 5 d at room temperature.
3. After evaporation under vacuum, the unreacted ciliatine is filtered off in ethyl acetate and the crude product purified by five preparative TLC plates (20 × 20 cm × 1 mm; Bracco-Merck, Milan, Italy) with a methylene chloride/methanol (80:20) eluent to give 85 mg of pure 8 (Rf = 0.18 in CH_2CI_2–MeOH [80:20]).

3.5. Determination of Lipophilic Character (Rm)

The lipophilic character of the synthesized compounds can be determined by a chromatographic Retardation measure (Rm) method ***(29,30)***.

1. Solutions of compounds are spotted 1 cm above the bottom of silanized silica-gel TLC plates (20 × 20 cm, RP-2, Bracco-Merck).
2. The plates are developed with various mixtures of water/methanol (from 50–90% in methanol).
3. The plates are then dried and sprayed with a 4% solution of vanillin in methanol and 2.5% concentrated sulphuric acid. After a few minutes at 80°C, reddish spots will appear.
4. The Rm are calculated from the following expression:

$$Rm = \log[(1/Rf)–1]$$

where Rf is the distance travelled by the compound divided by the distance travelled by the solvent front (18 cm).

Rm values higher than that of monensin are suggestive of higher lipophilicity. From this analysis, it appears that only compounds 7 and 8 are more polar than monensin; all other compounds are more lipophilic in an increasing order from compound 2 to 6.

3.6. Synthesis of Monensin–Tyramine and Labeling with ^{125}I

For particular applications, it might be useful to employ radiolabeled monensin. We herein describe a procedure yielding [^{125}I]-labeled monensin.

1. Monensin acid (100 mg, 0.149 mmol) is solubilized in 3 mL dry dimethylformamide with 20.3 mg (0.15 mmol) of 1-hydroxybenzotriazole and stirred at 5°C for 30 min. Dicycloexylcarbodiimide (32 mg, 0.155 mmol) is then added.
2. After stirring for 1 h, the reaction mixture is treated with a solution of tyramine (27.3 mg, 0.2 mmol) in 4 mL dry dimethylformamide. Stirring is continued at 5°C for 20 h.
3. The precipitated dicycloexylurea is removed by centrifugation and the solution dried under vacuum.
4. Monensin–tyramine is then purified by TLC on silica gel (with an elution buffer composed as follows: CH_2Cl_2/MeOH 9:1).
5. Aliquots of 0.5 mg monensin–tyramine in 200 μL benzene are placed in 3 mL glass vials.
6. Benzene is dried under N_2 and monensin–tyramine is labeled with ^{125}I using chloramine T ***(30)***.
7. ^{125}I-labeled monensin–tyramine is then extracted in benzene and washed in water to remove free ^{125}I.
8. Purity (>95%) of [^{125}I]-tyramine–monensin can be evaluated by TLC on silica gel (elution buffer MeOH/acetone 1:1); by this protocol specific activity is 0.25–0.54 μCi/μg in several different batches.

3.7. Protein Synthesis Assays

Protein synthesis measurements are performed to assay the intrinsic toxicity of monensin and its derivatives, and to evaluate their RTA-IT enhancing activity.

3.7.1. Nonselective Toxicity

1. Protein synthesis is assayed by incubating 5×10^4 Jurkat cells in 50 mL leucine-free RPMI, 5% fetal bovine serum in 96-well flat-bottomed microtitration plates (Costar, Cambridge, MA).
2. From a stock solution of 5 m*M* monensin in DMSO, 10-fold dilutions are prepared. DMSO alone (1% final concentration) has no effect on cell culture.
3. Monensin and its derivatives are then added to Jurkat-cell microcultures and target cells incubated for 22 h at 37°C in 5% CO_2 in a humidified atmosphere in 100 mL final volume. Final concentrations usually range from 500 μ*M* to 0.5 n*M*. Under these conditions and in the absence of monensin or derivatives, the cells proliferate monoexponentially.
4. One μCi of L-[U-^{14}C]-leucine (316 mCi/mmol, DuPont, Boston, MA) in 10 μL of RPMI is then added.
5. After 2 h, the cells are harvested onto glass fiber filters, washed with water, and dried.
6. Radioactivity incorporated by the cells is then measured in a beta spectrometer. The results are expressed as a percentage of the incorporation of control mock-treated cultures. The cytotoxicity of monensin or its derivatives can be compared by taking the molar concentration required to inhibit 50% protein synthesis (IC_{50}).

3.7.2. Enhancement of RTA-IT Cytotoxicity

1. Jurkat target cells (5×10^4/well) are treated with various concentrations of different RTA-IT for 22 h with or without monensin or its derivatives, used at the highest nontoxic concentration.
2. Protein synthesis is then measured as described above. Raw data expressed in cpm is also processed as above. Results of protein synthesis inhibition assays using monensin and its analogs, as well as the potentiating effects of monensin and protein–monensin conjugates, are shown in **Table 1**.
3. It can be observed that monensin–tyramide, monensin–squalene amide, and monensin–squalane amide show an RTA-IT potentiating activity comparable to monensin.
4. The squalane amide analog has a slightly higher enhancing effect (twofold) in comparison with the parent drug. However, it must be noted that the RTA-IT enhancement observed with monensin analogs is achieved at a 10-fold higher concentration than monensin (*see* **Table 1**), whereas the more polar compounds monensin taurine amide and monensin ciliatine amide require a 1000-fold higher concentration (not shown).
5. Derivatives with a positive ionizable charge (e.g., monensin–dimethylaminomethyl ester) or with a reduced negative charge (e.g., monensin–methyl ester) shows no RTA-IT–enhancing activity at the concentrations tested.

4. Notes

1. The buffer PB used in the synthesis procedure is a phosphate buffer, pH 7.0 (75 m*M* Na_2HPO_4 plus 50 m*M* KH_2PO_4).

Table 1
Effect of Monensin and Its Analogs on the Cytotoxic Activity of Immunotoxins

	IC_{50}(p*M*)/fold Potentiation[a] Immunotoxin	
Enhancer[b]	ST1–RTA	Tfn–RTA
None	1140/0	26/0
Monensin	0.46/2478	0.18/144
Monensin–tyramide	0.44/2590	0.16/162
Monensin–dimethylaminomethyl amide	800/1	26/1
Monensin–methyl ester	810/1.4	26/1
Monensin–squalene amide	0.4/2590	0.17/153
Monensin–squalane amide	0.28/4071	0.1/260
Monensin–taurine amide	710/1	26/1
Monensin–ciliatine amide	750/1.5	15/1.7

[a]Results are expressed as p*M* concentration of the immunotoxin inhibiting 50% of the protein synthesis in target cells. Fold potentiation is calculated based on the following formula: IC_{50} in the absence of the enhancer/IC_{50} in the presence of the enhancer. It represents the increase in cytotoxic effect obtained in the presence of monensin or of its analogs.

[b]The concentration of monensin is 50 n*M*, that of the analogs is 500 n*M*.

2. For SPDP derivatization, 20 mL HSA solution is placed in a 50 mL plastic tube. SPDP is weighed just before use and solubilized in ethanol. Do not exceed a 10 mg/mL concentration. The recommended HSA:SPDP ratio is 1:20 to 1:25. SPDP must be added dropwise to the stirred HSA solution.
3. For monensin derivatization with SAMSA, use glassware only. Monensin must first be solubilized in anhydrous chloroform. The recommended monensin: chloroform ratio (w:v) is 1:7 and the monensin:SAMSA ratio (w:w) is 1:2. Be careful not to add too much anhydrous Na_2SO_4, as monensin tends to be adsorbed onto it. Salt can be added as long as salt crystals can be solubilized. Stop Na_2SO_4 addition as soon as salt crystals become difficult to solubilize.

   At this stage, the preparation can be stopped and monensin stored at –20°C until needed.
4. A standard curve with known concentrations of derivatized monensin is first established by adding monensin–SAMSA in methanol to a solution of 3% vanillin in 0.5% sulfuric acid used as a color reagent. The samples are heated at 60°C (25 min) and cooled on ice (5 min); absorbance is measured at 518 nm. To estimate the monensin:HSA ratio, HSA–monensin conjugates are first treated with 1% β-mercaptoethanol for 1 h at room temperature; monensin is then extracted by four sequential chloroform extractions and the extracts are treated as described for the standard curve. Monensin concentration is determined from the standard curve. On average, 13.0 monensin molecules can be crosslinked to one HSA molecule.

Acknowledgments

The work described here was supported in part by grants from AIRC and MURST (to MC).

References

1. Youle, R. J. and Colombatti, M. (1986) lmmunotoxins: antibodies linked to toxic proteins for bone marrow transplantation and cancer therapy, in *Monoclonal Antibodies in Cancer: Advances in Diagnosis and Treatment* (Roth, I., ed.), Futura, Mount Kisco, NY, pp. 173–213.
2. Pastan, I., Willingham, M. C., and Fitzgerald, D. J. P. (1986) Immunotoxins. *Cell* **47,** 641–648.
3. Vitetta, E. S., Fulton, R. J., May, R. C., Tili, M., and Uhr, J. W. (1987) Redisigning nature's poisons to create anti tumor reagents. *Science* **238,** 1098–1104.
4. Olsnes, S. and Pihl, A. (1982) Toxin lectins and related proteins, in *Molecular Action of Toxins and Viruses* (Cohen, P. and Van Heyningen, S., eds.), Elsevier/North-Holland Biomedical Press, Amsterdam, pp. 51–105.
5. Youle, R. J. and Neville, D. M., Jr. (1982) Kinetics of protein synthesis inactivation by ricin-anti-Thy 1.1 monoclonal antibody hybrids. *J. Biol. Chem.* **257,** 1598–1601.
6. Barbieri, L. and Stirpe, F. (1982) Ribosome-inactivating proteins from plants: properties and possible uses. *Cancer Surv.* **1,** 489–520.
7. Stirpe, F. and Barbieri, L. (1986) Ribosome-inactivating proteins up to date. *FEBS Lett.* **195,** 1–8.
8. Ramakrishnan, S. and Houston, L. L. (1983) Inhibition of human acute lympho-blastic leukemia cella by immunotoxins: potentiation by chloroquine. *Science* **223,** 58–61.
9. Casellas, P., Bourrie, B. J., Gros, P., and Jansen, F. K. (1984) Kinetics of cytotoxicity induced by immunotoxins. Enhancement by lysosomotropic amines and carboxylic ionophores. *J. Biol. Chem.* **259,** 9359–9364.
10. Raso, V. and Lawrence J. (1984) Carboxylic ionophores enhance the cytotoxic potency of ligand- and antibody-delivered ricin A chain. *J. Exp. Med.* **160,** 1234–1240.
11. Akiyama, S., Seth, P., Pirker, R., Fitzgerald,D., Gottesman, M. M., and Pastan, I. (1985) Potentiation of cytotoxic activity of immunotoxins on cultured human cells. *Cancer Res.* **45,** 1005–1007.
12. Siena, S., Villa, S., Bregni, M., Bonadonna, G., and Gianni, A. M. (1987) Amantadine potentiates T-lymphocyte killing by an anti-pan-T cell (CD5) ricin A-chain immunotoxin. *Blood* **69,** 345–348.
13. Jansen, F. K., Blythman, H. E., Casellas, P., Derocq, J. M., and Dussossoy, D. (1987) Enhancement of ITs: in vitro and in vivo, in *Membrane-Mediated Cytotoxicity*, vol. 45 (Bonavida B. and Collier R. J., eds.), Alan R. Liss Inc., New York, pp. 167–173.
14. Mollenhauer H. H., Morrè D. J., and Rowe L. D. (1990) Alteration of intracellular traffic by monensin: mechanism, specificity and relationship to toxicity. *Biochim. Biophys. Acta* 1**031,** 225–246.
15. Colombatti M., Dell'Arciprete L., Chignola R., and Tridente G. (1990) Carrier protein-monensin conjugates: enhancement of immonotoxin cytotoxicity and potential in tumor treatment. *Cancer Res.* **50,** 1385–1391.

16. Casellas, P., Ravel, S., Bourrie, B. J., Derocq, J. M., Jansen, F. K., Laurent, G., et al. (1988) T-lymphocyte killing by T101-ricin A-chain immunotoxin: pH-dependent potentiation with lysosomotropic amines. *Blood* **72,** 1197–1202.
17. Candiani C., Franceschi A., Chignola C., Pasti M., Anselmi C., et al. (1992) Blocking effect of human serum but not of cerebrospinal fluid on ricin A chain immunotoxin potentiation by monensin or carrier protein monensin conjugates. *Cancer Res.* **52,** 623–630.
18. Jansen F. K., Jansen A., Derocq J. M., Carriere D., Carayon E., Veas F., et al. (1992) Golgi vacuolization and immunotoxin enhancement by monensin and perhexilin depend on a serum protein. *J. Biol. Chem.* **267,** 12,577–12,582.
19. Tartakoff, A. M. (1983) Perturbation of vesicular traffic with carboxylic ionophore monensin. *Cell* **32,** 663–667.
20. Duncan, R., J., S., Weston, P., D. (1983) A new reactive which may be used to introduce sulphydryl groups into proteins, and its use in the preparation of conjugates for immunoassay. *Anal. Biochem.* **132,** 68–74.
21. Higgins, W. and Miles, E., W. (1978) Affinity labeling of the pyridoxal phosphate binding site of the beta-2 subunit of *Escherichia coli* tryptophan synthase. *J. Biol. Chem.* **253,** 4648–4652.
22. Colombatti, M., Nabholz, M., Gros, O., and Bron, C. (1983) Selective killing of target cells by antibody-ricin A chain or antibody-gelonin hybrid molecules: comparison of cytotoxic potency and use in immunoselection procedures. *J. lmmunol.* **131,** 3091–3095.
23. Carlsson, J., Drevin, H., and Axen, R. (1978). Protein thiolation and reversible protein-protein conjugation. *N*-succinimidyl 3(2-pyridyldithio)propionate, a new heterobifunctional reagent. *Biochem. J.* **173,** 723–737.
24. Golab, T., Barton, S. J., and Scroggs, R. E. (1975) Colorimetric method for monensin. *J. Assoc. Anal. Chem.* **56,** 171–173.
25. Lowry, O. H., Rosebrough, N. J., Farr, A. J., and Randall, R. J. (1951) Protein measurement with the Folin phenol reagent. *J. Biol. Chem.* **193,** 265–275.
26. Cime, G. W. and Samir, B. R. (1988) Kinetics and mechanisms of the aminolysis of *N*-hydroxysuccinimide esters in aqueous buffers. *J. Org. Chem.* **53,** 3583–3586.
27. Ceruti, M., Viola, F., Dosio, F., Cattel, L., Bouvier-Navé, P., and Ugliengo, P. (1988) Stereospecific synthesis of squalenoid epoxide vinyl ethers as inhibitors of 2,3-oxidosqualene cyclase. *J. Chem. Soc. Perkin Trans.* I461–I469.
28. Tohda K., Suzuki K., Kosuge N., Watanabe K., Nagashima H., lnoue H., et al. (1990) Design and synthesis of lithium ionophores for an ion-selective electrode by chemicai modification of natural carboxylic polyether antìbiotic monensin. *Anal. Chem.* **62,** 936–942.
29. Biagi O. L., Barbaro A. M., and Guerra M. C. (1969) Partition data of cephalosporins determined by means of reversal-phase thin-layer chromatography. *J. Chromatogr.* **44,** 195–198.
30. Biagi O. L., Guerra M. C., and Barbaro A. M. (1970) Relationship between lipophilic character and hemolitic activity of testosterone esters. *J. Med. Chem.* **13,** 944–948.
31. Hunter, W. M. and Greenwood, F. C. (1962) Preparation of ^{131}iodine-labelled human growth hormone of high specific activity. *Nature* **194,** 495–498.

5

Purification and Conjugation of Type 1 Ribosome-Inactivating Proteins

Luigi Barbieri, Andrea Bolognesi, and Fiorenzo Stirpe

1. Introduction

Ribosome-inactivating proteins (RIPs, ***1***) are plant enzymes that damage ribosomes in an irreversible manner. They can be divided into type 1 RIPs, which are single-chain proteins, and type 2 RIPs, which are heterodimeric proteins consisting of an enzymatically active A-chain connected by a disulfide bond to a B-chain. The latter has the properties of a lectin specific for sugars with the galactose conformation and binds to galactosyl-terminated receptors on the cell surface, thus allowing the A-chain to enter the cytoplasm. Consequently, most type 2 RIPs are potent toxins, the best known being ricin, while type 1 RIPs are much less toxic.

Ribosome-inactivating proteins are rRNA *N*-glycosidases, that is, they remove a single adenine residue from rRNA (A^{4324} from rat liver rRNA; ***2***). More recently, it was observed than some RIPs remove more that one adenine from rRNA and that some act also on poly(A), while all RIPs remove adenine from DNA ***(3)***. For a protein to be identified as a RIP, it is necessary to ascertain that it inhibits protein synthesis and possesses rRNA *N*-glycosidase activity. This can be detected from the modification of rRNA or can be measured by determining the adenine released.

Ribosome-inactivating proteins have been linked to antibodies or other carriers (e.g., hormones, growth factors, cytokines) to form immunotoxins or conjugates specifically toxic to target cells. So far, these hybrid molecules have been studied mainly to remove malignant or immunocompetent cells, but other applications have been envisaged.

The type 2 RIPs as such cannot be used for this purpose; they must be modified to block the sugar-binding site, otherwise their B-chains would link to

From: *Methods in Molecular Biology, vol. 166: Immunotoxin Methods and Protocols*
Edited by: W. A. Hall

Table 1
Type 1 RIPs Used to Prepare Immunotoxins

Barley RIP
Bryodin
Dianthin
Gelonin
Luffin
Momordin
Pokeweed antiviral protein (PAP)
Saporin
Trichokirin
Trichosanthin

nontarget cells. More frequently, immunotoxins and other conjugates have been prepared with the A-chains of type 2 RIPs, that of ricin being the most widely employed, or with type 1 RIPs. These have the advantages over the A-chains: they are more stable, simpler and safer to prepare, and sometimes give more active conjugates. Also, they are diverse and often immunologically distinct, and consequently can be employed to overcome the immune response elicited by the administration of immunotoxins. A list of type 1 RIPs used to prepare immunotoxins is given in **Table 1**. Saporin is the most widely used RIP, as its conjugates are employed as experimental tools, especially for neurologic research ***(4,5)***.

Type 1 RIPs have molecular mass in the region of 30 kDa, are strongly basic proteins (with pI 9.5 or higher), and are generally resistant to proteases and various denaturating agents ***(1)***. These properties are exploited in the purification of these proteins and render them tolerant to the treatments for the insertion of linkers to obtain chemical conjugates. Some RIPs have been cloned, and fusion proteins have been prepared with appropriate carriers.

2. Purification of Type 1 Ribosome-Inactivating Proteins

Purification procedures for RIPs take into account the main physicochemical characteristics of RIPs. Thus, the strategies envisaged for the purification of type 1 and type 2 RIPs are quite different: type 1 RIPs may be purified by exploiting their high isoelectric points; purification of type 2 RIPs exploits the presence of a lectin chain capable of specific binding on galactose-containing matrices. The determination of RIP activity may be necessary during the adaptation of the methods here described to a particular RIP or to new plant tissues. A reticulocyte lysate mRNA-dependent translation system containing all the ingredients for in vitro translation is in our opinion the best system for unknown

RIPs, whereas ELISA or other antibody-dependent systems may do well when the RIP is known and antibodies to it are available. Direct measurements of the enzymatic activity (Endo's diagnostic fragment or direct released adenine-measurement) are more time consuming and often not feasible in the presence of crude extracts. RIP detection methods are beyond the purpose of present description and will not be described.

Type 1 RIPs are purified essentially by cation-exchange chromatography on carboxymethyl- or sulfopropyl-derivatized matrices ***(6)***, taking advantage of their pI in the extreme alkaline region. This general procedure was scaled up for pilot scale preparations with minor adaptation for each RIP ***(7)***.

2.1. Crude Enzyme Preparations for the Determination of Translational Inhibitory Activity

The following protocol may be applied to most plant tissues and is intended to obtain a crude enzyme preparation suitable to determine RIP presence and activity.

2.1.1. Materials

1. 500 m*M* sodium phosphate buffer, pH 6.67.
2. 5 m*M* sodium phosphate buffer, pH 7.0. The phosphate buffer may be prepared by dilution of a stock solution of 500 m*M* sodium phosphate buffer, pH 6.67: 100-fold dilution with double-distilled water gives pH 7.0.
3. Phosphate buffered saline (PBS): 0.14 *M* NaCl, 5 m*M* sodium phosphate buffer, pH 7.0.
4. 1 *M* sodium acetate buffer, prepared by adding under pH control 1 *M* acetic acid to 1 *M* sodium acetate.
5. 10 m*M* sodium acetate buffer, pH 4.5.
6. Liquid nitrogen.
7. Glacial acetic acid.
8. SP-sepharose (Pharmacia, Uppsala, Sweden).
9. Dialysis tubes.
10. Cheese cloth.

2.1.2. Special Equipment

1. Chromatography column 1 cm diameter × 10 cm height.
2. Optional: chromatography equipment including fraction collector, UV monitor, recorder.

2.1.3. Procedure

1. Put 10 mL SP-sepharose slurry in a vessel under vacuum with at least 5 vol of PBS at room temperature. Degas accurately. Pour the gel into the column. Wash sequentially with 1 vol of 0.5 *M* NaOH, 1 vol of 500 m*M* sodium phosphate buffer, pH 6.67, and 20 vol of 10 m*M* sodium acetate buffer, pH 4.5.

2. Freeze fresh plant material (1–2 g are a convenient quantity for assays of crude enzyme preparations) in liquid nitrogen, then grind in a mortar, adding liquid nitrogen to keep the material brittle. This operation should be performed in a protected environment to avoid spilling of the powders, which are potentially allergenic.
3. The powder is then extracted overnight at 4°C on a magnetic stirrer with 8 vol of PBS.
4. The extracts are adjusted to pH 4.0 with acetic acid under vigorous stirring and centrifuged at 16,000*g* for 30 min at 0–2°C. The temperature at which the centrifugation is performed is critical because the fatty materials often contained in high quantities in plant materials (some oily seeds may contain more than 10% fat) may be easily separated as a layer of floating solidified fat. The clear supernatant is decanted carefully and solidified fat is removed by filtering through a double layer of cheese cloth.
5. The supernatant is then applied to a column of SP-sepharose 1 cm in diameter × 5 cm in height. The column is sequentially eluted with 10 m*M* sodium acetate buffer, pH 4.5 (either 10 vol or alternatively to absorbance at 280 nm of the effluent lower than 0.1), 5 m*M* sodium phosphate buffer, pH 7.0 (1 vol), 1 *M* NaCl containing 5 m*M* sodium phosphate buffer, pH 7.0 (3 vol).
6. The last effluent contains the crude enzyme preparation and is dialysed against 100 vol of PBS overnight. (Alternatively, the buffer may be exchanged by chromatography on Sephadex G-25.)
7. This preparation may be stored frozen at –20°C. Activity is usually stable for years, but division in aliquots is recommended to avoid repeated cycles of freezing and thawing. This crude enzyme preparation is suitable for the determination of translational inhibitory activity, even in plant tissues with very low RIP content.

2.2. Small-Scale Purification of Type 1 RIPs

2.2.1. Materials

1. 500 m*M* sodium phosphate buffer, pH 6.67.
2. 5 m*M* sodium phosphate buffer, pH 7.0.
3. PBS.
4. 1 *M* sodium acetate buffer.
5. 10 m*M* sodium acetate buffer, pH 4.5.
6. Liquid nitrogen.
7. Glacial acetic acid.
8. Sephadex G-25, SP-Sepharose and CM-Sepharose from Pharmacia.
9. Dialysis tubes.
10. Cheese cloth.

2.2.2. Special Equipment

1. Tissue homogenizer: Ultra-Turrax apparatus.
2. Chromatography column 2 cm in diameter × 30 cm in height (two columns if possible).

3. Chromatography equipment including peristaltic pump, gradient maker, fraction collector, UV monitor, recorder.
4. Amicon concentrator equipped with a YM 2 or YM10 membrane.

2.2.3. Optional Materials and Equipment

1. Kitchen centrifuge.
2. If further purification steps are required, additional materials are necessary as specified in **Subheading 2.2.5.**

2.2.4. Methods

The procedure described here allows for the purification of milligrams quantities of RIPs from various plant sources and is a generalization of the procedure described for the purification from more than a dozen different plant materials ***(1)***. The preparations obtained with this procedure are often pure (more than 95% as judged by SDS electrophoresis or HPLC reverse-phase chromatography). In several cases, further purification is necessary. Purification may be monitored at each step by determining the inhibition of protein synthesis in the rabbit reticulocyte system.

1. In preparing crude extracts, the aim is to obtain a finely grounded slurry that can be conveniently agitated with a magnetic stirrer. Different procedures may be utilized depending on the type of plant tissue to be extracted. Using 500 g of leaves, prepare a powder with the aid of liquid nitrogen as described in **Subheading 2.1.3.**, then make a slurry with 5 vol of PBS and grind with an Ultra-Turrax apparatus. Using 100 g of roots, cut into small pieces and then subject to homogenization as above, or extract the juice in a kitchen centrifuge depending upon the water content of the tissue; in any case less, than 5 vol of PBS are generally sufficient to make a liquid slurry. Using 25 g of seeds, homogenize in 8 vol of PBS with an Ultra-Turrax apparatus.
2. Extract overnight at 4°C with a magnetic stirrer. Filter the extracts through cheesecloth, adjust to pH 4.0 with acetic acid, and centrifuge at 16,000*g* for 30 min at 0°C. Remove fatty material by filtering through cheese cloth if necessary. The clear supernatant is referred to as the crude extract.
3. Apply crude extract to an SP-sepharose (13 × 2 cm) column prepared as described above equilibrated with 10 m*M* sodium acetate buffer, pH 4.5, at room temperature. The column is washed with equilibration buffer until the A_{280} decreases to near the baseline and then with 5 m*M* sodium phosphate buffer, pH 7.0. Bound protein (crude extract) is eluted with 1 *M* NaCl in 5 m*M* sodium phosphate buffer, pH 7.0.
4. The crude extract is dialyzed overnight against 100 vol of 5 m*M* sodium phosphate buffer, pH 7.0. Any precipitated material is removed by centrifugation as above.
5. The crude extract is applied to a CM-sepharose column (25 × 2 cm) equilibrated with the dialysis buffer. The column is washed with the same buffer until the

effluent absorbance at 280 nm is near baseline and then eluted with 800 mL of a linear (0–0.3 *M*) gradient of NaCl in the equilibration buffer, flow rate 1 mL/min. Collect fractions of approx 3–4 mL. Test translation inhibitory activity of protein containing peaks at various dilutions (generally 1:1000 to 1:100,000, depending upon RIP content). As a rule, more than one active peak may be found in each plant material since RIPs are usually present in multiple isoforms.

6. Pool RIP-containing fractions, dialyze extensively against water, and then either (1) concentrate with an Amicon concentrator equipped with a YM2 or YM10 membrane (PM10 membranes allow for faster concentration and may be used but are somewhat more leaky) to approx 5 mg/mL and store in aliquots at –20°C (if required you may filter through 0.45 μm sterilization filters before freezing); or (2) freeze-dry and store at –20°C. The product of this second procedure is stable for years and may be transported at room temperature, but it may not redissolve completely, thus reducing the final yield of product.
7. RIPs purified in this way may not be pure enough. The first suggested procedure is to expand the gradient volume across the NaCl concentrations that elute the RIP-containing material. If this is not enough, several other methods have been envisaged to remove impurities from RIP preparations. The choice depends upon the nature of the contaminants to be removed. The most commonly used are described **Subheading 2.2.5.**

2.2.5. Further Purification Steps

1. Low–molecular-weight contaminants (3000–10,000 Mr) may be easily removed by either gel filtration on a Sephadex G-50 column, or by repeated concentrations and dilutions on an Amicon concentrator equipped with a PM10 membrane. Use a suitable column (2–5 cm diameter × 95 cm height); run in PBS at room temperature; do not apply samples larger than 5% of the volume of the column; and bear in mind that the first peak to be eluted contains the RIP.
2. Use gel filtration on a Sephacryl-S200 HR column to eliminate high–molecular-weight contaminants. Again, use a suitable column (2–5 cm diameter × 95 cm height); run in PBS (NaCl up to 0.3 *M* may be used if unspecific interactions appear) at room temperature; do not apply samples larger than 3% of the volume of the column; and calibrate the column with molecular-weight markers. The RIP peak is usually eluted with an apparent molecular weight somewhat lower than expected: 20,000–25,000. If not sure, test for translational inhibitory activity.
3. Nuclease (RNase and DNase) removal may be critical if the study of the mechanism of action is one use of the RIP preparation. Procion Red dye chromatography (red-sepharose, Pharmacia) may be useful for the removal of minute contamination with nucleases that are present in preparations appearing to be of great purity (>98% as judged by electrophoresis; ***8***). Up to 10 mg of protein per 10 mL of red sepharose may be applied at pH 8.0 in 20 m*M* Tris-HCl at room temperature. RIPs are retained under these conditions and can be eluted with a gradient of NaCl. The gradient has to be adjusted for each RIP with a starting condition of 0–300 m*M* NaCl in a total volume 20-fold that of the column. The

RIP will elute in a very broad peak; peak fractions usually contain nuclease-free RIP, whereas nucleases elute along with the tail of the peak. Due to tail elimination, this method is to be used only if rigorously nuclease-free RIP is necessary, since losses may be as high as 40–50%.

4. Several RIPs interact with Cibachrome blue (blue sepharose, Pharmacia; ***9–13***) not only through the charged groups of the dye, thus allowing purification with an easy method that can be added to previous steps. Because this interaction is fairly specific for each RIP, chromatography conditions have to be tuned for each protein. The conditions described here allow for the purification and the separations of several isoforms of pokeweed antiviral protein (PAP) from different tissues (Barbieri, L., Carnicelli, D., and Stirpe, F., unpublished results). Column dimensions: 2 cm diameter × 20 cm height; application and run buffer: 10 m*M* Tris-HCl, pH 8.0 (pH is critical for reproducibility of complex mixtures); gradient from 0–300 m*M* NaCl in the same buffer (gradient conditions have to be adapted to each RIP, e.g., gelonin requires gradients up to 1 *M*); the gradient volume has to be approx 20 column vol, run at room temperature. The drawbacks of this procedure are very diluted samples and dye-containing media that are not easily cleaned of all contaminants.
5. As a last resort (due to rather difficult reproducibility), try a step of hydrophobic chromatography between the two cation-exchange chromatographies. First, adjust S-sepharose fractions to 20% (w/v) ammonium sulphate, centrifuge to eliminate the precipitate, then apply to a phenyl-sepharose column (2 cm diameter × 10 cm height) equilibrated with 0.5 *M* NaCl containing 20% (w/v) ammonium sulphate and 20 m*M* sodium phosphate buffer, pH 6.7. The unretarded fraction is adjusted to 1 *M* NaCl plus 40% (w/v) ammonium sulphate, and is applied to a second column of phenyl-sepharose equilibrated with 1 *M* NaCl containing 40% (w/v) ammonium sulphate and 20 m*M* sodium PBS, pH 6.7. The column is washed with equilibration buffer and then bound protein is eluted with PBS. This method works fine with several tissues from *Saponaria officinalis* ***(14)***, but may need tuning to work with other plant extracts.

3. Preparation of Immunotoxins Containing Type 1 RIPs

It is well established that immunoconjugates that contain single-chain RIPs exhibit maximal cytotoxicity only when the toxin molecule is released from the targeting vehicle in a fully active form. The separation of the RIP molecule from the carrier is required to avoid steric hindrance and to allow an effective translocation of the toxin into the cytoplasm ***(15)***. At present, the disulfide bond is the only type of linkage that appears to fit these criteria, albeit not perfectly ***(16)***.

The coupling of two different protein macromolecules that results in heterodimer formation requires that each protein is modified prior to mixing them to react. In the case of the A-chains of type 2 RIPs, the modification is limited to the reductive cleavage of the native cystine residue that links the

active (A) and the binding (B) fragments of the molecule. For type 1 RIPs and for carrier molecules this is not possible, because cystine residues are absent or, when present, are involved in maintaining the tertiary and/or quaternary structure of the protein (i.e., it is not possible to reduce them without loss of the specific protein function). Moreover, presumably some of the cystine residues are not sterically accessible, as it was demonstrated by the 10 thiol groups per immunoglobulin that had to be generated for an optimal conjugation to an activated RIP ***(17)***.

For these reasons in type 1 RIPs and in most carrier molecules, thiol groups are chemically inserted using heterobifunctional reagents, and methods have been developed in order to generate heteroconjugates, avoiding or reducing to a minimum the formation of homopolymers. The most efficient and specific crosslinking techniques generally involve first the insertion of a free thiol group on a modified protein (usually the RIP) and secondly, the modification of the carrier protein to introduce a group that will react selectively with those thiols.

In most cases, the reagents used to introduce thiol groups react with amino groups, forming amide or amidine bonds. Amino groups are reactive, abundant, and in a limited way for most proteins, expendable. That is, one can modify a limited number of amino groups without diminishing the biological activity of the protein ***(17)***.

The most commonly used reagents for the introduction of free sulphydryl groups are *N*-succynimidyl 3-(2-pyridyl-dithiopropionate) (SPDP) and methyl 4-mercaptobutyrimidate (2-iminothiolane, Traut's reagent). SPDP introduces 2-pyridyl disulfide groups into the protein by reacting with amino groups to form neutral amides. 2-Iminothiolane introduces mercaptobutyrimidoil groups, reacting to form charged amidines and thus preserving the positive charge of the derivatized amino acid. Consequently, 2-iminothiolane has little or no effect on the conformation of the protein and biological activity is usually retained while SPDP produces a significant decrease. However, an excess of derivatization always results in a reduction of activity, probably owing to the modification of basic amino acid in the catalytic site of the RIP or in the binding sites of the carrier protein ***(16)***.

It should be noted that both linking reagents bring the thiol group on a spacer arm that make it much more accessible and reactive than free sulfhydryl groups generated by the reduction of native cystine residues. Usually, we introduce an average two groups per antibody molecule and 0.7–1.0 group per RIP molecule.

The preparation of conjugates is generally carried out by first modifying the single-chain RIP with 2-iminothiolane. The free thiol groups inserted are then reacted with a large molar excess of 5,5'-dithiobis (2-nitrobenzoic acid, Ellman's reagent) in order to avoid formation of homopolymer. The carrier (usually an antibody) can be modified in the same way or alternatively with

SPDP, in both cases introducing protected and activated disulfide. One of the two modified protein (usually the RIP without an accessible native disulfide) is then reduced in mild conditions and immediately mixed with the other modified protein. The thiopyridyl moiety (which protects the SPDP sulfhydryl group) and the 5-thio-2-nitrobenzoic acid (introduced with Ellman's reagent to protect the 2-iminothiolane sulfhydryl group) are also good leaving groups. Thus, the conjugate is finally formed in a thiol-disulfide exchange reaction ***(17)***.

Protein modification usually generates a mixture of modified species, both with respect to the site of modification and the number of groups introduced. With a given average number of inserted groups, the frequency of the various classes will follow the distribution of Poisson. The extent to which the proteins in a given conjugation reaction are modified is of considerable importance if one wishes to maximize the yield of the desired conjugate species. Undermodification of the proteins results in a poor yield of conjugate, while overmodification of the proteins results in the formation of large, highly crosslinked protein aggregates. With the degrees of derivatization mentioned above, and using a 5–7-fold molar excess of toxin over antibody, we optimized the yield of conjugate with respect to the antibody. Typically, we achieved, after careful purification, a conjugate preparation with a 40% yield with respect to the antibody.

3.1. Materials

1. 500 m*M* sodium phosphate buffer, pH 7.5.
2. 5 m*M* sodium phosphate buffer, pH 7.5.
3. PBS.
4. 1 *M* sodium borate buffer, pH 9.0, prepared by adding under pH control 1 *M* NaOH to 1 *M* boric acid.
5. 50 m*M* sodium borate buffer, pH 9.0, prepared by dilution of the 1 *M* sodium borate buffer stock solution, pH 9.0.
6. 2-Iminothiolane (Traut's reagent; Sigma-Aldrich, St. Louis, MO).
7. Glycine (Sigma-Aldrich).
8. 5,5'-dithiobis-(2-nitrobenzoic acid) (DTNB, Ellman's reagent; Sigma-Aldrich).
9. *N*-succynimidyl 3-(2-pyridyl-dithiopropionate; SPDP; Sigma-Aldrich).
10. Dimethylformamide for UV-spectroscopy (Fluka, Buchs, Switzerland).
11. DL dithiothreitol, or alternatively 2-mercaptoethanol (Sigma-Aldrich).
12. Sephadex G-25 and Sephacryl S-200 (or S-300; Pharmacia, Uppsala, Sweden).
13. Liquid nitrogen.

3.2. Special Equipment

1. Chromatography columns (30–50 cm height for the Sephadex G-25 desalting chromatography, and 100 cm height for the Sephacryl S-200 chromatography).
2. Chromatography equipment including peristaltic pump, fraction collector, UV monitor, and recorder.

3. Stirred ultrafiltration cell equipped with a YM10 membrane (Amicon, W.R. Grace & Co, Beverly, MA).
4. Nitrogen cylinder equipped with a manometer and pressure valve.
5. Gamma counter.

3.3. Derivatization of Type 1 RIPs

1. Dissolve the type 1 RIP in nine-tenths of the volume you need in distilled water. Add one-tenth in volume of 0.5 *M* sodium borate buffer, pH 9, and then add (^{125}I)RIP (1×10^6 cpm in few microliters) and centrifuge or pass through a 0.45-μm syringe filter. The final concentration of the single-chain RIP is usually 5–10 mg/mL in 50 m*M* sodium borate buffer, pH 9.
2. Add 2-iminothiolane in 50 μL to a final concentration of 1 m*M*. 2-Iminothiolane is dissolved immediately prior to use in 50 m*M* sodium borate buffer, pH 9.
3. After 60 min at 28°C, add solid glycine to a final concentration of 200 m*M*, and dissolve it immediately by vortex mixing.
4. After 30 min at room temperature, Ellman's reagent is added in 20–50 μL of *N*,*N*-dimethylformamide to a final concentration of 2.5 m*M* (the solution must be made immediately before use). To avoid protein denaturation, the volume of *N*,*N*-dimethylformamide in which the Ellman's reagent is dissolved must be kept to a minimum and added while mixing the protein solution on a vortex. Alternatively, Ellman's reagent can be dissolved in less denaturating (but less efficient) organic solvents like ethanol.
5. After 15 min at room temperature, the reaction mixture is applied to a Sephadex G-25 coarse column, equilibrated and eluted with 5 m*M* sodium phosphate buffer, pH 7.5, containing PBS. Many single chain RIPs start to denature during this reaction; for this reason the incubation must be stopped if some precipitate appears. For gelonin, an immediate chromatographic separation is advisable, reducing the reaction time to 1–2 min at maximum.
6. The protein peak that elutes first is collected following the absorbance at 280 nm.
7. The estimation of the number of mercaptobutyrimidoyl groups introduced is based on the differential absorbance at 412 nm of the 5-thio-2-nitrobenzoic acid, prior and after reduction (5-thio-2-nitrobenzoic acid is introduced by reacting with Ellman's reagent, *see* **step 4**); 0.2 mL are diluted to 1 mL with PBS, and the A_{280} and A_{412} are determined before and after the addition of 0.1 mL (1/10 vol/vol) of freshly prepared 0.55 *M* dithiothreitol or 0.22 *M* 2-mercaptoethanol.
   Typical absorbance values:

	A_{280}	A_{412}
–DTT	0.288	0.012
+DTT	—	0.146

   Normalization for the dilution:

A_{280} (–DTT): $0.288 \times (1000/200) = 1.440$
A_{412} (–DTT): $0.012 \times (1000/200) = 0.060$
A_{412} (+DTT): $0.146 \times (1100/200) = 0.803$

Calculation of derivatization ratio:

$$A_{412}\ (+DTT) - A_{412}\ (-DTT) = 0.803 - 0.060 = 0.743$$

This value, divided for the molar extinction coefficient at 412 nm of the 5-thio-2-nitrobenzoic acid (TNB) (13,600, as reported in ***(18)***) gives the concentration of the mercaptobutyrimidoyl groups introduced:

$$0.743/13{,}600 = 5.463 \times 10^{-5}\ M \text{ mercaptobutyrimidoyl groups inserted.}$$

The protein concentration is calculated by the A_{280} after the subtraction of the contribution due to TNB (ε_{280}^{M} 2490; ***13***), while the mercaptobutyrimidoyl group does not contribute.

$$5.463 \times 10^{-5}\ M \times 2490\ (\text{TNB } \varepsilon_{280}^{M}) = 0.136,$$
that is the contribution of TNB at A_{280}.

$$A_{280} - A_{280} \text{ due to TNB} = 1.440–0.136 = 1.280$$
(protein contribution to A_{280}).

Dividing this value for the molar extinction coefficient at 280 nm of the single-chain RIP (i.e., 24,000 for saporin-6 and many other RIPs), we have the molar concentration of the protein:

$$1.280/24{,}000 = 5.333 \times 10^{-5}\ M \text{ (RIP concentration).}$$

The number of mercaptobutyrimidoyl groups introduced per protein molecule can be finally calculated:

$$\text{mercaptobutyrimidoyl groups/RIP} = 5.463 \times 10^{-5}\ M/5.333 \times 10^{-5}\ M = 1.02.$$

3.4. Derivatization of IgG Antibody

1. The antibody can be modified with 2-iminothiolane, as reported above, with the following modification: The concentration of the linking reagent will be 0.3–0.6 m*M*, depending on the reactivity of the antibody used, and the protein molar extinction is 210,000.
2. Alternatively, IgG proteins can be modified with SPDP, which in the following conditions, do not significantly affect the antigen-binding property.

3.4.1. SPDP Reaction

1. Prepare an IgG solution in 50 m*M* sodium borate buffer, pH 9, to a final concentration ranging from 3–10 mg/mL.
2. Add SPDP, dissolved immediately prior to use in 20–50 μL of *N*,*N*-dimethylformamide, to a final 2.5–4.0 SPDP:IgG molar ratio (depending on the antibody reactivity).
3. After 30 min at room temperature, apply the reaction mixture to a Sephadex G-25 coarse column equilibrated and eluted with PBS, pH 7.5.
4. The protein peak that elutes first is collected following the absorbance at 280 nm.

5. The estimation of the number of 2-pyridyl disulfide groups introduced is based on the absorbance at 343 nm of the thiopyridyl moiety, released as a leaving group upon reaction with free thiols ***(20)***. The absorbance of an appropriate dilution of the sample, depending on the starting MoAb concentration, is determined at 280 and 343 nm before and after the addition of 1/10 vol/vol of freshly prepared 0.55 *M* DTT or 0.22 *M* 2-mercaptoethanol. Typical absorbance values:

	A_{280}	A_{343}
–DTT	0.312	0.014
+DTT	—	0.032

Normalization for the dilution:

A_{280} (–DTT): $0.305 \times (1000/200) = 1.525$
A_{343} (–DTT): $0.014 \times (1000/200) = 0.070$
A_{343} (+DTT): $0.036 \times (1100/200) = 0.180$

Calculation of the derivatization ratio:

$$A_{343}\ (+DTT) - A_{343}\ (-DTT) = 0.180–0.070 = 0.110$$

This value, divided for the molar extinction coefficient at 343 nm of the thiopyridyl moiety (8080; ***20***), gives us the concentration of the inserted groups:

$$0.110/8080 = 1.361 \times 10^{-5}\ M \text{ 2-mercaptopropionyl inserted groups.}$$

The protein concentration is calculated by the A_{280} after the subtraction of the contribution due to 2-pyridyl disulfide groups:

$$1.361 \times 10^{-5} \times 5100\ (\text{2-pyridyl disulfide } \varepsilon_{280}{}^{M})\ \textbf{\textit{(20)}} = 0.069,$$
which is the contribution of 2-pyridyl disulfide at A_{280}.

$$A_{280} - A_{280} \text{ due to 2-pyridyl disulfide} = 1.525 - 0.069 = 1.456$$
(IgG contribution to A_{280}).

Dividing this value for the molar extinction coefficient at 280 nm of the antibody (210,000 for IgG), we have the molar concentration of the protein:

$$1.456/210{,}000 = 6.933 \times 10^{-6}\ M \text{ (IgG concentration)}$$

$$\text{2-pyridyl disulfide groups/IgG} = 1.361 \times 10^{-5}\ M/6.933 \times 10^{-6}\ M = 1.96.$$

3.5. Conjugation

1. Take a 5–7-fold molar excess of the modified type 1 RIP.
2. Concentrate the protein solution under nitrogen pressure by using an Amicon concentrator to reach a volume of about one-tenth of the desalting column.
3. Remove 5-thio-2-nitrobenzoic acid by adding 1/10 in volume of freshly prepared 0.55 *M* DTT or 0.22 *M* 2-mercaptoethanol.
4. Apply the reduced protein to a Sephadex G-25 coarse column to remove excess reducent and the leaving protective group.
5. Collect the protein peak into an Amicon concentrator in which the modified IgG is stirred.

6. Concentrate the reaction mixture fourfold under nitrogen pressure.
7. Allowed the two proteins to react for 20 h at room temperature (or for 72 h at 4°C) in the concentrator cell with a nitrogen-saturated atmosphere.

3.6. Purification of Immunotoxins

Under the described conditions, the immunotoxin is predominantly a mixture of antibody linked to one or two toxin molecules, sometimes with the presence of high–molecular-weight aggregates (two IgG linked to several RIPs). Moreover, the reaction gives rise to a number of products other than immunotoxin, such as free and polymeric RIP and free antibody. A careful purification is needed to obtain a relatively pure product.

Size-exclusion chromatography is the purification procedure with least effect on the immunotoxin properties. However, immunotoxin and free antibody cannot be resolved in two distinct peaks. Thus, in order to eliminate free antibodies, it is necessary to follow the elution profile of the iodinated RIP, (*see* **Subheading 3.3.**).

1. The reaction mixture is applied to a Sephacryl S-200 (or S-300) high-resolution column (at least 100 cm of length; Pharmacia, Uppsala, Sweden). The column is equilibrated and eluted in PBS, which is the buffer of choice for storage and biological tests unless otherwise stated.
2. The radioactivity is reported on the absorbance elution profile at 280 nm.
3. First elute the high–molecular-weight conjugates (HMW), next the low–molecular-weight conjugates (LMW), and then in order trimeric, dimeric, and unreacted RIP. The free antibody elutes in the last part of the LMW absorbance peak. The fractions containing the immunotoxin are pooled following the radioactivity that is typically shifted from the absorbance profile in the LMW peak ***(21)***.
4. The RIP/IgG ratio is calculated as in the following example:

	A_{280}	cpm/mL
LMW conjugate	0.192	1427
Free RIP	0.376	18,891

$$18{,}891/0.376 = 50{,}242 \text{ cpm/1 OD unit (free RIP)}$$

$$1427/50{,}242 = 0.028 \text{ (RIP contribution to the } A_{280} \text{ of the conjugate)}$$

$$0.192–0.028 = 0.164 \text{ (IgG contribution to the } A_{280} \text{ of the conjugate)}$$

Dividing the absorbance of the two proteins for the respective molar extinction coefficient (24,000 for many RIP; 210,000 for IgG) we obtain the relative concentration:

$$0.028/24{,}000 = 1.166 \times 10^{-6}\ M \text{ (RIP in the immunotoxin)}$$

$$0.164/210{,}000 = 0.781 \times 10^{-6}\ M \text{ (IgG in the immunotoxin).}$$

The average RIP/IgG ratio is 1.166/0.782 = 1.49.

Immunotoxins can be frozen in liquid nitrogen or at –80°C for many years without loss of activity. It is advisable to divide the immunotoxin into aliquots to avoid repeated freeze-thawing procedures. Sterile solutions of immunotoxins are stable for months at 4°C.

References

1. Barbieri, L., Battelli, M. G., and Stirpe, F. (1993) Ribosome-inactivating proteins from plants. *Biochim. Biophys. Acta* **1154,** 237–282.
2. Endo, Y. (1988) Mechanism of action of ricin and related toxins on the inactivation of ribosomes, in *Immunotoxins* (Frankel, A. E., ed.), Kluwier Academic Publishers, Boston, MA, pp. 75–89.
3. Barbieri, L., Valbonesi, P., Bonora, E., Gorini, P., Bolognesi, A., and Stirpe, F. (1997) Polynucleotide:adenosine glycosidase activity of ribosome-inactivating proteins: effect on DNA, RNA and poly(A). *Nucleic Acids Res.* **25,** 518–522.
4. Rossner, S. (1997) Cholinergic immunolesions by 192IgG-saporin—Useful tool to simulate pathogenic aspects of Alzheimer's disease. *Int. J. Dev. Neurosci.* **15,** 835–850.
5. Wiley, R. G. and Lappi, D. A. (1995) *Suicide Transport and Immunolesioning*. R. G. Landes, Austin, TX.
6. Stirpe, F., Gasperi-Campani, A., Barbieri, L., Falasca, A. I., Abbondanza, A., and Stevens, W. A. (1983) Ribosome-inactivating protein from seeds of *Saponaria officinalis L.* (soapwort), of *Agrostemma githago L.* (corn cockle) and of *Asparagus officinalis L.* (asparagus), and from the latex of *Hura crepitans L.* (sand box tree). *Biochem. J.* **216,** 617–625.
7. Barbieri, L., Stoppa, C., and Bolognesi, A. (1987) Large scale chromatographic purification of ribosome-inactivating proteins. *J. Chromatogr.* **408,** 235–243.
8. Valbonesi, P., Barbieri, L., Bolognesi, A., Bonora, E., Polito, L., and Stirpe, F. (1999) Preparation of highly purified momordin II without RNase activity. *Life Sci.* **65,** 1485–1491.
9. Barbieri, L., Bolognesi, A., Cenini, P., Falasca, A. I., Garofano, L., Guicciardi, A., et al. (1989) Ribosome-inactivating proteins from plant cells in culture. *Biochem. J.* **257,** 801–807.
10. Sperti, S., Montanaro, L., Rambelli, F., and Zamboni, M. (1986) Interaction of alpha-sarcin and gelonin with Cibacron blue. *Biosci. Rep.* **6,** 901–908.
11. Dosio, F., Brusa, P., Delprino, L., Ceruti, M., Gerosa, G., Cattel, L., et al. (1993) A new "solid phase" procedure to synthesize immunotoxins (antibody-ribosome inactivating protein conjugates). *Farmaco* **48,** 105–115.
12. Sperti, S., Montanaro, L., and Rambelli, F. (1986b) Dye affinity chromatography of ricin subunits. *Biosci. Rep.* **6,** 1035–1040.
13. Watanabe, K. and Funatsu, G. (1987) Interaction of Cibacron blue F3GA and polynucleotides with ricin A-chain, 60S ribosomal subunit-inactivating protein. *Biochim. Biophys. Acta* **914,** 177–184.
14. Ferreras, J. M., Barbieri, L., Girbés, T., Battelli, M. G., Rojo, M. A., Arias, F. J., et al. (1993) Distribution and properties of major ribosome-inactivating proteins

(28 S rRNA N-glycosidases) of the plant *Saponaria officinalis* L. (Caryophyllaceae). *Biochim. Biophys. Acta* **1216,** 31–42.
15. Trush, G. R., Lark, L. R., Clinchy, B. C., and Vitetta, S. E. (1996) Immunotoxins: an update. *Annu. Rev. Immunol.* **14,** 49–71.
16. Lambert, J. M., Blattler, W. A., McIntyre, G. D., Goldmacher, V. S., and Scott, C. F. Jr. (1988) Immunotoxins containing single chain ribosome-inactivating proteins, in *Immunotoxins* (Frankel, A. E., ed.), Kluwer Academic Publishers, Boston, MA, pp. 175–209.
17. Marsh, J. W., Srinavasachar, K., and Neville, D. M., Jr. (1988) Antibody-toxin conjugation, in *Immunotoxins* (Frankel, A. E., ed.), Kluwer Academic Publishers, Boston, MA, pp. 213–237.
18. Ellman, G. L. (1959) Tissue sulfhydryl groups. *Arch. Biochem. Biophys.* **82,** 70–77.
19. Riddles, P. W., Blakeley, R. L., and Zerner, B. (1979) Ellman's reagent: 5-5'-dithiobis(2-nitrobenzoic acid)—a reexamination. *Anal. Biochem.* **94,** 75–81.
20. Carlsson, J., Drevin, H., and Axén, R. (1978) Protein thiolation and reversible protein-protein conjugation. *N*-succynimidyl 3-(2-pyridyldithio)propionate, a new heterobifunctional reagent. *Biochem. J.* **173,** 723–737.
21. Bolognesi, A., Tazzari, P. L., Tassi, C., Gromo, G., Gobbi, M., and Stirpe, F. (1992) A comparison of anti-lymphocyte immunotoxins containing different ribosome-inactivating proteins and antibodies. *Clin. Exp. Immunol.* **89,** 341–346.

6

Comparison of Immunotoxins Bearing a Single Saporin Molecule with Multiple Toxin Conjugates

David J. Flavell and Sopsamorn U. Flavell

1. Introduction

Immunotoxins (IT) constructed by conventional chemical means using heterobifunctional crosslinking reagents such as [*N*-succinimidyl 3-(2-pyridyldithio)propionate (SPDP) or 4-succinimidyloxycarbonyl-α methyl-α-(2-pyridyldithio) toluene (SMPT) are heterogeneous with regard to the site of attachment of toxin to antibody and to the number of toxin molecules linked per antibody molecule ***(1,2)***. Such constructs inevitably contain mixtures of hybrid molecules comprised of one antibody molecule coupled covalently via a disulfide bond to one, two, or even three toxin moieties ***(3)***. Such heterogeneity makes it difficult to accurately evaluate the pharmacologic and therapeutic properties of this class of molecule. A number of independent reports have in the past demonstrated that ITs containing more than one toxin moiety per unit antibody molecule are significantly more potent in vitro for the respective antigen expressing target cell ***(3,4)***. While this has been shown to be generally true for IT performance in vitro, the same has not been consistently demonstrable in vivo. For instance, Ghetie et al. have shown that anti-CD19 and anti-CD25 ricin A-chain (RTA) ITs containing two RTA moieties per unit antibody show an increased potency for target-antigen–expressing cell lines in vitro, compared with ITs containing a single RTA moiety ***(5)***. However, in SCID mice bearing the human B-cell lymphoma cell line Daudi, the IT containing two RTA performed no better therapeutically than the IT containing just one RTA molecule. In the same report, an anti-CD22 RTA-IT containing two RTA molecules was not only seven times more potent in vitro but also significantly better therapeutically in the same SCID mouse model of human lymphoma ***(5)***.

From: *Methods in Molecular Biology, vol. 166: Immunotoxin Methods and Protocols*
Edited by: W. A. Hall © Humana Press Inc., Totowa, NJ

Contradicting these findings, Myers and associates have shown that the anti-CD19 IT B43-PAP containing two pokeweed antiviral protein (PAP) molecules per antibody molecule is more potent both in vitro and also in vivo in a SCID mouse model of human acute lymphoblastic leukemia (ALL) than a similar IT containing only one PAP molecule per unit antibody ***(6)***. We have shown that an anti-CD7 IT HB2-saporin containing two saporin molecules (2-mer) per unit antibody is almost six times more potent in vitro against the human CD7+ T-ALL cell line HSB-2 than the one saporin molecule containing IT (1-mer; ***7***). However, the 2-mer IT performed no better than the 1-mer IT in vivo in SCID mice bearing the same human T-ALL cell line. We also found the 2-mer IT to be considerably more toxic for mice than the 1-mer equivalent. Similar increases in toxicity have generally not been seen for RTA- or PAP-ITs containing two toxin moieties. These results suggest that ITs containing two toxin moieties may perform differently when directed against different target molecules, though why this should be reflected in vitro but not always in vivo is not at all clear.

Arguably, the pharmacokinetic characteristics of the conjugates containing two toxins may differ and result in a reduction in the amounts of ITs available in the blood to levels that are suboptimal for a particular target molecule. It may be that target antigens such as CD22, which deliver toxin to the appropriate compartment within the cell interior with great efficiency, are more tolerant of lower blood levels of IT and remain capable, even at such lower levels of delivering what is effectively still a potent dose. We have shown that the HB2-saporin 2-mer IT has a prolonged half-life, compared with the equivalent 1-mer IT in the blood of normal and tumor-bearing SCID mice, and we have speculated that this might account for the increased toxicity that is seen with this particular IT species ***(7)***.

Thus, there is a lack of clarity as to whether it would be advantageous to utilize ITs containing two or more toxin molecules per unit antibody. In attempting to improve the therapeutic index of IT-based therapies, it is important to establish this clearly, thus justifying the development of such therapeutics for use in humans. Identifying the best target molecules and toxins in terms of the most favorable potencies and lack of toxicity should be a high priority for pursuit. One strategy would be to explore these issues as expeditiously as possible utilizing chemically constructed ITs, and to use the emerging results to guide and justify an effort to eventually construct appropriate and better-defined recombinant ITs.

2. Materials

1. CM-Sepharose: CM-Sepharose was purchased from Amersham-Pharmacia.
2. 5 m*M* phosphate buffer (various pHs): 5 m*M* sodium phosphate buffer is prepared by mixing together component A with component B in different propor-

tions to yield buffer with the desired pH value. Detailed below is the composition of components A and B (*see* **Note 1**).

3. Component A:
   Potassium dihydrogen phosphate (KH_2PO_4) 9.1 g
   H_2O 1000 mL
4. Component B:
   Sodium dihyrogen phosphate (NaH_2PO_4) 4.75 g
   H_2O 500 mL
   Table 1 below details the amounts of A + B required to yield buffers with the desired pH value.

Table 1

	Volume required (mL)		
Desired pH	Component A	Component B	Water
6.5			
7.0	400 mL	600 mL	4000 mL
7.5	200 mL	800 mL	4000 mL
8.0	50 mL	950 mL	4000 mL

Other pH values may be arrived at within a useful range from 6 to 8.5 by altering the proportions of A and B mixed together.

5. Low-pressure chromatography equipment: We favor either the BioRad Econo System or the BioLogic system for the type of low-pressure chromatography work demanded here. In particular, the software interface on the BioLogic system combined with the precision of the pump head allows for gradients to be designed and applied with a high degree of precision and reproducibility. Any low-pressure column with appropriate adaptors and meshes is suitable, though we tend to favor the Pharmacia KX series of columns for ease of use.
6. Isoelectric focusing equipment: Though not absolutely essential, a flat-bed or vertical isoelectric focusing apparatus (IEF) is useful for determining the isoelectric points (PI) of antibodies. This allows one to make predictions about the binding and elution characteristics of both unconjugated antibody and immunoconjugates on CM-sepharose. Precast IEF gels within a working range from 6–9 are available from several suppliers.
7. Conductivity meter: An accurate conductivity meter is an essential item of equipment needed to measure the conductivities of buffers and samples prior to application to the CM-sepharose column.
8. SDS-PAGE equipment: An apparatus for conducting sodium dodecyl polyacrylamide gel electrophoresis (SDS-PAGE), according to the method of Laemmli, is essential for determining molecular weights of species eluted from the CM-sepharose column. SDS-PAGE analysis is conducted in these circumstances

under nonreducing conditions to retain the integrity of each IT species (composed of two immunoglobulin heavy and light chains, and one, two, or three saporin components coupled covalently via reducible disulfide bonds). Reductive cleavage of these bonds would thus prevent the determination of the molecular weight of the entire hybrid IT molecule made from these subunits. We have found 5% polyacrylamide gels to be the most appropriate for resolving the various unconjugated antibodies and IT species generated in the molecular weight range between 150–240 kDa. There are several manufacturers of SDS-PAGE equipment and precast gels, which include BioRad and Amersham-Pharmacia.

3. Methods

1. The ribosome-inactivating protein (RIP) saporin is highly basic with a measurable PI for the SO6 isoform between 9 and 9.4. The highly basic nature of this RIP can be exploited in preparative procedures to separate the different molecular species comprised of conjugates of one, two, or three saporin molecules coupled to each antibody molecule. We have had some success in achieving chromatographic partial separation of these species on columns of the weak cation exchanger carboxymethyl (CM) sepharose as modified from a previously described method ***(8)***. It must be stressed that the elution conditions (pH and ionic strength) that allow the effective separation of these molecular species will vary for conjugates made with different monoclonal antibodies. This is a result of idiosyncratic variations in the amino acid sequences for individual antibody clones, which in turn confers variation in molecular charge and the site(s) to which the toxin moiety attaches to the protein backbones of the antibody subunits. Thus, the conditions under which immunoconjugates bind to CM-sepharose, and the specific conditions required to elute them sequentially as distinct molecular species, requires empirical investigation and optimization for each individual immunoconjugate (*see* **Note 2**). As we shall see, not all immunoconjugates are amenable to separation of the various molecular species by this method, owing to the individual characteristic properties of the antibody.
2. The immunotoxin HB2-saporin is comprised of a murine IgG1 antibody directed against the CD7 antigen expressed on the surface of virtually all human T-lymphocytes, coupled covalently by a disulfide bridge to the saporin moiety utilizing the heterobifunctional crosslinking agent SPDP ***(9)***. This conjugation method involves substituting primary amine groups of both antibody and saporin with the 2-pyridyl moiety of SPDP, and is followed by reduction of only 2-pyridyl-substituted saporin. The covalent disulfide bond between the two is formed following a sulfydryl exchange reaction between the antibody's SH group and the 2-pyridyl disulfide group of substituted saporin.

   The heterobifunctional nature of SPDP, and the fact that only one of the partners is reduced before conjugation (i.e., saporin), means that homoconjugates between antibody–antibody or saporin–saporin molecules are not formed. However, the reaction is relatively inefficient, with an excess of free unconjugated

antibody and saporin remaining in the reaction mix. (The efficiency of the conjugation process in our hands varies between 10% and 40%, depending upon the antibody employed, but is highly consistent for any given individual antibody.)

It is necessary to remove free antibody (and saporin) from the reaction mixture, as this will reduce the potency of the immunotoxin due to its competitive binding on the target cell surface. Saporin is relatively easy to remove by gel filtration, as the molecular weight difference between it (30 kDa) and unconjugated antibody (approx 160 kDa) or immunoconjugates (approx 190 kDa, 210 kDa) is sufficiently great enough to allow full resolution by gel filtration. We routinely use a 1000 cm × 1.6 cm column of Sephacryl S200HR for this purpose and have never encountered any problems in completely separating free saporin from antibody and conjugates. However, gel filtration, even on high resolution supports such as Superdex, provides insufficient separation of the various molecular species of immunoconjugate with only molecular weight differences between them in multiples of 30 kDa. The real challenge lies with the separation of free antibody from conjugate(s), and then the further separation of conjugates containing one, two, or three saporin molecules per antibody molecule.

3. Among the various technologies that have been exploited to separate free antibody from immunoconjugates is the use of the dye Cibacron blue. Ricin binds to Cibacron blue-sepharose whereas antibody does not; thus immunoconjugates of ricin–antibody bind to a column of immobilized blue sepharose CL6B (cibacron blue; ***10***), allowing free unconjugated antibody to pass. The bound ricin immunoconjugates can then be selectively eluted. However, saporin does not bind to blue sepharose, thus obviating the use of this particular method.
4. In our experience, the utility of a weak cationic exchanger such as CM-sepharose has proven the most effective and gentlest way of separating antibody from saporin-based immunotoxins. Stronger cation exchangers such as monoS have proven far less discriminating because of the avidity of their interaction with saporin immunoconjugate species and the subsequent relative difficulties we have had in eluting these. All of our separations are now conducted on CM-sepharose, a cation support that has proven forgiving and yet robust enough to allow for consistently reproducible separations, providing a few simple rules are followed. The basic method is adapted from a low pressure chromatography method first described by Lambert and colleagues ***(8)*** which is straightforward and easy to apply. However, customizing the binding conditions and then the precise elution conditions (pH and ionic strength) is something that has to be designed for each immunoconjugate and can only be arrived at by empirical investigation.
5. Weak phosphate buffers (generally 5 m*M*) are generally employed for running CM-sepharose columns, and as a general rule, the pH of the running buffer should approximate the PI of the antibody component of the immunoconjugate (*see* **Note 3**). This can be determined easily by isoelectrically focusing the antibody in question together with protein standards of known PI.

3.1. Elution Gradient

1. Changing the ionic conditions on the CM-sepharose column determines which molecular species elute. This is usually achieved by changing the salt concentration, and sodium chloride is most commonly used with this type of molecule where it is desired that full biologic function is retained. However, it is not only the ionic conditions themselves but also the *rate* at which these are applied to the material on the column that determines which molecular species elute. **Figure 1** illustrates this clearly for the anti-CD7 IT HB2-saporin.

   The PI of the HB2 antibody is between 7.2–7.4. When this IT is applied to a CM-sepharose column running in 5 m*M* phosphate buffer (without sodium chloride), pH 6.5; conductivity approx 620 μS, both antibody and immunoconjugate bind to the column. If the sodium chloride concentration is increased in a stepwise fashion from 0–105 m*M*, a single peak comprised of unconjugated antibody plus IT containing covalently coupled antibody and saporin in a 1:1 ratio is eluted (**Fig. 1A**). Increasing the salt concentration to 300 m*M* elutes a second peak comprised of a mixture of ITs containing antibody and saporin in 1:1 and 1:2 ratios.

   If the column-bound material is eluted with a gradient of sodium chloride (**Fig. 1B**), then it is possible to separate both unconjugated HB2 antibody from immunoconjugates and immunoconjugates containing one and two saporin moieties per antibody molecule from each other. The salt gradient (**Fig. 1B**) was arrived at by empirical investigation.

Fig. 1. *(opposite page)* The effects of stepwise vs semistepwise gradient elution with sodium chloride of HB2-saporin IT species from CM-sepharose. **(A)** A sample comprised of a mixture of unconjugated antibody, 1-mer ITs and 2-mer ITs was applied to a column of CM-sepharose running in 5 m*M* phosphate buffer, pH 6.5. The majority of sample material bound to the column with a small fall through peak (peak 1) composed exclusively of unconjugated HB2 antibody. Stepwise elution with 105 m*M* sodium chloride gave peak 1 comprised of unconjugated HB2 antibody and 1-mer IT. A second stepwise elution with 300 m*M* sodium chloride resulted in the elution of peak 3, which contained a mixture of 1-mer and 2-mer ITs. **(B)** In an alternative strategy, a semistepwise elution technique has been adopted. Here, the sample was applied to the CM-sepharose column in 5 m*M* phosphate buffer, pH 6.5, and all components with the exception of a small amount of unconjugated antibody bound as previously. A stepwise increase to 60 m*M* sodium chloride did not result in elution of any component from the column. A very gradual gradient of sodium chloride from 60 m*M* to 105 m*M* over a 96 min period resulted in the partial resolution of two peaks, peak 2 containing predominantly unconjugated HB2 antibody eluting with between 60–80 m*M* sodium chloride, and peak 3 eluting between 80–105 m*M* containing mainly 1-mer IT with a small amount (<5%) of unconjugated antibody. A second stepwise elution step with 300 m*M* sodium chloride gave rise to peak 4 containing mainly 2-mer IT with a small amount of contaminating 1-mer IT.

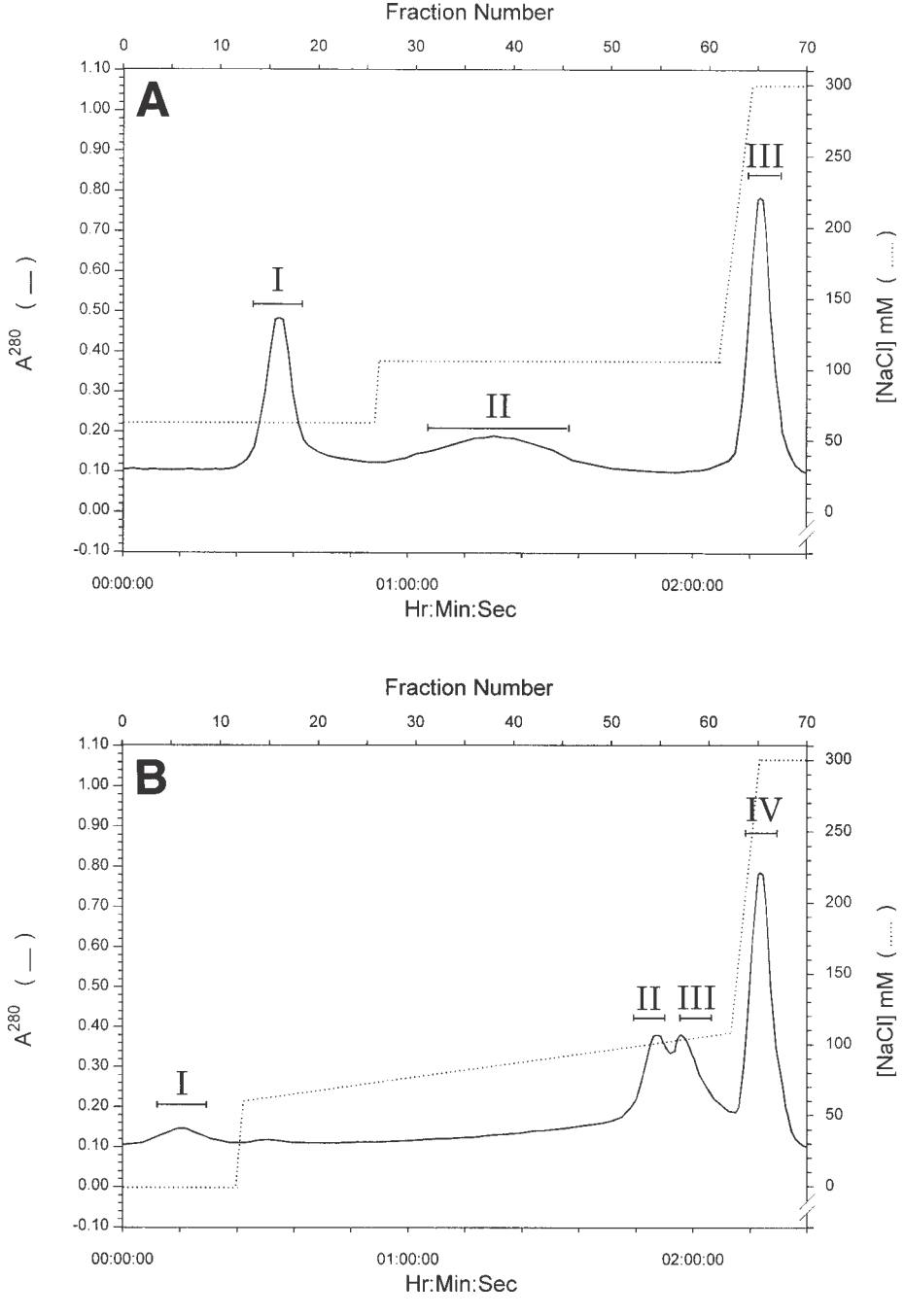

Fig. 1

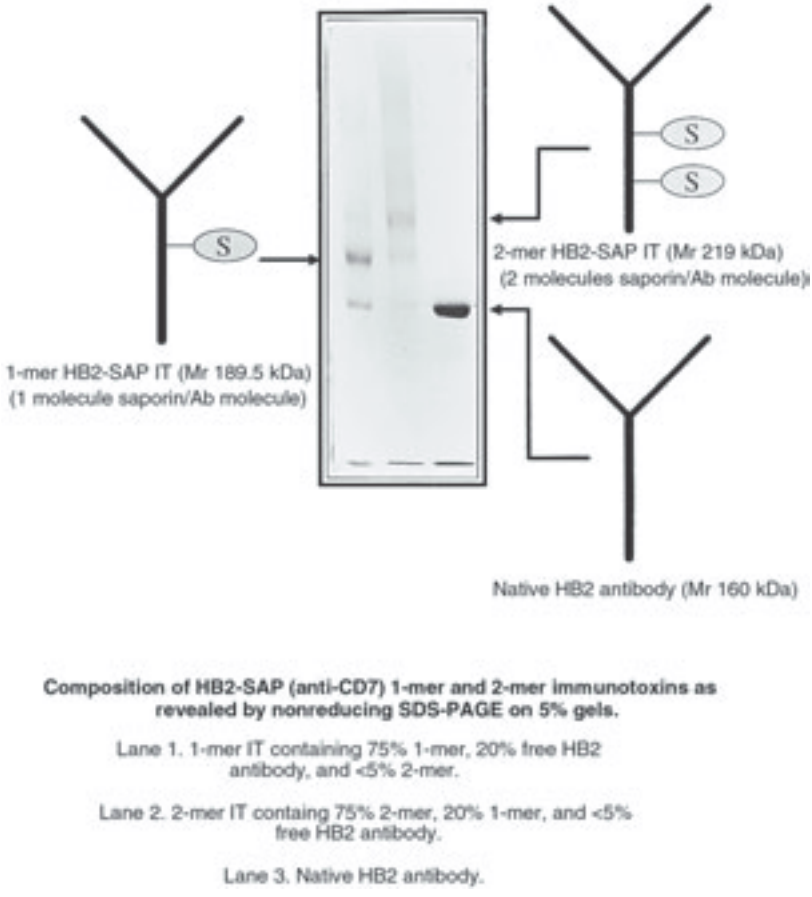

Fig. 2. SDS-PAGE analysis of IT species eluted from CM-sepharose with a semistepwise gradient of sodium chloride.

As we have seen when a mixture of unconjugated HB2 antibody and HB2-saporin immunoconjugates are applied to a CM-sepharose column running in 5 m*M* phosphate buffer at pH 6.5, virtually all molecular species bind to the column. If the salt concentration is then increased stepwise from 0–60 m*M*, then virtually nothing elutes from the column. However, if the antibody/immunoconjugate mixture is applied to a column running in 5 m*M* phosphate buffer (pH 6.5) containing 60 m*M* sodium chloride, then unconjugated antibody and a significant amount of IT comprised of antibody–saporin in a 1:1 ratio fails to bind to the column and is collected as fall-through (**Fig. 1B**). Thus, unconjugated HB2 antibody and IT that has bound to CM-sepharose in the absence of sodium chloride does not elute with 28 m*M* sodium chloride, and its prelocalization to binding

sites on the CM-sepharose confers resistance to elution with a concentration of salt that would not otherwise allow the same material to bind in the presence of the same concentration of salt. This phenomenon is instrumental to the separation of molecular species of IT. The analytical details of this chromatographic separation are shown in **Fig. 2**.

3.2. Elution Characteristics

Figure 3 shows the effects of three different pHs on the elution characteristics of the anti-CD7 IT HB2-saporin from a CM-sepharose column running in 5 m*M* phosphate buffer. The different pHs of each running buffer were obtained by mixing components A and B of the buffer in different proportions (*see* **Subheading 2**). The gradient of sodium chloride used is the same as that described above (**Fig. 1B**) for separating free antibody from IT and species of IT containing antibody to saporin in ratios of 1:1 and 1:2 from each other (**Fig. 2**). At a pH of 6.5 (**Fig. 3A**), this separation is readily achievable. However, at pH 7.0 (**Fig. 3B**), a small proportion of unconjugated HB2 antibody falls through (peak 1), while the rest leeches off as a long shallow peak (peak 2) for the duration of the shallow salt gradient (60–105 m*M*; **Fig. 3B**). Stepwise increase of salt concentrations to 300 m*M* results in peak 3 eluting, which contains both 1-mer and 2-mer plus a sizable amount (approx 30%) of unconjugated HB2 antibody.

At pH 7.5, the majority of the unconjugated HB2 antibody falls through and a long shallow peak (peak 2) elutes over the duration of the shallow salt gradient (**Fig. 3C**). This peak predominantly contains 1-mer IT with a small amount (approx 10%) of unconjugated HB2 antibody. The third peak eluted with 300 m*M* sodium chloride contains both 1-mer and 2-mer IT in a ratio of approx 3:1, with a very small amount (<5%) of free unconjugated HB2 antibody. Thus, one unit of change in pH has completely changed the elution profile obtained with the same sodium chloride gradient.

3.3. Different ITs, Different Conditions

We have already stressed that the binding and elution conditions of different IT constructs will vary, and this is determined largely by the characteristic properties of the antibody component. Unfortunately, customizing the right binding and elution conditions for each individual construct can only be arrived at through careful trial and error experimentation, an approach that is both time consuming and laborious. However, once this has been achieved, then providing that the conditions are rigorously controlled, separations can be accomplished with a very high degree of reliability and reproducibility.

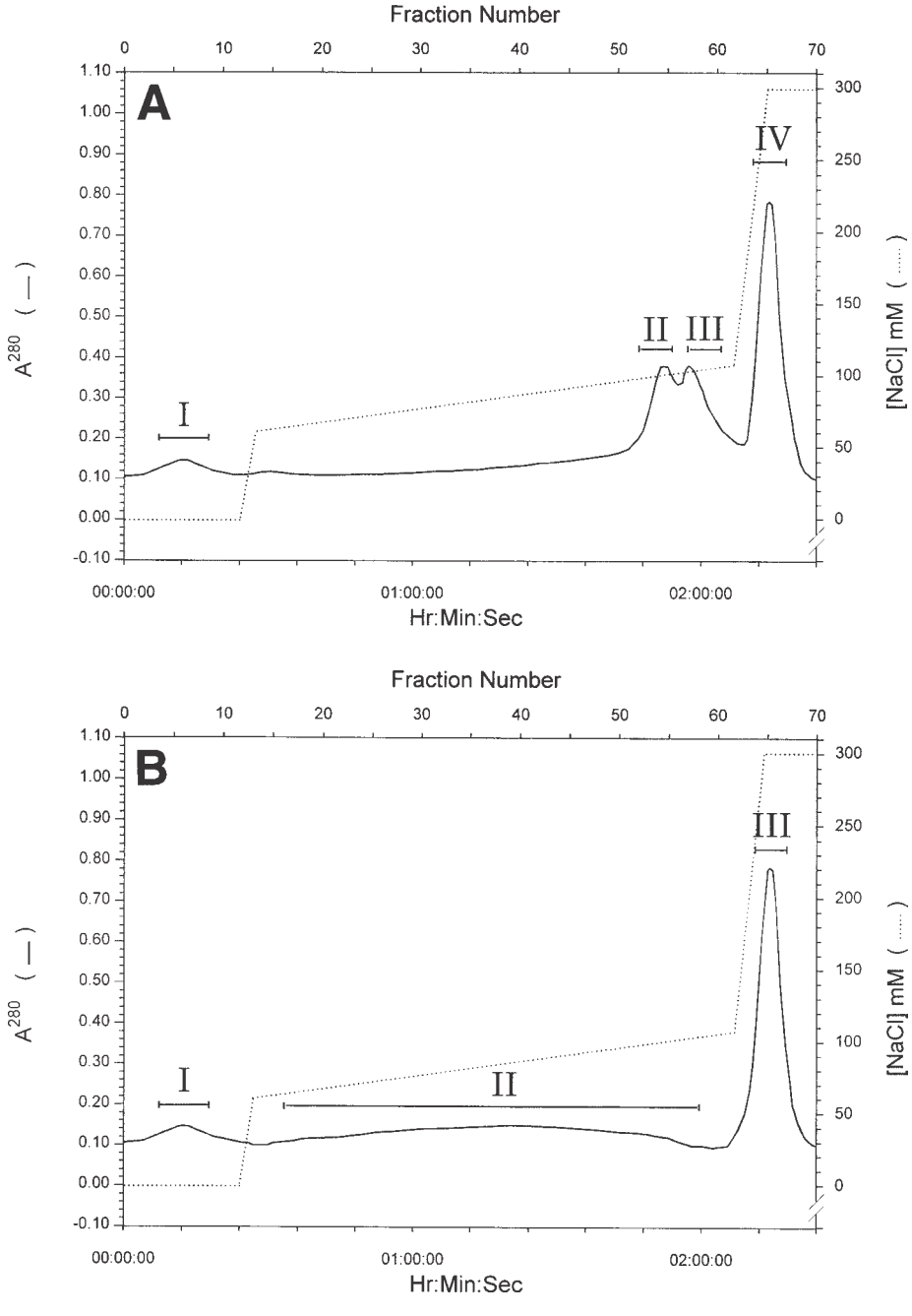

Fig. 3. The effects of pH on the elution of unconjugated HB2 antibody and HB2-saporin IT species from CM-sepharose. **A** = pH 6.5, **B** = pH 7.0, **C** = pH 7.5.

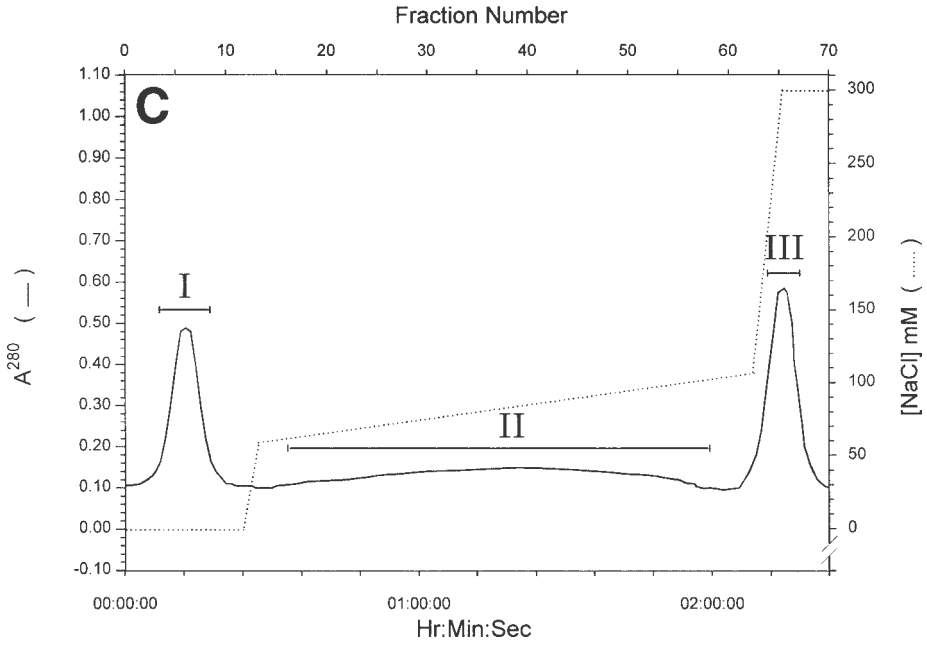

Fig. 3. *(continued)*

Illustrated in **Fig. 4** are the elution profiles and conditions ascribed to them for three different IT constructs that are routinely undertaken in this laboratory. Each separation illustrated here yields IT comprised of a mixture of 1-mer and 2-mer in ratios ranging from 3:1 to 6:1 (1-mer–2-mer ratio). We have succeeded in separating 1-mer from 2-mer for the BU12-saporin (anti-CD19) and OKT10-saporin (anti-CD38) constructs, but the separation of 1-mer and 2-mer for 4KB128-saporin still remains problematic largely because of the unusually basic nature of the 4KB128 antibody (PI 8.2). For this reason, separation of 4KB128-saporin IT has to be undertaken on a CM-sepharose column running in 5 m*M* phosphate buffer at pH 8.2; any lower, and the antibody and immunoconjugates precipitate and bind irreversibly to the column.

4. Notes

1. Small differences in the conductivity (i.e., ionic strengths) of buffers can have profound effects on the elution characteristics and hence, separation of molecular species being sought. We use only ultrapure water for making buffers. This is produced on a Milli Q apparatus that has a measurable impedance of 18.2 mΩ and a very low conductivity of 1.6 μS. The pH and conductivity of all buffers

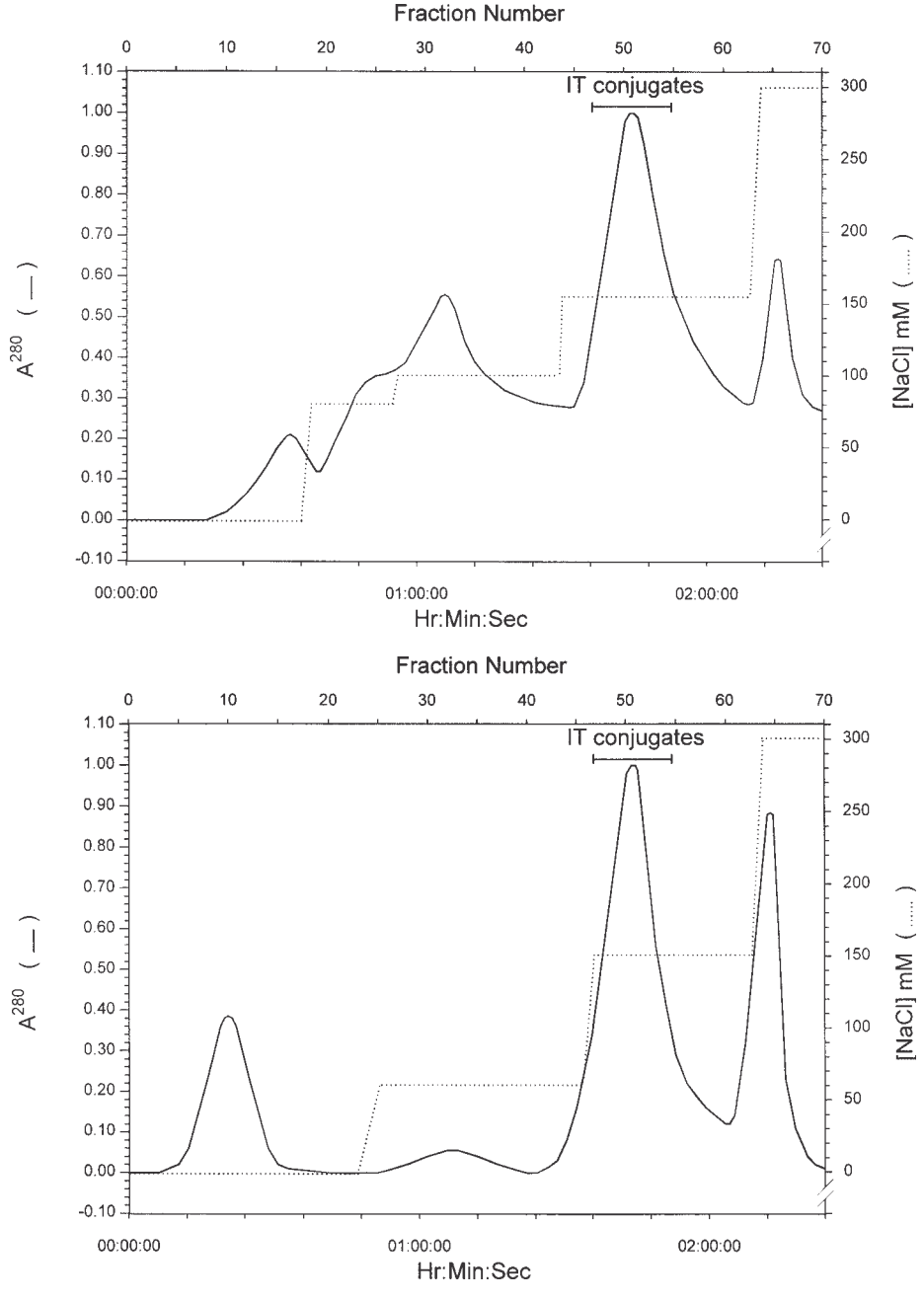

Fig. 4. Elution profiles of three different saporin ITs, BU12-saporin (anti-CD19) *(top)*, OKT10-saporin (anti-CD38) *(bottom)*, and 4KB128-saporin (anti-CD22) *(top right)*, to illustrate the wide variation that exists in elution characteristics between different conjugates. These differences are dictated entirely by the individual physico-chemical properties of the particular antibody used in the construction.

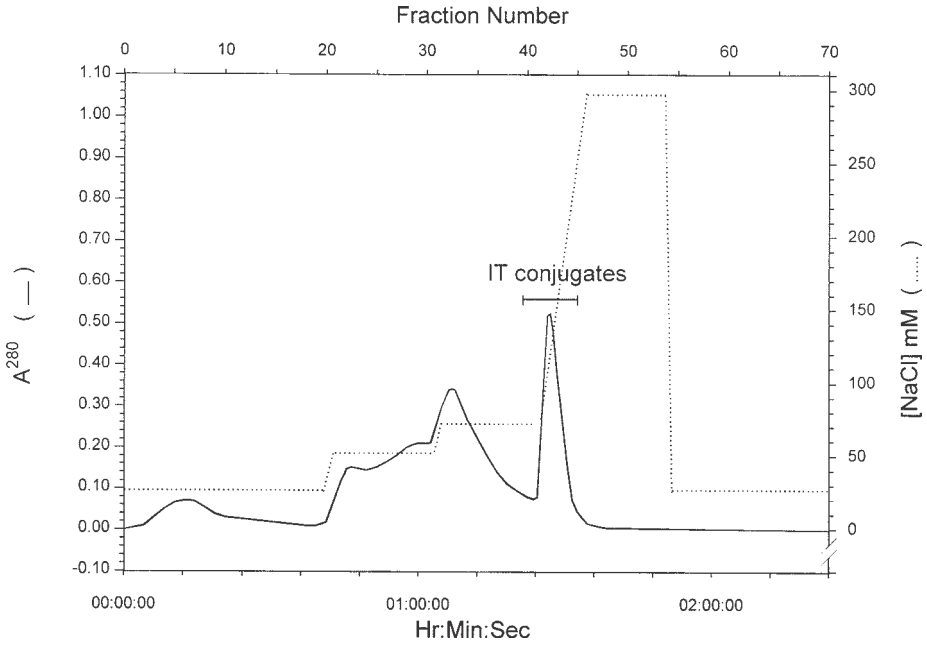

Fig. 4. *(continued)*

should be checked before use and should fall within a predetermined working range.

2. It is essential that the sample is applied to the CM-sepharose column in the same buffer at the same pH and conductivity in which the column is running. We achieve this by buffer exchange when we separate unconjugated saporin from unconjugated antibody and immunoconjugates by gel filtration on Sephacryl S200HR. Both the pH and conductivity of the sample should be checked before applying to the column and should be near identical to the running buffer.
3. As a general rule, the pH of the running phosphate buffer should approximate the PI of the antibody component. This should allow the majority of the unconjugated antibody to fall through the column, leaving only immunoconjugate species bound to the column. However, this may not always prove to be the best strategy for the separation of molecular species of ITs constructed with some antibodies. Unfortunately, the best separation strategy for each new construct will have to be evaluated on an individual basis.

5. Conclusions

There are suggestions that some ITs constructed with more than one toxin moiety per antibody molecule may exert more potent therapeutic effects in vivo. This needs to be balanced against potential increases in toxicity that might

be encountered due to increased serum half-lives and retention in the kidney or liver. Ultimately, increasing the therapeutic index of such immunotherapeutics would represent a major step forward for this class of drug. There is a need to determine whether there would be a therapeutic benefit from constructing the next generation of ITs for human therapy with more than one toxin molecule per unit antibody.

References

1. Cumber, A. J., Worrell, N. R., Parnell, G. D., Forrester, J. A., and Ross, W. J. (1985) Effect of linkage variation on pharmacokinetics of Ricin A chain antibody conjugates. *Br. J. Cancer* **52,** 433.
2. Cumber, A. J., Forrester, J. A., Foxwell, B. M. J., Ross, W. C. J., and Thorpe, P. E. (1985) Preparation of antibody-toxin conjugates, in *Methods in Enzymology,* vol. 112, Academic Press, New York, pp. 207–224.
3. Ghetie, V., Swindell, E., Uhr, J. W., and Vitetta, E. S. (1993) Purification and properties of immunotoxins containing one vs. two deglycosylated ricin A chains. *J. Immunol. Meth.* **166,** 117–122.
4. Marsh, J. W., Jr. and D. M. N. (1986) Kinetic comparison of ricin immunotoxins: biricin conjugate has potentiated cytotoxicity. *Biochem.* **25,** 4461–4467.
5. Ghetie, V., Engert, A., Schnell, R., and Vitetta, E. S. (1985) The in vivo anti-tumour activity of immunotoxins containing two versus one deglycosylated ricin A chains. *Cancer Lett.* **98,** 97–101.
6. Myers, D. E., Yanishevski, Y., Masson, E., Irvin, J. D., Evans, W. E., and Uckun, F. M. (1995) Favorable pharmacodynamic features and superior anti-leukemic activity of B43 (Anti-CDl9) immunotoxins containing two pokeweed antiviral protein molecules covalently linked to each monoclonal antibody molecule. *Leuk. Lymphoma* **18,** 93–102.
7. Flavell, D. J., Boehm, D. A., Noss, A., and Flavell, S. U. (1997) Comparison of the potency and therapeutic efficacy of the anti-CD7 immunotoxin HB2-saporin constructed with one or two saporin moieties per immunotoxin molecule. *Br. J. Cancer* **75,** 1035–1043.
8. Lambert, J. M., Senter, P. D., Yau-Young, A., Blattler, W. A., and Goldmacher, V. S. (1985) Purified immunotoxins that are reactive with human lymphoid cells. *J. Biol. Chem.* **260,** 12035–12041.
9. Carlsson, J., Drevin, H., and Axen, R. (1978) Protein thiolation and reversible protein-protein conjugation. *J. Biochem.* **173,** 723–727.
10. Knowles, P. P. and Thorpe, P. E. (1987) Purification of immunotoxins containing ricin A-chain and abrin A-chain using blue sepharose CL-6B. *Anal. Biochem.* **160,** 440–443.

7

Modulation of Growth Factor Receptor Expression by Irradiation for Immunotoxin Targeting

Ki-Uk Kim, Hsiao-Tzu Ni, Stephen R. Spellman, Kwan H. Cho, Walter C. Low, and Walter A. Hall

1. Introduction

Immunotoxins, characterized by tumor-specific cytotoxicity and high potency, have been developed as one of the new promising treatment modalities for primary malignant brain tumors ***(1–3)***. Fusion toxins bind to the cell-surface receptor specific for them, are internalized by receptor-mediated endocytosis, and inhibit protein synthesis, causing apoptotic cell death ***(4,5)***. The cytotoxic activity of the immunotoxin can be influenced by many factors, such as binding to the receptor, intracellular routing, degradation in the lysosome by enzymes, and immunogenicity ***(3)***. The first step in the mechanism of action of the immunotoxin is binding to its receptor.

Many receptors for growth factors are composed of an extracellular ligand-binding domain, transmembrane domain, and an intracellular domain with tyrosine kinase activity ***(6–10)***. When ligands bind to these receptors, tyrosine residues located in the intracellular domain become phosphorylated, endocytosis of receptor–ligand complex proceeds, and the receptors are down-regulated due to receptor endocytosis and lysosomal degadation ***(11–15)***. After exposure to epidermal growth factor (EGF), the EGF receptors are internalized and EGF binding activity disappears ***(12,13)***.

Studies were done to investigate the molecular mechanisms for internalization, focusing on the importance of kinase activity of the receptors's intracellular domain. Ligand-induced internalization of EGF receptors is blocked by mutational inactivation of tyrosine kinase, indicating the importance of kinase activity in the internalization process ***(16–18)***. Activation of the receptor is related to phosphorylation at the tyrosine and serine/threonine amino acid sites

From: *Methods in Molecular Biology, vol. 166: Immunotoxin Methods and Protocols*
Edited by: W. A. Hall

that are phosphorylated by stimulation ***(19,20)***. Reduced receptor phosphorylation was related to the reduced receptor kinase activity and internalization of both EGF and platelet-derived growth factor (PDGF) receptors ***(19,21)***. EGF receptor internalization was also blocked by antiphosphotyrosine antibodies, implying that a phosphorylated substrate is required in the ligand-induced receptor internalization ***(16)***. Even though there are controversies regarding the importance of tyrosine phosphorylation in receptor function, it is thought that tyrosine phosphorylation is crucial for receptor endocytosis in some cases ***(22)***.

Transferrin receptors (TR) and interleukin-4 receptors (IL-4R) are those frequently used as targets for immunotoxin therapy ***(23–26)***. The TR is a transmembrane glycoprotein that binds transferrin and mediates cellular iron uptake ***(27)***. This receptor is a disulfide-bonded dimer and the bulk of TR are exposed on the cell surface. When the TR is exposed to trypsin, it can be cleaved, thereby releasing a large soluble fragment ***(28)***. The cytoplasmic domain of the TR is small and contains serine residues where phosphorylation principally occurs ***(20,28)***. IL-4R mediate the biologic function of IL-4 and are identified on many kinds of human and mouse cells ***(29–32)***. The precise mechanisms of IL-4R–mediated signaling is not known, but tyrosine phosphorylation is thought to be related to the molecular sequence. The CT.4R cell line has shown a striking increase in tyrosine phosphorylation after treatment with IL-4 ***(33)***.

Insulin-like growth factors (IGF) act as growth promotors on malignant astrocytomas in an autocrine, stimulatory manner, and their biologic effect is mediated by two types of IGF receptor ***(34–36)***. In malignant gliomas, the expression of the IGF receptor is increased and subunit structures are altered. The type 1 receptor (IGF-1R) is composed of an α subunit, which binds IGF, and a β-subunit with tyrosine kinase activity ***(34,37,38)***. When IGF type 1 binds to the α-subunit of IGF-1R, intracellular tyrosine kinase activity is increased and autophosphorylation occurs ***(39–41)***.

DNA is the main intracellular target of ionizing radiation and is damaged by the direct and indirect action of radiation ***(42,43)***. Also, ionizing radiation affects the signal transduction pathway, causing programmed cell death ***(44,45)***. Tyrosine kinase is one of the enzymes shown to be activated by ionizing radiation ***(46)***, and radiation-activated tyrosine kinase mediates subsequent cellular responses to radiation ***(47–50)***. The receptor's tyrosine kinase can be phosphorylated by activated cellular tyrosine kinase, directly by ionizing radiation, or by activated posttranscriptional factors. In addition, irradiation-induced phosphorylation of the receptor will produce conformational changes that can either activate or inactivate the receptor. The EGF receptor in human keratinocytes exposed to ionizing radiation and surgical samples in patients with basal cell carcinoma undergoing radiation therapy show increased expression ***(51)***. In human malignant mammary epithelial

cell lines, the expression of the estrogen receptor was reduced after exposure to ionizing radiation, and phosphorylation of the EGF receptor was reported to be increased after irradiation ***(52–54)***.

In this chapter, we demonstrate the detailed methods of detecting altered expression of TR, IL-4R, and IGF-1R on brain-tumor cell lines after exposure to ionizing irradiation using fluorocytometric analysis. Cell-surface receptors are stained with appropriate antibodies before and after irradiation, and their fluorescence intensity is compared to that of controls. Using CELLQuest software, histograms are taken and the absolute expression index is calculated.

2. Materials

2.1. Cell and Irradiation

1. Human medulloblastoma (Daoy) and glioblastoma (U373 and T98) cell lines (ATCC, Rockville, MD), *see* **Note 1**.
2. Minimum essential medium (GibcoBRL, Grand Island, NY), supplemented with 10% fetal bovine serum, 1% L-glutamine, and 1% penicillin/streptomycin.
3. Flasks, 75 cm^2 and 25 cm^2.
4. Mark-1 ^{137}Cs irradiator (JL Shepherd, Glenwood, CA).

2.2. Staining of the Receptors

1. EDTA 0.5 m*M* (F.W., 372.24), *see* **Note 1**.
2. Polystyrene round-bottom tube.
3. Phycoerythrin (PE)-labeled anti–IGF-1R antibody (1H7); FITC-labeled anti-TR antibody (CD71); PE-mouse IgG1; FITC-mouse IgG2 (Pharmingen, San Diego, CA). These antibodies are stored at 4°C with protection from light.
4. Buffer for resuspension of the cells for FACScan (FACS buffer).
5. Hank's balanced salt solution with 2% fetal bovine serum and 0.02% sodium azide stored at 4°C.
6. Formaldehyde 1% in PBS.
7. For the staining of IL-4R, use the Fluorokine biotinylated human IL-4 kit (R&D Systems, Minneapolis, MN).

2.3. Flowcytometric Analysis

1. FACScan (Becton Dickinson, San Jose, CA).
2. CELLQuest software.

3. Methods

3.1. Preparation of the Tumor Cell Lines and Irradiation

1. Maintain the cells in minimum essential medium supplemented with 10% fetal bovine serum (vol/vol), 1% L-glutamine, and 1% penicillin/streptomycin.

Table 1
Staining of TR and IGF-1R

	Control	TR and IGF-IR
Cell suspension	100 μL[a]	100 μL[a]
PE-labeled mouse IgG1	1 μL	
FITC-labeled mouse IgG2	1 μL	
PE-labeled IGF-1R		20 μL
FITC-labeled CD71		20 μL

[a]100 μL of cell suspension contain about 0.5×10^6 cells.

2. For irradiation, the cells were harvested with trypsin, and $1.5–2 \times 10^6$ cells were taken and transferred into the 25 cm^2 flasks in 13 mL of total volume of cell suspension, *see* **Note 2**. They were incubated at 37°C for 24 h (*see* **Note 3**).

   In order to detect the changes of receptor expression sequentially, the cells are grouped as follows: No irradiation; and receptor staining 1, 3, 6, and 24 h after irradiation. Each group was tested in triplicate.
3. The cells were irradiated with 500 cGy using a Mark-1 ^{137}Cs irradiator. The irradiated cells were returned to the incubator until staining.

3.2. Staining of TR and IGF-1R

1. The cells in the flask were harvested with cold 0.5 m*M* EDTA (*see* **Note 4**). Centrifuge and resuspend in cold PBS (*see* **Note 5**).
2. Count the cells and take a cell suspension containing 10^6 cells.
3. Centrifuge at 1200*g* and resuspend the pellet in 200 μL of cold PBS.
4. Put 100 μL of cell suspension in a polystyrene round-bottom tube for receptor staining, and put 100 μL in another tube for control staining.
5. Add 20 μL of PE-labeled IGF-1R and 20 μL of FITC-labeled CD71 into the tube for receptor staining. Add 1 μL PE-labeled mouse IgG1 and 1 μL FITC-labeled mouse IgG2 into the control tube. Incubate the reaction mixture for 20 min in the dark on ice (**Table 1**, *see* **Note 6**).
6. For washing the excess antibody, add 3 mL of FACS buffer and centrifuge.
7. Remove the supernatant and resuspend the pellet in 500 mL of 1% formaldehyde. Keep the fixed cells at 4°C in the dark until fluorocytometric analysis.

3.3. Staining of the IL-4R

1. The cells in the flask were harvested with cold 0.5 m*M* EDTA.
2. Centrifuge and resuspend in cold PBS to a final concentration of 4×10^6 cells/mL.
3. Transfer 25 mL cell suspension into polystyrene tubes and add 10 μL of biotinylated cytokine reagent. For the negative control, add 10 μL biotinylated negative reagent to 25 mL of cell suspension (**Table 2**).
4. Incubate the reaction mixture for 60 min in the dark on ice.
5. Add 10 μL of avidin-FITC reagent to each tube and incubate on ice for 30 min in the dark.

Table 2
Staining of IL-4R

	Control	IL-4R
Cell suspension	25 μL[a]	25 μL[a]
Biotinylated cytokine reagent		10 μL
Biotinylated negative reagent	10 μL	
Avidin-FITC reagent	10 μL	10 μL

[a]25 μL of cell suspension contain about 10^5 cells.

6. Wash the cells twice with 2 mL of RDF 1 cell wash buffer.
7. Fix the stained cells by resuspending in 0.2 mL of 1% formaldehyde in RDF 1 cell wash buffer and store the cells at 4°C with light protection until flow cytometric analysis.

3.4. Flowcytometric Analysis

1. FACScan was used and 10,000 events were collected.
2. Analyze the data using CELLQuest software. Histograms were made, the cells were gated, and the M1 marker was applied (**Fig. 1**). The histogram statistics will show the data, including mean fluorescence intensity and the percent gated.

   Histogram statistics (receptor staining).

Marker	% gated	Mean
All	M1	100.00
82.84	13.97	15.55

   Histogram statistics (background staining).

Marker	% gated	Mean
All	M1	100.00
16.45	5.28	10.67

3. Calculate the fluorescein intensity (FI) within the M1 marker by multiplying the mean with percent gated for receptor staining FI(R) and background staining FI(B).

$$FI(R) = \text{mean} \times \% \text{ gated}$$

Example) $FI(R) = 15.55 \times 82.84$

$$FI(B) = \text{mean} \times \% \text{ gated}$$

Example) $FI(B) = 10.67 \times 16.45$

4. Calculate the absolute expression index (AEI) of the receptor by subtracting the fluorescein intensity of background staining from that of receptor staining, and compare the AEI of each irradiated group to that of the control group.

$$\text{Absolute Expression Index} = FI(R) - FI(B)$$

Example) Absolute Expression Index = 1112

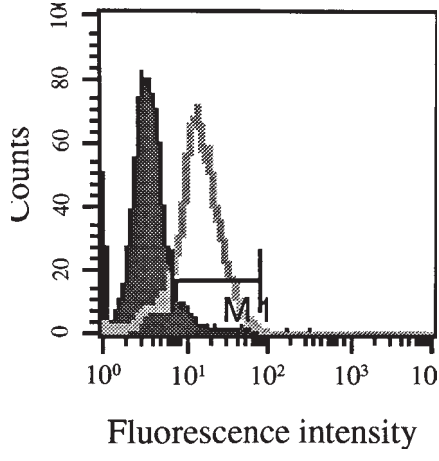

Fig. 1. Histogram showing expression of TR on the medulloblastoma (DAOY) cell line. Solid, background staining; Blank, receptor staining.

3.5. Effect of Irradiation on TR, IGF-1R, and IL-4R Expression

1. Transferrin receptor: In the Daoy cell line, the AEI was increased 62.7% in the 1-h group, 45.9% in the 3-h group, and 94% in the 6-h group, but decreased 11.4% in the 24-h group. Statistically significant changes were noticed in the 1-h, 3-h, and 6-h groups ($P < 0.05$). In the T98 cell line, the AEI was not changed significantly.
2. Type-1 insulin-like growth factor receptor: In the Daoy cell line, the AEI was increased 22.1%, 30.1%, 57.6%, and 8.6% in the 1-h, 3-h, 6-h, and 24-h groups, respectively. Statistically significant changes were noticed in the 3-h and 6-h groups. In the U373 cell line, the AEI was increased 7.6% in the 1-h group, 37.5% in the 3-h group, 37.1% in the 6-h group, but decreased 24.2% in the 24-h group. Statistically significant changes were noticed in the 3-h and 6-h groups.
3. Interleukin-4 receptor: In the Daoy cell line, the AEI was decreased 61.4% in the 1-h group, 36.7% in the 3-h group, 36.6% in the 6-h group, but increased 4.4% in the 24-h group. Statistically significant changes were noticed in the 1-h, 3-h, and 6-h groups. In the U373 cell line, the AEI was decreased 49.6% in the 1-h group, 24.7% in the 3-h group, 23.7% in the 6-h group, and 15.3% in the 24-h group. No statistically significant changes were noticed in any group.

4. Notes

1. It is difficult to harvest the adherent cells using EDTA, and only 30–50% of the cells can be obtained using EDTA. The doubling time of the tumor cells was 1.1 d for Daoy, 1.5 d for U373, and 1.2 d for T98. In order to get 1×10^6 cells after the 24 h of incubation which is needed for staining, it is desirable to incubate $1.5–2 \times 10^6$ cells 1 d before staining.

2. In order to irradiate the cells in each flask at the same dose, the total volume of the media should be the same.
3. Incubation for 24 h is sufficient for the receptors to restore normal function after possible changes due to trypsinization.
4. To harvest the cells effectively, EDTA has to be used in large amounts 10–15 mL per 25 cm^2 flask, and incubation for 10–15 min with intermittent mechanical shaking.
5. The harvested cells should be resuspended in cold PBS and kept on ice to prevent internalization of receptors.
6. When staining the receptors, an excess of antibody compared to the number of receptors on the cells can be used, because the excess antibody will be washed out later. The reverse is not allowed because it will cause false negative results.

Acknowledgments

This chapter was supported in 1998 by a Dong-A University Research Fund.

References

1. Hall, W. A. and Fodstad, Ø. (1992) Immunotoxins and central nervous system neoplasia. *J. Neurosurg.* **76,** 1–12.
2. Hall, W. A. (1997) Targeted toxin therapy, in *Advances in Neuro-Oncology II* (Kornblith, P. L. and Walker, M. D., eds.), Futura Publishing Co., Armonk, NY, pp. 505–516.
3. Youle, R. J. (1996) Immunotoxins for central nervous system malignancy. *Semin. Cancer Biol.* **7,** 65–70.
4. Pastan, I., Willingham, M. C., and FitzGerald, D. J. P. (1986) Immunotoxins. *Cell* **47,** 641–648.
5. Youle, R. J. and Neville, D. M. Jr. (1987) Role of endocytosis and receptor recycling in ligand-toxin and antibody-toxin conjugate activity, in *Immunoconjugates: Antibody Conjugates in Radioimaging and Therapy of Cancer* (Vogel, C. W., ed.), Oxford University Press, New York, NY, pp. 153–169.
6. Yarden, Y. and Ullrich, A. (1988) Growth factor receptor tyrosine kinases. *Annu. Rev. Biochem.* **57,** 443–478.
7. Ullrich, A. and Schlessinger, J. (1990) Signal transduction by receptors with tyrosine kinase activity. *Cell* **61,** 203–212.
8. Goumnerova, L. C. and Guha, A. (1993) Oncogenes and growth factors in human astrocytomas, in *Astrocytomas: Diagnosis, Treatment, and Biology* (Black, P. M., Schoene, W. C., and Lampson, L. A., eds.), Blackwell Scientific Publications, Cambridge, MA, pp. 211–227.
9. van der Geer, P., Hunter, T., and Lindberg, R. A. (1994) Receptor protein-tyrosine kinases and their signal transduction pathways. *Annu. Rev. Cell Biol.* **10,** 251–337.
10. Lala, P., Angelov, L., Provias, J., and Guha, A. (1997) Growth factors and nervous system tumors, in *Cancer of the Nervous System* (Black, P. M. and Loeffler, J. S., eds.), Blackwell Science, Cambridge, MA, pp. 744–772.

11. Heldin, C. H., Wasteson, A., and Westermark, B. (1982) Interaction of platelet-derived growth factor with its fibroblast receptor. *J. Biol. Chem.* **257,** 4216–4221.
12. Beguinot, L., Lyall, R. M., Willingham, M. C., and Pastan, I. (1984) Down-regulation of the epidermal growth factor receptor in KB cells is due to receptor internalization and subsequent degradation in lysosomes. *Proc. Natl. Acad. Sci. USA* **81,** 2384–2388.
13. Stoscheck, C. M. and Carpenter, G. (1984) Down regulation of epidermal growth factor receptors: direct demonstration of receptor degradation in human fibroblasts. *J. Cell Biol.* **98,** 1048–1053.
14. Subtil, A., Hemar, A., and Dautry-Varsat, A. (1994) Rapid endocytosis of interleukin 2 receptors when clathrin-coated pit endocytosis is inhibited. *J. Cell Sci*. **107,** 3461–3468.
15. Hemar, A., Subtil, A., Lieb, M., Morelon, E., Hellio, R., and Dautry-Varsat, A. (1995) Endocytosis of interleukin 2 receptors in human T lymphocytes: distinct intracellular localization and fate of the receptor α, β, and γ chains. *J. Cell Biol*. **129,** 55–64.
16. Glenney, J. R. Jr., Chen, W. S., Lazar, C. S., Walton, G. M., Zokas, L. M., Rosenfeld, M. G., et al. (1988) Ligand-induced endocytosis of the EGF receptor is blocked by mutational inactivation and by microinjection of anti-phosphotyrosine antibodies. *Cell* **52,** 675–684.
17. Sorkin, A., Westermark, B., Heldin, C. H., and Claesson-Welsh, L. (1991) Effect of receptor kinase inactivation on the rate of internalization and degradation of PDGF and the PDGF β-receptor. *J. Cell Biol.* **112,** 469–478.
18. Felder, S., LaVin, J., Ullrich, A., and Schlessinger, J. (1992) Kinetics of binding, endocytosis, and recycling of EGF receptor mutants. *J. Cell Biol.* **117,** 203–212.
19. Sorkin, A., Helin, K., Waters, C. M., Carpenter, G., and Beguinot, L. (1992) Multiple autophosphorylation sites of the epidermal growth factor receptor are essential for receptor kinase activity and internalization. *J. Biol. Chem.* **267,** 8672–8678.
20. Schneider, C., Sutherland, R., Newman, R., and Greaves, M. (1982) Structural features of the cell surface receptor for transferrin that is recognized by the monoclonal antibody OKT9. *J. Biol. Chem.* **257,** 8516–8522.
21. Joly, M., Kazlauskas, A., Fay, F. S., and Corvera, S. (1994) Disruption of PDGF receptor trafficking by mutation of its PI-3 kinase binding sites. *Science* **263,** 684–687.
22. Sorkin, A. (1996) Receptor-mediated endocytosis of growth factors, in *Signal Transduction* (Heldin, C. H. and Purton, M., eds.), Chapman & Hall, London, pp. 109–123.
23. Johnson, V. G., Wrobel, C., Wilson, D., Zovickian, J., Greenfield, L., Oldfield, E. H., et al. (1989) Improved tumor-specific immunotoxins in the treatment of CNS and leptomeningeal neoplasia. *J. Neurosurg.* **70,** 240–248.
24. Laske, D. W., Youle, R. J., and Oldfield, E. H. (1997) Tumor regression with regional distribution of the targeted toxin TF-CRM 107 in patients with malignant brain tumors. *Nature Med.* **3,** 1362–1368.

25. Husain, S. R., Behari, N., Kreitman, R. J., Pastan, I., and Puri, R. K. (1998) Complete regression of established human glioblastoma tumor xenograft by interleukin-4 toxin therapy. *Cancer Res.* **58,** 3649–3653.
26. Puri, R. K., Hoon, D. S., Leland, P., Snoy, P., Rand, R. W., Pastan, I., et al. (1996) Preclinical development of a recombinant toxin containing circularly permuted interleukin 4 and truncated *Pseudomonas* exotoxin for therapy of malignant astrocytoma. *Cancer Res.* **56,** 5631–5637.
27. Trowbridge, I. S., Newman, R. A., Domingo, D. L., and Sauvage, C. (1984) Transferrin receptors: structure and function. *Biochem. Pharmacol.* **33,** 925–932.
28. Trowbridge, I. S. and Shackelford, D. A. (1986) Structure and function of transferrin receptors and their relationship to cell growth. *Biochem. Soc. Symp.* **51,** 117–129.
29. Ohara, J. and Paul, W. E. (1987) Receptors for B-cell stimulatory factor-1 expressed on cells of haematopoietic lineage. *Nature* **325,** 537–540.
30. Park, L. S., Friend, D., Sassenfeld, H. M., and Urdal, D. L. (1987) Characterization of the human B cell stimulatory factor 1 receptor. *J. Exp. Med.* **166,** 476–488.
31. Park, L. S., Friend, D., Grabstein, K., and Urdal, D. L. (1987) Characterization of the high-affinity cell-surface receptor for murine B-cell-stimulating factor 1. *Proc. Natl. Acad. Sci. USA* **84,** 1669–1673.
32. Lowenthal, J. W., Castle, B. E., Christiansen, J., Schreurs, J., Rennick, D., Arai, N., et al. (1988) Expression of high affinity receptors for murine interleukin 4 (BSF-1) on hemopoietic and nonhemopoietic cells. *J. Immunol.* **140,** 456–464.
33. Paul, W. E. (1991) Interleukin-4: A prototypic immunoregulatory lymphokine. *Blood* **77,** 1859–1870.
34. Gammeltoft, S., Haselbacher, G. K., Humbel, R. E., Fehlmann, M., and Van Obberghen, E. (1985) Two types of receptor for insulin-like growth factors in mammalian brain. *EMBOJ* **4,** 3407–3412.
35. Gammeltoft, S., Ballotti, R., Kowalski, A., Westermark, B., and Van Obberghen, E. (1988) Expression of two types of receptor for insulin-like growth factors in human malignant glioma. *Cancer Res.* **48,** 1233–1237.
36. Glick, R. P., Lichtor, T., and Unterman, T. G. (1997) Insulin-like growth factors in central nervous system tumors. *J. Neurooncol.* **35,** 315–325.
37. Ullrich, A., Gray, A., Tam, A. W., Yang-Feng, T., Tsubokawa, M., Collins, C., et al. (1986) Insulin-like growth factor 1 receptor primary structure: comparison with insulin receptor suggests structural determinants that define functional specificity. *EMBOJ* **5,** 2503–2512.
38. Ballotti, R., Nielsen, F. C., Pringle, N., Kowalski, A., Richardson, W. D., Van Obberghen, E., et al. (1987) Insulin-like growth factor 1 in cultured rat astrocytes: expression of the gene, and receptor tyrosine kinase. *EMBOJ* **6,** 3633–3639.
39. Jacobs, S., Kull, F. C. Jr., Earp, H. S., Svoboda, M. E., Van Wyk, J. J., and Cuatrecasas, P. (1983) Somatomedin-C stimulates the phosphorylation of the beta-subunit of its own receptor. *J. Biol. Chem.* **258,** 9581–9584.
40. Rubin, J. B., Shia, M. A., and Pilch, P. F. (1983) Stimulation of tyrosine-specific phosphorylation in vitro by insulin-like growth factor I. *Nature* **305,** 438–440.

41. Zick, Y., Sasaki, N., Rees-Jones, R. W., Grunberger, G., Nissley, S. P., and Rechler, M. M. (1984) Insulin-like growth factor-I (IGF-I) stimulates tyrosine kinase activity in purified receptors from a rat liver cell line. *Biochem. Biophys. Res. Commun.* **119,** 6–13.
42. Hall, E. J. (1994) *Radiobiology for the Radiologist*. J. B. Lippincott Co., Philadelphia, PA.
43. Kolker, J. D. and Weichselbaum, R. R. (1997) Radiobiology update, in *Advances in Neuro-Oncology II* (Kornblith, P. L. and Walker, M. D., eds.), Futura Publishing Co., Armonk, NY, pp. 283–305.
44. Matsuo, T., Ohtsuru, A., Ito, M., Komatsu, K., Okumura, Y., Numba, H., et al. (1995) Inhibition of epidermal growth factor binding system by ionizing radiation in A431 human squamous carcinoma cells. *Cancer Lett.* **89,** 153–159.
45. Dulic, V., Kaufmann, W. K., Wilson, S. J., Tlsty, T. D., Lees, E., Harper, J. W., et al. (1994) p53-Dependent inhibition of cyclin-dependent kinase activities in human fibroblasts during radiation-induced G1 arrest. *Cell* **76,** 1013–1023.
46. Chae, H. P., Jarvis, L. J., and Uckun, F. M. (1993) Role of tyrosine phosphorylation in radiation-induced activation of c-*jun* protooncogene in human lymphohematopoietic precursor cells. *Cancer Res.* **53,** 447–451.
47. Fuks, Z., Haimovitz-Friedman, A., Hallahan, D. E., Kufe, D. W., and Weichselbaum, R. R. (1993) Stress response genes induced in mammalian cells by ionizing radiation. *Radiat. Oncol. Invest.* **1,** 81–93.
48. Uckun, F. M., Schieven, G. L., Tuel-Ahlgren, L. M., Dibirdik, I., Myers, D. E., Ledbetter, J. A., et al. (1993) Tyrosine phosphorylation is a mandatory proximal step in radiation-induced activation of the protein kinase C signaling pathway in human B-lymphocyte precursors. *Proc. Natl. Acad. Sci. USA* **90,** 252–256.
49. Uckun, F. M., Tuel-Ahlgren, L., Song, C. W., Waddick, K., Myers, D. E., Kirihara, J., et al. (1992) Ionizing radiation stimulates unidentified tyrosine-specific protein kinases in human B-lymphocyte precursors, triggering apoptosis and clonogenic cell death. *Proc. Natl. Acad. Sci. USA* **89,** 9005–9009.
50. Kharbanda, S., Yuan, Z. M., Rubin, E., Weichselbaum, R., and Kufe, D. (1994) Activation of Src-like p56/p53^{lyn} tyrosine kinase by ionizing radiation. *J. Biol. Chem.* **269,** 20,739–20,743.
51. Peter, R. U., Beetz, A., Ried, C., Michel, G., van Beuningen, D., and Ruzicka, T. (1993) Increased expression of the epidermal growth factor receptor in human epidermal keratinocytes after exposure to ionizing radiation. *Radiat. Res.* **136,** 65–70.
52. Schmidt-Ullrich, R. K., Valerie, K., Chan, W., Wazer, D. E., and Lin, P. S. (1992) Expression of oestrogen receptor and transforming growth factor in MCF-7 cells after exposure to fractionated irradiation. *Int. J. Radiat. Biol.* **61,** 405–415.
53. Schmidt-Ullrich, R. K., Valerie, K. C., Chan, W., and McWilliams, D. (1994) Altered expression of epidermal growth factor receptor and estrogen receptor in MCF-7 cells after single and repeated radiation exposures. *Int. J. Radiat. Oncol. Biol. Phys.* **29,** 813–819.
54. Schmidt-Ullrich, R. K., Valerie, K., Fogleman, P. B., and Walters, J. (1996) Radiation-induced autophosphorylation of epidermal growth factor receptor in human malignant mammary and squamous epithelial cells. *Radiat. Res.* **145,** 81–85.

8

Quantification of Immunotoxin Number for Complete Therapeutic Response

Robert J. Kreitman

1. Introduction

1.1. Purpose for Biodistribution Studies

Radiolabeled antibodies are commonly administered to patients, and their biodistribution to tumor and normal tissues is routinely quantitated by nuclear medicine scanning for dosimetry ***(1)***. Only a few studies have examined the uptake of radiolabeled immunotoxins into tumors or normal tissues ***(2–7)***. These studies used toxin-ligand chemical conjugates and determined uptake by percentage of injected dose per gram of tissue (%id/g). The present review details the methods involved in determining the uptake of the recombinant immunotoxin LMB-2, and the calculations necessary to convert %id/g to the number of molecules binding specifically to each tumor cell. These methods can also be used for any radiolabeled ligand, including monoclonal antibodies (MAbs), to determine numbers of molecules per cell that bind to the target antigen in vivo. With immunotoxins, however, one can compare the number of molecules per cell needed for complete tumor regression with the need for eradication of tumor cells in monolayer culture.

1.2. Protein Toxins

Toxins are proteins produced by plants or bacteria that internalize into animal cells and kill them by inhibition of protein synthesis. Plant toxins inhibit protein synthesis by inactivating ribosomes ***(8)***, while bacterial toxins inactivate elongation factor 2 (EF-2) ***(9,10)***. Toxins are active in minute quantities because they function enzymatically, and in fact only one molecule in the cytoplasm is sufficient to kill cells ***(8,11)***. Plant toxins include ricin A-chain (RTA),

From: *Methods in Molecular Biology, vol. 166: Immunotoxin Methods and Protocols*
Edited by: W. A. Hall © Humana Press Inc., Totowa, NJ

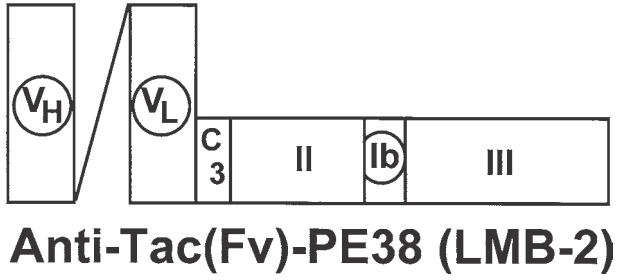

Fig. 1. Schematic diagram of LMB-2. The 63-kDa recombinant immunotoxin LMB-2 used as an example in this protocol is a single-chain protein composed of the variable domains (V_H and V_L) of the anti-Tac MAb to CD25, connected with the peptide linker $(G_4S)_3$ and then fused to PE38, a truncated form of *Pseudomonas* exotoxin. The C3 connector (ASGGPE) peptide connects V_L with PE38. The toxin is devoid of its binding domain Ia and part of domain Ib. PE38 contains the translocating domain II (residues 253–364), and the ADP ribosylating domain III (residues 400–613).

a form of RTA that is deglycosylated to prevent binding to the liver (dgA), full-length but mutated "blocked" ricin, pokeweed antiviral protein (PAP), and saporin. Bacterial toxins administered clinically include *Pseudomonas* exotoxin (PE) and diphtheria toxin (DT).

1.3. Structure and Production of Recombinant Immunotoxins

Anti-Tac(Fv)-PE38 (LMB-2), (**Fig. 1**) is a 63-kDa single-chain protein containing the variable heavy domain of the monoclonal antibody anti-Tac ***(12)*** fused via a 15–amino-acid linker to the variable light domain, which in turn is fused to PE38, the 38-kDa truncated form of PE ***(13)***. PE38 is devoid of the toxin domain, which binds to normal cells but contains the translocating and ADP-ribosylating domains.

Based on structural ***(14,15)*** and functional ***(16)*** studies, intoxication by LMB-2 has been shown to require binding to CD25; internalization and processing of the toxin within its translocation domain ***(17–19)***; binding of the 35-kDa carboxy terminal fragment of the toxin to the intracellular KDEL receptor that carries it to the endoplasmic reticulum ***(20,21)***; translocation of the toxin into the cytoplasm ***(22,23)***; and finally ADP ribosylation of EF-2, leading to apoptosis and cell death ***(9,24)***. LMB-2 is produced in *E. coli* as insoluble inclusion bodies. The insoluble recombinant protein is purified free of bacterial proteins and endotoxin; denatured and reduced in a guanidine-dithioerythritol solution; refolded by dilution into a redox buffer containing oxidized glutathione; and purified by anion-exchange and sizing chromatography ***(20)***.

1.4. Preclinical and Clinical Development

Preclinical studies have shown that LMB-2 is cytotoxic toward fresh leukemic cells from patients ***(25–28)***, and produced complete regressions of CD25+ tumors in mice ***(13)*** at serum concentrations that were well tolerated by monkeys. LMB-2 binds to both human and primate CD25 but not to the murine antigen. To determine the clinical activity of LMB-2 in humans, phase I testing was undertaken in patients with CD25+ hematologic malignancies. All toxicity was reversible. At the maximum tolerated dose—40 μg/kg intravenous every other day for 3 doses—the most common toxicity was transaminase elevations, which may be cytokine related since they were usually preceded by fever. The half-life in patients was 4–8 h and only 6 of 35 patients made high levels of neutralizing antibodies after one cycle. Of 20 patients receiving the highest doses (> 60 μg/kg/cycle total dose), the response rate was 40%, including four of four patients with hairy cell leukemia and one patient each with chronic lymphocytic leukemia, adult T-cell leukemia, cutaneous T-cell lymphoma, and Hodgkin's disease ***(29)***. LMB-2 is now being prepared for additional clinical trials, and phase I testing is now underway with another recombinant immunotoxin, BL22, for CD22+ chronic lymphocytic leukemia, hairy cell leukemia and B-cell lymphoma ***(30)***.

1.5. Quantifying Tumor Uptake In Vivo

As shown by the flow chart in **Fig. 2**, determining the number of molecules of radiolabel that bind to a target antigen in vivo requires subcutaneous injection of antigen-positive transfected cell lines and antigen-negative parental cell lines. Therefore, the amount of radiolabel specifically binding to the target antigen may be determined by subtraction, as explained in **Subheading 3.8.**

2. Materials

2.1. Recombinant Immunotoxin

The recombinant immunotoxin used for this study was LMB-2; its production was previously published ***(20)***. The methods were very similar to those published previously for IL6-toxin ***(31)*** and also those detailed for the fusion toxin GM-CSF-PE38KDEL ***(32)***.

2.2. Radiolabeling

1. Chloramine T: 3 μL/10 μg.
2. Sodium metabisulfite: 52 mg/mL in H_2O.
3. Na(^{125}I).
4. Human serum albumin (HSA).

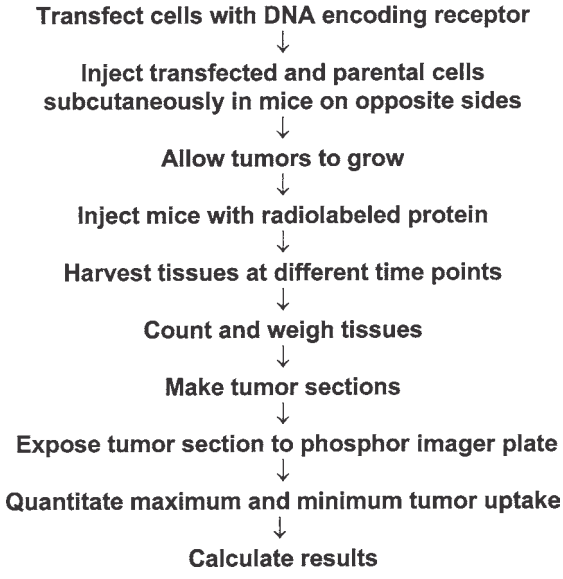

Fig. 2. Flow diagram for quantifying immunotoxin number in vivo.

5. Phosphate-buffered saline (PBS).
6. G-25 Sephadex (PD-10) column (Pharmacia, Piscataway, NJ).

2.3. Characterization

1. Binding buffer: Dulbecco's modified Eagle's medium (DMEM) containing 0.1% BSA and 0.1% sodium azide.
2. Cell culture medium.

2.4. Immunodeficient Animals

1. Nude or SCID mice.

2.5. Cell Lines

1. Transfected cells.
2. Parental cells.

2.6. Apparatus

1. Phosphor imager.

3. Methods

3.1. Radiolabeling of the Recombinant Immunotoxin

A variety of different radionuclides (i.e., ^{125}I, ^{131}I, or ^{111}In) may be used to quantitate binding sites in vivo. Owing to the relatively long half-life of ^{125}I

(60 d), LMB-2 in the present example was radiolabeled with ^{125}I. Methods for radioiodination differ depending on whether it is desirable to label tyrosine or lysine residues. Chloramine T was used to label the tyrosine residues (*see* **Note 1**).

1. In a 0.6 mL microfuge tube, a solution is prepared containing 150 μg of protein and 150 m*M* sodium phosphate buffer, pH 7.5, in a minimal volume, optimally 80–100 μL. Store on ice.
2. A PD-10 column is washed with 4 × 5 mL of 0.2% HSA in PBS (HSA-PBS).
3. Chloramine T (3 μL/10 μg) is added to the 150 μg protein and allowed to come to room temperature.
4. ^{125}I (10 μL/1 mCi) is added and incubated at room temperature for 2 min (*see* **Note 2**).
5. Sodium metabisulfite (1.6 μL of a 52 mg/mL solution) is added to quench the reaction (*see* **Note 3**).
6. The protein is added to a PD-10 column fitted over the first collection tube.
7. Washings from the 0.6 mL tube are used to quantitatively transfer, allowing a total of 2–2.5 mL HSA-PBS to elute through the column into the first collection tube; 0.5 mL HSA-PBS are then eluted for each of nine subsequent collection tubes.
8. Two microliters of each fraction is diluted to 200 μL, and 10 μL are counted. The peak fractions are pooled, which will typically include 2–3 fractions between fraction 3 and fraction 7.
9. The amount of protein present is estimated by multiplying the starting protein amount (150 μg in this example) by the percentage of pooled radioactivity, compared to total radioactivity in the 10 fractions collected, multiplied by 90% to account for nonspecific losses (*see* **Note 4**).
10. The μCi/mL in the pooled fractions is determined, followed by the specific activity in μCi/μg.
11. HSA 25% is added to bring the total albumin concentration to 10 mg/mL (1%).

3.2. Characterization of Radiolabeled Immunotoxin

The fraction that is able to bind is determined. This is best done using a cell line that expresses a high level of the target antigen. For LMB-2, the adult T-cell leukemia cell line HUT-102, which expresses about 500,000 CD25 sites/cell, was used ***(33)***.

1. A constant concentration of the radiolabeled protein close to its K_d (0.5 n*M*) is incubated with 0.2 mL aliquots of binding buffer containing increasing numbers of cells up to 5×10^7/mL.
2. Cells are harvested either by centrifuging the cells, removing the supernant, and washing twice; or by centrifuging the cells once through 150 μL of phthalate oil and counting the bottoms of the tubes.
3. If practical, a duplicate assay is performed in parallel using an excess of unlabeled protein to block the target antigens on the cells and to determine nonspecific binding.

4. To determine the fraction that is able to bind, which is equal to the fraction of radiolabel bound at an infinite concentration of cells, the reciprocal of the fraction bound is plotted on the *y*-axis and the reciprocal of cell concentration on the *x*-axis. The *y*-intercept is the reciprocal of the bindable fraction. The true specific activity of the sample may be adjusted to reflect only those molecules which are capable of binding antigen.

3.3. Measurement of Binding Affinity

The procedure for determining the bindable fraction is repeated with a chosen constant cell number and increasing concentrations of radiolabeled protein (with and without an excess of unlabeled protein). A Scatchard plot is constructed containing the amount specifically bound (in units of molecules per cell) on the *x*-axis and the ratio between specific amount bound and free concentration (in units of mol/cell/n*M*) on the *y*-axis. The *x*-intercept indicates the number of molecules per cell bound at an infinite free concentration, which is the number of binding sites on the cells. The inverse-reciprocal of the slope is equal to the K_d in units of n*M*.

3.4. Determination of Purity

1. A small fraction of radiolabeled protein (10^4–10^5 cpm) is applied to an HPLC column and small fractions (approx 0.25 mL) are collected and counted. Before applying the protein to the column, it may be advisable to centrifuge it through a 0.2 μm filter to remove macroaggregates that could damage the column. After filtering, the radioactivity in the sample is rechecked to verify that the percentage lost by filtering was small.
2. About 1 μL of radiolabeled protein (not more than 10 μg of HSA) is electrophoresed on reducing and nonreducing gels, and exposed to a phosphor imager plate for several hours or overnight. The reducing gel will detect low–molecular-weight degradation products of the radiolabeled protein, and the nonreducing gel will detect disulfide-bonded aggregates (*see* **Note 5**).
3. If a cytotoxic protein such as LMB-2 is radiolabeled, it is possible to determine the loss of cytotoxicity caused by radiolabeling important residues on the toxin. A typical cytotoxicity assay is performed by incubating target cells in media with immunotoxin overnight, pulsing with (^{3}H) leucine, and then determining inhibition of (^{3}H) leucine incorporation into the protein as an estimate of the inhibition of protein synthesis.

3.5. Preparation of Cell Lines and Subcutaneous Injection

Both antigen-positive and negative cell lines must be growing exponentially prior to subcutaneous injection.

1. The cells for injection are washed in PBS, collected by centrifugation, and resuspended in DMEM at a suitable concentration for injection.

2. Immunodeficient mice (i.e., athymic nude) are injected subcutaneously on the flank with antigen-positive cells on one side and antigen-negative cells on the other.
3. The number of cells to inject will vary from 7.5×10^5/mouse to 3×10^6/mouse, depending on the speed of growth in vivo.
4. The volume of cells to inject is 0.1 mL (*see* **Note 6**).

3.6. Injection of Radiolabeled Protein

1. Radiolabeled protein is prepared for injection containing the injected dose in 0.2 mL of HSA-PBS.
2. Injected doses contain approx 10 μCi of radiolabeled protein.
3. If an immunotoxin is injected, its quantity should equal that capable of inducing complete regression of the antigen-positive tumor. This amount must be determined in prior antitumor experiments, since mice injected with radiolabeled protein are not followed long enough to undergo complete remission.
4. Doses for injection of 0.2 mL are drawn up in 0.5 mL insulin syringes containing 27.5 gauge needles. Syringes containing manually attached needles should not be used due to excessive dead volumes.
5. Mice are injected via the tail vein with 0.2 mL of radiolabeled protein.

3.7. Harvesting, Weighing, and Counting Tissues

All tissues, unless otherwise specified, are collected in preweighed scintillation vials suitable for γ-counting. For tissues that require sectioning, such as tumors or liver, the scintillation vial should contain 0.37% formaldehyde or a similarly appropriate preservative (*see* **Note 7**). Harvesting should be performed at different times depending on the pharmacokinetic properties of the radiolabeled protein (*see* **Note 8**).

1. Mice are anesthetized by inhalation (i.e., methoxyflurane) so as not to alter hepatic metabolism.
2. Blood is withdrawn from the orbital sinus. Some blood may be placed in a 0.6 mL microfuge tube in addition to a scintillation vial if it is desired later to analyze serum from the animal by cytotoxicity assay and SDS-PAGE.
3. Animals are sacrificed immediately after blood is withdrawn.
4. The receptor-positive and receptor-negative tumors are harvested separately.
5. Various tissues are harvested. In mice undergoing complete necropsy, it is possible to account for all radioactivity administered by counting entire organs, carcass, and waste. Some organs, particularly the liver and kidneys, should be rinsed briefly with PBS immediately after harvesting to remove contaminating blood which may be very high in radioactivity.
6. Tissues, including tumors, are counted. An aliquot of the radiolabeled protein prior to injection is also counted to accurately determine the injected dose in units of cpm. For each harvested tissue, the concentration of radiolabel is determined in units of %id/g of tissue.

7. Sections are produced of the antigen-positive tumor suitable for staining. These sections are exposed to a phospor imager plate, with the thin coverslip side of the slide closest to the plate. In parallel, twofold dilutions of standard amounts of radioactivity are added to filter paper, and these control samples are also exposed to the phospor imager plate.
8. The phospor imager plate is developed into a computer image, which divides the image into 88 μm pixels. By light microscopy, it is possible to estimate how many cells are present in a pixel. For the CD25+ ATAC-4 tumor targeted by LMB-2, the number of cells per pixel is approx 75.
9. To determine whether the radiolabeled protein reaches every pixel of the tumor, the sensitivity of the image is increased to determine if a setting exists where all pixels of the tumor become "black."
10. If such a setting exists, the minimum concentration (in terms of cpm/mm^2) of LMB-2 within the tumor may be determined by recording cpm/mm^2 of the faintest spot on the control filter paper that is visible.

3.8. Calculations to Determine Binding In Vivo

1. A table is prepared to list the %id/g values for each tissue at each time point.
2. The amount of radiolabeled protein specifically binding to the target antigen at each time point may be calculated by subtracting uptake in the antigen-negative tumor from that in the antigen-positive tumor. The result is the net %id/g that actually binds to the target antigen.
3. This net %id/g can be converted to molecules per cell as shown in the following example at 6 h, where the injected dose is 4 μg, the net %id/g is 4.34 (6.31 – 197), the molecular weight of LMB-2 is 63 kDa, and the number of cells per gram of tumor is approx 10^9:

$$(4.34\ \%\text{id/g tumor}) \times (4\ \mu\text{g/id}) \times (1\ \text{nmol}/63\ \mu\text{g}) \times (6.02 \times 10^{14}\ \text{mol/nmol}) \times (1\ \text{g tumor}/10^9\ \text{cells}) = 1659\ \text{mol/cell}$$

4. Thus at 6 h in the present example, there are 1659 mol/cell specifically bound to the tumor cells in the antigen-positive tumor. However, this is an average across the tumor, with some cells binding more and some cells binding less radiolabeled protein.
5. At 6 h after injection of LMB-2, it was determined by the phospor imager procedure that the part of the tumor containing the least quantity of radiolabeled protein had 22.2 cpm/mm^2 ***(33)***. This can be converted to molecules per cell using a specific activity of 8.8 μCi/μg, a molecular weight of 63 kDa for LMB-2, and 10^4 cells per single cell layer with an area of 1 mm^2 by the following equation:

$$(22.2\ \text{cpm/mm}^2) \times (1\ \mu\text{Ci}/2.2 \times 10^6\ \text{CPM}) \times (1\ \mu\text{g}/8.8\ \mu\text{Ci}) \times (1\ \text{nmol}/63\ \mu\text{g}) \times (6.02 \times 10^{14}\ \text{mol/nmol}) \times (1\ \text{mm}^2/10^4\ \text{cells}) = 1100\ \text{mol/cell}.$$

6. Thus, 1100 mol/cell is the amount of radiolabel associated with the antigen-positive tumor in the region of minimum uptake. However, only some of these molecules are specifically bound to antigen and the remainder are nonspecifically

associated. To estimate the minimal amount of specifically bound immunotoxin necessary for complete regression, this 1100 mol/cell must be multiplied by the fraction of total radiolabel within the tumor that is specifically bound. In the present example, the total uptake in the antigen-positive tumor was 6.31 %id/g, and that specifically bound was 4.34 %id/g. Thus, (4.34/6.31) × 1100 mol/cell = 750 mol/cell were specifically bound in the region of lowest uptake of radiolabeled protein. This is the minimum number of molecules needed to bind in vivo to induce complete tumor regression.

3.9. Quantitation of Immunotoxin Needed for Cytotoxicity in Monolayer

1. The antigen-positive cell line is seeded to obtain a monolayer culture in a 96-well plate with a total volume of 0.2 mL/well.
2. The cells are then incubated with different concentrations of immunotoxin for the same time period as tested in vivo, and then incubated with fresh medium without immunotoxin for a total of 24 h. Thus, in the example with LMB-2, the CD25+ ATAC-4 cells are incubated with different concentrations of LMB-2 for 6 h, and then incubated an additional 18 h with fresh medium.
3. The cells are then trypsinized, split fivefold, and cultured with fresh media in 24-well plates (1 mL/well.)
4. The cells are cultured until they become confluent in wells corresponding to no treatment with immunotoxins. At this time point (3 d in the present example), the cells in all wells of the 24-well plate are trypsinized and counted for viability.
5. In the example with LMB-2 it was determined that a 6 h incubation of CD25+ ATAC-4 cells in monolayer with 10 p*M* LMB-2 resulted in more than 99.9% eradication of cells. To determine how many molecules of radiolabeled immunotoxin need to bind to monolayer cultures to result in cell death, monolayer cells are exposed to immunotoxin concentrations above and below that determined to be lethal (determined in the previous example to be 10 p*M*) and the number of molecules bound per cell measured. In this example, ATAC-4 cells in 24-well plates were exposed to (^{125}I) LMB-2 at 37°C for 6 h at concentrations between 4 and 128 p*M*, and uptake determined in the washed cells in units of molecules per cell. The results showed that at these low nonsaturating concentrations of LMB-2, uptake was directly proportional to the (^{125}I) LMB-2 concentration added and was 400 sites/cell at a concentration of 10 p*M* ***(33)***.

3.10. Conclusion

It is possible, using a combination of in vivo and ex vivo experiments, to determine the minimum number of molecules of immunotoxin needed to bind to each target cell in vivo to result in complete regression of tumor, and to then determine how this result compares with the minimum number of molecules per cell needed to eradicate tumor cells in monolayer culture. The most important requirement for this model is that the antigen-positive and antigen-negative cell

lines must be identical with respect to their nonspecific uptake of radiolabeled protein, and they must differ only in expression of the target antigen.

There are several assumptions made in this model which cannot be verified at this time. One is that a pixel of 88 μm in width is representative of the approx 75 cells inside. Another is that all cells of a tumor need to be killed directly in order for complete tumor regression to occur. Nevertheless, we believe the model presented should be helpful in better understanding the extent to which immunotoxin molecules reach tumors in vivo, and can be applied also to nontoxic radiolabeled proteins, including MAbs. Owing to the responses induced by LMB-2 in phase I testing ***(29)***, phase II studies are planned. As part of these studies, we plan to administer (^{111}In) LMB-2 to better quantify biodistribution and tumor uptake in humans.

4. Notes

1. The goal in radiolabeling is to avoid destruction of the binding activity of the ligand. MAbs are optimal molecules to radiolabel because their constant regions comprise most (greater than two-thirds) of the 155-kDa protein and often may be radiolabeled without harming binding activity. In contrast, recombinant immunotoxins like LMB-2 are only 63 kDa in size and radiolabeling of the 25-kDa Fv ligand is difficult to avoid. Thus when radioiodinating with ^{125}I, low specific activities of 5–10 μCi/μg are best, which equates to an average of about one radiolabel per three molecules. In this way, molecules that are multiply labeled are avoided. In this example, the tyrosine residues of LMB-2 were labeled with chloramine T (rather than the lysine residues with Bolton-Hunter reagent) because the toxin portion contains 11 tyrosines and only three lysine residues, while the ligand contains 15 tyrosines and 13 lysine residues.
2. **Steps 4–7** in **Subheading 3.1.** must be performed under a certified exhaust hood capable of preventing volatile radioactive iodine from entering the atmosphere.
3. Failure to quench the reaction will result in radiolabeling of the albumin in the elution buffer of the PD-10 column, which will contaminate the 63-kDa recombinant immunotoxin.
4. A direct measure of protein concentration is possible if HSA is taken out of the elution buffer. This can be done in parallel to verify the protein estimation in the presence of HSA. HSA is desired because it enhances the stability of the radiolabeled protein.
5. Both reducing and nonreducing gels are required to judge purity. If the protein is cleaved within a disulfide loop, the resulting lower–molecular-weight contaminants will not be observed on a nonreducing gel because the protein fragments are still held together by a disulfide bond. Also, the nonreducing gel can detect contaminating aggregates only if they are covalently linked. Multimeric protein may be connected by electrostatic interactions, and these multimers would only be visible by sizing chromatography and not by nonreducing SDS-PAGE.

6. The injection volume of 0.2 mL has been previously published ***(13,34)***, but a volume of 0.1 mL has been found to produce more consistently reproducible tumors. Not only must the size of antigen-positive and negative tumors be similar in each mouse tested, but all mice tested should have tumors of comparable size.
7. It is most efficient to tare the balance with a collection vial that does or does not contain formaldehyde immediately before addition of tissue, so that the net weight can be quickly recorded.
8. For radioiodinated proteins, it must be considered that after 6 h, a large percentage of the radiolabeled protein is deiodinated and no longer detected, and free iodine remains in the peripheral blood with a very long half-life ***(33)***. To follow the biodistribution of the radiolabeled protein longer than 6 h, it is optimal to use an alternate radionuclide like (^{111}In). Unlike iodine, indium remains attached to tissues and gives a more accurate measure of the total radiolabel accumulating in a given tissue over time. Results of (^{111}In) LMB-2 in general confirmed those of (^{125}I) LMB-2, except that uptake in catabolic organs such as the liver and kidneys was increased ***(35)***.

References

1. Wilder, R. B., Shen, S., and DeNardo, G. (1999) Dosimetry for radioimmunotherapy: a rapidly evolving field. *Cancer Biotherapy and Radiopharmaceuticals* **14,** 67–70.
2. Buchsbaum, D. J., Nelson, L. A., Hanna, D. E., and Vallera, D. A. (1987) Human leukemia cell binding and killing by anti-CD5 radioimmunotoxins. *Int. J. Radiat. Oncol. Biol. Phys.* **13,** 1701–1712.
3. Manske, J. M., Buchsbaum, D. J., Hanna, D. E., and Vallera, D. A. (1988) Cytotoxic effects of anti-CD5 radioimmunotoxins on human tumors in vitro and in a nude mouse model. *Cancer Res.* **48,** 7107–7114.
4. Perkins, A. C., Pimm, M. V., and Baldwin, R. W. (1987) Demonstration of the hepatic uptake of radiolabelled immunotoxins using gamma scintigraphy. *Eur. J. Cancer Clin. Oncol.* **23,** 1225–1227.
5. Byers, V. S., Pimm, M. V., Pawluczyk, I. Z. A., Lee, H. M., Scannon, P. J., and Baldwin, R. W. (1987) Biodistribution of ricin toxin A chain-monoclonal antibody 791T/36 immunotoxin and influence of hepatic blocking agents. *Cancer Res.* **47,** 5277–5283.
6. Skilleter, D. N. Price, R. J. and Thorpe, P. E. (1985) Modification of the carbohydrate in ricin with metaperiodate and cyanoborohydride mixtures: effect on binding, uptake and toxicity to parenchymal and non-parenchymal cells of rat liver. *Biochem. Biophys. Acta* **842,** 12–21.
7. Fulton, R. J., Tucker, T. F., Vitetta, E. S., and Uhr, J. W. (1988) Pharmacokinetics of tumor-reactive immunotoxins in tumor-bearing mice: effect of antibody valency and deglycosylation of the ricin A chain on clearance and tumor localization. *Cancer Res.* **48,** 2618–2625.
8. Eiklid, K., Olsnes, S., and Pihl, A. (1980) Entry of lethal doses of abrin, ricin and modeccin into the cytosol of HeLa cells. *Exp. Cell Res.* **126,** 321–326.

9. Carroll, S. F. and Collier, R. J. (1987) Active site of *Pseudomonas aeruginosa* exotoxin A. Glutamic acid 553 is photolabeled by NAD and shows functional homology with glutamic acid 148 of diphtheria toxin. *J. Biol. Chem.* **262,** 8707–8711.
10. Uchida, T., Pappenheimer, A. M., Jr., and Harper, A. A. (1972) Reconstitution of diphtheria toxin from two nontoxic cross-reacting mutant proteins. *Science* **175,** 901–903.
11. Yamaizumi, M., Mekada, E., Uchida, T., and Okada, Y. (1978) One molecule of diphtheria toxin fragment A introduced into a cell can kill the cell. *Cell* **15,** 245–250.
12. Uchiyama, T. A., Broder, S., and Waldmann, T. A. (1981) A monoclonal antibody (anti-Tac) reactive with activated and functionally mature human T cells. I. Production of anti-Tac monoclonal antibody and distribution of Tac (+) cells. *J. Immunol.* **126,** 1393–1397.
13. Kreitman, R. J., Bailon, P., Chaudhary, V. K., FitzGerald, D. J. P., and Pastan, I. (1994) Recombinant immunotoxins containing anti-Tac(Fv) and derivatives of *Pseudomonas* exotoxin produce complete regression in mice of an interleukin-2 receptor-expressing human carcinoma. *Blood* **83,** 426–434.
14. Allured, V. S., Collier, R. J., Carroll, S. F., and McKay, D. B. (1986) Structure of exotoxin A of *Pseudomonas aeruginosa* at 3.0 Angstrom resolution. *Proc. Natl. Acad. Sci. USA* **83,** 1320–1324.
15. Li, M., Dyda, F., Benhar, I., Pastan, I., and Davies, D. R. (1996) Crystal structure of the catalytic domain of *Pseudomonas* exotoxin A complexed with a nicotinamide adenine dinucleotide analog: implications for the activation process and for ADP ribosylation. *Proc. Natl. Acad. Sci. USA* **93,** 6902–6906.
16. Hwang, J., FitzGerald, D. J., Adhya, S., and Pastan, I. (1987) Functional domains of *Pseudomonas* exotoxin identified by deletion analysis of the gene expressed in *E. coli. Cell* **48,** 129–136.
17. Chiron, M. F., Fryling, C. M., and FitzGerald, D. J. (1994) Cleavage of *Pseudomonas* exotoxin and diphtheria toxin by a furin-like enzyme prepared from beef liver. *J. Biol. Chem.* **269,** 18,167–18,176.
18. Fryling, C., Ogata, M., and FitzGerald, D. (1992) Characterization of a cellular protease that cleaves *Pseudomonas* exotoxin. *Infect. Immun.* **60,** 497–502.
19. Ogata, M., Fryling, C. M., Pastan, I., and FitzGerald, D. J. (1992) Cell-mediated cleavage of *Pseudomonas* exotoxin between Arg^{279} and Gly^{280} generates the enzymatically active fragment which translocates to the cytosol. *J. Biol. Chem.* **267,** 25,396–25,401.
20. Kreitman, R. J. and Pastan, I. (1995) Importance of the glutamate residue of KDEL in increasing the cytotoxicity of *Pseudomonas* exotoxin derivatives and for increased binding to the KDEL receptor. *Biochem. J.* **307,** 29–37.
21. Hessler, J. L. and Kreitman, R. J. (1997) An early step in *Pseudomonas* exotoxin action is removal of the terminal lysine residue, which allows binding to the KDEL receptor. *Biochemistry* **36,** 14,577–14,582.
22. Theuer, C., Kasturi, S., and Pastan, I. (1994) Domain II of *Pseudomonas* exotoxin A arrests the transfer of translocating nascent chains into mammalian microsomes. *Biochemistry* **33,** 5894–5900.
23. Theuer, C. P., Buchner, J., FitzGerald, D., and Pastan, I. (1993) The N-terminal region of the 37-kDa translocated fragment of *Pseudomonas* exotoxin A aborts

translocation by promoting its own export after microsomal membrane insertion. *Proc. Natl. Acad. Sci. USA* **90,** 7774–7778.

24. Brinkmann, U., Brinkmann, E., Gallo, M., and Pastan, I. (1995) Cloning and characterization of a cellular apoptosis susceptibility gene, the human homologue to the yeast chromosome segregation gene CSE1. *Proc. Natl. Acad. Sci. USA* **92,** 10,427–10,431.
25. Kreitman, R. J., Chaudhary, V. K., Waldmann, T., Willingham, M. C., FitzGerald, D. J., and Pastan, I. (1990) The recombinant immunotoxin anti-Tac(Fv)-*Pseuodomonas* exotoxin 40 is cytotoxic toward peripheral blood malignant cells from patients with adult T-cell leukemia. *Proc. Natl. Acad. Sci. USA* **87,** 8291–8295.
26. Kreitman, R. J., Chaudhary, V. K., Waldmann, T. A., Hanchard, B., Cranston, B., FitzGerald, D. J. P., et al. (1993) Cytotoxic activities of recombinant immunotoxins composed of *Pseudomonas* toxin or diphtheria toxin toward lymphocytes from patients with adult T-cell leukemia. *Leukemia* **7,** 553–562.
27. Saito, T., Kreitman, R. J., Hanada, S.-I., Makino, T., Utsunomiya, A., Sumizawa, T., et al. (1994) Cytotoxicity of recombinant Fab and Fv immunotoxins on adult T-cell leukemia lymph node and blood cells in the presence of soluble interleukin-2 receptor. *Cancer Res.* **54,** 1059–1064.
28. Kreitman, R. J., Batra, J. K., Seetharam, S., Chaudhary, V. K., FitzGerald, D. J., and Pastan, I. (1993) Single-chain immunotoxin fusions between anti-Tac and *Pseudomonas* exotoxin: relative importance of the two toxin disulfide bonds. *Bioconjug. Chem.* **4,** 112–120.
29. Kreitman, R. J., Wilson, W. H., Robbins, D., Margulies, I., Stetler-Stevenson, M., Waldmann, T. A., et al. (2001) Responses in refractory hairy cell leukemia to a recombinant immuntoxin, submitted.
30. Kreitman, R. J., Wang, Q. C., FitzGerald, D. J. P., and Pastan, I. (1999) Complete regression of human B-cell lymphoma xenografts in mice treated with recombinant anti-CD22 immunotoxin RFB4(dsFv)-PE38 at doses tolerated by Cynomolgus monkeys. *Int. J. Cancer* **81,** 148–155.
31. Kreitman, R. J. and Pastan, I. (1993) Purification and characterization of IL6-PE^{4E}, a recombinant fusion of interleukin 6 with *Pseudomonas* exotoxin. *Bioconjug. Chem.* **4,** 581–585.
32. Kreitman, R. J. and Pastan, I. (2000) Making fusion toxins to target leukemia and lymphoma. *Methods in Molecular Medicine; Drug Targeting: Strategies, Principles and Applications.* **25,** 215–216.
33. Kreitman, R. J. and Pastan, I. (1998) Accumulation of a recombinant immunotoxin *in vivo*: less than 1000 molecules per cell is sufficient for complete responses. *Cancer Res.* **58,** 968–975.
34. Brinkmann, U., Pai, L. H., FitzGerald, D. J., Willingham, M., and Pastan, I. (1991) B3(Fv)-PE38KDEL, a single-chain immunotoxin that causes complete regression of a human carcinoma in mice. *Proc. Natl. Acad. Sci. USA* **88,** 8616–8620.
35. Kobayashi, H., Kao, C. K., Kreitman, R. J., Le, N., Kim, M., Brechbiel, M. W., et al. (1999) Pharmacokinetics of ^{111}In- and ^{125}I-labeled anti-Tac single-chain Fv recombinant immunotoxin. *J. Nucl. Med.* **41,** 755–762.

9

In Vitro Studies of Ricin A-Chain–Induced Vascular Leak Syndrome

Alan L. Lindstrom and Christopher A. Pennell

1. Introduction

The major dose-limiting toxicity associated with ricin-conjugated immunotoxins (ITs) is vascular leak syndrome (VLS). IT-induced VLS appears to be dose dependent, occurs 2–4 d posttreatment ***(1–6)***, and is thought to be a result of the toxin moiety, rather than the targeting moiety, because VLS is associated with ITs containing targeting moieties with different specificities. In addition, whole antibodies and FAb fragments can cause VLS, suggesting that this toxicity is not a result of Fc receptor binding or complement fixation ***(1–6)***.

There are two general ways that IT-induced VLS might occur. First, IT-induced VLS could result from a direct effect of the toxin on the endothelium, similar to that observed for toxic shock syndrome toxin-1 (TSST-1) ***(7)***. The simplest hypothesis is that the toxin enters the cell, leading to cytotoxicity and eventual cell death. Evidence for this hypothesis is based upon the inhibition of protein synthesis inhibition in human umbilical-vein–derived endothelial cell (HUVEC) monolayers exposed to ricin toxin A-chain (RTA) ***(8)***. Another hypothesis for RTA-induced VLS is based on the observation that RTA binds to endothelial cells and can cause morphologic changes prior to the detectable protein synthesis inhibition ***(8,9)***. The binding of RTA to endothelial cells may be due to a specific interaction with a three–amino-acid motif present in RTA ***(10)***. Because this interaction can be blocked by fibronectin, it was suggested that the early morphologic changes observed following RTA treatment were due to the disruption of endothelial cell–cell interactions or interactions between endothelial cells and the extracellular matrix ***(9)***.

Another possibility is that ITs induce VLS indirectly, as seen with IL-2–induced VLS ***(11–13)***. A rat model has been reported for *Pseudomonas* exotoxin

From: *Methods in Molecular Biology, vol. 166: Immunotoxin Methods and Protocols*
Edited by: W. A. Hall © Humana Press Inc., Totowa, NJ

(PE)-induced VLS in which VLS was inhibited by prophylactic treatment with anti-inflammatory drugs ***(14)***. The presence of leukocyte infiltrates in the lungs of these animals (the primary site of disease) suggests that these cells may play a pathogenic role. Although this rat model appears to be a good one for PE-induced VLS, ricin-mediated VLS cannot be mimicked in rats, suggesting that there may be differences in the pathogenesis of PE- vs ricin-mediated VLS. Additional animal species have been utilized in preclinical trials with IT conjugated to ricin or RTA, or with RTA alone, and no species adequately mimics the toxicity observed in humans. Mice, for instance, develop a late weight gain and hypoalbuminemia similar to VLS. However, these symptoms are primarily attributed to renal pathology rather than VLS ***(15)***. In addition, guinea pigs also reportedly do not exhibit symptoms related to VLS ***(8)***. Most surprisingly, monkeys do not develop VLS-like symptoms in response to RTA treatment ***(16)***. Because there are no reported animal models for RTA-induced VLS, in vitro model systems are required ***(8,9)***.

This chapter describes in detail an in vitro system that was developed to study the effects of RTA on endothelial cell monolayers. Because VLS is manifested as alterations in the permeability of the endothelium in vivo, we chose a model system that measures the permeability of endothelial monolayers in vitro as a function of RTA treatment. In our model system, a hydrostatic pressure differential is generated across the monolayer similar to that found in vivo. The permeability of the monolayers is then measured in terms of the volume of medium that flows across the monolayer per unit of time, or transendothelial fluid flux (TEFF) ***(17–19)***. Our studies show that RTA has a direct effect on the endothelium, leading to alterations in endothelial cell permeability in vitro consistent with VLS observed in vivo ***(20)***. Details of how the endothelial cells are cultured and how the TEFF apparatus is assembled and operated are provided.

2. Materials

2.1. Cells

A HUVEC culture frozen at passage 12 was purchased from the American Type Culture Collection. This is a nontransformed, near-diploid cell line with a life expectancy of 50–60 population doublings. Cells at passage 16 through 19 were used in our studies. Pooled primary HUVEC can also be purchased from Clonetics Corporation (Walkersville, MD) and used at low passage number.

2.2. Solutions and Reagents

1. Phosphate-buffered saline (PBS): 137 m*M* NaCl, 2.7 m*M* KCl, 9.5 m*M* sodium phosphate, pH 7.4.

2. Trypsin-EDTA: 0.5% trypsin, 0.53 m*M* EDTA.
3. HUVEC culture medium: M199 medium supplemented with 15% fetal bovine serum, 1 m*M* sodium pyruvate, 4.8 m*M* L-glutamine (Life Technologies, Grand Island, NY), 5 U/mL heparin (Sigma, St. Louis, MO), 100 U/mL penicillin/ streptomycin (Cellox, Hopkins, MN), and 1.0 μg/mL Endo-Gro (VEC TEC, Inc., Schenectady, NY; *see* **Note 1**).
4. Ricin toxin A-chain (RTA; Inland Laboratories, Austin, TX): used at concentrations ranging from 10^{-8} to 10^{-7} M.

2.3. TEFF Apparatus Supplies

1. Reusable polycarbonate cell culture insert support (*see* **Note 2**).
2. Collagen IV-coated cell culture inserts (Collaborative Biomedical Products, Bedford, MA).
3. Metal file.
4. Acrylic insert sealing fixture.
5. Twenty-eight 1/4" × 1/2" stainless steel socket head cap screws.
6. 5/32" Hexkey wrench.
7. 70% Ethanol or isopropanol in a plastic container large enough to submerse apparatus parts.
8. Medical-grade silicone sealant.
9. 6 cc syringe.
10. Polycarbonate culture tray.
11. 35 mm Petri dish bases.
12. Two stainless steel forceps.
13. Small surgical wire cutters.
14. 7.5" × 15" × 1/4" Plate glass.
15. 1/8" Autoclavable tubing (*see* **Note 3**).
16. 15" × 24" Plastic or metal base with aluminum angle supports for 3-way stopcocks.
17. Twelve 3-way stopcocks.
18. Twelve 3 cc syringes.
19. Twelve 1 mL graduated pipets (used for permeability measurements).
20. Twelve 100-mL HDPE bottles with tubing connectors in cap (used for medium waste receptacle).
21. Two silicone gaskets.
22. Acrylic base support.
23. Acrylic insert base.
24. Upper manifold.
25. Twenty-eight 1/4" × 1.5" stainless steel socket-head–cap screws.
26. 1/4" Tygon tubing with in-line HEPA air filters.
27. Gas cylinder pressure regulator.
28. Needle valve with 1/4" tubing connectors.

3. Methods

3.1. Preparation of Cell-Culture–Insert Support

1. Sterilize the reusable polycarbonate cell-culture–insert support, metal file, insert sealing fixture, and 1/4" × 1/2" stainless steel socket-head–cap screws by soaking the items for 15 min in a plastic container filled with 70% ethanol or isopropanol.
2. Remove the items and stand them up to dry in a sterile biologic safety cabinet under continuous air flow.
3. Fix the reusable polycarbonate cell-culture–insert support onto the insert sealing fixture using the 1/4" × 1/2" stainless steel head-socket–cap screws as shown in **Fig. 1**.
4. Scuff up the outside middle-third of 12 collagen IV-coated cell culture inserts using a small sterilized metal file and place the inserts into the tray. This step is performed to improve silicone sealant adhesion.
5. Fill a 6 cc syringe with a medical-grade nonleveling silicone sealant and connect it to a plastic pipet tip with the end trimmed at a 45° angle where the tip is approx 2 mm wide.
6. Apply the silicone around each of the cell culture inserts on the upper surface of the polycarbonate cell-culture–insert support.
7. In order to establish precise placement of the insert into the tray, the entire fixture is turned upside down onto a sterilized piece of plate glass and allowed to cure for 24 h in the biologic safety cabinet with the cabinet fan and UV light on.
8. When the silicone sealant is cured, the upper lip of the cell culture inserts is removed using a small surgical wire cutter.
9. Remove the socket-head–cap screws and flip the insert tray upside down so that the top of the inserts is in the wells of the insert sealing fixture.
10. Apply a second bead of sealant around the inserts.
11. Allow the sealant to cure for an additional 24 h.

3.2. HUVEC Cell Culture (see Fig. 1)

1. Grow HUVEC to near confluence in a 75 cm^2 flask.
2. Sterilize the polycarbonate cell-culture–insert tray with 70% ethanol or isopropanol as described previously.
3. When dry, place one drop of silicone sealant in the center of the location where each of the cell culture inserts will line up (use a spare cell-culture–insert support to the mark proper location).
4. Place 35 mm sterile Petri dish bases on the drops of silicone in the center of where each cell culture insert will be placed.
5. Harvest by adding 4 mL trypsin/EDTA solution, allow it to incubate for 1–2 min at 37°C and wash off by repeated pipeting up and down.
6. Spin cell suspension for 10 min at 400*g* in a benchtop centrifuge.
7. Resuspend the cell pellet to a density of 1.5–1.8 × 10^5/mL.
8. Add 1 mL of cell suspension to each cell culture insert.
9. Place the cell culture tray in a 37°C 5% CO_2 incubator for approx 7 d.

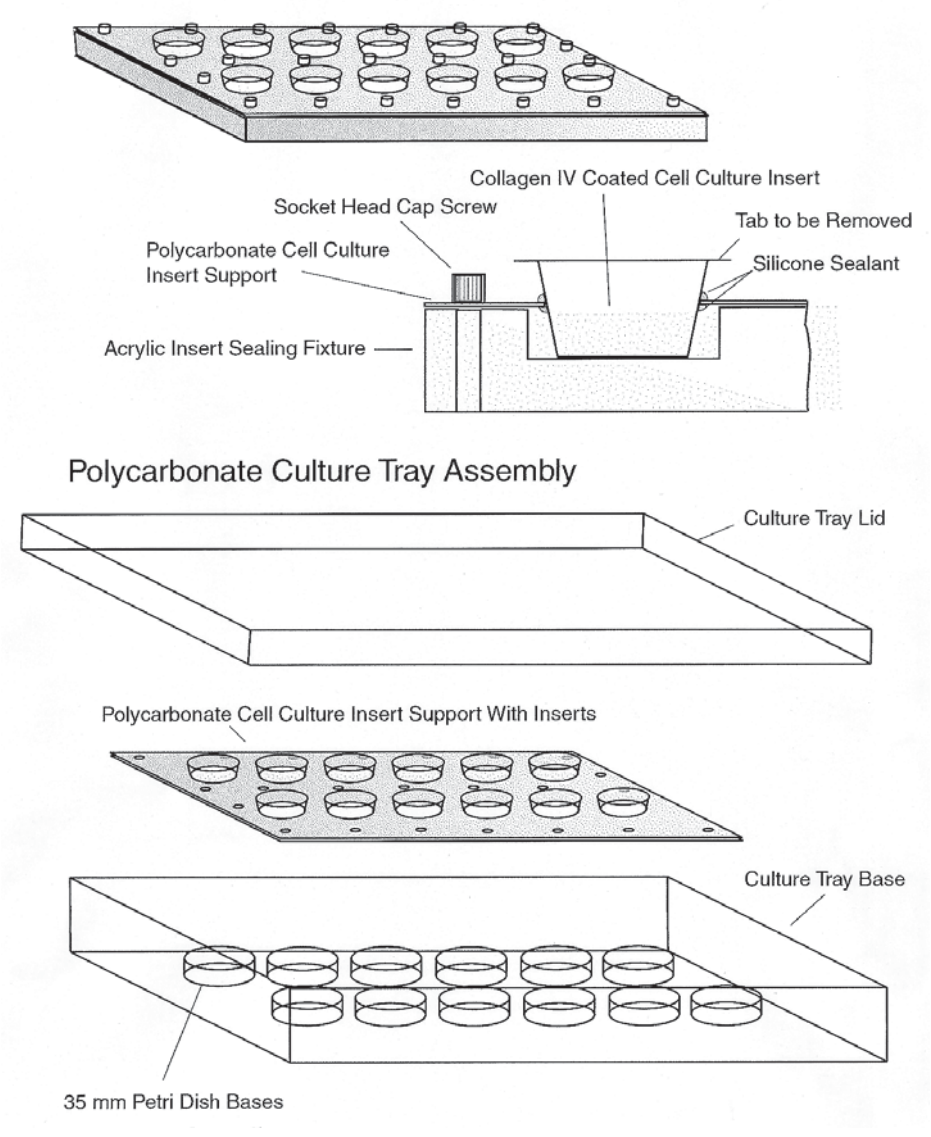

Fig. 1. Collagen IV-coated cell culture insert preparation and culture tray assembly.

10. Replace the cell culture media every other day by removing the polycarbonate cell-culture–insert support from the tray and placing it on a sterilized piece of plate glass. Replace the medium in the lower reservoir and place the polycarbonate cell-culture–insert support back into the tray, then replace the medium in the cell-culture–inserts themselves.

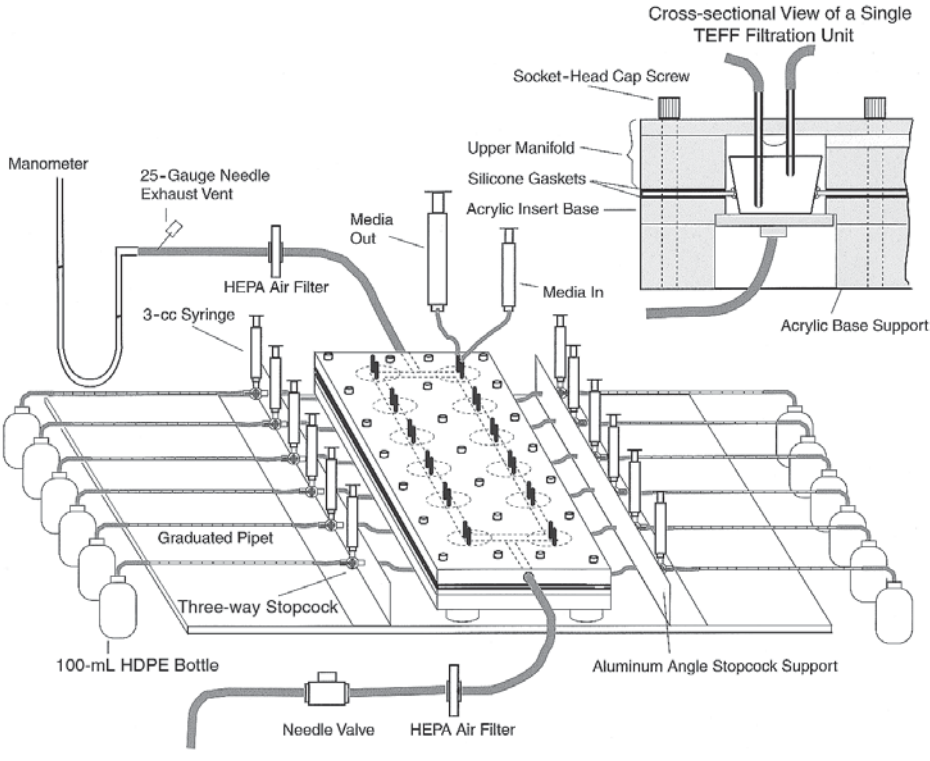

Fig. 2. Cross-sectional and 3D views of the TEFF apparatus.

3.3. Assembly of TEFF Apparatus (see Fig. 2)

1. After the cells have been cultured for a period of approx 7 d in a standard CO_2 incubator, the TEFF apparatus is assembled.
2. The parts of the apparatus must be thoroughly sterilized prior to assembly. The flexible tubing, graduated pipets, waste reservoirs, aluminum angle stopcock support, and HEPA filters with tygon tubing are made of materials suitable for autoclaving in an autoclave bag (or other autoclavable container covered with aluminum foil). The other parts must be thoroughly soaked for 15 min in 70% ethanol or isopropanol and allowed to dry in a biologic safety cabinet prior to assembly (*see* **Note 4**).
3. Attach 3-way stopcocks to the aluminum stopcock support, remembering to be careful not to contaminate the hose and Luer-Lok ports.
4. Attach 3 cc syringes to the vertical ports of the 3-way stopcocks and turn the valves of the stopcocks so that the levers are facing toward the waste reservoir.
5. Connect the female Luer-Lok fittings of the outflow tubing to the underside of the insert base unit.

6. Slip the free end of the outflow tubing through the holes of the base unit and attach each line to its respective 3-way stopcock.
7. Attach graduated pipets and waste reservoirs to the other end of stopcocks.
8. Place one of the silicone gaskets on the acrylic insert base, making certain that the holes match up, and add 2 mL of medium to each well of the insert base.
9. Prime the outflow tubing using the 3 mL syringe attached to the stopcock until there is approx 0.5 cc of medium in the syringe.
10. Place the polycarbonate cell-culture–insert support onto the insert base carefully using two pair of forceps (*see* **Note 5**).
11. Place a second silicone gasket on the upper surface of the polycarbonate cell-culture–insert support, again making certain that all of the holes match up.
12. Add additional medium to the cell-culture–inserts to bring the medium to approx 5 mm from the top of the insert.
13. Carefully place the upper manifold onto the upper silicone gasket. Place 1/4" × 2" stainless steel socket-head–cap screws into the holes of the manifold and finger-tighten.
14. Carefully tighten cap screws further, starting with the center screws and working outward.
15. Attach the media input and output tubing to the stainless steel ports in the manifold.
16. Attach a syringe with 3 mL of medium to the Luer-Lok end of the media input tubing and an empty 12 cc syringe to the medium output tubing.
17. Attach air-vent tubing and HEPA air filters to the air supply and exhaust ports of the manifold.
18. Transport the entire apparatus to a 37°C controlled atmosphere room and connect the air supply line to a regulated compressed air tank containing 95% air and 5% CO_2 (*see* **Note 6**).
19. Connect the air exhaust line to an open tube manometer.
20. Vent the tubing before the manometer with a 25 gauge needle.
21. Turn on the air supply and adjust airflow so that the net pressure equals 10 cm H_2O.
22. Allow the cells and medium to equilibrate for at least 2 h prior to establishing a baseline fluid flux.

3.4. Measurement of Transendothelial Fluid Flux

1. Open up the three-way valves to allow medium to flow from the pressurized chamber and allow several minutes to stabilize.
2. Use the syringe to calibrate the fluid in the graduated tube such that the meniscus is at zero on the scale.
3. Measure fluid flux by determining the volume of medium that flows from the pressurized chamber per unit of time.
4. Take six permeability measurements for each insert, close the three-way stopcocks, and average the results to obtain a good estimate of the baseline permeability for the monolayers (*see* **Note 7**).
5. If a satisfactory flow rate is achieved, initiate treatments by removing the medium from each well using the syringe attached to the medium output tubing, and

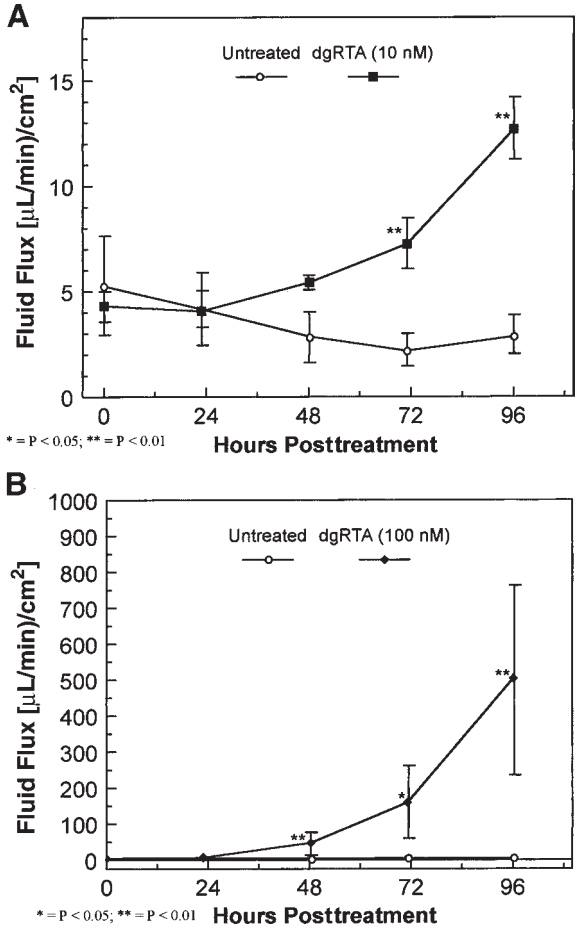

Fig. 3. dgRTA-induced permeability. **(A)** HUV-EC-C monolayers cultured on collagen IV-coated microporous cell culture inserts either left untreated (n = 4; ○) or treated with 1×10^{-8} M (0.3 µg/mL) dgRTA (n = 2; ■). **(B)** HUVEC monolayers were left untreated (n = 5; ○) or were exposed to 1×10^{-7} M (3.0 µg/mL) dgRTA (n = 4; ◆). Monolayer permeability was measured by TEFF and is expressed as the mean ± standard deviation.

replace the medium with fresh medium alone or medium containing RTA (*see* **Notes 8** and **9**).

6. Replace the medium and take fluid flux measurements on a daily basis as described in **steps 1–4** (**Fig. 3**).
7. After the final fluid flux measurement has been taken, treat all monolayers with cytochalasin D (1 µg/mL) to ensure that all endothelial cell monolayers are capable of producing high levels of permeability when disrupted (**Fig. 4**; **Note 10**).

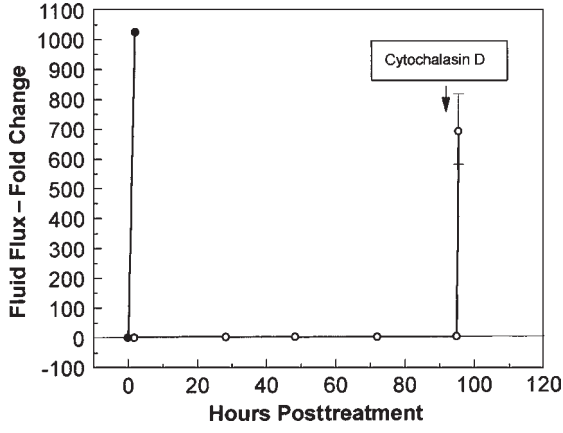

Fig. 4. Cytochalasin D-induced permeability. Baseline transendothelial fluid flux was determined for each monolayer. The monolayers were then either treated with cytochalasin D (1 μg/mL) (n = 1; ●) or were left untreated (n = 2; ○). Permeability was measured 15 min posttreatment for all monolayers and on a daily basis 4 d in the untreated monolayers. Following the d 4 permeability measurements, the two remaining monolayers were also treated with cytochalasin D. The data are expressed as the mean fold change in fluid flux relative to pretreatment values of fluid flux ± standard deviation.

8. Close the valve on the compressed air tank and disassemble the TEFF apparatus, being careful to clean each part thoroughly (*see* **Note 11**).

4. Notes

1. Do not filter the medium with Endo-gro added. Add all of the reagents except the Endo-gro, filter sterilize, and then add the Endo-gro.
2. Many of the components of the TEFF apparatus are not commercially available but may be constructed by a knowledgeable machinist. More detailed specifications for these components are available upon request.
3. One can use either silicone or other autoclavable tubing such as C-FLEX tubing (Cole Parmer, Vernon Hills, IL). Silicone tubing is much more gas permeable and allows air bubbles to form in the tubing, which can interfere with accurate permeability measurements in the graduated pipet.
4. Parts such as the three-way stopcocks should be sterilized by forcing 70% alcohol through each of the ports with a syringe while turning the valve.
5. Minimize air bubbles in the space between the insert base and insert tray as they could compromise the permeability data.
6. The gas pressure regulator should be set to less than 5 psi prior to connecting to the TEFF apparatus to avoid possible injury and damage to the apparatus.
7. The plastic three-way stopcocks on occasion leak slightly and may result in depletion of medium within the cell culture inserts. To avoid running the insert dry

overnight, pinch off the tubing between the cell culture insert and the three-way stopcock using a tubing clamp.

8. Monolayers were used only if the baseline fluid flux for HUVEC monolayers was less than 15 (μL/min)/cm^2.
9. When changing medium in the cell culture inserts, care must be taken to avoid contamination. Before removing the syringes, irrigate Luer-Lok fittings generously with 70% ethanol.
10. Treatment with cytochalasin D (1 μg/mL) results in a several hundred-fold increase in permeability and is useful for measuring a maximal permeability response and ensuring that monolayers are capable of responding to a permeabilty-inducing substance (**Fig. 4**).
11. If contamination is observed in the wells when disassembling the apparatus, soak all parts in a 10% bleach solution for 20 min, followed by thorough rinsing in RO/DI H_2O.

References

1. Ghetie, M. A. and Vitetta, E. S. (1994) Recent developments in immunotoxin therapy. *Curr. Opin. Immunol.* **6,** 707–714.
2. Amlot, P. L., Stone, M. J., Cunningham, D., Fay, J., Newman, J., Collins, R., et al. (1993) A phase I study of an anti-CD22-deglycosylated ricin A chain immunotoxin in the treatment of B-cell lymphomas resistant to conventional therapy. *Blood* **82,** 2624–2633.
3. Vitetta, E. S., Stone, M., Amlot, P., Fay, J., May, R., Till, M., et al. (1991) Phase I immunotoxin trial in patients with B-cell lymphoma. *Cancer Res.* **51,** 4052–4058.
4. LeMaistre, C. F., Rosen, S., Frankel, A., Kornfeld, S., Saria, E., Meneghetti, C., et al. (1991) Phase I trial of H65–RTA immunoconjugate in patients with cutaneous T-cell lymphoma. *Blood* **78,** 1173–1182.
5. Weiner, L. M., Dwyer, J., Kitson, J., Comis, R. L., Frankel, A. E., Bauer, R. J., et al. (1989) Phase I evaluation of an anti-breast carcinoma monoclonal antibody 260F9-recombinant ricin A chain immunoconjugate. *Cancer Res.* **49,** 4062–4067.
6. Conry, R. M., Khazaeli, M. B., Saleh, M. N., Ghetie, V., Vitetta, E. S., Liu, T., et al. (1995) Phase I trial of an anti-CD19 deglycosylated ricin A chain immu–notoxin in non-Hodgkin's lymphoma: effect of an intensive schedule of administration. *J. Immunother. Emphasis Tumor Immunol.* **18,** 231–241.
7. Lee, P. K., Vercellotti, G. M., Deringer, J. R., and Schlievert, P. M. (1991) Effects of staphylococcal toxic shock syndrome toxin 1 on aortic endothelial cells. *J. Infect. Dis.* **164,** 711–719.
8. Soler-Rodriguez, A. M., Ghetie, M. A., Oppenheimer-Marks, N., Uhr, J. W., and Vitetta, E. S. (1993) Ricin A-chain and ricin A-chain immunotoxins rapidly damage human endothelial cells: implications for vascular leak syndrome. *Exp. Cell Res.* **206,** 227–234.
9. Baluna, R., Ghetie, V., Oppenheimer-Marks, N., and Vitetta, E. S. (1996) Fibronectin inhibits the cytotoxic effect of ricin A chain on endothelial cells. *Int. J. Immunopharmacol.* **18,** 355–361.

10. Baluna, R., Rizo, J., Gordon, B. E., Ghetie, V., and Vitetta, E. S. (1999) Evidence for a structural motif in toxins and interleukin-2 that may be responsible for binding to endothelial cells and initiating vascular leak syndrome. *Proc. Natl. Acad. Sci. USA* **96,** 3957–3962.
11. Rosenstein, M., Ettinghausen, S. E., and Rosenberg, S. A. (1986) Extravasation of intravascular fluid mediated by the systemic administration of recombinant interleukin 2. *J. Immunol.* **137,** 1735–1742.
12. Ettinghausen, S. E., Puri, R. K., and Rosenberg, S. A. (1988) Increased permeability in organs mediated by the systemic administration of lymphokine-activated killer cells and recombinant interleukin-2 in mice. *J. Natl. Cancer Inst.* **80,** 177–188.
13. Bechard, D. E., Gudas, S. A., Sholley, M. M., Grant, A. J., Merchant, R. E., Fairman, R. P., et al. (1989) Nonspecific cytotoxicity of recombinant interleukin-2 activated lymphocytes. *Am. J. Med. Sci.* **298,** 28–33.
14. Siegall, C. B., Liggitt, D., Chace, D., Tepper, M. A., and Fell, H. P. (1994) Prevention of immunotoxin-mediated vascular leak syndrome in rats with retention of antitumor activity. *Proc. Natl. Acad. Sci. USA* **91,** 9514–9518.
15. Soler-Rodriguez, A. M. Uhr, J. W., Richardson, J., and Vitetta, E. S. (1992) The toxicity of chemically deglycosylated ricin A-chain in mice. *Int. J. Immunopharmacol.* **14,** 281–291.
16. Shah, S. A., Lambert, J. M., Goldmacher, V. S., Esber, H. J., Levin, J. L., Chungi, V., et al. (1993) Evaluation of the systemic toxicity and pharmacokinetics of the immunoconjugate anti-B4-blocked ricin in non-human primates. Delivered by multiple bolus injections and by continuous infusion. *Int. J. Immunopharmacol.* **15,** 723–736.
17. Powers, M. R., Blumenstock, F. A., Cooper, J. A., and Malik, A. B. (1989) Role of albumin arginyl sites in albumin-induced reduction of endothelial hydraulic conductivity. *J. Cell Physiol.* **141,** 558.
18. Suttorp, N., Hessz, T., Seeger, W., Wilke, A., Koob, R., Lutz, F., et alD. (1988) Bacterial exotoxins and endothelial permeability for water and albumin in vitro. *Am. J. Phys.* **255,** C368–C376.
19. Suttorp, N., Polley, M., Seybold, J., Schnittler, H., Seeger ,W., Grimminger, F., et al. (1991) Adenosine diphosphate-ribosylation of G-actin by botulinum C2 toxin increases endothelial permeability in vitro. *J. Clin. Invest.* **87,** 1575–1564.
20. Lindstrom, A. L., Erlandsen, S. L., Kersey, J. H., and Pennell, C. A. (1997) *An* in vitro model for toxin-mediated vascular leak syndrome: ricin Toxin A chain increases the permeability of human endothelial cell monolayers. *Blood* **90,** 2323–2334.

10

Immunotoxin Treatment of Brain Tumors

Walter A. Hall

1. Introduction

Current treatment for malignant gliomas, which includes surgery, radiation therapy, and chemotherapy, is associated with a poor prognosis ***(1,2)***. Patients with glioblastoma multiforme have an estimated 2 yr survival of less than 20% ***(1)***. Leptomeningeal carcinomatosis carries an estimated mean survival of 2–3 mo ***(3)***. Localized radiation therapy techniques such as brachytherapy and stereotactic radiosurgery often fail to prevent disease progression at the primary tumor site ***(4)***. Unfortunately, the lack of specificity of both radiation therapy and chemotherapy for malignant cells has resulted in central nervous system (CNS) toxicity and unacceptable side effects ***(1,2)***.

Monoclonal antibody technology has enabled investigators to develop agents that recognize cell-surface antigens preferentially expressed by tumors compared to normal cells, particularly for hematologic malignancies ***(1,5,6)***. Neoplastic cells often overexpress growth factor receptors or carbohydrate antigens that can act as targets for cytotoxic molecules ***(7)***. Compounds designed to take advantage of this difference in antigen expression are targeted toxins or immunotoxins. Immunotoxins are molecules composed of two components: a protein toxin with extraordinary potency that is conjugated to a carrier ligand, such as a monoclonal antibody, that has cell-type selectivity ***(1,2)***. Growth factors such as transferrin have been substituted for the antibody component to create fusion proteins called oncotoxins or mitotoxins ***(7)***.

Paul Erlich first introduced the concept of immunotoxins in 1906, although their application to the CNS spans little more than 10 yr. Initial in vitro studies using glioblastoma- and medulloblastoma-derived cell lines demonstrated the profound cytotoxic effects of immunotoxins and oncotoxins ***(8–10)***. Modest therapeutic results were obtained in the first in vivo studies where immunotoxins

From: *Methods in Molecular Biology, vol. 166: Immunotoxin Methods and Protocols*
Edited by: W. A. Hall © Humana Press Inc., Totowa, NJ

were administered into the CNS compartment *(3,11)*. More recently, immunotoxins have been delivered directly into tumors in animals and in patients with malignant brain tumors in a phase I clinical trial with encouraging results *(12–14)*. The ability to safely deliver agents to brain tumors with limited neurologic morbidity has stimulated an interest in the generation of immunotoxins targeted to different cell surface antigens found on malignant gliomas for future use in clinical trials *(15)*.

2. Immunotoxin Construction

2.1. Rationale

Conventional chemotherapeutic drugs rely on the difference in proliferative rate of malignant cells compared to normal cells to achieve a cytotoxic response *(1)*. Unfortunately, the therapeutic window between normal dividing hematopoietic stem cells and neoplastic cells is usually too narrow for chemotherapy to prove curative *(2)*. Immunotoxins, guided by their cell-type selective carrier ligand to tumor cells, have a mechanism of action that is much different than that of chemotherapeutic agents *(2)*. Factors that make tumor cells resistant to radiation therapy and chemotherapy, such as hypoxia, do not influence the potency of immunotoxins *(1,2)*. The natural or acquired resistance that cancer cells develop to chemotherapy has not been demonstrated with immunotoxins.

For most chemotherapeutic agents that act stoichiometrically, more than 10^4–10^5 mol are required to kill a single tumor cell *(1)*. In contrast, immunotoxins react enzymatically with multiple intracellular targets and one molecule can kill a tumor cell *(1,2)*. Irrespective of the cell cycle or cellular division, immunotoxins can inactivate 200 ribosomes or elongation factor 2 molecules per minute *(1,2)*. The concentration of the alkylating agent BCNU required to kill 50% of glioma cells in tissue culture is 10^{-3}–10^{-6} *M* in comparison to an intact ricin immunotoxin, which had the same effect at 10^{-13} *M (1,10)*. Although exact comparisons between chemotherapy and immunotoxins are difficult because of a difference in assay techniques, the extraordinary potency of immunotoxins by 7–10 orders of magnitude is apparent *(1,2)*.

2.2. Toxins

The toxins that have been used to construct immunotoxins are natural byproducts of plants, bacteria, and fungi that all inactivate protein synthesis (**Table 1**). Fewer than 1000 mol bound per cell are sufficient for complete tumor regression in vivo *(16)*. Plant toxins that have been used in the construction of immunotoxins are ricin and abrin or their A-chains, pokeweed antiviral protein, gelonin, saporin, modeccin, and momordica charanthia inhibitor *(1,2)*. Bacterial toxins include diphtheria toxin (DT), crossreacting material (CRM)

Table 1
Toxins

Plant toxins
Ricin
Abrin
Ricin A-chain
Abrin A-chain
Abrin variant
Modeccin
Gelonin
Saporin
Pokeweed antiviral protein (PAP)
Momordica charanthia inhibitor
Bacterial toxins
Diphtheria toxin (DT)
Crossreacting material 107 (CRM-107)
DAB_{486} & DAB_{389}
Pseudomonas aeruginosa exotoxin A (PE)
Pseudomonas aeruginosa exotoxin 38 (PE38)
Pseudomonas aeruginosa exotoxin 40 (PE40)
Pseudomonas aeruginosa exotoxin 4E (PE4E)
Fungal toxins
α-sarcin

107, *Pseudomonas aeruginosa* exotoxin A (PE), and three mutated forms of PE (PE4E, PE38, and PE40). Alpha-sarcin is a fungus-derived toxin. Most toxins such as ricin and DT contain two polypeptide chains, A and B, that are joined by a disulfide bond. The B-chain binds nonspecifically to cell surface receptors and promotes translocation and internalization of the A-chain into the cell, where the latter chain inhibits protein synthesis ***(1)***.

Plant toxins are classified as type I or type II ribosome-inactivating proteins based on their chemical structure. Type I plant toxins such as saporin have a single protein chain and maintain their catalytic activity but do not have cell-binding or translocation functions ***(2,7)***. Type II plant toxins, which include ricin and abrin, inactivate the 60S ribosomal subunit through the cleavage of the *N*-glycosidic bond of the adenine residue at position 4324 of 28S ribosomal RNA ***(2,7)***. The carboxylic ionophore monensin potentiates the action of plant toxins through an unknown mechanism ***(1,2,10)***.

Bacterial toxins used for immunotoxin construction have been primarily from DT or PE. The cell surface receptors for DT and PE have not been

Table 2
Immunotoxin Mechanisms of Action

Toxins	Mechanism[a]
Plant	
Ricin	Inactivates ribosomes
Abrin	Inactivates ribosomes
Ricin A-chain	Inactivates ribosomes
Bacterial	
Diphtheria toxin	Catalyzes transfer of ADP–ribose to EF-2
Crossreacting material 107	Catalyzes transfer of ADP–ribose to EF-2
Pseudomonas aeruginosa exotoxin A	Catalyzes transfer of ADP–ribose to EF-2
Pseudomonas aeruginosa exotoxin 38	Catalyzes transfer of ADP–ribose to EF-2
Fungal	
α-sarcin	Inactivates ribosomes

[a]ADP = adenosine diphosphate; EF = elongation factor.

characterized. The DT A-chain catalyzes the transfer of ADP-ribose to elongation factor 2 (**Table 2**), preventing the transfer of peptidyl-tRNA on ribosomes and blocking protein synthesis, thus killing the cell ***(1,2)***. CRM 107 is a genetically engineered toxin that is identical to DT except for two amino acid substitutions in the B chain that inactivate toxin binding and increase tumor-specific toxicity ***(1,2)***. *Pseudomonas* exotoxin A has three separate domains, Ia/Ib, II, and III, which are located on one polypeptide chain. Domain Ia binds to the PE receptor present on most animal cells; the function of Ib is unknown. Domain II mediates the translocation of the carboxy terminal fragment into the cell cytosol, and domain III is responsible for the ADP ribosylation of elongation factor 2 in the cytosol ***(1)***. The COOH terminus REDLK is not necessary for ADP ribosylation activity, and replacing it with KDEL increases the cytotoxicity of PE ***(17)***. The removal of domain Ia from PE results in the molecule PE40, which retains its translocation function and enzymatic activity but does not bind to cell surface receptors ***(7)***. The fungal toxin α-sarcin cleaves a phosphodiester bond in the 28S ribosomal RNA near the binding site for elongation factor 2, thereby inhibiting protein synthesis ***(1,2)***.

The recent isolation of genes that encode for many protein toxins now allows for the development of chimerics composed of DNA, encoding for a growth factor, cytokine, or cloned antibody variable region plus the gene encoding for a toxin ***(2,7)***. These gene-fusion products can be expressed rapidly, efficiently, and inexpensively in bacteria to yield a homogenous polypeptide chain or fusion protein known as an oncotoxin or single-chain immunotoxin ***(7)***. Toxins that have been used to create fusion proteins include PE40, PE38, PE4E, CRM107,

and two binding-defective DT molecules DAB_{486} and DAB_{389} *(7)*. Compared to these fusion proteins, chemical conjugates prepared using radioisotopes, protein toxins, or chemotherapeutic drugs such as adriamycin are more heterogenous in nature *(7)*. All of these molecules are immunogenic and will elicit an immune response, particularly with repeat administration *(2)*.

2.3. Carrier Ligands

The carrier ligand is extremely important when constructing immunotoxins and has a functional relevance similar to that of the toxin moiety of the compound. Chemical conjugation of the toxin to monoclonal antibodies, polyclonal antibodies, growth factors, lectins, hormones, and antigens has been performed using either a disulfide or thioether bond. Although the function of most antigens is unknown, binding of the carrier ligand to the cell-surface antigen is essential for these agents to exert their therapeutic effect. The ligand–antigen complex is internalized into the cytosol, where the toxin is later released to inhibit protein synthesis. Immunotoxins must enter the cell to be effective in comparison to monoclonal antibody-linked high-energy radionuclides, which are cytotoxic after binding to the cell. The "bystander effect" that occurs with gene therapy for brain tumors does not occur with immunotoxins.

A number of cell-surface receptors that are expressed on malignant brain tumor cells in both tissue culture and on surgical samples have been identified as potential targets for immunotoxins. These brain tumor antigens include the epidermal growth factor receptor (EGFR), a rearranged deletion-mutant tumor-specific EGFR, the transferrin receptor (TR), and the interleukin-4 (IL4) receptor *(1,2,5,15,18,19)*. Amplification of the *EGFR* gene and overexpression of *EGFR* has been demonstrated in glioblastomas multiforme and in human glioma biopsy specimens *(19–23)*. Laboratory techniques that have been used to demonstrate EGFR expression in malignant gliomas include Scatchard analysis, immunoprecipitation, a competitive radioreceptor assay, Western immunoblot analysis, affinity reaction, and immunohistochemistry *(19,21)*.

The TR, a mediator of cellular iron uptake, is expressed in greater numbers in dividing cells than in nonreplicating cells. Because of their high requirement for iron, glioblastomas multiforme and medulloblastomas have increased expression of TR, as found using solid-phase indirect radioimmunoassay, radioreceptor assay, and immunohistochemistry *(10,19,24)*. Normal brain tissue was not found to express TR, although TR are expressed by endothelial cells of cerebral blood vessels *(10,19,24)*. A method for the rapid detection of TR expression using monoclonal antibody-coated magnetic microspheres has been reported *(5)*. Flow cytometry has been used to detect TR, human leukocyte antigen (HLA)-DR antigens, and the glioma associated antigen GE-2 on glioma cells *(2)*.

Previously, monoclonal antibodies have been used to construct immunotoxins targeted to HLA-DR antigens, glioma-associated antigens, and TR ***(1,2,8–10,24)***. Iron-loaded transferrin as a growth factor has been conjugated to CRM107, ricin A-chain, abrin variant, and PE to yield potent in vitro and in vivo agents ***(1,2,8,9,12)***. Transferrin conjugated to CRM107 was the first immunotoxin used to treat malignant brain tumors using high-flow interstitial microinfusion in clinical trials ***(14)***.

IL4 is a cytokine that causes signal transduction, up-regulation of major histocompatibility antigens and intercellular adhesion molecule 1, and inhibits tumor cell growth ***(15)***. Recently, the high-affinity IL4 receptor was found in high numbers on malignant glioma cell lines using flow cytometric analysis and (^{125}I)-IL4 binding ***(15,18)***. Using Northern blot analysis, four malignant glioma cell lines were found to express the mRNA for the IL4 receptor ***(15)***. In 21 patients with malignant astrocytomas who underwent surgical resection, IL4 receptor expression was demonstrated in 16/21 (76%) samples using reverse transcriptase-polymerase chain reaction (RT-PCR) and Southern blot analysis ***(15)***. One of six samples of normal brain tissue was weakly positive for IL4 receptors using RT-PCR and Southern blotting ***(15)***. In low numbers, IL4 receptors are expressed on normal T-cells, B-cells, monocytes, basophils, eosinophils, fibroblasts, and endothelial cells ***(15)***. The overexpression of this receptor on tumor cells compared to normal cells provides the rationale for the creation of a recombinant toxin containing circularly permuted IL4 and truncated PE for the treatment of malignant astrocytoma in a phase I trial ***(15)***.

3. In Vitro Studies

In 1987, the first report demonstrating in vitro efficacy in a malignant glioma cell line was published ***(10)***. More than 50% of glioblastoma- and medulloblastoma-derived cell lines were killed after 18 h using an anti-TR monoclonal antibody–ricin immunotoxin at a concentration of 5.6×10^{-13} *M* in the presence of monensin ***(10)***. A 150–1380-fold selective toxicity was seen between target cells and nontarget normal brain cells ***(2,10)***. Using an anti-TR–ricin A-chain immunotoxin, 50% of protein synthesis was inhibited (IC_{50}) at concentrations ranging from 1.9×10^{-9} to 1.8×10^{-8} *M* with the addition of monensin, increasing toxicity by 16–842-fold ***(25)***. In three medulloblastoma cell lines treated with an anti-TR monoclonal antibody-ricin A-chain immunotoxin, the IC_{50} ranged from 8.5×10^{-11} to 1×10^{-9} *M* ***(2,26)***. Using an anti-TR monoclonal antibody–CRM107 immunotoxin, the IC_{50} ranged from 3.2×10^{-9} to 5.7×10^{-9} *M* for these same medulloblastoma cell lines ***(2,26)***. Surgical samples from glioblastoma multiforme and medulloblastoma patients had IC_{50} values of 10^{-12} *M* ***(2,26)***. The time to growth inhibition was after 6 h

of incubation for the anti-TR-CRM107 immunotoxin and not until 16 h for the anti-TR–ricin A-chain conjugate in the one medulloblastoma cell line that was tested ***(2,26)***.

Excellent in vitro results in glioma cell lines have been reported when transferrin was used as the carrier ligand in the construction of immunotoxins. A 10,000-fold increase in tumor-specific toxicity was seen in glioblastoma and medulloblastoma cell lines when transferrin–CRM107 was compared to CRM107 alone ***(9)***. The IC_{50} for transferrin–CRM107 in glioblastoma cell lines ranged from 2.6×10^{-12} to 6.5×10^{-11} *M*, and 3.9×10^{-13} to 1.1×10^{-10} *M* in medulloblastoma cells ***(9)***. Immunotoxins constructed of an anti-TR monoclonal antibody and either CRM107 or ricin A-chain had comparable potency but were not as effective as transferrin–CRM107 in the cell lines tested. The addition of monensin increased the efficacy of transferrin–ricin A-chain 5000-fold over the toxin alone in glioma cell lines and was 100,000 times more potent than BCNU ***(27)***.

Three immunotoxins constructed with human diferric transferrin as the carrier ligand and abrin variant, CRM107, and PE as the toxin moieties were tested against the SNB19 and SF295 glioma cell lines ***(8)***. Transferrin receptor expression on these glioma cell lines was confirmed by direct ^{125}I-transferrin binding assays. For each cell line, the transferrin–abrin variant and transferrin–PE had comparable IC_{50} values and were both more potent than transferrin–CRM107. Monensin potentiated the effect of transferrin–abrin variant by 35-fold in both cell lines where the IC_{50} values were 4.0×10^{-13} *M* (SNB19) and 4.7×10^{-12} *M* (SF295). The DAOY medulloblastoma cell line had IC_{50} values of 1.3×10^{-12} *M* for transferrin–abrin variant with monensin, 3.4×10^{-11} *M* for transferrin–PE, and 1.8×10^{-10} *M* for transferrin–CRM107 ***(28)***. When the genetically engineered immunotoxin composed of epidermal growth factor (EGF) and the DT mutant DAB_{389} was tested against U87 glioma cells, the IC_{50} for DAB_{389}–EGF was 10^{-11} *M* ***(2)***.

Three chimeric immunotoxins, IL4-PE4E, IL4(38-37)-PE38KDEL, and IL4-PE38KDEL, were tested for 20 h against the A172, U251, U373MG, T98G, SNB19, SF295, H638, and U87MG glioma cell lines ***(15,18)***. The IC_{50} values for the glioblastoma cell lines ranged from 5 to 180 ng/mL (~60–2000 p*M*) for IL4-PE4E and were 3–28-fold lower for IL4(38-37)-PE38KDEL ***(15)***. The IL4-PE38KDEL fusion toxin, which is not circularly permuted, was the least effective ***(15)***.

The immunoconjugate constructed with an antiglioma monoclonal antibody (SZ39) and adriamycin had an eightfold increase in toxicity against glioma cells compared to adriamycin alone ***(29)***. Adriamycin had an IC_{50} of 7.08×10^{-8} *M* in contrast with 9.16×10^{-9} *M* for SZ39–adriamycin. Adriamycin was 11 times more toxic to nontarget K560 leukemia cells than SZ39–adriamycin.

4. In Vivo Studies

4.1. Efficacy Studies

Diphtheria toxin is frequently used as a positive control in immunotoxin research because of its extreme potency ***(30)***. Mice are resistant to the effects of DT and humans are extremely sensitive to the toxin. Complete regression of a large human glioblastoma multiforme grown in the flank of a nude mouse treated with intraperitonal DT has been reported ***(30)***. Advanced intraperitoneal human mesothelioma was consistently cured by a single intraperitoneal or intravenous injection of 1.0–3.0 μg DT ***(31)***. Survival was extended in an intracerebral nude rat model of human small-cell lung cancer after intravenous DT administration ***(32)***. Control animals had a median survival of 15 d compared with 19 d for animals receiving 0.1 μg DT, and 26.5 d for animals receiving 1.0 μg DT ***(32)***. Ninety percent of the initial concentration of DT was cleared within 6 h of administration.

The first immunotoxin experiments to involve the CNS were in a syngeneic guinea pig model of leptomeningeal neoplasia ***(33)***. Animals were treated 24 h after the intrathecal inoculation of L_2C leukemia cells with an anti-idiotype monoclonal antibody (M6)–intact ricin immunotoxin administered into the cisterna magna ***(33)***. The results were consistent with a 2–5 log cell kill of L_2C leukemia cells.

In a nude rat model of human neoplastic meningitis from LOX melanoma, untreated animals developed lower extremity paralysis at 10.7 ± 2.75 d, compared with 15.5 ± 4.58 d for animals that were treated 24 h after tumor cell inoculation with 1 μg of intrathecal transferrin–PE immunotoxin ***(3)***. The mean delay in the onset of paraplegia by 5 d (31%) was statistically significant. Animals with intrathecal DAOY medulloblastoma treated 7 d after tumor cell inoculation with 1 μg transferrin–PE developed paraplegia at 56 ± 27 d compared with 38 ± 16 d ($P < 0.05$) for control animals ***(28)***. Even though transferrin receptor expression was found to be decreased in vivo, a significant therapeutic response was found that emphasizes the extreme potency of these compounds ***(28)***.

In another animal model of carcinomatous meningitis from human H-146 small-cell lung cancer injected into the cisterna magna, neurologic symptoms developed after a mean latency of 20 d ***(34)***. Animals received 1.5 μg of an immunotoxin as a single intrathecal injection 24 h after tumor cell inoculation ***(34)***. The immunotoxins tested in this animal model were transferrin–PE and one of two immunotoxins constructed with anticarcinoma monoclonal antibodies (MOC-31 or NrLu10) conjugated to PE. Symptom-free latency was increased by 35%–46% with either MOC-31–PE or MrLu10–PE. MOC-31–PE coinstilled with 10% glycerol increased the symptom-free latency to 72% ***(34)***.

A single bolus injection of MOC-31–PE was more effective that repeat or delayed injections.

Direct intratumoral administration of immunotoxins into a human glioma flank-tumor model in a nude mouse resulted in greater than 95% tumor regression by d 14, and recurrence was not seen by d 30 ***(12)***. When tumors measured 0.5–1.0 cm in diameter, animals received 10 μg of either transferrin–CRM107 or anti-TR monoclonal antibody–ricin A-chain (454A12–RA) immunotoxin every 2 d for 4 doses ***(12)***. By d 14, 454A12–RA had caused a 30% decrease in tumor volume. A significant dose–response relationship was seen for 10, 1.0, and 0.1 μg transferrin–CRM107 injected intratumorally. Direct intratumoral injection of 1 or 10 μg of DAB_{389}–EGF twice a day for three doses into U87 human glioblastoma flank tumors in nude mice significantly inhibited tumor growth compared to control animals ***(2)***. Complete regression of small and large U251 human glioblastoma flank tumors was seen in all animals that received intratumoral administration of 250 μg/kg IL-4(38-37)-PE38KDEL on alternate days for three or four doses ***(13)***. Intraperitoneal and intravenous administration of IL-4(38-37)-PE38KDEL also resulted in significant antitumor activity ***(13)***.

Animals with subcutaneous human glioma xenografts that were treated with SZ39–adriamycin had a greater antitumor effect than animals receiving a nonspecific IgG–adriamycin conjugate ***(29)***. Tumor volumes were 0.30 for animals receiving SZ39–adriamycin, 0.78 for those that received IgG–adriamycin, and 0.84 for animals treated with adriamycin alone. In animals with intracerebral xenografts that received intraperitoneal SZ39–adriamycin, the median survival was 51 d, compared with 36 d for adriamycin alone, and 33 d for phosphate-buffered saline treatment ***(29)***.

4.2. Distribution Studies

Immunotoxin penetration into solid tumor has been investigated after intraperitoneal, intracarotid, and intratumoral administration ***(12,35,36)***. Following an intracarotid injection of 1×10^5 LOX melanoma cells, nude rats developed a skull base tumor with local infiltration into the brain that caused neurologic symptoms at a median of 19 d ***(35)***. With the onset of symptoms, animals received a retrograde external carotid artery injection of 2.5 μg of ^{125}I-anti-melanoma monoclonal antibody–abrin immunotoxin prior to sacrifice at 10 min. Tissue samples were taken from the tumor, ipsilateral cerebral hemisphere, contralateral hemisphere, and brain stem and cerebellum for analysis in a standard gamma counter to determine the tissue immunotoxin concentration (counts × 100/total counts/g tissue). The uptake of immunotoxin in the tumor was 4.9–9.0 times higher than in the ipsilateral brain tissue, demonstrating specificity for targeted tissue ***(35)***.

Quantitative autoradiography has been used to determine the spatial distribution of immunotoxins in solid tumors ***(36)***. Immunotoxins labeled with radioactive iodine targeted to the TR were administered intravenously to animals with a subcutaneous rhabdomyosarcoma that expressed the receptor. Spatial distribution within the tumor was evaluated at 2, 6, and 24 h. Diphtheria toxin had an extremely uniform distribution throughout the tumor compared to either a monoclonal antibody FAb' fragment–CRM107 immunotoxin or a monoclonal IgG_1 antibody–CRM107 conjugate which displayed a punctate pattern on autoradiography ***(36)***. A nonbinding immunotoxin had a more homogenous pattern of distribution than either targeted toxin but was not as uniformly distributed as DT ***(36)***. The heterogenous distribution of both targeted immunotoxins was due to binding to tumor cells that retarded penetration.

When the 454A12–RA chain immunotoxin was administered into the cerebral spinal fluid (CSF) of monkeys, a biphasic clearance pattern was seen with an early phase half-life of 1.4 h and a late-phase half-life of 10.9 h ***(37)***. The clearance of 454A12–RA from the CSF was 4.4 mL/h, which was twice what would be expected from clearance by bulk flow. The immunotoxin was found to be stable for up to 24 h after administration into the CSF, and the volume of distribution was 10.1 mL, or three-fourths the total CSF volume for the monkey ***(37)***.

4.3. Toxicity Studies

Direct delivery of immunotoxins into the intrathecal space is appealing because of the ability to achieve high local concentrations and potentially avoid systemic toxicity ***(2)***. Intrathecal immunotoxin toxicity trials have demonstrated that a maximum dose of 2×10^{-9} *M* transferrin–CRM107 was tolerated in guinea pigs ***(9)***. When this same dose was administered intrathecally in monkeys it was nontoxic and represented a concentration of 20–5000-fold higher than that which was effective against glioma cells in vitro. Neurologic toxicity, which was manifest as hemorrhagic degeneration around the central canal or a pathological cleft in the cervical spinal cord, was seen in rats that were treated intrathecally with 2.5 μg or 5.0 μg of transferrin-PE ***(3)***.

The IL-4(38-37)-PE38KDEL immunotoxin was not associated with any toxicity in mice with subcutaneous human glioblastomas that were treated by intratumoral, intravenous, or intraperitoneal routes ***(13)***. Upon the intrathecal injection of IL-4(38-37)-PE38KDEL in monkeys, high CSF concentrations were achieved without evidence of neurologic toxicity using 2 and 6 μg/kg doses ***(15)***. No monkey demonstrated detectable levels of IL-4(38-37)-PE38KDEL in the serum after intrathecal administration. Injection of IL-4(38-37)-PE38KDEL into the right frontal lobe of a rat resulted in localized necrosis with 1000 μg/mL doses but not at ≤100 μg/mL doses ***(15)***.

In monkeys receiving intrathecal 454A12–RA, the maximally tolerated dose yielded a CSF concentration of 1.2×10^{-7} *M* ***(37)***. In rats, the 10% lethal dose (LD_{10}) of the antihuman TR immunotoxin in the CSF was 8.8×10^{-7} *M*. When the antirat transferrin receptor monoclonal antibody–ricin A-chain (OX26-RA) immunotoxin was tested in rats, the LD_{10} was 1.2×10^{-7} *M*, representing a concentration that is one-seventh of the immunotoxin constructed with the irrelevant antibody. Selective elimination of Purkinje cells was the dose-limiting toxicity seen in rats and monkeys and was manifest clinically as ataxia and uncoordination. The ataxia in monkeys occurred within 5 d and was reversible with time for the more mild form ***(37)***. No evidence of systemic toxicity was apparent, and only mild inflammation was visible in the CSF ***(37)***.

5. Clinical Trials

The encouraging results obtained in animal studies, particularly with intratumoral administration of transferrin–CRM107 and IL-4(38-37)-PE38KDEL, provide the basis for proceeding with the development of immunotoxins for phase I/II clinical trials ***(12,13)***. Two clinical trials have been completed that address the safety and efficacy of immunotoxins administered either into the CSF of patients with leptomeningeal neoplasia, or directly in malignant brain tumors by convection-enhanced delivery ***(14,38)***. The first clinical trial was for the treatment of neoplastic meningitis using 454A12–RA, and the second trial used human diferric transferrin linked to the diphtheria toxin mutant CRM107 (Tfn–CRM107) to treat brain tumors ***(14,38)***.

5.1. Leptomeningeal Neoplasia

A pilot study was performed using 454A12–RA to treat eight patients with leptomeningeal spread of systemic cancer that included breast cancer and lung cancer ***(38)***. Patients received a single intrathecal dose of 454A12–RA that ranged from 1.2–1200 μg. A total of 10 different doses were given during the trial. The early-phase half-life of 454A12–RA in the ventricular CSF averaged 44 ± 21 min, and the late-phase half-life averaged 237 ± 86 min ***(38)***. The clearance of 454A12–RA was 2.4 times faster than that of coinjected technetium-99m–diethylenetriamine penta-acetic acid. There was no degradation of 454A12–RA for a period of 24 h as determined by Western blot analysis, and bioactivity paralleled the concentration of the immunotoxin in the CSF. Bioassays of CSF from treated patients demonstrated retained cytotoxicity for 48 h after immunotoxin administration ***(2)***.

No acute or chronic drug toxicity was seen in any patient that received an intrathecal dose of 454A12–RA less than or equal to 38 μg ***(38)***. Doses greater than or equal to 120 μg caused a CSF inflammatory response that was associated with transient headache, nausea, vomiting, lethargy, and mental status

changes. Corticosteroid administration and CSF drainage was necessary for these patients. Four of eight patients had >50% reduction in their lumbar CSF tumor cell counts within 5–7 d, with a >95% reduction seen at the highest administered dose *(38)*. No patient completely cleared their CSF of tumor cells, and clinical and radiographic progression was seen in seven of eight patients after treatment *(38)*.

5.2. Malignant Brain Tumors

In a phase I/II clinical trial, Tfn–CRM107 was delivered directly into malignant brain tumors using a high-flow interstitial microinfusion technique that induced fluid convection within the brain *(14)*. Eighteen patients were enrolled in the trial, of which ten had glioblastomas multiforme, five had anaplastic astrocytomas, two had lung cancer, and one had an anaplastic oligodendroglioma. One patient withdrew from the study, and the two patients with metastatic disease had surgical resections after treatment and could not be evaluated for response to treatment.

Of the 15 evaluable patients, nine experienced a ≥50% decrease in tumor volume. Reduction in tumor volume did not occur prior to one month after completing the first treatment and was not maximal in four patients for 6–14 mo. Two complete responses were seen. In one complete responder with a glioblastoma multiforme, no tumor progression was seen for 23 mo. The second patient with an anaplastic astrocytoma recurred 5 mo after treatment. Of the 16 patients that could be evaluated by magnetic resonance imaging (MRI) ≤6 wk after treatment, 14 (88%) demonstrated a zone of necrosis or a reduction in tumor volume.

Only two of eight patients had partial responses in the first two treatment groups where the Tfn–CRM107 concentration was 0.1 and 0.32 μg/mL and the total dose was 0.5–12.8 μg. In comparison, two complete and two partial responses were seen in four patients that received ≥1.0 μg/mL or a total dose of 20–128 μg. At intermediate treatment levels, the responses correlated more with total dose level than with the concentration of the drug. Pretreatment tumor volume did not correlate with the likelihood of response. The median survival in the treatment group of nine responders was 74 wk, compared with 36 wk for nonresponders.

Intratumoral infusions of 5–180 mL were well tolerated and there were no treatment-related deaths or life-threatening toxicity *(38)*. Transient worsening of a pre-existing neurologic deficit occurred in 3 of 44 infusions. These deficits resolved with steroid and hyperosmolar therapy. Four patients with seizures had them during treatment, and peritumoral edema was seen in three of these four patients. Peritumoral focal brain injury was seen at the higher concentrations of Tfn–CRM107 (≥1.0 μg/mL) and occurred 2–4 wk after infusion. Three

patients developed a hemiparesis, which resolved in two patients and was associated with magnetic resonance imaging (MRI) changes characterized by serpentine strips of increased signal on the unenhanced T1-weighted scan ***(38)***. Stereotactic biopsy of these abnormal areas revealed thrombosed cortical venules and capillaries. No peritumoral toxicity was seen in patients who received 40 mL of Tfn–CRM107 ≤0.66 μg/mL. Two of three patients who received 120 mL at 0.5 μg/mL (total dose 60 μg) developed peritumoral injury.

No systemic toxicity occurred, although 14 patients had transient elevation of serum AST and ALT transaminases and 12 experienced mild hypoalbuminemia. All patients had antidiphtheria antibodies before treatment that increased at least twofold in 6 of 14 patients > 4 wk after treatment. Increases in antibody titer did not correlate with tumor response. No evidence of systemic toxicity was seen in any of the organs of five patients examined at autopsy. Examination of the brain at autopsy in six patients showed changes that were felt to be consistent with radiation therapy and chronic vasogenic edema, and not due to the effects of Tfn–CRM107 infusion ***(38)***.

6. Future Directions

Present immunotoxin trials are directed at treating recurrent or residual primary malignant disease in the CNS. Because of a different mechanism of action than conventional chemotherapy and radiation therapy, immunotoxins may act synergistically with these forms of treatment without subsequent cumulative side effects. Administering a combination of immunotoxins that target different tumor antigens may result in an improved clinical response.

The immune response against mouse monoclonal antibodies and protein toxins presents a potential problem that may influence their overall efficacy. Antibodies to immunotoxins interfere with their binding ability and accelerate plasma clearance. The generation of antibodies from different animal species, the use of human monoclonal antibodies or antibody fragments that bind antigens, or the creation of chimeric rodent–human monoclonal antibodies may stimulate less of an immune response ***(1)***. Immunosuppressive drugs, such as cyclophosphamide and cyclosporin A, may diminish or delay the immune response to immunotoxins and allow for repeat treatments ***(1)***. The "immunologically privileged" nature of the CNS may offer protection from the immune system.

Because of the large size of immunotoxin molecules and their inability to diffuse into tumor tissue in the presence of an intact blood–brain barrier, investigators have considered alternative routes of administration for these agents. Convection-enhanced intratumoral delivery appears to effectively allow immunotoxins to reach tumor cells with minimal neurologic morbidity ***(14)***. Blood–brain barrier disruption using hyperosmolar mannitol may also represent another route for delivering these compounds in sufficient quantities to be

therapeutically effective. Producing smaller carrier ligands such as antibody fragments and FAbs, and using recombinant technology to generate fusion proteins, may increase tumor penetration and reduce antigenicity ***(1,7)***. The coadministration of drugs that potentiate the action of immunotoxins—such as α-interferon, monensin, chloroquine, and the calcium-channel blockers verapamil and diltiazem—may enhance their effect ***(1)***.

Immunotoxins are an effective class of compounds against malignant brain tumors in vitro and in vivo. The extreme potency of these agents allows them to retain significant efficacy despite reduced antigen receptor expression that has be seen in vivo ***(28)***. Although no tumor-specific antigen has been identified on malignant glioma cells, there appears to be a therapeutic window between transferrin and IL-4 receptor expression on neoplastic cells, compared to normal brain tissue, that can be exploited in the CNS. Although the prognosis for malignant brain tumors remains poor, immunotoxins represent an exciting therapeutic modality with tremendous potential that offers future promise for patients with this disease.

References

1. Hall, W. A. and Fodstad, Ø. (1992) Immunotoxins and central nervous system neoplasia. *J. Neurosurg.* **76,** 1–12.
2. Hall, W. A. (1997) Targeted toxin therapy, in *Advances in Neuro-Oncology II* (Kornblith, P. L. and Walker, M. D., eds.), Futura, Armonk, NY, pp. 505–516.
3. Hall, W. A., Myklebust, A., Godal, A., Nesland, J. M., and Fodstad, Ø. (1994) In vivo efficacy of transferrin-*Pseudomonas* exotoxin A immunotoxin against LOX melanoma. *Neurosurgery* **34,** 649–656.
4. Hall, W. A., Djalilian, H. R., Sperduto, P. W., Cho, K. H., Gerbi, B. J., Gibbons, J., et al. (1995) Stereotactic radiosurgery for recurrent malignant gliomas. *J. Clin. Oncol.* **13,** 1642–1648.
5. Wen, D. Y., Hall, W. A., and Fodstad, Ø. (1993) Rapid detection of transferrin receptor expression on glioma cell lines by using magnetic microspheres. *Neurosurgery* **33,** 878–881.
6. Multani, P. S. and Grossbard, M. L. (1998) Monoclonal antibody-based therapies for hematologic malignancies. *J. Clin. Oncol.* **16,** 3691–3710.
7. Siegall, C. B. (1994) Targeted toxins as anticancer agents. *Cancer* **74,** 1006–1012.
8. Hall, W. A., Godal, A., Juell, S., and Fodstad, Ø. (1992) In vitro efficacy of transferrin-toxin conjugates against glioblastoma multiforme. *J. Neurosurg.* **76,** 838–844.
9. Johnson, V. G., Wrobel, C., Wilson, D., Zovickian, J., Greenfield, L., Oldfield, E. H., et al. (1989) Improved tumor-specific immunotoxins in the treatment of CNS and leptomeningeal neoplasia. *J. Neurosurg.* **70,** 240–248.
10. Zovickian, J., Johnson, V. G., and Youle, R. J. (1987) Potent and specific killing of human malignant brain tumor cells by an anti-transferrin receptor antibody-ricin immunotoxin. *J. Neurosurg.* **66,** 850–861.

11. Zovickian, J. and Youle, R. J. (1988) Efficacy of intrathecal immunotoxin therapy in an animal model of leptomeningeal neoplasia. *J. Neurosurg.* **68,** 767–774.
12. Laske, D. W., Ilercil, O., Akbasak, A., Youle, R. J., and Oldfield, E. H. (1994) Efficacy of direct intratumoral therapy with targeted protein toxins for solid human gliomas. *J. Neurosurg.* **80,** 520–526.
13. Husain, S. R., Behari, N., Kreitman, R. J., Pastan, I., and Puri, R. K. (1998) Complete regression of established human glioblastoma tumor xenograft by interleukin-4 toxin therapy. *Cancer Res.* **58,** 3649–3653.
14. Laske, D. W., Youle, R. J., and Oldfield, E. H. (1997) Tumor regression with regional distribution of the targeted toxin TF-CRM107 in patients with malignant brain tumors. *Nature Med.* **3,** 1362–1368.
15. Puri, R. K., Hoon, D. S., Leland, P., Snoy, P., Rand, R. J., Pastan, I., et al. (1996) Preclinical development of a recombinant toxin containing circularly permuted interleukin 4 and truncated *Pseudomonas* exotoxin for therapy of malignant astrocytoma. *Cancer Res.* **56,** 5631–5637.
16. Kreitman, R. J. and Pastan, I. (1998) Accumulation of a recombinant immunotoxin in a tumor *in vivo*: fewer than 1000 molecules are sufficient for complete responses. *Cancer Res.* **58,** 968–975.
17. Kreitman, R. J., Puri, R. K., and Pastan, I. (1995) Increased antitumor activity of a circularly permuted interleukin 4–toxin in mice with interleukin 4 receptor-bearing human carcinoma. *Cancer Res.* **55,** 3357–3363.
18. Puri, R. K., Leland, P., Kreitman, R. J., and Pastan, I. (1994) Human neurological cancer cells express interleukin-4 (IL-4) receptors which are targets for the toxic effects of IL-4-*Pseudomonas* exotoxin chimeric protein. *Int. J. Cancer* **58,** 574–581.
19. Hall, W. A., Merrill, M. J., Walbridge, S., and Youle, R. J. (1990) Epidermal growth factor receptor receptors on ependymomas and other brain tumors. *J. Neurosurg.* **72,** 641–646.
20. Libermann, T. A., Nusbaum, H. R., Razon, N., Kris, R., Lax, I., Spreq, H., et al. (1985) Amplification, enhanced expression and possible rearrangement of EGF receptor gene in primary human brain tumours of glial origin. *Nature* **313,** 144–147.
21. Humphrey, P. A., Wong, A. J., Vogelstein, B., Friedman, H. S., Werner, M. H., Bigner, D. D., et al. (1988) Amplification and expression of the epidermal growth factor receptor gene in human gliomas xenografts. *Cancer Res.* **48,** 2231–2238.
22. Helseth, E., Unsgaard, G., Dalen, A., Fure, H., Skandsen, T., Odegaard, A., and Vik, R. (1988) Amplification of the epidermal growth factor receptor gene in biopsy specimens from human intracranial tumours. *Br. J. Neurosurg.* **2,** 217–225.
23. Whittle, I. R., Hawkins, R. A., Killen, E., and Miller, J. D. (1988) Epidermal growth factor binding in intracranial neoplasms: preliminary biochemical and clinicopathological findings. *Br. J. Neurosurg.* **2,** 211–215.
24. Recht, L., Torres, C. O., Smith, T. W., Raso, V., and Griffin, T. W. (1990) Transferrin receptor in normal and neoplastic brain tissue: implications for brain-tumor immunotherapy. *J. Neurosurg.* **72,** 941–945.

25. Recht, L.D, Griffin, T. W., Raso, V., and Salimi, A. R. (1990) Potent cytotoxicity of an antihuman transferrin receptor-ricin A chain immunotoxin on human glioma cells in vitro. *Cancer Res.* **50,** 6696–6700.
26. Martell, L. A., Agrawal, A., Ross, D. A., and Muraszko, K. M. (1993) Efficacy of transferrin-receptor targeted immunotoxins in brain tumor cell lines and pediatric brain tumors. *Cancer Res.* **53,** 1348–1353.
27. Colombatti, M., Bisconte, M., Dell'Arciprete, L., Gerosa, M. A., and Tridente, G. (1988) Sensitivity of glioma cells to cytotoxic heteroconjugates. *Int. J. Cancer* **42,** 441–448.
28. Wen, D. Y., Hall, W. A., Conrad, J., Godal, A., Flørenes, V. A., and Fodstad, Ø. (1995) In vitro and in vivo variation in transferrin receptor expression on a human medulloblastoma cell line. *Neurosurgery* **36,** 1158–1164.
29. Zhu, J.-H., Du, Z.-W., Huang, Q., Yang, W.-L., and Wang, Y. (1990) Drug-targeting by monoclonal antibody in neurooncology. *Child's Nerv. Syst.* **6,** 309.
30. Reid, L. M., Colburn, P., Sato, G., and Kaplan, N. O. (1978) Approaches to chemotherapy using the athymic nude mouse, in *Proccedings of the Symposium on the Use of Atyhymic* (Nude) *Mice in Cancer Research* (Houchens, D. P. and Ovejera, A. A., eds.), Gustav Fischer, NY, pp. 123–131.
31. Raso, V. and McGrath, J. (1989) Cure of experimental human malignant mesothelioma in athymic mice with diphtheria toxin. *J. Natl. Cancer Inst.* **81,** 622–627.
32. Wrobel, C. J., Wright, D. C., Dedrick, R. L., and Youle, R. J. (1990) Diphtheria toxin effects on brain-tumor xenografts: implications for protein-based brain-tumor chemotherapy. *J. Neurosurg.* **72,** 946–950.
33. Zovickian, J. and Youle, R. J. (1988) Efficacy of intrathecal immunotoxin therapy in an animal model of leptomeningeal neoplasia. *J. Neurosurg.* **68,** 767–774.
34. Myklebust, A. T., Godal, A., and Fodstad, Ø. (1994) Targeted therapy with immunotoxins in a nude rat model for leptomeningeal growth of human small cell lung cancer. *Cancer Res.* **54,** 2146–2150.
35. Myklebust, A. T., Helseth, A., Breistøl, K., Hall, W. A., and Fodstad, Ø. (1994). Nude rat models for human tumor metastasis to the CNS: procedures for intracarotid delivery of cancer cells and drugs. *J. Neuro-Oncol.* **21,** 215–224.
36. Sung, C., Dedrick, R.L, Hall, W. A., Johnson, P. A., and Youle, R. J. (1993) The spatial distribution of immunotoxins in solid tumors: assessment by quantitative autoradiography. *Cancer Res.* **53,** 2092–2099.
37. Muraszko, K., Sung, C., Walbridge, S., Greenfield, L., Dedrick, R. L., Oldfield, E. H., et al. (1993) Pharmacokinetics and toxicology of immunotoxins administered into the subarachnoid space in nonhuman primates and rodents. *Cancer Res.* **53,** 3752–3757.
38. Laske, D. W., Muraszko, K. M., Oldfield, E. H., DeVroom, H. L., Sung, C., Dedrick, R. L., et al. (1997) Intraventricular immunotoxin therapy for leptomeningeal neoplasia. *Neurosurgery* **41,** 1039–1049.

11

Cytotoxins Directed at Interleukin-4 Receptors as Therapy for Human Brain Tumors

Raj K. Puri

1. Introduction

Interleukin-4 (IL-4) is a pleiotropic immune regulatory cytokine that has been extensively studied in the last decade. Activated T-lymphocytes, mast cells, and basophils ***(1–3)*** produce it. Consistent with the pleiotropic nature of this molecule, the receptors for IL-4 have been identified on many different cell types, including hematopoietic and nonhematopoietic cells ***(2–4)***. We have reported that a variety of solid tumor cells express a greater number of high-affinity IL-4 receptors (IL-4R) than normal cells ***(5–12)***. We were first to report that murine solid cancer cells expressed high affinity IL-4R ***(4)***. We later reported that human renal-cell carcinoma and other solid tumor cells expressed functional IL-4R ***(6,7)***. These receptors are functional because IL-4 can cause signal transduction, inhibit growth of some tumor cell lines, and increase expression of major histocompatibility antigens and the intercellular adhesion molecule-1 (ICAM-1) on some tumor cell lines ***(11–17)***. IL-4R is also expressed, although in low numbers, in normal immune cells such as T-cells, B-cells, monocytes, other blood cells such as eosinophils, basophils, and fibroblasts, and endothelial cells ***(1–3)***.

The significance of overexpression of IL-4R and its subunit structure on solid cancer cells is not completely clear. IL-4R is comprised of a 140-kDa protein originally termed as IL-4Rα ***(4,11)***. Because of similarities in extracellular domains (WSXWS motif and four cysteine residues at the fixed location) and long intracellular domains between IL-4Rα and β chains of receptors for IL-3, IL-5, and GM-CSF, this chain was renamed IL-4Rβ ***(11,18)***. This redesignation was also based on its similarity with the IL-2Rβ chain which,

From: *Methods in Molecular Biology, vol. 166: Immunotoxin Methods and Protocols*
Edited by: W. A. Hall © Humana Press Inc., Totowa, NJ

like IL-4Rp140, binds IL-2 but does not transmit signals on its own. The renaming of this chain is still controversial, and the IL-4Rα designation is still commonly used.

The second subunit of the IL-4R system was shown to be the γ chain of the IL-2 receptor system ***(19,20)***. It has been named γ_c because it was also shown to be a component of IL-7, IL-9 and IL-15 receptor systems ***(21–23)***. Recently, we demonstrated that a 60–70 kDa protein form of the interleukin-13 receptor (IL-13R) can substitute γ_c in mediating IL-4 signaling; thus, this chain forms a third subunit of the IL-4R system (termed IL-13Rα' or αl.) ***(15,16,24–26)***. Whether all three chains form an IL-4R complex in immune or tumor cells is not known. The differences in subunit structure between IL-4R in cancer cells and immune cells are also not completely known. Our extensive studies have demonstrated that the γ_c chain expressed in immune cells is not expressed by human solid cancer cell lines ***(10,15,16,24–27)***. Instead, these cells express the IL-13Rα' chain along with the IL-4Rβ chain ***(16,28)***. By reconstitution experiments, we have demonstrated that IL-4 can activate the STAT6 protein in cells expressing the IL-4Rβ and IL-13Rα' chains ***(16)***, confirming that these chains form an alternate form of the IL-4R complex. Further studies on the structure and function of IL-4R on cancer cells are ongoing. Regardless of differences in IL-4R between normal and cancer cells, we have been able to exploit the overexpression of IL-4R by cancer cells by targeting them with a cytotoxic chimeric protein composed of IL-4 and *Pseudomonas* exotoxin (PE) ***(29–40)***.

PE-based cytotoxins have been used previously to target cancer cells ***(41)***. PE is a 66-kDa protein produced by *Pseudomonas aeruginosa*. It has three domains: domain Ia binds to PE receptors, domain II catalyzes the translocation of the toxin into the cytosol, and domain III inhibits protein synthesis and eventually kills the cells by adenosine diphosphate (ADP) ribosylation of elongation factor 2 ***(42)***. The domain Ia of PE binds α2-macroglobulin receptors that are expressed ubiquitously and these cells die after binding to PE. By deleting or mutating the binding domain, one can substantially decrease or abrogate PE's cytotoxic activity. By replacing the binding domain of PE with IL-4, one assigns a new function to PE: This molecule (IL4-PE) will only bind cells that express IL-4R, and these cells will only die if they are able to internalize PE molecules that are processed in the right intracellular compartment of the cytoplasm. This chapter will review the expression of IL-4R by brain tumor cells, the targeting of these receptors by IL4-PE, the use of circular permutated IL-4 toxin on brain tumor cells, preclinical results that support initiation of a phase I clinical trial for the therapy of human glioblastoma muliforme, and preliminary observations made in the clinical trial so far.

Table 1
IL-4 Receptor Expression by Brain Tumor Cells

Tumor	IL-4 molecules/cell[a]
A 172 glioblastoma	2156 ± 109
SF295 glioblastoma	1043 ± 60
U251 glioma	37 ± 19
T98G glioblastoma	1532 ± 60

[a]Determined by binding (^{125}I)IL-4 (500–600 p*M*) to tumor cells at 4°C. Specific binding was calculated by subtracting nonspecific binding (determined in the presence of a 250 mol excess of unlabeled IL-4 from total binding. Data are represented as mean IL-4 molecules bound/cell ± SEM of triplicate or quadruplicate determination. Adapted from **ref. *34***.

2. IL-4R Expression

2.1. Expression of IL-4R on Glioblastoma

Human brain-cancer cell lines express IL-4R ***(34)***. Using (^{125}I)-IL-4 binding studies, glioblastoma, glioma, and neuroblastoma cells were found to express IL-4R. These receptors were of high affinity (K_d = 100–700 × 10^{-12} *M*) on glioblastoma cells (**Table 1**). By flow cytometric analysis, 100% of glioma cells were positive for IL-4R expression (**Fig. 1**). Surgical samples of high-grade astrocytoma and glioblastoma were assessed for IL-4R expression by reverse-transcriptase polymerase chain reaction (RT-PCR) and Southern blot analysis; 16 of 21 surgical samples expressed IL-4R ***(37)***. Five of six normal brain tissue samples (five from the frontal lobe and one from the temporal cortex) did not express IL-4Rβ chain as determined by RT-PCR and Southern blot analysis ***(37)***. However, our recent study suggests that normal human astrocytes express mRNA and proteins for IL-4Rβ and IL-13Rα' chains ***(43)***. Additional samples should be examined to confirm this observation.

2.2. Structure of IL-4R on Glioma Cells

To determine the subunit structure of IL-4R on glioma cells, crosslinking and RT-PCR studies were performed. Complexes crosslinked with (^{125}I)-IL-4 were analyzed by SDS-PAGE analysis, resulting in crosslinks to p140 and 70–80 kDa doublet proteins. Monoclonal antibodies to the IL-4Rβ chain immunoprecipitated faint 70–80 kDa and the IL-4Rβ bands, suggesting that IL-4Rβ chain forms a complex with the 70-kDa IL-13Rα' chain (**Fig. 2**). Antibodies to the γ chain did not immunoprecipitate any bands, indicating that γ_c does not participate in the formation of the IL-4R complex in two brain-tumor cell lines examined.

We further examined the interaction between IL-4R and IL-13R in these cells. Since IL-4R has been shown to share two chains with the IL-13R sys-

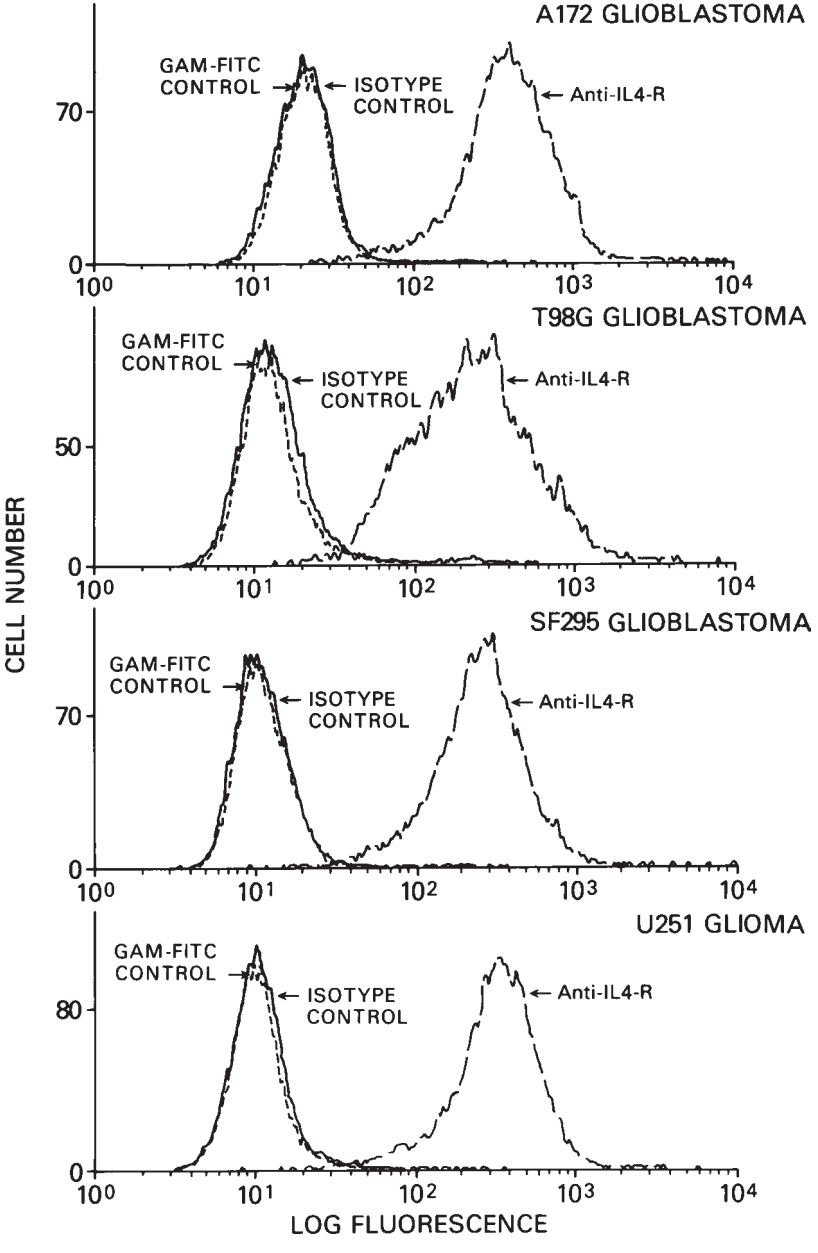

Fig. 1. IL-4 receptor expression by glioblastoma, neuroblastoma, and glioma cells. Tumor cells were stained with anti-IL4-R antibodies (M-57) or an isotype-matched control for 60 min at 4°C. Cells were then washed and stained with FITC-labeled secondary Fab' fragment antibody for an additional 60 min and then analyzed for specific staining. Data is representative of two experiments.

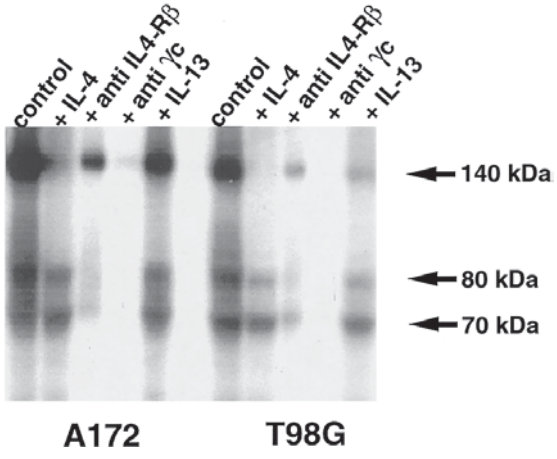

Fig. 2. Crosslinking of (^{125}I)IL-4 to its receptors. A172 and T98G cells (5–10 × 10^6) were incubated with (^{125}I)-IL-4 in the presence or absence of excess IL-4 or IL-13 for 2 h at 4°C. The bound ligand was crosslinked to its receptor with disuccinimidyl suberate and then cells were lysed. The cell lysates were precleared and cleared by boiling in sample buffer containing 2-mercaptoethanol and analyzed by electrophoresis through an 8% SDS polyacrylamide gel. The gel was subsequently dried and autoradiographed. In some instances, the receptor–ligand complex was captured from the precleared total cell lysate on protein A sepharose beads previously incubated with receptor-specific antibodies. The complex was washed in lysis buffer, boiled in sample buffer, and analyzed by SDS-PAGE and autoradiography. Arrows mark protein bands of interest (Puri et al., unpublished data).

tem ***(24)***, we examined whether binding of (^{125}I)-IL-4 to any receptor chain was competed by excess IL-13. In A172 cells, IL-13 did not displace (^{125}I)-IL-4 binding, indicating that IL-4R does not interact with IL-13 in these cells. However, in T98G cells, (^{125}I)-IL-4 binding to IL-4Rβ and IL-13Rα' chains was slightly displaced by IL-13, indicating that IL-13R and IL-4R may be related. RT-PCR studies demonstrated the presence of IL-4Rβ and IL-13Rα' chains but not IL-2 receptor γ chain (IL-2Rγ) in these cells, confirming results of crosslinking studies. Since the IL-2Rγ chain was not expressed on glioma cells, our studies indicate that glioma cells express type II IL-4R on their cell surfaces (**Table 2**; ***43***).

3. Targeting IL-4R on Glioblastoma

To target IL-4R on brain cancer cells, we utilized a recombinant chimeric cytotoxin composed of IL-4 and a mutated form of PE (IL4-PE^{4E}) ***(29,34)***. This chimeric toxin was produced by the fusion of a human IL-4 cDNA to the 5' end of a cDNA encoding a full-length PE mutated in domain Ia. These

Table 2
Expression of IL-4R Chains by Human Glioblastoma Tumor Cell Lines[a]

Cell Lines	IL-4Rβ	IL-13α'	γ_c
U251	+	+	–
A172	+	+	–
T98G	+	+	–

[a]Total RNA from different cell lines was isolated and reversely transcribed using specific primers as described by Murata et al. ***(48)***. The PCR products were analyzed by 2% Nusieve 3:1 agarose gel. The mRNA was visualized by ethdium bromide staining (Puri et al., unpublished data).

Table 3
Cytotoxicity of IL4-PE^{4E}

Tumor	IC_{50} (ng/mL)[a]
Glioblastoma	
T98G	9.0
A172	9.0
U-87MG	50.0
U-373MG	20.0
SN19	30.0
SF295	150.0
Neuroblastoma	
$LA1–5_s$	45.0
IMR-32	70.0
SK-N-SH	110.0
Glioma	
U251	35.0
H638	25.0

[a]Represents the concentration of IL4-PE^{4E} at which 50% inhibition of protein synthesis is observed compared with untreated cells. Adapted from **ref. *34***.

mutants prevent the binding of PE to the PE receptor, hence preventing cytotoxic activity that would otherwise be directed against many types of normal cells. The purified IL-4PE^{4E} was highly cytotoxic toward human glioblastoma, neuroblastoma, and glioma tumor cells (**Table 3**). The IC_{50} ranged between 9–150 ng/mL. The cytotoxicity of IL4-PE^{4E} was specific, as it was neutralized

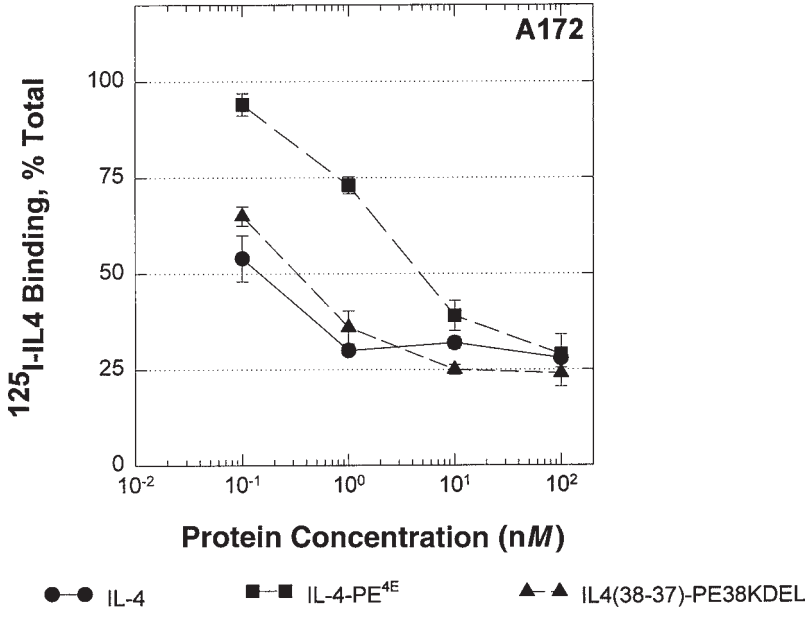

Fig. 3. Displacement of (^{125}I)-IL-4 binding by IL4-PE. A172 glioblastoma cells were incubated at 4°C with 200 p*M* (^{125}I)IL-4 and various concentrations of either IL-4, IL4(38-37)-PE38KDEL, or IL4-PE^{4E}. After 2 h, cells were centrifuged through a mixture of phthalate oils and cell pellets were counted in a gamma counter. The data points shown are the mean ± SD of duplicate determinations.

by excess IL-4 and by an anti-IL-4 monoclonal antibody in all types of brain tumors tested. The cytotoxins comprised of IL-2, IL-6, and PE were not cytotoxic, nor an IL4-PE^{4E} mutant lacking ADP-ribosylating activity, indicating the IL4-PE^{4E}-mediated cytotoxicity of the brain tumor cells require both IL-4R binding and enzymatic toxin activity ***(34)***.

3.1. Activity of Circularly Permuted IL4-PE on Glioma cells

Because IL4-PE^{4E} bound to IL-4R in glioma cells with 37-fold less affinity than native IL-4 (**Fig. 3**), we produced a circularly permuted IL4-PE termed IL4(38-37)-PE38KDEL ***(30,33,36)***. This molecule contains amino acid residues 38–129 of IL-4 fused via a peptide linker to residues 1–37, which in turn is fused to residues 353–364 and 381–608 of PE, with KDEL (an endoplasmic retaining sequence) at positions 609–612. This purified toxin was found to be highly cytotoxic to IL-4R–positive glioblastoma cells and bound to glioblastoma cells with 16-fold higher affinity than the native IL4-toxins, IL4-PE^{4E} (**Fig. 3**) or IL4-PE38KDEL (not shown). More importantly, IL4(38-37)-

Table 4
Cytotoxicity of IL4(38-37)-PE38KDEL vs IL4-PE38KDEL and IL4-PE^{4E}

Cells	IC_{50}[a] (ng/mL) IL4(38-37)-PE38KDEL	IL4-PE38KDEL	IL4-PE^{4E}
U251	7[b]	100	34
A172	1	23	23
U373	4	142	34
T98G	2	38	5
SN19	10	233	40

[a]Ten thousand cells were cultured with IL4-PE for 20 h at 37°C, pulsed with 1 μCi of [^{3}H]-leucine, and further incubated for 4 h. Cells were harvested and counted.

[b]Values are presented as the mean of four experiments performed in quadruplicate. However, individual IC_{50s} are shown for other tumor cell lines from two independent experiments performed in quadruplicate. Adapted from **ref. *37***.

PE38KDEL was 3–30-fold more cytotoxic to glioblastoma cell lines compared with the first-generation toxins IL4-PE38KDEL or IL-PE^{4E} (**Table 4**) ***(37)***. The cytotoxic activity of circularly permuted IL4-PE was specific, as excess IL-4 neutralized its activity (**Fig. 4**).

The cytotoxicity of IL4(38-37)-PE38KDEL was also tested on normal human bone marrow-derived cells, EBV-transformed B-cells, promonocytic (U937) cells, H9 T-cells, and normal endothelial cells. Consistent with the expression of low numbers of IL-4R, IL4-PE was not cytotoxic at all or mediated only slight cytotoxicity in these resting human cells (**Fig. 5**; ***30***).

3.2. Antitumor Activity of IL4(38-37)-PE38KDEL

IL4(38-37)-PE38KDEL was also very cytotoxic to glioma cells as determined by clonogenic assay. More than 50% of colonies were inhibited at <1 ng/mL of IL4-PE. (**Table 5**). Thus, in vitro data indicated that glioblastoma cells are very sensitive to IL-4 toxins. To assess in vivo activity of the toxin, nude mice were injected subcutaneously (sc) with human U251 glioma cells, resulting in the development of tumors with a mean size of 13–60 mm^3 by d 3–4. These cells consistently generated solid tumors in all injected animals. The efficacy of IL4(38-37)-PE38KDEL when administered by different routes and dosing schedules was evaluated ***(39)***.

3.2.1. Intraperitoneal Treatment

Intraperitoneal administration of IL4(38-37)-PE38KDEL on every other day for a total of 3 d significantly inhibited U251 tumor growth in a dose-dependent manner (at doses of 25, 50, or 100 μg/kg). Therapy was well tolerated,

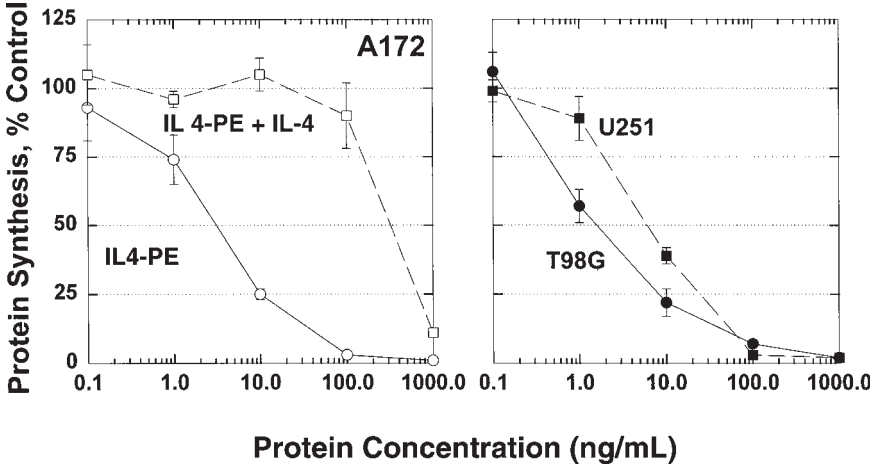

Fig. 4. Cytotoxicity of IL4(38-37)-PE38KDEL. Ten thousand A172 (**A**), T98G, or U251 **(B)** glioma cells were cultured with various concentrations of IL4(38-37)-PE38KDEL. In some wells, excess IL-4 (2 μg/mL) was added 30 min prior to the addition of IL-4 toxin. Protein synthesis was measured after 20 h of culture by incorporation of (^{3}H)-leucine. The results are presented as the mean ± SD % control of untreated cells from quadruplicate determinations.

with no signs of apparent toxicity or deaths. Complete tumor regressions were seen at the two highest doses. Three of five mice remained tumor-free at a long-term follow-up (**Fig. 6**; ***39***).

3.2.2. Intravenous Treatment

Antitumor activity of IL4(38-37)-PE38KDEL was also assessed by intravenous administration of IL4(38-37)-PE38KDEL ***(39)***. Tumor-bearing mice were injected intravenously with three different doses (50, 100, and 200 μg/kg) of IL4(38-37)-PE38KDEL on alternate days for a total of 3 d; tumor volumes were then measured three times a week. Tumor regression was noted in 100% of the IL4(38-37)-PE38KDEL–treated mice, irrespective of the dose administered, beginning as early as d 6. The effect of IL4(38-37)-PE38KDEL was clearly dose-dependent; however, complete regressions were not observed.

3.2.3. Intratumoral Treatment

To determine whether intratumoral treatment would lead to better antitumor activity, nude mice with SC U251 tumors were injected intratumorally with various doses of IL4(38-37)-PE38KDEL (up to 1000 μg/kg; ***39***). Tumors in the mice treated with three 250 μg/kg doses of IL4(38-37)-PE38KDEL every other

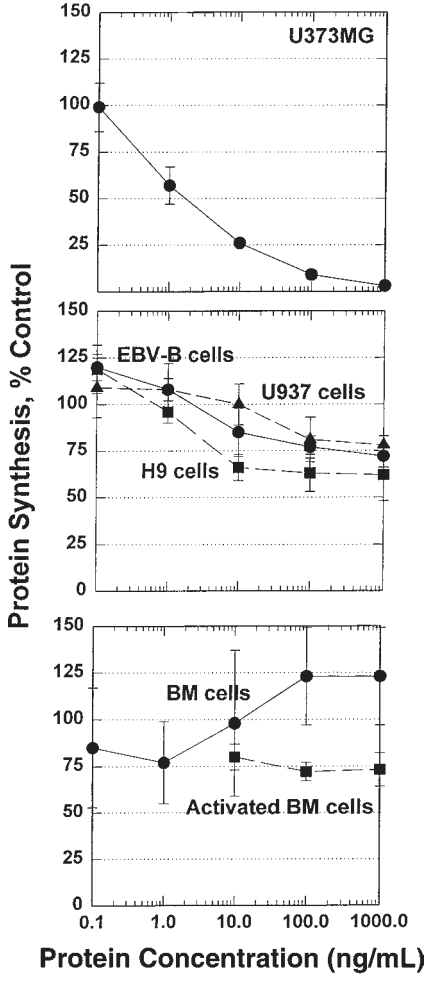

Fig. 5. IL4(38-37)-PE38KDEL is not cytotoxic to normal immune cells. Ten thousand U373MG glioma cells (*top*), EBV immortalized B, U937 promonocytic, and H9 T-cells (*middle*) or resting or activated bone marrow cells (*bottom*) were cultured with various concentrations of IL4(38-37)-PE38KDEL. Protein synthesis was measured as described in **Fig. 4** legend.

day began to decrease significantly in size by d 10, with 100% of mice exhibiting complete regression by d 24. Although tumors recurred in 50% of mice by d 37 from tumor implantation, the mean size of the tumors remained significantly smaller than the control group (2% of control tumor size, or 20 mm^3 vs 1135 mm^3) through d 58.

Table 5
Inhibition of U251 Brain-Tumor Cell Colony Formation by IL4(38-37)-PE38KDEL[a]

IL4(38-37)-PE38KDEL (ng/mL)	Colonies ± SD (% of control)
1	49.1 ± 9.1
5	7.3 ± 1.9
0	4.0 ± 2.8
20	0
100	0

[a]Five hundred cells were allowed to adhere to 100 mm Petri dishes and culture media was replaced with medium containing various concentrations of IL4(38-37)-PE38KDEL. Cells were cultured for 10 d and colonies consisting of at least 50 cells were scored after washing with PBS and staining with crystal violet. Adapted from **ref. *39***.

All four mice treated with four 250 μg/kg doses of IL4(38-37)-PE38KDEL, every other day for 4 d showed complete responses by d 12 and remained tumor-free for 64 d. One mouse displayed tumor growth (approx 3 mm^3) that increased very slowly thereafter and reached a size of 26 mm^3 by the end of the experiment (91 d).

We also evaluated the antitumor activity of IL4(38-37)-PE38KDEL against relatively larger U251 glioblastoma tumors of 60 mm^3 size ***(39)***. Treatment with 750 μg/kg of IL4(38-37)-PE38KDEL was initiated on d 4, with additional doses administered on d 6 and 8. All treated animals showed substantial tumor regression as early as d 6. Complete tumor regression in 100% of the mice was observed by d 8. These mice remained tumor-free for more than 100 d. All control animals injected with excipient quickly developed tumors and were sacrificed by d 60 (**Fig. 7**).

To assess the distribution of IL4(38-37)-PE38KDEL after intratumoral injection as it relates to its antitumor activity, we implanted tumors in both flanks of each nude mouse. The tumors in the right flank were injected intratumorally with three 750 μg/kg doses of IL4-PE every other day, and tumors in the left flank received excipient solution. Additional mice intratumorally received excipient only in both flanks (designed as control). On the day of the third injection, the IL4-PE–treated tumors in the right flank were completely regressed in all animals; these flanks remained tumor-free until termination of the study. Excipient-treated tumors in the left flank continued to grow in all mice at a rate comparable to the controls. These studies indicated that most of the IL4-PE remained localized after intratumor administration (**Fig. 8**).

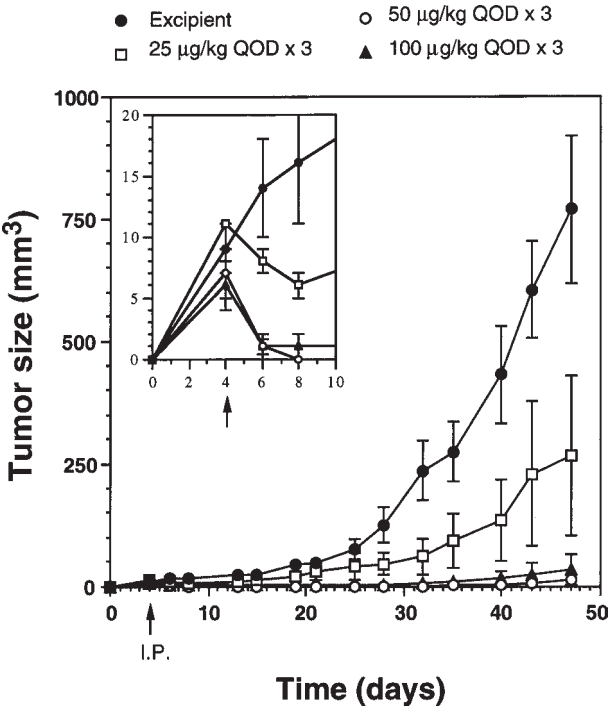

Fig. 6. In vivo antitumor activity of IL4(38-37)-PE38KDEL against established glioblastoma tumors. Nude mice received subcutaneous injections of U251 cells on d 0. Animals were injected intraperitoneally on d 4, 6, and 8, with different doses of IL4(38-37)-PE38KDEL in 100 µL volume. Tumor sizes were measured two to three times per week by a Vernier caliper. Tumor volumes were calculated as: Volume = (length)(width)^2(0.4).

4. Toxicology and Pharmacokinetics

In vivo toxicology and pharmacokinetics studies in mice, rats, guinea pigs, and cynomolgus monkeys have been conducted ***(36,40)***. The LD_{50} (IL4-PE dose causing death in 50% of animals) in mice was determined to be 475 µg/kg given every other day for a total of three injections. Liver enzymes were elevated at doses of 400 µg/kg and higher. This toxicity was most likely related to nonspecific uptake of the toxin by the liver, since human IL-4 does not bind murine cells ***(44)***. The serum half-life of IL(38-37)-PE38KDEL was 10 min after single intravenous administration of IL4-PE.

To determine the concentration of IL4-PE required to cause necrosis of normal brain tissue by nonspecific internalization, we used rats whose IL-4R did not bind human IL-4. Six groups of rats received various doses of IL4(38-37)-

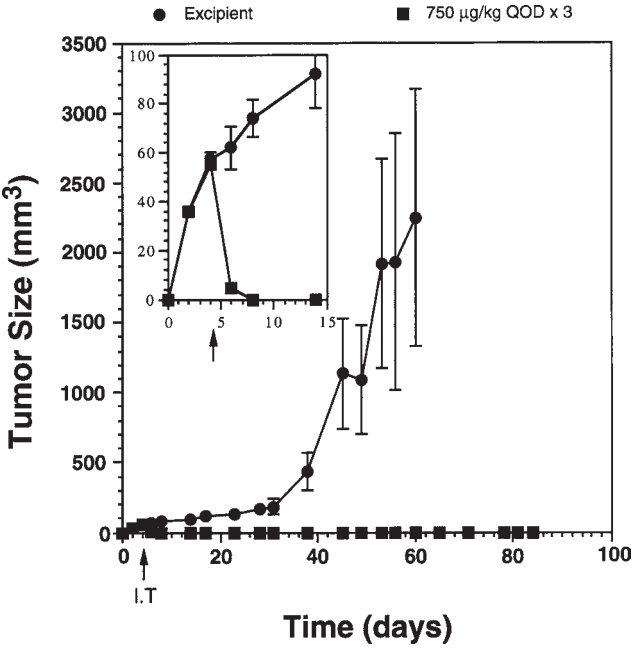

Fig. 7. Antitumor activity by intratumor IL4-PE administration. Nude mice received subcutaneous injections of U251 cells on d 0. Animals were injected intratumorally on d 4, 6, and 8, with different doses of IL4(38-37)-PE38KDEL when tumor size had reached approx 60 mm^3. The toxin was injected with a total volume of 20 μL in each half of the tumor at each sitting.

PE38KDEL injected into the frontal cortex. On d 4, the animals were sacrificed and their brain tissues were examined microscopically. All animals survived until the terminal necropsy. No abnormalities in behavior were noted and the mean body weights did not change for all groups; there were no remarkable gross pathological findings. No IL4(38-37)–PE38KDEL induced histopathologic changes were observed at concentrations ≤100 μg/mL. Microscopic evaluation revealed necrosis of the right cortical hemisphere at the injection site in the group receiving 1000 μg/mL IL4(38-37)-PE38KDEL ***(37)***.

We then performed intrathecal administration of IL4(38-37)-PE38KDEL in monkeys as a toxicology model for the intratumor injection of patients, because in both cases the drug would form a fluid space bound by normal brain tissue. In addition, intrathecal administration would provide maximum exposure of the brain to high concentrations of IL4-PE. Because human IL-4 is primate-specific, produces many effects in cynomolgus monkeys, and can bind to monkey fibroblast and gibbon ape leukemia cells ***(19,45,46)***, this model allowed us

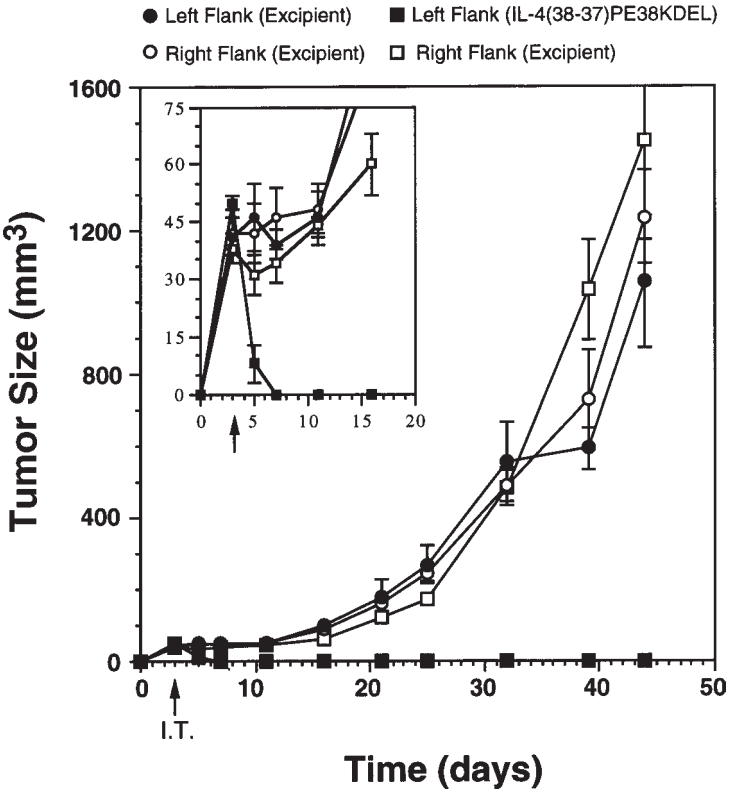

Fig. 8. IL4-PE remains localized by intratumoral administration. Tumors were implanted on both flanks of mice and treatment began on d 4 with intratumoral injection of 20 μL of either excipient or 750 μg/kg IL4(38-37)PE38KDEL on alternate days for a total of three doses. Circles represent the tumors in each flank of control group that received excipient only. The squares represent the groups treated with IL4(38-37)-PE38KDEL in the left flank only (closed square) or treated with excipient only in the right flank (open square). The arrow on the *x*-axis points the day of initiation of treatment. The data presented are the mean ± SEM of four to seven animals in each group.

to evaluate the pharmacologic and toxicologic consequences of IL4(38-37)-PE38KDEL injection into normal brain tissue.

To determine the levels of IL4(38-37)-PE38KDEL in the cerebral spinal fluid (CSF) after intrathecal administration, cynomolgus monkeys were dosed on d 1, 3, and 5 with 0.2% human serum albumin–phosphate buffered saline containing 0, 2, or 6 μg/kg of IL4(38-37)-PE38KDEL ***(37)***. The samples were drawn at various points in time, including 2 h after injection on d 3 and 5 at

Table 6
CSF and Serum Levels After Intrathecal Administration of IL4(38-37)-PE38KDEL in Monkeys

	IL4(38-37)-PE38KDEL levels (ng/mL)[a]		
Day	Control	2 μg/kg	6 μg/kg
CSF			
Day 1, preinjection	<2	<2	<2
Day 2, 24 h post-1st injection	<2	<2	<2
Day 3, preinjection	<2	<2	<2
Day 3, 2 h post-2nd injection	<2	428	680
Day 4, 24 h post-2nd injection	<2	<2	<2
Day 5, preinjection	<2	<2	<2
Day 5, 2 h post-3rd injection	<2	323	1417
Serum			
Day 3, 2 h post-2nd injection	<2	<2	<2
Day 5, 2 h post-3rd injection	<2	<2	<2

[a]IL4(38-37)-PE38KDEL levels were determined by cytotoxicity assay utilizing Daudi Burkitt's lymphoma cell line. Concentrations were determined using a standard curve generated from purified IL4(38-37)-PE38KDEL. Results are expressed as the average of three simultaneous experiments. Adapted from **ref. *37***.

each dose level. High CSF levels of IL4(38-37)-PE38KDEL were measurable after administration of the drug (**Table 6**). Since the CSF volume is approx 1 mL/kg, the levels at 2 h were >15% of peak values expected if the drug were to immediately distribute throughout the CSF. IL4(38-37)-PE38KDEL was cleared rapidly from the CSF, since at 24 h after injection, less than 1% of the drug remained. No detectable serum levels of IL4(38-37)-PE38KDEL were observed in any group.

The same monkeys utilized for pharmacokinetics studies were also evaluated for any signs or alterations in hematology and clinical chemistry as indicators of toxicity. No systemic toxicity was observed as expected by the absence of the drug in the serum. No changes in hematology and serum chemistry were observed in any of the monkeys studied, consistent with the absence of IL4(38-37)-PE38KDEL in the serum. Creatinine phosphokinase (CPK) BB (brain) bands, which can be a sensitive enzyme indicator for brain injury, were not elevated in any of the monkeys examined.

Cynomolgus monkeys were also injected intravenously with two doses of IL4-PE, and serum chemistry and hematologic parameters were studied. These monkeys were administered 50 and 200 μg/kg doses every other day for 3 d. These monkeys tolerated the doses well; however, reversible hepatic toxicities

were observed. High peak serum levels of drug were observed at both doses *(37,38)*. These studies suggested that high concentrations of this drug are well tolerated without major toxicities.

It is important to note that only approx 10–100 ng/mL of IL4(38-37)-PE38KDEL was sufficient to kill >95% of glioblastoma cells in tissue culture. However, 17-fold higher concentrations of IL4(38-37)-PE38KDEL at the 6 μg/kg dose and approx 3–4-fold higher concentrations at the 2 μg/kg dose by intrathecal route did not causing any noticeable pathology *(37)*. These studies predict that sufficient levels of IL4(38-37)-PE38KDEL could be achieved for therapeutic efficacy by administration of only 1–2 μg/kg of IL4(38-37)-PE38KDEL.

5. Phase I Clinical Trial

To determine safety and antitumor activity of IL4(38-37)-PE38KDEL against human brain tumors, we performed a phase I clinical trial at the John Wayne Cancer Institute and St. John's Hospital, Santa Monica, California. Nine patients with progressive malignant brain tumors despite standard therapy who received no other treatment within 3 wk of inclusion were enrolled in this clinical trial. All patients were previously treated with external beam radiation and had adequate baseline organ function as assessed by the standard laboratory parameters on their preoperative visit (e.g., within 21 d of commencement of study drug infusion). Patients with diffuse subependymal or CSF disease, anaplastic oligodendroglioma, tumors involving the brainstem, cerebellum, or both hemispheres, or who were unable or unwilling to give informed consent, had an active infection requiring treatment, or had an unexplained febrile illness were excluded from the study. Our protocol was approved by the institutional review boards of the Food and Drug Administration and St. John's Hospital. IL4-PE was infused by Dr. Robert Rand, John Wayne Cancer Institute.

All patients underwent a standard stereotactic biopsy under magnetic resonance/computerized tomography (MR/CT) guidance and appropriate anesthesia before placement of catheters as described by Laske et al. *(47)*. Up to three silastic infusion catheters (2.1 mm outer diameter for Pudenz catheters) were placed with the tip at a selected site in the tumor using stereotactic guidance through small twist-drill holes. The numbers of catheters were selected based on the volume to be infused and to ensure maximal saturation of the tumor bed and margins in the designated period of time. After surgery, the externalized catheters were connected to Medex 2010 micropumps (Medtronic, Minneapolis, MN) that were filled with IL4(38-37)-PE38KDEL. Infusion within each catheter began within 24 h after catheter insertion at a very slow pace over a 4–8 d period (0.3–0.6 mL/h).

The starting dose was selected based on the preclinical animal studies. The first dose level of 0.2 μg/mL was 1/500 times lower than the dose that produced

histologic damage to normal brain tissue when administered intra–brain parenchyma in rats and 1/30 of maximum tolerated doses injected intrathecally in monkeys. The dose was escalated one log to the next cohort of three patients and then one-half log to the highest dose (6 μg/mL) in this initial trial. The volume of fluid infused was determined based on the tumor volume determined by MR scan including 1–2 cm margins of normal brain tissue.

No apparent systemic toxicity occurred in any patient. The infusion of IL4-PE in six of nine patients showed glioma necrosis. One patient remained disease-free 18 mo after the procedure. We conclude that direct glioma injection of IL-4(38-37)-PE38KDEL is safe without systemic or neurotoxicity, causing necrosis of malignant gliomas that were refractory to conventional therapy ***(49)***.

6. Conclusion

Human brain-tumor cells express receptors for an immune regulatory pleiotropic cytokine, IL-4. By utilizing a monoclonal antibody to IL-4R and radioligand binding, it was demonstrated that human neuroblastoma, glioma, and glioblastoma cells express IL-4R. The affinity of IL-4 binding to its receptors on glioblastoma cells was found to be of high affinity similar to that reported on other human tumor cells or immune cells ***(3)***. At least 76% of malignant astrocytoma biopsies obtained from patients undergoing surgical resection were positive for the IL-4R, and all glioblastoma cell lines examined were positive for the expression of high-affinity IL-4R by binding studies and RT-PCR plus Southern blot analyses. The PCR data corroborated with the binding results, demonstrating surface expression of IL-4R protein on malignant astrocytoma cells. In contrast to tumors, five normal brain tissues obtained from six individuals were found negative and one sample weakly positive for IL-4R mRNA.

The significance of IL-4R expression by brain-tumor cells is not known. It is possible that IL-4R are expressed as a result of dedifferentiation or that the IL-4R act to stimulate cell growth like an oncogene. Because IL-4R expression in normal brain tissues was not observed, our data indicate that receptor expression by brain-tumor cells is not a consequence of dedifferentiation. IL-4 was not mitogenic to these cells, thus supporting that IL-4R is not an oncogene. However, it is possible that IL-4R is someway associated with a oncogene.

To target brain-tumor cells, we have produced two generations of IL4-R–targeted cytotoxins. However, a circular permuted IL4-PE, IL4(38-37)-PE38KDEL, was more effective against brain tumors compared with first the generation IL4-PE^{4E}. These results show that as the binding affinity of IL4-PE to IL-4R increases, the cytotoxicity of IL4-PE is also increased. This is a desirable characteristic of a chimeric molecule that is expected to result in a more effective targeting agent with no increase in nonspecific toxicity.

To further develop IL4(38-37)-PE38KDEL for clinical studies, we undertook preclinical studies in various animal models to determine its toxicity and pharmacokinetics. The route of administration was chosen to ensure maximum exposure of brain tissue to assess possible toxicity. Monkeys serve as good models because their cells can bind human IL-4 ***(19)*** and human IL4-PE is cytotoxic to monkey COS-7 cells (Puri et al, unpublished data). At doses up to 6 μg/kg, no toxicity was observed even though very high CSF levels of IL4(38-37)-PE38KDEL were achieved. The CSF protein levels were within normal limits and no inflammatory cells were observed (results not shown).

Since IL4(38-37)-PE38KDEL was highly cytotoxic to IL-4R–bearing brain-cancer cells in vitro, we investigated whether it is also active in vivo. These experiments successfully demonstrated that administration of IL4(38-37)-PE38KDEL to human-tumor–bearing mice can cause significant antitumor activity without any evidence of toxicity. Intratumoral injection of IL4(38-37)-PE38KDEL was most effective in eliminating established gliomas. This is because intratumor administration resulted in saturation of the tumor bed, with subsequent complete eradication of established large tumors. Thus, it is reasonable to believe that intraglioma administration of IL4(38-37)-PE38KDEL will saturate the entire tumor bed and, because of bulk flow action, it may also saturate the immediate proximity of the bed that contains tumor cells that cause recurrence ***(47)***. Based on these results, we have initiated a phase I clinical trial for the treatment of recurrent grade IV astrocytoma by intratumoral administration of IL4(38-37)-PE38KDEL. Since intratumoral administration surpasses toxicity that may be associated with systemic exposure, and since glioblastoma multiforme is generally not a systemic disease, intratumoral injection of IL4(38-37)-PE38KDEL offers a promising new treatment for brain tumors.

Our preliminary clinical results suggest that IL4(38-37)-PE38KDEL can be administered safely at doses that are associated with no systemic or neurologic toxicities. Promising antitumor activity has been documented in patients treated with doses of 2 μg/mL or more. A phase I clinical trial is currently ongoing at various centers in the United States and Germany to explore the antitumor activities of IL4(38-37)-PE38KDEL.

Acknowledgments

All studies reported in this chapter were performed in collaboration with Ms. Pam Dover, Drs. Rafat Husain, Bharat Joshi, and Nick Obiri of the Laboratory of Molecular Tumor Biology, Center for Biologics Evaluation and Research, and Drs. Robert Kreitman and Ira Pastan of the Laboratory of Molecular Biology, National Cancer Institute. The initial clinical trial was performed in collaboration with Dr. Robert Rand of the John Wayne Cancer Institute, Santa Monica, California.

References

1. Paul, W. E. (1990) Interleukin-4, A prototypic immunoregulatory lymphokine. *Blood* **77,** 1859–1870.
2. Puri, R. K. and Siegel, J. P. (1993) Interleukin-4 and cancer therapy. *Cancer Invest.* **11,** 473–486.
3. Puri, R. K. (1995) Structure and function of interleukin-4 and its receptors, in *Cytokines: Interleukins and Their Receptors* (Kurzrock, R. and Talpaz, M., eds.), Kluwer Academic Publishers, Norwell, MA, pp. 143–186.
4. Idzerda, R. L., March, C. J., Mosley, B., Lyman, S. D., Bos, T. V., Girupel, S. D., et al. (1990) Human interleukin 4 receptor confers biological responsiveness and defines a novel receptor superfamily. *J. Exp. Med.* **171,** 861–873.
5. Puri, R. K., Ogata, M., Leland, P., Feldman, G. M. , and Pastan, I. (1991) Expression of high affinity IL4 receptors on murine sarcoma cells and receptor mediated cytotoxicity of tumor cells to chimeric protein between IL-4 and Pseudomonas exotoxin. *Cancer Res.* **51,** 3011–3017.
6. Obiri, N. I., Hillman, G., Haas, G. P., Sud, S., and Puri, R. K. (1993) Expression of high affinity interleukin-4 receptors on human renal cell carcinoma cells and inhibition of tumor cell growth in vitro by interleukin-4. *J. Clin. Invest.* **91,** 88–93.
7. Obiri, N. I., Siegel, J. P., Varricchio, F., and Puri, R. K. (1994) Expression and function of high affinity interleukin-4 receptors on human melanoma, ovarian and breast carcinoma cells. *Clin. Exp. Immunol.* **95,** 148–155.
8. Obiri N. I. and Puri, R. K. (1994) Characterization of interleukin-4 receptors expressed on human renal cell carcinoma cells. *Oncology Res.* **6,** 419–427.
9. Varricchio, V., Obiri, N. I., Haas, G. P., and Puri, R. K. (1993) Immunostaining of interleukin-4 receptor on human renal cell carcinoma. *Lymphokine Cytokine Res.* **12,** 465–469.
10. Varricchio, F., Husain, R., Dover, P. Gill, P., and Puri, R. K. (1997) Interleukin-4 receptor expression in vivo on human AIDS-related Kaposi's sarcoma. *Oncology Res.* **9,** 495–503.
11. Murata, T., Noguchi, P. D., and Puri, R. K. (1995) Receptors for Interleukin (IL)-4 do not associate with the common γ chain, and IL-4 induces the phosphorylation of JAK2 tyrosine kinase in human colon carcinoma cells. *J. Biol. Chem.* **270,** 30,829–30,836.
12. Mehrotra, R., Varricchio, F., Husain, S. R., and Puri, R. K. (1998) Head and neck cancers but not benign lesions express interleukin-4 receptors *in situ. Oncology Reports* **5,** 45–48.
13. Obiri, N. I., Tandon, N., and Puri, R. K. (1995) Upregulation of intercellular adhesion molecule-1 on human renal cell carcinoma cells by interleukin-4. *Int. J. Cancer* **61,** 635–642.
14. Leland, P., Obiri, N. I., Aggarwal, B. B., and Puri, R. K. (1995) Suramin blocks binding of interleukin-4 to its receptors and interleukin-4 induced mitogenic response. *Oncology Res.* **7,** 227–235.
15. Murata, T., Obiri, N. I., and Puri, R. K. (1998) Structure of and signal transduction through interleukin 4 and interleukin 13 receptors. *Int. J. Mol. Med.* **1,** 551–557.

16. Murata, T., Taguchi, J., and Puri, R. K. (1998) Interleukin-13 receptor α' chain but not α chain: A functional component of interleukin-4 receptor. *Blood* **91,** 3884–3891.
17. Husain, S. R., Leland, P., Aggarwal, B. B., and Puri, R. K. (1996) Transcriptional up-regulation of interleukin 4 receptors by human immunodeficiency virus type 1 *tat* gene. *AIDS Res. Human Retroviruses* **12,** 1349–1359.
18. Aman, M. J., Tayebi, N., Obiri, N. I., Puri, R. K., Modi, W. S., and Leonard, W. J. (1996) cDNA cloning and characterization of the human interleukin-13 receptor α chain. *J. Biol. Chem.* **271,** 29,265–29,270.
19. Russell, S. M., Keegan, A. D., Harada, N., Nakamura, Y., Noguchi, M., Leland, P., et al. (1993) Interleukin-2 receptor gamma chain: A functional component of the interleukin-4 receptor. *Science* **262,** 1880–1883.
20. Kondo, M., Takeshita, T., Ishi, N., Nakamura, M., Watanabe, S., Arai, K., and Sugamura, K. (1993) Sharing of interleukin-2 (IL-2) receptor γ_c chain between receptors for IL-2 and IL-4. *Science* **262,** 1874–1877.
21. Noguchi, M., Nakamura, Y., Russell, S. M., Ziegler, S. F., Tsang, M., Cao, X., et al. (1993) Interleukin-2 receptor γ chain: A functional component of interleukin-7 receptor. *Science* **262,** 1877–1880.
22. Russell, S. M., Johnston, M., Noguchi, M., Kawamura, M., Bacon, C., Friedman, M., et al. (1994) Interaction of IL-2 receptor beta and gamma chain with Jak 1 and Jak 3, implications for XSCID and XCID. *Science* **266,** 1042–1045.
23. Giri, J. G., Ahdieh, M., Eisenman, J., Snanebeck, K., Grabstein, K., Kumaki, S., et al. (1994) Utilization of beta and gamma chains of the IL-2 receptor by novel cytokine IL-15. *EMBO J.* **13,** 2822–2830.
24. Obiri, N. I., Leland, P., Murata, T., Debinski, W., and Puri, R. K. (1997) The interleukin-13 receptor structure differs on various cell types and may share more than one component with interleukin 4 receptor. *J. Immunol.* **158,** 756–764.
25. Murata, T. and Puri, R. K. (1997) Comparison of IL-13 and IL-4 induced signalling in EBV-immortalized human B cells. *Cell. Immunol.* **175,** 33–40.
26. Murata, T., Obiri, N. I., and Puri, R. K. (1997) Human ovarian carcinoma cell lines express IL-4 and IL-13 receptors: comparison between IL-4 and IL-13 signaling. *Int. J. Cancer* **70,** 230–240.
27. Murata, T., Taguchi, J., Puri, R. K., and Mohri, H. (1999) Sharing of receptor subunits and signal transduction pathway between the IL-4 and IL-13 receptor system. *Int. J. Hematol.* **69,** 13–20.
28. Obiri, N. I., Murata, T., Debinski, W., and Puri, R. K. (1997) Modulation of interleukin-13 binding and signaling in human renal cell carcinoma cells by the γ_c chain of the IL-2 receptor. *J. Biol. Chem.* **272,** 20,251–20,258.
29. Debinski, W., Puri, R. K., Kreitman, R. J., and Pastan, I. (1993) A wide range of human cancers express IL-4 receptors that can be targeted with chimeric toxin composed of IL-4 and *Pseudomonas* exotoxin. *J. Biol. Chem.* **268,** 14,065–14,070.
30. Puri, R. K., Leland, P, Obiri, N. I., Husain, S. R., Mule, J., Pastan, I., et al. (1996) An improved circularly permutated interleukin 4–toxin is highly cytotoxic to human renal cell carcinoma cells: Introduction of $_c$ chain in RCC cells does not improve sensitivity. *Cell. Immunol.* **171,** 80–86.

31. Puri, R. K., Mehrotra, P. T., Leland, L., Kreitman, R, Siegel, J. P., and Pastan, I. (1994) Chimeric protein comprised of IL-4 and *Pseudomonas* exotoxin (IL4–PE4E) is cytotoxic for activated human lymphocytes. *J. Immunol.* **152,** 3693–3700.
32. Debinski, W., Puri, R. K., and Pastan, I. (1994) Chimeric toxin composed of human Interleukin 4 and derivatives of *Pseudomonas* exotoxin A are potent antitumor agents in mice. *Int. J. Cancer* **58,** 744–748.
33. Kreitman, R. J., Puri, R. K., and Pastan, I. (1994) A circularly permutated recombinant interleukin-4 toxin with increased activity. *Proc. Natl. Acad. Sci. USA* **91,** 6889–6893.
34. Puri, R. K., Leland, P., Kreitman, R. J., and Pastan, I. (1994) Human neurological cancer cells express interleukin-4 (IL-4) receptors which are targets for the cytotoxic effect of IL4-*Pseudomonas* exotoxin chimeric protein. *Int. J. Cancer* **58,** 574–581.
35. Kreitman, R. J., Puri, R. K., Leland, P., Lee, B., and Pastan, I. (1994) Site directed mutagenesis of IL-4, Improved binding and cytotoxicity of mutant IL4–Toxins by conjugation through cysteine substitutions in IL-4. *Biochemistry* **33,** 11,637–11,644.
36. Kreitman, R. J., Puri, R. K., and Pastan, I. (1995) Increased antitumor activity of a circularly permuted IL4–toxin in mice with IL-4 receptor bearing human carcinoma. *Cancer Res.* **55,** 3357–3363.
37. Puri, R. K., Hoon, D. S., Leland, P., Snoy, P., Rand, R. W., Pastan, I., et al. (1996) Preclinical development of a recombinant toxin containing circularly permuted interleukin-4 and truncated *Pseudomonas* exotoxin for therapy of malignant astrocytoma. *Cancer Res.* **56,** 5631–5637.
38. Husain, S. R., Gill, P., Kreitman, R. J., Pastan, I., and Puri, R. K. (1997) Interleukin-4 receptor expression on AIDS-associated Kaposi's sarcoma cells and their targeting by a chimeric protein comprised of circularly permuted interleukin-4 and *Pseudomonas* exotoxin. *Mol. Med.* **3,** 327–338.
39. Husain, S. R., Bihari, N., Kreitman, R. J., Pastan, I., and Puri, R. K. (1998) Complete regression of established glioblastoma tumor xenografts by interleukin-4 toxin therapy. *Cancer Res.* **58,** 3649–3653.
40. Husain, S. R., Kreitman, R. J., Pastan, I., and Puri, R. K. (1999) Interleukin-4 receptor directed cytotoxin therapy of AIDS-associated Kaposi's sarcoma tumors in xenograft model. *Nature Med.* **5,** 817–822.
41. Pastan, I. and FitzGerald, D. (1991) Recombinant toxins for cancer treatment. *Science* **254,** 1173.
42. Pastan, I., Chaudhary, V. K., and FitzGerald, D. J. (1992) Recombinant toxins as novel therapeutic agents. *Annu. Rev. Biochem.* **61,** 331.
43. Joshi, B., Plautz, G., and Puri, R. K. (2000) Interleukin-13 receptor α chain: A novel tumor associated antigen on malignant glioma cells. *Cancer Res.* (Advances in Brief). **60,** 1168–1172.
44. Morrison, B. and Leder, P. (1992) A receptor binding domain of mouse interleukin-4 defined by a solid phase binding assay and in vitro mutagenesis. *J. Biol. Chem.* **267,** 11,957–11,963.

45. Gossett, K. A., Barbolt, T. A., Cornacoff, J. B., Zelinger, D. J., and Dean, J. H. (1993) Clinical pathologic alterations associated with subcutaneous administration of recombinant interleukin-4 to cynomolgus monkeys. *Toxicol. Pathol.* **21,** 46–53.
46. Cornacoff, J. B., Gossett, K. A., Barbolt, T. A., and Dean J. H. (1992) Preclinical evaluation of recombinant interleukin-4. *Toxicol. Lett.* **64/65,** 299–310.
47. Laske, D. W., Youle, R. J., and Oldfield, E. H. (1997) Tumor regression with regional distribution of the targeted toxin TF-CRM107 in patients with malignant brain tumors. *Nature Med.* **3,** 1362–1368.
48. Murata, T., Obiri, N. I., Debinski, W., and Puri, R. K. (1997) Structure of IL-13 receptor: Analysis of subunit composition in cancer and immune cells. *Biochem. Biophys. Res. Commun.* **238,** 90–94.
49. Rand, R. W., Kreitman, R. J. Patronas, N., Varrichio, F., Pastan, I., and Puri, R. K. (2000) Intratumoral administration of recombinant circularly permuted interleukin-4-*Pseudomonas* exotoxin in patients with high grage glioma. *Clin. Cancer Res.* **6,** 2157–2165.

12

Bispecific Monoclonal Antibodies for the Targeting of Type I Ribosome-Inactivating Proteins Against Hematological Malignancies

Silvano Ferrini, Sabrina Sforzini, and Silvana Canevari

1. Introduction

Monoclonal antibodies (MAbs) recognizing tumor-associated antigens (TAA) have been widely used to selectively deliver toxic compounds to neoplastic cells. In most studies, tumor targeting was achieved by the use of immunotoxins (IT) generated by chemical conjugation of an antibody to a toxin ***(1)***. In addition, several recombinant antibody–toxin chimeric molecules have been generated by genetic engineering ***(2)***. Ricin A-chain, which enzymatically damages ribosomal RNA, has been most commonly used for the generation of ITs, although several other single-chain ribosome-inactivating proteins (RIPs) or type I RIPs are also available ***(3)***. Type I RIPs are RNA *N*-glycosidases displaying potent inhibition of protein synthesis in cell-free assays, but they lack a lectin B-chain for cell entry, and thus have a low toxicity for whole cells. Type I RIPs such as saporin can be easily purified ***(4)*** and have been successfully used to generate potent ITs, displaying antitumor activity both in vitro ***(5)*** and in vivo ***(6)***.

An alternative approach to the IT for the delivering of toxic compounds is based on the use of bispecific monoclonal antibodies (biMAbs). These are hybrid antibodies that possess two different antigen-binding sites and therefore act as highly specific crosslinking agents between two different antigenic molecules ***(7)***. BiMAbs directed to a TAA and to a cytotoxic agent—such as a radioactive hapten ***(8)***, a toxin ***(9)*** or a triggering receptor of cytotoxic cells of the immune system ***(10)***—can be used to selectively eliminate neoplastic cells.

In previous studies, we have demonstrated the possibility to use biMAbs to efficiently deliver type I RIPs against human lymphoma cells expressing CD30

From: *Methods in Molecular Biology, vol. 166: Immunotoxin Methods and Protocols*
Edited by: W. A. Hall

or CD25 target molecules ***(11,12)***. Lymphocyte activation antigens, such as CD25 and CD30, have been regarded as suitable target molecules for hematological malignancies, because they are not expressed in resting lymphoid cells and in other normal tissues. The CD25 antigen (IL-2R α chain) has been proposed as a suitable target molecule in adult T-cell leukemia and Hodgkin's lymphomas ***(13)***. The CD30 antigen (a member of the TNF-receptor superfamily) is typically expressed at high levels on Hodgkin's lymphoma and anaplastic large cell lymphomas ***(14)***, and anti-CD30–saporin IT displayed antitumor activity in chemotherapy-refractory Hodgkin's lymphoma ***(15)***. In our previous studies, anti-CD30–antisaporin or anti-CD25–antisaporin biMAbs produced by hybrid hybridomas strongly enhanced saporin toxicity against $CD30^+$ Hodgkin's lymphoma cells ***(11,12)***. It should be pointed out that biMAbs secreted by hybrid hybridomas are monovalent for each antigen and thus may perform in a similar fashion as ITs made with monovalent Fab' fragments. Several pieces of experimental evidences indicated that the use of a combination of two biMAbs reacting with different non-crossreactive epitopes of a toxin results in a cooperative effect of toxin delivery ***(9,12,16,17)***. This may depend both on increased avidity for the toxin and on the induction of crosslinking and internalization of the target molecule.

One of the potential advantages in the use of the biMAb approach over the use of conventional immunotoxins is the possibility to perform "pretargeting" strategies based on the administration of biMAb, followed in a second step by the free RIP. This should be possible by the use of two cooperative monovalent biMAbs which internalize at a reduced rate upon antigen binding. Administration of free RIP in the second step may allow capture of the RIP at the tumor site by biMAbs, followed by target TAA crosslinking and internalization. This approach will result in a reduced plasmatic half-life of the RIP, as compared to that of a RIP antibody conjugate, thus reducing the possibility of a vascular-leak syndrome, a frequent side effect of IT.

In this chapter, we will describe the following to produce and characterize pairs of cooperative biMAbs recognizing distinct epitopes of a type I RIP and a TAA.

1. Selection and characterization of hybridomas producing anti-RIP MAbs.
2. Identification of MAbs reacting to nonoverlapping epitopes.
3. Construction of hybrid-hybridomas secreting anti-TAA/anti-RIP biMAbs.
4. Purification of biMAbs.
5. Evaluation of anti-tumor activity.

Alternative methods for biMAb construction will also be mentioned.

2. Materials

In addition to the materials listed below, purified toxin selected by the investigator (dissolved in PBS and stored at –20°C), tumor cell lines express-

ing a TAA of interest, HGPRT-deficient myeloma P3U1, hybridoma secreting anti-TAA MAb, the standard reagents (RPMI 1640 or DMEM high glucose, heat-inactivated fetal calf serum, antibiotics) equipment for cell culture maintenance and sterile handling, and the materials and buffers for SDS-PAGE are required (***18***; *see* **Note 1**)

Columns, materials, and buffers common to more than one methodology are listed separately.

Columns, materials, and buffers:

1. Empty, low-pressure glass columns (2.5 cm × 10 cm).
2. Desalting columns.
3. Dialysis membrane tubing. Any commonly used dialysis membrane tubing with a molecular mass cutoff of 12 kDa or smaller can be used.
4. 0.22 μm filters.
5. Automated microprocessor-driven Phastsystem apparatus (Pharmacia).
6. Precasted gels for SDS-PAGE and isoelectrofocusing (Pharmacia).
7. Phosphate buffered saline (PBS), pH 7.4: 8.0 g NaCl, 0.2 g KCl, 0.2 g KH_2PO_4, 1.13 g/L Na_2HPO_4 (store at 4°C); alternate PBS recipes may be used.
8. 10 m*M* sodium or potassium phosphate buffer, pH 6.8.
9. Blocking solution: 2% BSA–PBS.

2.1. Selection and Characterization of Hybridomas Producing Anti-RIP MAbs

1. 6-wk-old female BALB/c mice.
2. Complete Freund's adjuvant (CFA).
3. Incomplete Freund's adjuvant (IFA).
4. Polyethylene glycol (PEG 4000 GK; Merck).
5. Hypoxantine, aminopterin, thymidine (HAT) medium.
6. Flat-bottomed, 24- and 96-well microtiter plates for tissue culture, and 96-well plates for ELISA.
7. ELISA washing buffer: 0.02% Tween 20–PBS.
8. Peroxidase-conjugated antimouse antiserum and peroxidase substrate (ABTS).
9. Multiscan fluorimeter.
10. Erythrocyte lysis buffer: 10 m*M* $KHCO_3$, 150 m*M* NH_4Cl.

2.2. Identification of MAbs Reacting to Nonoverlapping Epitopes

1. 96-well microtiter flexible polyvinylchloride (PVC) plates.
2. Bovine serum albumin (BSA; fatty-acid–free, fraction V; Sigma, St. Louis, MO).

2.3. Construction of Hybrid-Hybridomas Secreting Anti-TAA–Anti-RIP biMAbs

1. 100× Iodoacetamide stock solution (0.5 *M*) in PBS; store at –20°C in the dark.

2.4. Purification of biMAbs

2.4.1. Affinity Chromatography on Immobilized Protein A

1. Sepharose-protein A fast-flow column (HiTrap Protein A; Pharmacia, Sweden).
2. 20 m*M* sodium phosphate buffer, pH 7.0.
3. 0.1 *M* sodium citrate buffer.
4. 1.0 *M* Tris-base.

2.4.2. Affinity Chromatography on Immobilized Toxin

1. CNBr-activated sepharose 4B freeze-dried powder (Pharmacia LKB Biotechnology, Sweden).
2. Swelling buffer: 1 m*M* HCl.
3. Coupling buffer: 0.1 *M* $NaHCO_3$, 0.5 *M* NaCl, pH 8.3.
4. Blocking buffer: 0.2 *M* glycine, pH 8.0.
5. Washing buffer: 0.1 *M* CH_3COONa, 0.5 *M* NaCl, pH 4.0.
6. 1.0 *M*, 100 m*M* or 10 m*M* Tris-base (pH adjusted to 8.8, 8.0, and to 7.5 with HCl immediately prior to use).
7. 100 m*M* glycine-HCl, pH 2.5 or pH 4.5.

2.5. Tumor Cytotoxicity Assay

1. 96-well U-bottomed plates.
2. ^{3}H-leucine (1 mCi/mL; Amersham), store at –20°C.
3. Glass fiber filters.
4. Cell harvester (ICN-flow).
5. Scintillation cocktail (Filler Count, Packard Int., Netherlands).
6. Liquid scintillation counter.

3. Methods

3.1. Selection and Characterization of Hybridomas Producing Anti-RIP MAbs

3.1.1. Mice Immunization with RIPs

Several methods to immunize mice and produce MAbs have been reported ***(19)***. We describe a technique that was successfully applied to select anti-saporin and antigelonin hybridomas.

1. Dilute RIP up to 20 mg/mL in PBS. Mix 1:1 with CFA (for the first injection), or with IFA (for further injections). Sonicate in a bath sonicator or mix by repeatedly aspirating in a syringe through a 22 gauge needle to obtain a stable emulsion.
2. Inject 6-wk-old Balb/c mice subcutaneously in at least two sites of the back.
3. Repeat injections at two-week intervals for a total of four injections.
4. Bleed animals and test serum (from 1:10 to 1:10,000 dilution in blocking buffer) by ELISA.

5. If ELISA titer is higher than 1:1000, perform one intraperitoncal booster injection of RIP in PBS 3 d before mice sacrifice and splenectomy.

3.1.2. ELISA Assay for Anti-RIP Antibody

1. Dilute RIP in PBS at 2 μg/mL.
2. Add 50 μL to each well and incubate for 2 h to overnight at 4°C.
3. Empty plate and tap on a towel.
4. Wash twice with washing solution.
5. Add 150 μL/well of blocking solution and incubate for 2 h to overnight. Discard fluid and tap to dry. After coating, plates can be kept at –20°C for several months or used directly.
6. Add 50 μL of hybridoma supernatant or diluted serum to be tested in duplicate wells, and incubate 1 h at room temperature.
7. Wash three times with 200 μL/well of washing solution.
8. Add 50 μL/well of peroxidase-conjugated antimouse antiserum diluted in blocking buffer and incubate 1 h at room temperature.
9. Wash four times with 200 μL/well of washing solution.
10. Add substrate solution in 50 μL.
11. Incubate 10–30 min at room temperature, inspect for reaction, and read at 405 nm by a multiscan fluorimeter.

3.1.3. Cell Fusion and Hybridoma Selection

1. Collect P3U1 myeloma cells from exponentially growing cultures. Count and wash twice in medium without FCS.
2. Prepare splenocytes by teasing apart the spleen using a syringe with a 21 gauge needle in a petri dish containing complete medium.
3. Collect splenocyte suspension, spin down, and resuspend pellet in 1 mL erythrocyte lysis buffer. Mix for 1 min and add 10 mL complete medium. Spin down, discard supernatant, wash twice in medium without FCS, and count cells.
4. Melt an aliquot of 0.5 g PEG in boiling water and dilute 1:1 with medium without FCS. Keep at 37°C in water bath.
5. Add 5×10^7 splenocytes and 5×10^6 myeloma cells in medium without FCS to a 50 mL tube. Spin down, discard the supernatant, and dry the pellet.
6. Keep cells at 37°C in a water bath for a few minutes. Add dropwise to the pellet the diluted PEG within 1 min while mixing the cells by stirring with the pipet. Keep the tube at 37°C shaking gently for 3 min. Add dropwise 10 mL of prewarmed (37°C) medium without FCS while gently shaking, followed by 10 mL of prewarmed complete medium.
7. Spin down at 400*g* for 5 min. Discard supernatant and resuspend in complete medium. Avoid vortexing or strong shaking, instead resuspend by very slowly pipetting and inverting the tube. Dilute suspension in up to 80 mL of complete medium.
8. Add 0.1 mL of cell suspension to 96-well flat-bottom plates .
9. After 18 h, add 0.1 mL complete medium containing 2% of a 50X HAT solution.

10. Replace 50% medium with HAT every 4 d and inspect periodically for growth.
11. Screen supernatants of growing cultures before confluence by ELISA, and immediately clone positive cultures by limiting dilution in 96-well flat-bottom plates.
12. Screen clones by ELISA and expand and characterize positive clones (at least one round of subcloning is recommended).

3.2. Detection of Antibodies Directed to Different Toxin Epitopes by Binding Crosscompetition Assays

Epitope mapping studies are performed to determine whether different antitoxin antibodies recognize the same or different epitopes on the toxin molecule. An example of this type of reactions is given below using the toxin bound to 96-well plates and the ^{125}I-labeled antitoxin antibody ***(19,20)*** (*see* **Note 2**). Alternative methods are reported in **Note 3**.

1. Make a solution of approx 2 μg/mL of the toxin diluted in 1X PBS (*see* **Note 4**).
2. Add 50 μL of the toxin solution to each well of a microtiter flexibile PVC plate and incubate at room temperature for 2 h or overnight at 4°C.
3. Remove the content of the wells (it can be stored at –20°C and used again). If the toxin solution will not be saved, it can be removed by flicking the liquid into a waste container.
4. Wash the plate three times with PBS (a 500 mL squirt bottle is advisable; *see* **Note 5**).
5. Fill the wells with 200 μL of blocking buffer and incubate for at least 2 h at room temperature (*see* **Note 6**).
6. Wash the plate twice with PBS.
7. Add 50 μL of the competitor antibodies at several concentrations ranging from 50–0.05 μg/mL in blocking buffer and a fixed amount (50,000 cpm/50 μL/well) of the ^{125}I-labeled antitoxin antibody (*see* **Note 7**).
8. Incubate 1 h at room temperature.
9. Aspirate the supernatant in a suitable radioactive waste and wash extensively (five times) with PBS.
10. Cut the wells, put them in vials, and evaluate the radioactivity in a gamma counter.

3.3. Construction of Hybrid-Hybridomas Secreting Anti-TAA–Anti-RIP biMAbs

Somatic fusion to achieve a biMAb-secreting cell can be performed either between two different hybridomas (the resulting cell has been referred to as "quadroma" or "hybrid-hybridoma") or between a hybridoma and spleen cells from an immunized animal ***(7)***. Different selection markers and procedures can be utilized to achieve in vitro selection of hybrid cells that express the genes of four antibody chains (*see* **Note 8**). Here we describe a method based

on chemical inactivation of one HGPRT$^+$ HAT-resistant hybridoma, and subsequent fusion with cells from a HGPRT$^-$ HAT-sensitive hybridoma ***(21)***. Different association patterns of the two heavy and the two light chains may occur in hybrid-hybridoma cells, resulting in the secretion of a mixture of different antibodies. Most frequently a preferential reassociation of homologous heavy and light chains occurs, allowing the formation of functional antigen binding sites, and the secretion of only the two parental antibodies and of the biMAb. In addition to somatic fusion techniques, several alternative approaches have been developed for the production of biMAbs including: chemical conjugation of two different MAbs or their fragments (excessive chemical manipulation frequently generates a low yield of the final product and a partial loss of activity) ***(16,17,22)***; methods based on antibody genetic engineering ***(23,24)*** such as linkage of two single-chain antibodies (scFv; ***25***); or generation of complex self-assembling molecules known as "diabodies" (**Fig. 1**; ***26***).

3.3.1. Generation of a HGPRT-Negative HAT-Sensitive Revertant of a Hybridoma "A"

1. Subculture hybridoma "A" in complete medium containing 1 μg/mL 8-azaguanine in a 75 cm^2 flask for 2–3 passages.
2. In subsequent subcultures, progressively increase the 8-azaguanine concentration by doubling its concentration up to 64 μg/mL. Before each increasing step, inspect cultures for the presence of groups of viable cells.
3. As soon as cells regrow, subclone hybridoma cells and check for antibody production and HAT sensitivity. Keep and expand suitable clones.

3.3.2. Somatic Fusion Between HGPRT-Negative HAT-Sensitive Hybridoma "A" and HAT-Resistant Chemically Inactivated Hybridoma "B"

1. Harvest subconfluent cultures of the two hybridomas, keep without any selection for at least 1 wk before fusion, and count cells.
2. Wash 10^7 HGPRT$^+$ hybridoma cells "B" twice with PBS and incubate the cells for 30 min at 4°C in 5 mL of 5 m*M* iodoacetamide in PBS in a tube; keep cells in suspension. Wash three times in medium without FCS at 4°C.
3. Wash 2×10^7 cells from HGPRT$^-$ hybridoma cells "A" twice in medium without FCS. Add hybridoma cells "B" resuspended in medium without FCS to the tube containing hybridoma cells "A."
4. Proceed as described in **Subheading 3.1.3.**
5. Screen proliferating culture supernatants for reactivity against RIP by ELISA (25–50 μL of supernatant for each assay) and against TAA by standard indirect immunofluorescence. Use supernatants from double-positive wells to perform cytotoxicity assays as described using a 1:10, 1:100, and 1:1000 final concentration of supernatant in the test wells and one RIP concentration (a concentration 100-fold lower than the IC_{50} for RIP determined in preliminary titration assays in the absence of antibody).

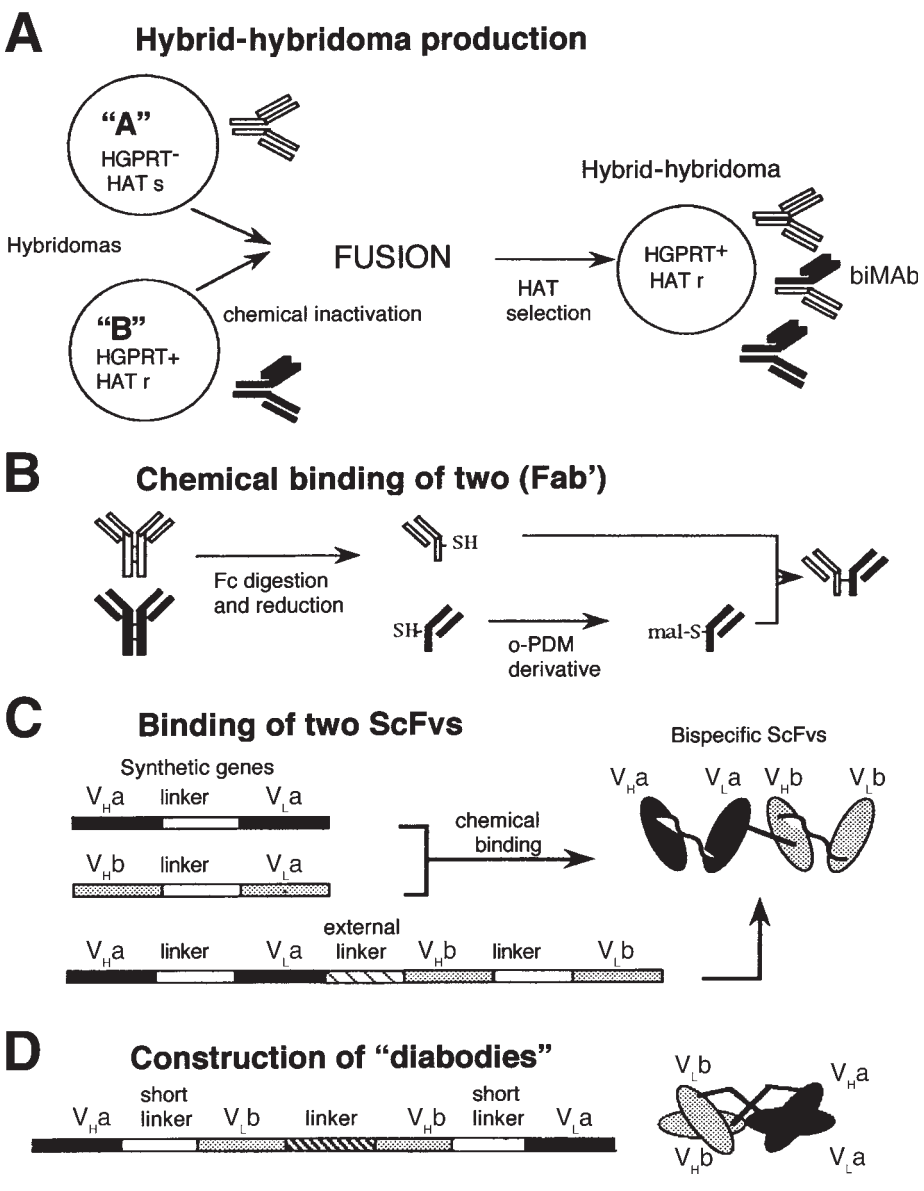

Fig. 1. Schematic representation of different approaches suitable for the generation of biMAbs: **(A)** Construction of a biMAb-secreting hybrid-hybridoma generated by somatic fusion of an HGPRT-negative, HAT-sensitive anti-RIP hybridoma, and a chemically inactivated anti-TAA hybridoma. **(B)** Chemical conjugation of two Fab' fragments of two MAbs. **(C)** Binding of two different scFv by either chemical binding, or joining of the two constructs through an external linker. **(D)** Construction of self-assembling diabodies.

6. Clone double-positive wells as soon as possible by limiting dilution, giving priority to cultures also producing enhanced RIP toxicity in the cytotoxicity assay, and repeat screening. Repeated subcloning is suggested to stabilize hybrid-hybridomas.
7. Scale up recently subcloned hybridoma cultures for antibody production and biMAb purification.

3.4. biMAb Purification by Affinity Chromatography (see Note 9)

Ascitic fluids or culture supernatants from hybrid-hybridoma contain all possible combinations of the light and heavy chains of the two parental antibodies (anti-TAA and antitoxin), and functional biMAbs with appropriate pairing of heavy and light chains, represent only a fraction of the antibody molecules produced *(7)*. Suitable methods that enable separation of the different molecular species should be applied. Two methods are presented for purifying heteroisotypic biMAbs (*see* **Note 10**). In **Subheading 3.4.1.**, we describe immunoaffinity chromatography on protein A that can be applied alone or possibly in combination with the second method. This method exploits the different affinities for protein A of IgG_1 and IgG_{2a} murine antibodies *(19)* and is suited for separation of bispecific molecules from the parental contaminants; however it does not allow the removal of nonfunctional biMAbs derived from inappropriate heavy- and light-chain pairings. In **Subheading 3.4.2.**, we describe immunoaffinity chromatography on immobilized toxin *(11)*. This method is suited for selection of functional MAbs for one of the two antigenic specificity of the biMAb.

3.4.1. biMAb Purification by Affinity Chromatography on Protein A Column

1. Thaw the ascitic fluid or cell culture supernatant and centrifuge to eliminate cell debris and flocculates.
2. Dilute ascitic fluid 1:1 with binding buffer or extensively dialyze at 4°C the cell culture supernatant against 20 m*M* sodium phosphate buffer, pH 7.0 .
3. Load into a sepharose-protein A fast-flow column at a flowrate of 1 mL/min.
4. Wash with three column volumes of 20 m*M* sodium phosphate buffer, pH 7.0.
5. Elute with 0.1 *M* sodium citrate buffer by using a three-stepwise (pH 5.5, 5.0, and 3.5) or a linear pH gradient (from pH 6.0–3.5). The parental IgG_1 MAbs usually start to elute at pH 5.5, the IgG_1/IgG_{2a} biMAbs at around pH 5.0, and the parental IgG_{2a} at around pH 4.0–3.5. The eluted proteins should be easily detected by UV absorbance at 280 nm.
6. Immediately neutralize collected fractions with 1.0 *M* Tris-base (to avoid denaturation induced by the acidic buffer).
7. Pool the protein-containing fractions according to the elution profile. Dialyze extensively against 10 m*M* sodium phosphate buffer, pH 6.8–7.0 (or 10 m*M* potassium phosphate buffer in the case of further fractionation or analysis in hydroxylapatite column; *see* **Note 11**).

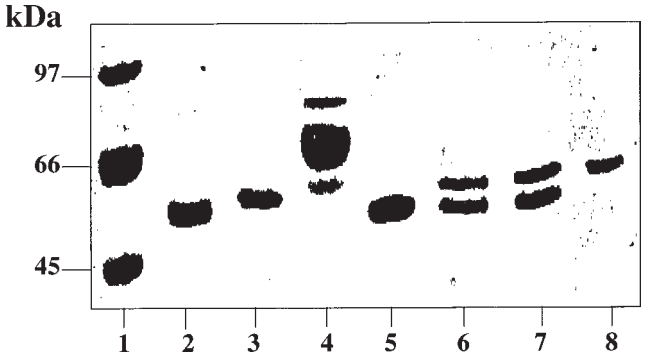

Fig. 2. Characterization of hybrid-hybridoma–secreted MAbs following fractionation by protein A chromatography. SDS-PAGE analysis of parental MAbs and of elution peaks from protein A (reducing conditions, 12.5% polyacrylamide). Lanes: 1, molecular weight standards; 2, IgG_1 parental MAb (heavy-chain band with an apparent 58,000 mol wt); 3, IgG_{2a} parental MAb (heavy-chain band with an apparent 61,000 mol wt); 4, unbound material (note the broad band of albumin); 5, peak A eluted when applying pH 5.5; 6 and 7, doublet peak B eluted at pH 5.5; 8, peak C eluted at pH 5.0. By comparison of the retention times in hydroxylapatite column, peak A was found to contain at least 70% of parental IgG_1 MAb, peak B more than 90% of biMAb, and peak C more than 95% of parental IgG_{2a} MAb.

8. Determine protein concentration by UV absorbance at 280 nm, applying the extinction coefficient of immunoglobulin (13.3). If necessary, concentrate to about 1 mg/mL in an Amicon Centricon or Centriprep concentrator, an Amicon stirred-cell concentrator, or the equivalent.
9. The column can be used at least several times without appreciable loss of the binding capacity for antibodies. After each use, the column is washed with 0.1 *M* sodium citrate (pH 3.0) to remove any biological materials. The resin is then equilibrated with 20% ethanol and stored at 4°C.

An example of effective purification of biMAbs by pH gradient elution from a protein A column is reported in **Fig. 2**.

3.4.2. biMAb Purification by Affinity Chromatography on Toxin—Sepharose Column

This purification technique allows the removal of antibody species not reacting with the toxin (such as parental anti-TAA MAbs or mismatched paired biMAbs) while parental antitoxin MAbs coeluted together with functional biMAbs. Despite this limitation, the advantages of this simple and rapid purification are the possibility to obtain a good yield and a sufficient purity for most purposes ***(11,19)***.

Protocol for toxin–sepharose coupling is modified from coupling procedures suggested by the manufacturer.

1. Dialyze the purified toxin (10 mg at a concentration ranging from 1–2 mg/mL) against coupling buffer (1 mL bead binds approx 5 mg of toxin).
2. Suspend 1 g of freeze-dried powder (CNBr-activated sepharose) in swelling buffer (SB) (1 g gives about 3.5 mL swollen gel; *see* **Note 12**).
3. Wash with swelling buffer for 15 min on a sintered glass filter (use approx 200 mL/g).
4. Transfer the gel in a tube, add coupling buffer to the beads (10 mL buffer/mL beads) and gently rotate for 20 min at room temperature.
5. Activate beads with eight alternate washings with swelling and coupling buffers (centrifuge each time at 1000*g* for 5 min).
6. Add the purified toxin solution to the pellet and rotate overnight at 4°C.
7. Centrifuge, take the supernatant, and measure the protein concentration by UV absorbance at 280 nm (*see* **Note 13**) to confirm that toxin–sepharose coupling has taken place (usually an efficient coupling should be at least 70%).
8. Wash four times with 10 mL of coupling buffer and incubate with 5 mL of coupling buffer overnight at 4°C.
9. Wash eight times alternately with wash buffer and coupling buffer followed three times with PBS.
10. Resuspend the resin in 10 mL of 10 m*M* Tris-HCl (pH 7.5) and transfer to a column.
11. Wash the column extensively with 10 bed-volumes of the following buffers: 100 m*M* Tris-HCl, pH 7.5; 100 m*M* glycine pH 2.5; 10 m*M* Tris-HCl, pH 8.8 (assess if the pH at the end reaches 8.8, otherwise apply other buffer); 10 m*M* Tris-HCl, pH 7.5, until the pH is 7.5.

Protocol for affinity chromatography on immobilized toxin.

1. Load the culture supernatant or the ascitic fluid to the column and allow to recirculate 5–10 times to be sure that complete binding has taken place.
2. Wash the column with 30 bed-volumes of 10 m*M* Tris-HCl pH 7.5.
3. Elute by acid-sensitive binding, with 5 bed-volumes of 100 m*M* glycine (pH 4.5) followed by 5 bed-volumes of 100 m*M* glycine (pH 2.5).
4. Continue from **Subheading 3.4.1., steps 6–9**.

3.5. Tumor Cytotoxicity Assay

Anti-TAA–antitoxin biMAbs can be analyzed for their ability to induce cytotoxicity against various cell types in a protein synthesis inhibition assay (the described method is based on ^{3}H-leucine uptake; *see* **Note 14**; ***27***). These experiments allow one to determine the toxin concentration inhibiting 50% of protein synthesis (IC_{50}) in the target cells.

1. Count and plate the cells in 96-well U-bottomed plate in a volume of 100 µL of complete medium. (By a preliminary assay determine the optimum number of cells per well; *see* **Note 15**).

Table 1
Inhibition of Protein Synthesis in Human Tumor Cells Expressing the Relevant TAA (CD30) by biMAbs Delivering Saporin Used as Single Agents or in Combination[a]

Saporin (*M*) +	5×10^{-8}	5×10^{-9}	5×10^{-10}	5×10^{-11}	5×10^{-12}	5×10^{-13}	5×10^{-14}
No biMAb	11.3	78.1	93.1	89.4	85.7	95.7	102.2
CD30xsap1	2.9	3.1	12.8	54.9	91.7	98.3	104.7
CD30xsap2	3.0	5.1	19.3	70.9	107.5	118.1	130.7
CD30xsap1+ CD30xsap2	2.6	2.8	3.3	3.5	13.2	40.6	80.5

[a]Data are expressed as % mean values of the untreated cells.

2. Add 100 μL of different concentrations of the toxin and biMAbs to each well. Each point is run in duplicate or triplicate (*see* **Note 16**).
3. Incubate the plate for 24 h in a humidified atmosphere of 5% CO_2 in air. Longer incubation periods can be used.
4. Add 1 μCi of ^{3}H-leucine to each well in a volume of 20 μL of complete medium.
5. After 18 h harvest the cells onto glass fiber filters.
6. Dry the filter in a stove and put each circle filter in a vial containing 3 mL of scintillation cocktail.
7. Evaluate the radioactivity by a β-counter. Calculate the percentage of the amount of ^{3}H-leucine incorporation with respect to untreated control values using the formula:

$$\% \text{ Uptake} = \text{cpm sample/cpm control} \times 100$$

An example of results obtained using two different anti-CD30–antisaporin synergistic biMAbs, saporin (type I RIP), and their combinations is reported in **Table 1**.

3.6. Conclusion

To reduce immunogenicity of murine MAbs, genetic engineering techniques for the "humanization" of murine antibodies have been established. The grafting of the CDR regions (part of the V regions encoding for the antigen binding site) into a human framework allows one to construct fully reshaped antibodies with reduced immunogenicity ***(23)***. More recently, phage-display libraries have been developed to directly produce human antibodies or small antibody fragments formed by V_H and V_L joined by a linker sequence (single-chain Fv; ***24***). These constructs can be used to construct human or humanized bispecific monoclonal antibodies according to different strategies (*see* **Fig. 1**).

The availability of several nonimmunologically crossreactive toxins may be of importance to avoid side effects and resistance phenomena due to anti-RIP antibody responses.

4. Notes

1. Owing to their toxicity, care should be exercised when handling toxin and some of the chemicals used in the described methods.
2. The labelling of the MAbs can be done according to standard methods ***(19,20)***.
3. Alternative detection methods can be used (e.g., Iasys resonant mirror biosensor ***(16)***, biotin labeling of one of the MAbs, and detection with ^{125}I-streptavidin).
4. The performance and optimal coating concentration may need to be adjusted for different toxins.
5. Plates can be prepared in advance and stored at –70°C.
6. If background signals are excessive, other blocking solutions (5% dry milk in PBS or 5% FCS in PBS) can be used.
7. It is very important to include an irrelevant MAb as a negative control and the same unlabelled MAb as a positive control.
8. Alternative methods can be utilized for the selection of hybrid-hybridomas and for the purification of hybrid biMAbs ***(7)***. Hybridoma–hybridoma fusion can be performed by: chemical inactivation of both hybridomas by the use of two distinct inhibitors of macromolecular synthesis, such as emetine and actinomycin-D; use of two different complementing enzyme-deficient hybrids (one deficient in HGPRT obtained by selection in 8-azaguanine, the other deficient in thymidine kinase obtained by selection in bromodeoxyuridine. Both enzyme-deficient mutants are sensitive to HAT, which is used for hybrid-hybridoma cell selection).
9. Entire biMAbs with intact Fc portions could interact with the three types of IgG Fc receptors differently expressed on various human leukocytes (NK cells, monocytes, polymorphonuclear cells, B-lymphocytes, microglial cells; ***28***). Use of F(ab')2 fragments obtained by pepsin digestion ***(29)*** prevents this interaction.
10. In the case of homoisotypic biMAbs, a different purification strategy should be applied ***(30)***.
11. The purity and integrity of the biMAbs are analyzed by SDS-PAGE, isoelectrofocusing, HPLC analytical gel filtration and/or interaction with hydroxilapatite ***(31)***. The maintenance of the binding reactivity of the purified biMAbs is evaluated by immunofluorescence on the target cells expressing the relevant TAA and by ELISA test on the toxin (11,12).
12. Swollen sepharose can be diluted and stored in PBS plus 0.02% NaN_3 at 4°C.
13. The quickest method for protein concentration detection may be performed by 280 nm absorbance owing mainly to the residues of tyrosine and tryptophan. The extinction coefficient is 6.67 for BSA and for other toxins an approximation may be used (e.g., 6.47 for gelonin).
14. The toxins used act by inhibiting protein synthesis, so the best evaluation of their cytotoxicity is the measure of radioactive amino acid. However, alternative non-radioactive methods can be used ***(32)***.

15. Negative control with TAA negative cell line.
16. Several dilutions of biMAbs in the presence or absence of toxin must be tested preliminarily in order to obtain the IC_{50} of both reagents. Usually the assay is performed in a titration curve with a dilution factor of 10. Remember to dilute the reagents in complete medium at double the final concentration, because the cells were plated in 100 μL/well. Appropriate control samples are run with cells alone, toxin alone, biMAbs alone, parental MAb alone or toxin plus parental MAbs mixed together.

Acknowledgments

S.S. is a recipient of a fellowship from Fondazione Italiana Ricerca sul Cancro (FIRC). Most of the techniques reported were developed by the authors at the Department of Biotechnology in Oncology, Istituto Nazionale per la Ricerca sul Cancro, Genoa, and the Department of Experimental Oncology, Istituto Nazionale Tumori, Milan, Italy.

References

1. Thrush, G. R., Lark, L. R., Clinchy, B. C., and Vitetta, E. S. (1996) Immunotoxins: an update. *Annu. Rev. Immunol.* **14,** 49–71.
2. Reiter, Y. and Pastan, I. (1996) Antibody engineering of recombinant Fv immunotoxins for improved tageting of cancer: disulphide-stabilized Fv immunotoxins. *Clin. Cancer Res.* **2,** 245–252.
3. Barbieri, L., Battelli, M. G., and Stirpe, F. (1993) Ribosome-inactivating proteins from plants. *Biochim. Biophys. Acta* **1154,** 237–282.
4. Barbieri, L., Stoppa, C., and Bolognesi, A. (1987) Large scale chromatographic purification of ribosome-inactivating proteins. *J. Chromatogr.* **408,** 235–243.
5. Bolognesi, A., Tazzari, P. L., Tassi, C., Gromo, G., Gobbi, M., and Stirpe, F. (1992) A comparison of anti-lymphocyte immunotoxins containing different ribosome-inactivating proteins and antibodies. *Clin. Exp. Immunol.* **89,** 341–346.
6. Pasqualucci, L., Wasik, M., Teicher, B., Flenghi, L., Bolognesi, A., Stirpe, F., et al. (1995) Antitumor activity of anti-CD30 immunotoxin (Ber-H2/saporin) in vitro and in severe combined immunodeficiency disease mice xenografted with human CD30+ anaplastic large cell lymphoma. *Blood* **85,** 2139–2146.
7. Suresh, M., Cuello, A., and Milstein, C. (1986) Bispecific monoclonal antibodies from hybrid hybridomas. *Methods Enzymol.* **121,** 210–228.
8. Le Doussal, J-M., Barbet, J., and Delaage, M. (1992) Bispecific monoclonal antibody-mediated targeting of radiolabeled bivalent haptens: theoretical, experimental and clinical results. *Int. J. Cancer* Suppl. **7,** 58–62.
9. French, R. R., Courtenay, A. E., Ingamells, S., Stevenson, G. T., and Glennie, M. J. (1991). Cooperative mixtures of bispecific F(ab') antibodies for delivering saporin to lymphoma in vitro and in vivo. *Cancer Res.* **51,** 2353–2361.
10. Ferrini, S., Cambiaggi, A., Cantoni, C., Canevari, S., Mezzanzanica, D., Colnaghi, M. I., et al. (1992). Targeting of T or NK lymphocytes against tumor cells by

bispecific monoclonal antibodies: role of different triggereing molecules. *Int. J. Cancer* (Suppl.) **7,** 15–18.

11. Tazzari, P. L., Zhang, S., Chen, Q., Sforzini, S., Bolognesi, A., Stirpe, F., et al. (1993) Targeting of saporin to CD25-positive normal and neoplastic lymphocytes by an anti-saporin/anti-CD25 bispecific monoclonal antibody: in vitro evaluation. *Br. J. Cancer* **67,** 1248–1253.
12. Sforzini, S., De Totero, D., Gaggero, A., Ippoliti, R., Glennie, M. J., Canevari, S., et al. (1998) Targeting of saporin to Hodgkin's lymphoma cells by anti-CD30 and anti-CD25 bispecific antibodies. *Br. J. Haematol.* **102,** 1061–1062.
13. Engert, A., Diehl, V., Schnell, R., Radszuhun, A., Hatwig, M., Drillich, S., et al. (1997) A phase-I study of an anti-CD25 ricinA-chain immunotoxin (RFT5-SMPT-dgA) in patients with refractory Hodgkin's lymphoma. *Blood* **2,** 403–410.
14. Stein, H., Mason, D. Y., Gerdes, J., O'Connor, N., Wainscoat, J., Pallesen ,G., et al. (1985) The expression of the Hodgkin's disease-associated antigen Ki-1 in reactive and neoplastic tissue: evidence that Reed-Sternberg cells and histiocytic malignancies are derived from activated lymphoid cells. *Blood* **66,** 848–858.
15. Falini, B., Bolognesi, A., Flenghi, L., Tazzari, P. L., Broe, M. K., Stein, H., et al. (1992) Response of refractory Hodgkin's disease to therapy with anti-CD30 monoclonal antibody linked to saporin (BER-H2/SO6) immunotoxin. *Lancet* **339,** 1195–1196.
16. French, R. R., Penney, C. A., Browning, A. C., Stirpe, F., George, A. J. T., and Glennie, M. J. (1995). Delivery of the ribosome-inactivating protein, gelonin, to lymphoma cells via CD22 and CD38 using bispecific antibodies. *Br. J. Cancer* **71,** 986–994.
17. Bonardi, M. A., French, R. R., Amlot, P., Gromo, G., Modena, D., and Glennie, M. J. (1993) Delivery of saporin to human B cell lymphoma using bispecific antibody: targeting via CD22 but not CD19, CD37 or immunoglobulin results in efficient killing. *Cancer Res.* **53,** 3015–3021.
18. Laemmli, U. K. (1970) Cleavage of structural proteins during the assembly of the head of bacteriophage T4. *Nature* **227,** 680–685.
19. Harlow, E. and Lane, D. (1988) *Antibodies a Laboratory Manual.* Cold Spring Harbor Laboratory, New York.
20. Casalini, P., Mezzanzanica, D., Canevari, S., Della Torre, G., Miotti, S., Colnaghi, M. I., et al. (1991) Use of combination of monoclonal antibodies directed against three distinct epitopes of a tumor-associated antigen: analysis of cell binding and internalization. *Int. J. Cancer* **48,** 284–290.
21. Clark, M. R. and Waldmann, H. (1987) T-cell killing of target cells induced by hybrid antibodies: comparison of two bispecific monoclonal antibodies. *J. Natl. Cancer Inst.* **79,** 1393–1401.
22. Glennie, M. J., McBride, H. M., Worth, A. T., and Stevenson, G. T. (1987) Preparation and performance of bispecific F(ab')2 antibody containing thioether-linked Fab' Fragments. *J. Immunol.* **139,** 2367–2375.
23. Riechmann, L., Clark, M., Waldmann, H., and Winter, G. (1988) Reshaping human antibodies for therapy. **332,** 323–327.

24. Nissim, A., Hoogenboom, H. R., Tomlinson, I. M., Flynn, G., Midgley, C., Lane, D., et al. (1994) Antibody fragments from a "single pot" phage display library as immunochemical reagents. *EMBO J.* **13,** 692–698.
25. Mack, M., RiethmÄller, G., and Kufer, P. (1995) A small bispecific antibody construct expressed as a functional single-chain molecule with high tumor cell cytotoxicity. *Proc. Natl. Acad. Sci. USA* **92,** 7021–7025.
26. Holliger, P., Prospero, T., and Winter, G. (1993) "Diabodies": Small bivalent and bispecific antibody fragments. *Proc. Natl. Acad. Sci. USA* **90,** 6444–6448.
27. Tazzari, P. L., Bolognesi, A., De Totero, D., Falini, B., Lemoli, R. M., Soria, M. R., et al. (1992) Ber-H2 (anti-CD30)-saporin immunotoxin: a new tool for the treatment of Hodgkin's disease and CD30+ lymphoma: in vitro evaluation. *Br. J. Haematol.* **81,** 203–211.
28. Fanger, M. W., Shen, L., Graziano, R. F., and Guyre, P. M. (1989) Cytotoxicity mediated by human Fc receptors for IgG. *Immunol. Today* **10,** 92–99.
29. Parham, P. (1983) On the fragmentation of monoclonal IgG1, IgG2a, and IgG2b from balb/c mice. *J. Immunol.* **131,** 2895–2902.
30. Warnaar, S. O., De Paus, V., Lardenoije, R., Machielse, B. N. M., De Graaf, J., Bregonje, M., et al. (1994) Purification of bispecific $F(ab')_2$ from murine trinoma OC/TR with specificity for CD3 and ovarian cancer. Hybridoma, **13,** 519–526.
31. Roosnek, E. and Lanzavecchia, A. (1989) Triggering T cells by otherwise inert hybrid anti-CD3/anti-tumor antibodies requires encounter with the specific target cell. *J. Exp. Med.* **170,** 297–302.
32. Mosmann, T. (1983) Rapid colorimetric assay for cellular growth and survival: application to proliferation and cytotoxicity assays. *J. Immunol. Methods* **65,** 55–63.

13

Tyrosine Kinase Inhibitors Against EGF Receptor-Positive Malignancies

Elise A. Sudbeck, Sutapa Ghosh, Xing-Ping Liu, Yaguo Zheng, Dorothea E. Myers, and Fatih M. Uckun

1. Introduction

The role of protein tyrosine kinases (PTKs) in the survival of cancer cells and their potential use in anticancer therapy has led to their selection as anticancer drug targets. Tyrosine kinases which are being studied for this purpose include epidermal growth factor receptor (EGFR) ***(1–6)***, Janus kinases (JAKs) ***(7–13)***, Bruton's tyrosine kinase (BTK) ***(14–16)***, platelet-derived growth factor (PDGF) ***(17)***, protein kinase C (PKC) ***(18–24)***, Lck ***(25,26)***, Trk ***(27–30)***, and others. The strategies used to attenuate or disable kinases implicated in cancer include the use of antibodies, immunoconjugates, ligand-binding cytotoxic agents, and small-molecule inhibitors. Each of these strategies has shown some promise for the treatment of cancer. Herceptin ***(31–35)***, for example, is an immunotherapeutic agent that binds to the extracellular domain of HER2 (also referred to as ErbB-2, a tyrosine kinase belonging to the same family as EGFR) at nanomolar levels. EGF-genistein (EGF-gen) is an EGFR-binding cytotoxic agent that also shows potency in the nanomolar range ***(2,36)*** and will be discussed in this chapter. The search for new small molecules that inhibit kinases has involved traditional approaches, including the testing of natural products, random screening of chemical libraries, the use of classical structure–activity relationship studies, and the incorporation of structure-based drug design approaches and combinatorial chemistry techniques. As a result, several promising small-molecule inhibitors have also been identified in recent years that may prove useful as potent new anticancer drugs.

Small-molecule inhibitors of kinases that show promise as anticancer agents include inhibitors of EGFR. EGF exerts pleiotropic biologic effects by binding

From: *Methods in Molecular Biology, vol. 166: Immunotoxin Methods and Protocols*
Edited by: W. A. Hall © Humana Press Inc., Totowa, NJ

to ErbB-1 ***(37–40)***. In breast cancer, the expression of EGFR is a significant and independent indicator for recurrence and poor survival ***(41–43)***. Recent studies provided evidence that EGFR serves as an endogenous negative regulator of apoptosis in breast cancer cells ***(2)***. Many classes of small molecules have been reported in recent years that inhibit EGFR kinase ***(1,3–6,44–47)***. Genistein (**Fig. 1**), a naturally occurring isoflavone found in soybeans, is an inhibitor of EGFR ***(6)***. When genistein is linked to EGF, the potency against EGFR increases from an IC_{50} value of >10 μ*M* to a value in the nanomolar range ***(2)***.

Pyrazolopyrimidines (*see* **Fig. 1**) were found to inhibit EGFR with IC_{50} values ranging around 1–8 n*M* ***(3)***. Two pyrazolopyrimidines with reported IC_{50} values below 10 n*M* ***(3)*** also showed high selectivity towards some nonreceptor tyrosine kinases (c-*Src*, v-*Abl*, and serine/threonine kinases such as PKC-α and CDK1). The quinazoline derivative CP-358,774 ***(45)*** inhibits EGFR with an IC_{50} of 2 n*M* and reduces EGFR autophosphorylation in intact tumor cells with an IC_{50} of 20 n*M*. This inhibition is selective for EGFR relative to other tyrosine kinases examined as determined by assays of isolated kinases and whole cells. Despite the reported profound in vitro potency (K_i = 5 p*M*) and selectivity of the ATP-competitive brominated quinazoline derivative PD153035 (**Fig. 1**; ***4,5***), the compound failed to show significant in vitro or in vivo efficacy against cancer cells. Other quinazolines reported include PD168393 and PD160678, which selectively target and irreversibly inactivate EGFR through covalent modification of a cysteine (Cys^{773}) residue present in the ATP-binding pocket ***(44)***. These compounds also interact in an analogous fashion with ErbB2 (which has a conserved Cys residue at the same position) but have no activity against IR, PDGF receptor, FGFR, and PKC. The compounds have not been tested against BTK and JAK3, which also contain conserved cysteine residues at the corresponding position.

A series of new quinazoline compounds targeting EGFR have been designed more recently using structure-based methods. In this study, a three-dimensional model of the kinase domain of EGFR was constructed ***(1)*** using known coordinates of homologous kinase domains as reference coordinates (Hematopoietic cell putative protein tyrosine kinase [HCK; ***48***], fibroblast growth factor receptor [FGFR; ***49,50***], and insulin receptor kinase [IRK; ***51***]). The EGFR model was used along with an inhibitor docking procedure for the rational design of compounds predicted to bind favorably to EGFR. The EGFR model indicated that inhibition may be significantly improved by increasing the size of the functional groups attached to the 4-anilinoquinazoline molecular scaffold. Chemically relevant substitutions at the 3', 4' and 5' positions on the anilino ring lead to the successful design of a dibromo quinazoline derivative, WHI-P97, with an IC_{50} value of 2.5 μ*M* in EGFR kinase inhibition assays. WHI-P97 effec-

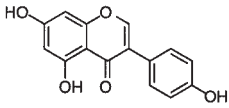

Genistein
(5,7,4'-trihydroxyisoflavone)
EGFR IC_{50} > 10μM

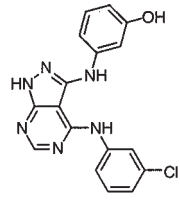

Pyrazolopyrimidine derivative
EGFR IC_{50} = 1 nM

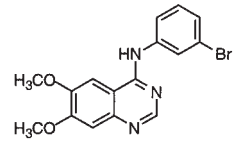

PD153035
EGFR K_i = 5.2 pM (4)
EGFR IC_{50} = 25 pM (5),
4-6 nM (3), 10μM (46)

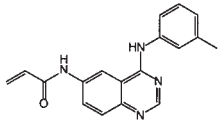

PD168393
EGFR IC_{50} = 0.45 nM

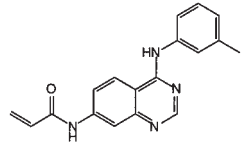

PD160678
EGFR IC_{50} = 0.70 nM

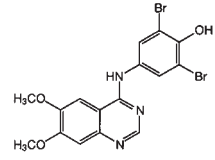

WHI-P97
EGFR IC_{50} = 2.5 μM

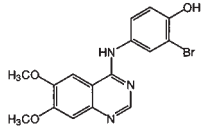

WHI-P154
EGFR IC_{50} = 5.6 μM

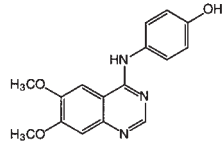

WHI-P131
JAK3 IC_{50} = 9.1 μM
EGFR IC_{50} = 4.2 μM

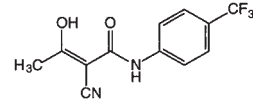

LFM (A77 1726)
EGFR IC_{50} = 5.4 μM

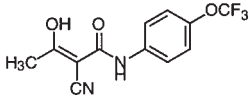

LFM-A12
EGFR IC_{50} = 1.7 μM

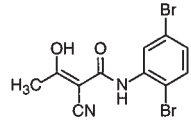

LFM-A13
BTK IC_{50} = 2.5 μM

Fig. 1. Examples of tyrosine kinase inhibitors.

tively inhibited the in vitro invasiveness of EGFR-positive human cancer cells in a concentration-dependent manner. The quinazoline derivatives WHI-P97, WHI-P131, WHI-P154, WHI-P180, and WHI-P197 with 3' or 4'OH substitution on the anilino moiety were predicted to form an additional hydrogen bond with Asp^{831} in the ATP-binding region of EGFR that may enhance binding. The EGFR inhibition values for WHI-P97, WHI-P131, WHI-P154, WHI-P180, and WHI-P197 ranged from 2.5 to 5.6 μ*M* in kinase assays. However, the

quinazolines tested were not specific for EGFR. For example, the EGFR inhibitor WHI-P154 (EGFR IC_{50} = 5.6 μ*M*) also inhibited other tyrosine kinases such as HCK (IC_{50} = 12 μ*M*), JAK3 (IC_{50} = 130 μ*M*) and spleen tyrosine kinase (SYK) (IC_{50} = 150 μ*M*) ***(46)***.

In terms of selectivity for EGFR, leflunomide metabolites may show the most promise. Earlier studies reported that the immunosuppressive activity of leflunomide is due to its metabolite A77 1726 (α-cyano-β-hydroxy-β-methyl-*N*-[4–(trifluromethyl)phenyl]-propenamide, or LFM), which is rapidly formed in vivo, functions as a pyrimidine synthesis inhibitor ***(52)*** and also inhibits the tyrosine kinase activity of EGFR ***(53)***. The leflunomide metabolite analog LFM-A12 (**Fig. 1**) showed inhibition of EGFR with an IC_{50} value of 1.7 μ*M* and killed >99% of human breast cancer cells in vitro by triggering apoptosis ***(1)***. Both LFM-A12 and WHI-P97 inhibited the in vitro invasiveness of EGFR-positive human breast cancer cells at micromolar concentrations and induced apoptotic cell death. In addition, LFM-A12 inhibited the proliferation (IC_{50} = 26.3 μ*M*) and in vitro invasiveness (IC_{50} = 28.4 μ*M*) of EGFR-positive human breast-cancer cells in a concentration-dependent fashion.

Like the quinazolines WHI-P97 and WHI-P154, the design of LFM-A12 was aided by a model of the EGFR kinase domain. In kinase assays, LFM-A12 was found to be specific for EGFR and did not inhibit other PTKs such as BTK, HCK, JAK1, JAK3, IRK, and SYK at concentrations ranging from 175 to 350 μ*M*. The observed selectivity of LFM-A12 for EGFR likely results from its molecular shape and from favorable interactions with unique EGFR residues that are not present in the kinase domains of other PTKs. Likewise, unfavorable interactions with unique residues of other PTKs that are not found in the EGFR kinase domain may also contribute to this selectivity. This observation is in contrast to the observed inhibition of several kinases (EGFR, HCK, JAK3 and SYK) by WHI-P154. The first contributing factor for the nonselectivity of WHI-P154 may be the inhibitor's complementary shape with the hinge region of the binding cavity of all seven kinases, which in turn leads to favorable hydrophobic contact between the compound and the residues in this cavity. Additionally, predicted hydrogen bonding interactions with all seven kinases may enhance its binding with each of them.

The structure-based method used to design leflunomide inhibitors of EGFR was also successful for the identification of small-molecule inhibitors of JAK3 ***(7)***. JAK3 is expressed abundantly in primary leukemic cells from children with acute lymphoblastic leukemia (ALL). The construction of a three-dimensional model of JAK3 ***(7)*** was used to design a quinazoline inhibitor, WHI-P131 (**Fig. 1**), shown to have specificity for JAK3. WHI-P131 inhibited JAK3 (IC_{50} = 9.1 μ*M*) but not JAK1 or JAK2 and did not inhibit the ZAP/SYK-family tyrosine kinase SYK, TEC-family tyrosine kinase BTK, *Src*-family tyrosine kinase LYN, or

the receptor-family tyrosine kinase IRK, even at concentrations as high as 350 μ*M* ***(7)***. WHI-P131 induced apoptosis in JAK3-expressing human leukemia cell lines but not in JAK3-negative melanoma or squamous carcinoma cells.

Another study to identify kinase inhibitors focused on inhibitors of BTK as antileukemic agents with apoptosis-promoting properties ***(14)***. A three-dimensional homology model of the BTK kinase domain was constructed ***(14)*** and inhibitor docking procedures led to the identification of an LFM analog, LFM-A13 (**Fig. 1**), which was found to be a potent and specific inhibitor of BTK. LFM-A13 inhibited recombinant BTK with an IC_{50} value of 2.5 μ*M*, but it did not affect the enzymatic activity of other protein tyrosine kinases including JAK1 and JAK2, *Src*-family kinase HCK, and receptor-family tyrosine kinases EGFR and IRK, at concentrations as high as 278 μ*M*. LFM-A13 also enhanced the chemosensitivity of BTK-positive B-lineage leukemia cells to vincristine and ceramide.

Although several agents have been identified in recent years that inhibit tyrosine kinases such as EGFR, JAK3, and BTK, a future challenge is to ensure the specificity of inhibitors for one targeted tyrosine kinase. A successful strategy to accomplish this involves conjugating small-molecule inhibitors to ligand-binding entities; this enables the inhibitor to be delivered to a specific tyrosine kinase. An example of this strategy is to link a kinase inhibitor (soybean-derived genistein, 5,7,4'-trihydroxyisoflavone) to a protein (recombinant human EGF) that binds to a receptor kinase (EGFR). The resulting protein–inhibitor conjugate is an EGFR-directed cytotoxic agent (EGF-gen) with PTK inhibitory activity ***(2,36)***, which will be described in further detail in this chapter. (A similar method was successfully applied to the targeted delivery of genistein to CD19-receptor–associated vital PTK and shows considerable promise for more effective treatment of human leukemias and lymphomas ***[25,54]***)

2. Materials and Methods

2.1. Structure-Based Design of Small-Molecule Inhibitors of EGFR

The three-dimensional coordinates of the EGFR kinase domain used in protein–inhibitor modeling studies (**Fig. 2**) were constructed based on a structural alignment of the sequence of EGFR with the sequences of known crystal structures of other protein kinases (kinase domains of HCK ***[48]***, FGFR ***[50]***, IR ***[55]***, and cAPK ***[56]***) as described previously ***(1)***. The procedure was also used to construct homology models for JAK1, JAK3 ***(7)***, BTK ***(14)***, and SYK (Mao, C., unpublished data). Molecular docking and scoring procedures were used to estimate binding of inhibitors in the catalytic site of EGFR (**Tables 1** and **2**, **Figs. 3** and **4**) ***(1,47)***. Leflunomide metabolite analogs such as LFM-A12 (**Scheme 1**) and quinazoline compounds such as WHI-P97 (**Schemes 2**&**3**) were synthesized, and their ability to inhibit EGFR in breast cancer cells was tested as previously described ***(1,57)***.

2.2. EGF-Genistein Immunoconjugates

2.2.1. Preparation of EGF-Genistein Immunoconjugates

Recombinant human EGF (rhEGF) was produced in *E. coli* harboring a genetically engineered plasmid that contains a synthetic gene for human EGF fused at the N-terminus to a hexapeptide leader sequence for optimal protein expression and folding. The rhEGF fusion protein precipitated in the form of inclusion bodies, and the mature protein was recovered by trypsin cleavage followed by purification using ion-exchange chromatography and HPLC ***(2,36)***. The recently published photochemical conjugation method using the hetero bifunctional, photoreactive crosslinking agent sulfosuccinimidyl 6-(4'azido-2'-nitrophenylamino)hexanoate (Sulfo-SANPAH) ***(25)*** was used to prepare the EGF-genistein (EGF-gen) conjugate. Photolytic generation of a reactive singlet nitrene on the other terminus of EGF-SANPAH in the presence of a 10-fold molar excess of differentially hydroxyl-protected genistein (gen) resulted in the attachment of gen via its available C7-hydroxyl group to the Lys^{28} or Lys^{48} residues of EGF. The resulting sample was purified using size-exclusion HPLC, and reverse-phase HPLC ***(2)***. Electrospray-ionization mass spectrometry ***(62,63)*** was used to determine the stoichiometry of gen and EGF in EGF-gen. ^{125}I-gen was also used to confirm the stoichiometry of gen and EGF in EGF-gen and to verify the removal of free gen and gen-labeled EGF–EGF homoconjugates by the described purification procedure. The purity of EGF–^{125}I-gen was assessed by SDS-PAGE and autoradiography.

2.2.2. Binding of EGF–^{125}I-Gen to Breast Cancer Cells

Ligand-binding assays using EGF–^{125}I-gen (2.0×10^8 cpm/μmol), ^{125}I-gen (3.8×10^8 cpm/μmol) and ^{125}I-EGF (2.2×10^{12} cpm/μmol; Amersham) were performed using standard procedures as previously described ***(25,64)***. The cell lines in ligand-binding assays included the EGFR-positive breast cancer cell lines MDA-MB-231 and BT-20, as well as the EGFR-negative human leukemia cells lines NALM-6 (pre-B leukemia) and HL-60 (promyelocytic leukemia).

Fig. 2. *(opposite page)* The molecular-surface representation of the homology model of the EGFR kinase domain. A small-molecule inhibitor (multicolor) is shown docked into the ATP-binding site (active site, yellow) of EGFR. Taken from Ghosh et al., (1998) *Clin. Cancer Res.* **4,** 2657–2668 ***(1)***.

Fig. 3. *(opposite page)* Docked position of LFM-A12 (yellow) in the catalytic site of the EGFR kinase domain model. The EGFR catalytic site residues are shown as space-filling atoms. Taken from Ghosh et al. (1999) *Clin. Cancer Res.* **5,** 4264–4272 ***(46)***.

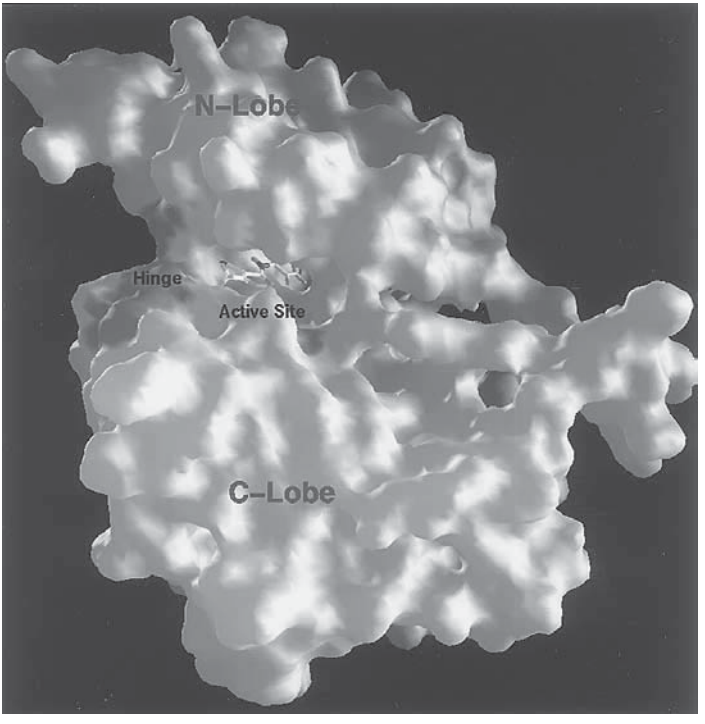
N–Lobe
Hinge
Active Site
C–Lobe

Fig. 2.

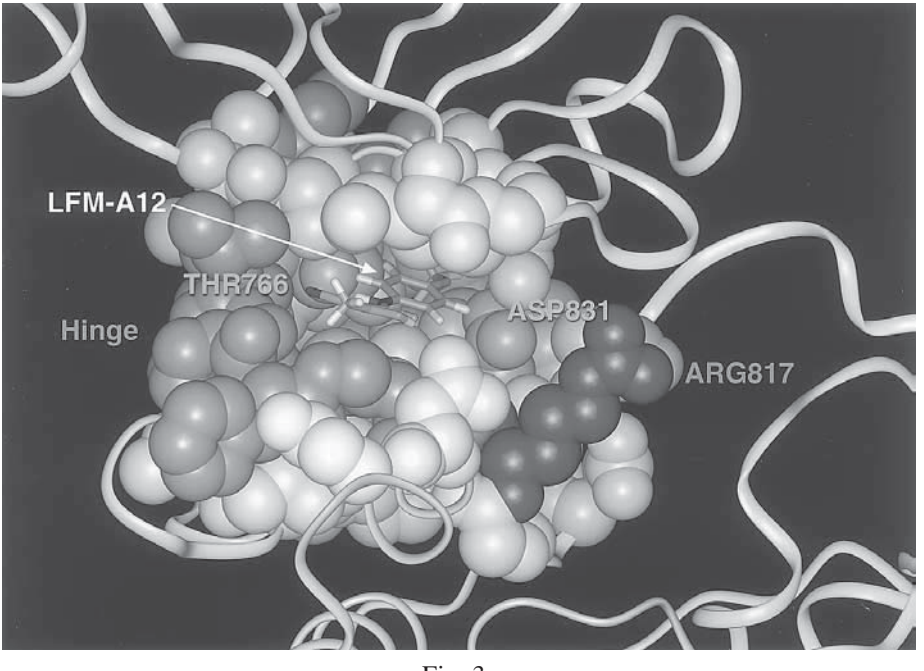
LFM-A12
THR766
Hinge
ASP831
ARG817

Fig. 3.

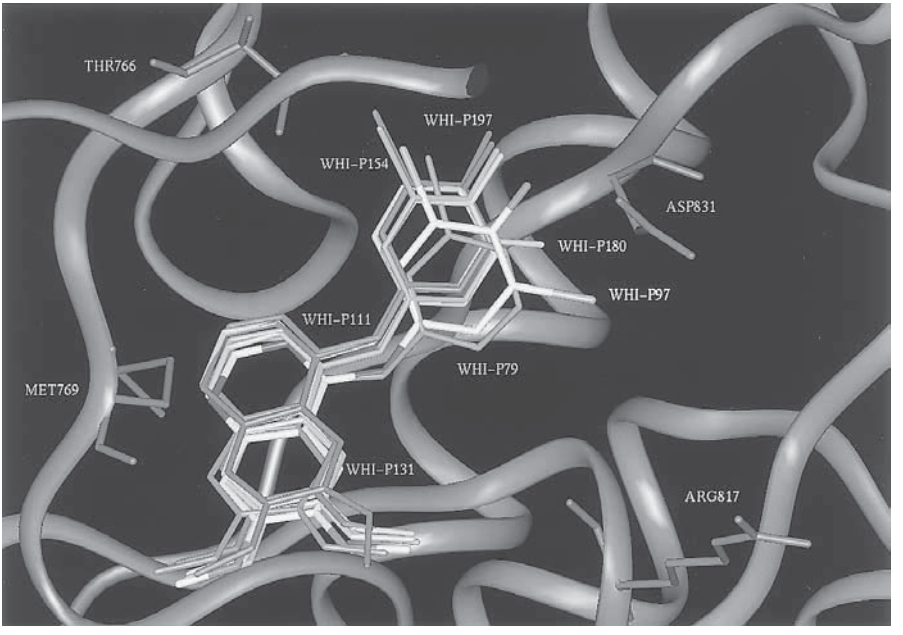

Fig. 4. The superimposed docked positions of several 4-anilinoquinazolines in the catalytic site of the EGFR kinase domain model. Taken from Ghosh et al. (1999) *Anticancer Drug Des.,* **14,** 403–410 ***(47)***.

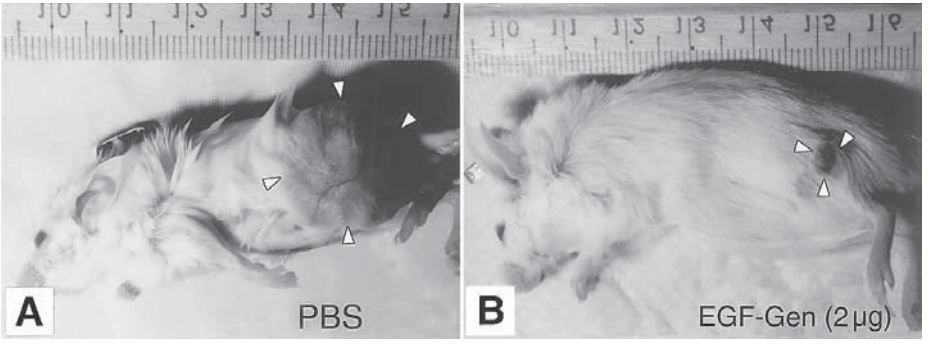

Fig. 5. The effects of EGF-gen on tumor progression in SCID mice xenografted with MDA-MB-231 human breast cancer cells. White arrows indicate the approximate size of the tumors in **(A)** a PBS-treated mouse (control) and **(B)** an EGF-gen–treated mouse after 60 d. Ruler units shown are in centimeters.

Table 1
Interaction Scores, Calculated K_i Values, EGFR Inhibition (IC_{50}), and EGFR-Positive Cancer Cell Cytotoxicity of LFM Analogs *(1)*

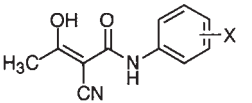

Compound	X	MS[a] (Å)	BS[b] (%)	Lipo Score	Ludi Score	Ludi[c] *Ki* (μ*M*)	EGF-R Inhibition IC_{50} (μ*M*)	Cancer Cell Cytotoxicity IC_{50} (μ*M*) MDA-MB-231	MDA-MB-361
LFM	*p*-CF_3	250	205	522	508	8	5.4	198.9	190.5
LFM-A1	*p*-Br	226	177	462	449	32	> 100	> 300	> 300
LFM-A2	*p*-Cl	228	180	456	443	37	> 100	> 300	> 300
LFM-A3	*p*-F	221	164	397	362	> 100	> 100	> 300	> 300
LFM-A4	*o*-CF_3	239	181	442	354	> 100	> 100	> 300	> 300
LFM-A5	*o*-Br	230	168	424	383	> 100	> 100	> 300	> 300
LFM-A6	*o*-Cl	227	157	385	345	> 100	> 100	> 300	> 300
LFM-A7	*o*-F	220	170	430	416	69	74.5	> 300	> 300
LFM-A8	*m*-CF_3	246	189	492	465	22	> 100	> 300	> 300
LFM-A9	*m*-Br	236	168	367	354	> 100	> 100	> 300	> 300
LFM-A10	*m*-Cl	236	165	391	344	> 100	> 100	> 300	> 300
LFM-A11	*m*-F	218	163	400	387	> 100	> 100	> 300	> 300
LFM-A12	*p*-OCF_3	260	195	510	489	13	1.7	53.4	26.3
LFM-A13	2,5-diBr	246	170	436	340	> 100	> 100	> 300	> 300
LFM-A14	None	214	158	397	367	> 100	> 100	> 300	> 300

[a]Molecular surface area calculated using Connolly's MS program ***(69)***. Defined as the boundary of volume within any probe sphere (meant to represent a water molecule) of given radius sharing no volume with hard sphere atoms that make up the molecule.

[b]Buried surface, the percentage of molecular surface in contact with protein calculated by Ludi, based on docked positions.

[c]Ludi K_i based on the empirical score function in the Ludi program (Insight II, Molecular Simulations, San Diego, CA) ***(70)***.

Taken from Ghosh et al. (1998) *Clin. Cancer Res.* **4,** 2657–2668 ***(1)***.

Table 2
EGFR Interaction Scores, Estimated K_i Values, and Measured IC_{50} Data for 4-Anilinoquinazolines

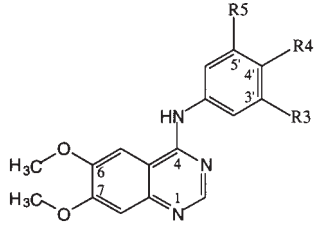

Compound	R3	R4	R5	MS[a] (Å^2)	BS[b] (Å^2)	Lipo Score	HB[c]	Ludi Score	Ludi[d] K_i (μM)	EGFR Inhibition IC_{50} (μM)
WHI-P79 (PD153035)	Br	H	H	302	208	610	1	570	2.0	10.0
WHI-P97	Br	OH	Br	329	224	655	2	701	0.09	2.5
WHI-P111	Br	CH_3	H	305	226	661	1	622	0.60	4.0
WHI-P131	H	OH	H	290	202	593	2	639	0.40	4.2
WHI-P154	Br	OH	H	307	218	639	2	685	0.14	5.6
WHI-P180	OH	H	H	292	204	599	2	645	0.36	4.0
WHI-P197	Cl	OH	H	298	215	629	2	675	0.18	3.5

[a]Molecular surface area calculated using Connolly's MS program ***(69)***. Defined as the boundary of volume within any probe sphere (meant to represent a water molecule) of given radius sharing no volume with hard sphere atoms that make up the molecule.

[b]Buried surface, the molecular surface in contact with protein calculated by Ludi based on docked positions.

[c]The number of hydrogen bonds between the protein and the inhibitor.

[d]Ludi K_i values were calculated based on the empirical score function in the Ludi program ***(71)***. Ideal hydrogen bond distances and angles between compounds and protein are assumed in all cases for Ludi score and K_i calculation.

Taken from Ghosh et al. (1999) *Anticancer Drug Des.* **14,** 403–410 ***(47)***.

2.2.3. Immunocytochemistry of EGF-Gen

Immunocytochemistry was used to examine the surface expression of EGFR on breast cancer cells, to evaluate the uptake of EGF-gen by breast cancer cells, and to examine the morphologic features of EGF-gen–treated cancer cells. To detect the EGFR–EGF-gen complexes, cells were incubated with a mixture of a monoclonal antibody directed at the extracellular domain of human EGFR and a polyclonal rabbit anti-gen antibody ***(2)***. After rinsing with PBS, cells were incubated with a mixture of a goat antimouse IgG antibody conjugated to FITC, and donkey antirabbit IgG conjugated to Texas Red. Cells were washed in PBS, counterstained with toto-3, and viewed using a confocal microscope.

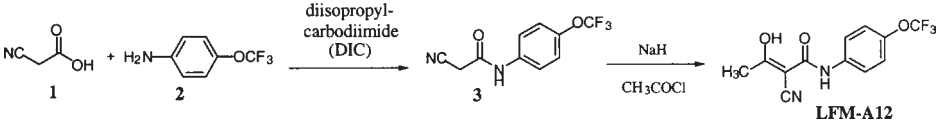

Scheme 1. Synthesis of LFM-A12 ***(59,60)***.

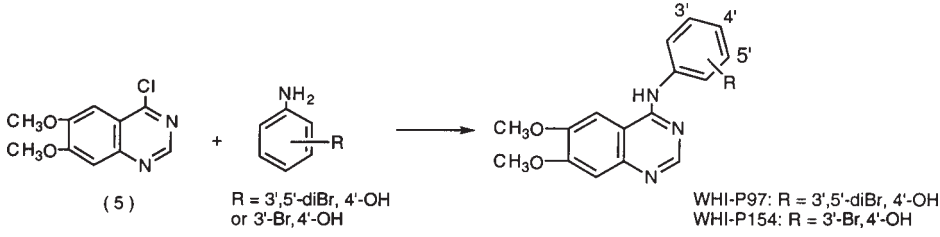

Scheme 2. Synthesis of quinazoline derivatives WH1-P97 and WH1-P154 ***(58)***.

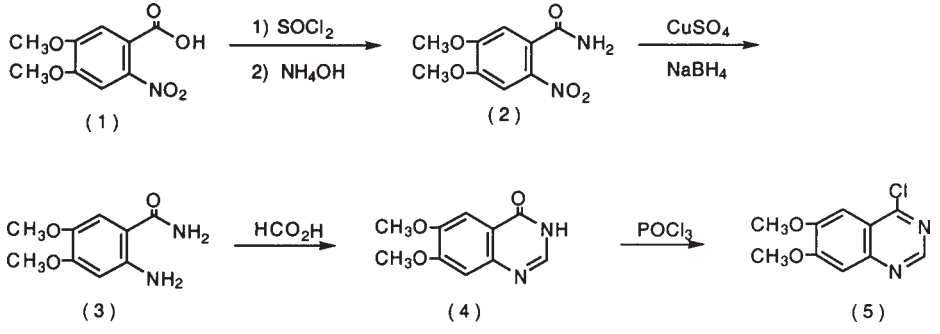

Scheme 3. Synthesis of a quinazoline derivative precursor ***(61,62)***.

2.2.4. In Vitro Treatment of Cells with EGF-Gen

In order to determine the cytotoxic activity of EGF-gen against breast cancer cells, cells were treated with various concentrations of EGF-gen and then used in either apoptosis assays or clonogenic assays ***(2)***. Controls included cells treated with G-CSF-gen (an irrelevant cytokine–gen conjugate that does not react with EGFR), cells treated with unconjugated EGF plus unconjugated gen, cells treated with unconjugated gen or unconjugated EGF, and cells treated with PBS, pH 7.4. In some experiments, excess G-CSF or EGF was added to the EGF-gen–containing treatment medium to show that the cytotoxicity of EGF-gen can be selectively blocked by excess EGF but not G-CSF.

2.2.5. Immune-Complex Kinase Assays and Antiphosphotyrosine Immunoblotting

After treatment with EGF-Gen, cells were stimulated with EGF and cell lysates were immunoprecipitated with an anti-EGFR antibody reactive with the Ala^{351}-Asp^{364} sequence of human EGFR. EGFR immune complexes were examined for tyrosine phosphorylation by Western blot analysis as previously described ***(66)***. All antiphosphotyrosine Western blots were subjected to densitometric scanning and for each time point a percent inhibition value was determined.

2.2.6. Apoptosis Assays Using EGF-Gen

MC540 binding and propidium iodide (PI) permeability (indicators of apoptosis) were simultaneously measured in breast cancer cells after exposure to EGF-gen (either without any cytokine preincubation or following preincubation with excess unconjugated EGF or G-CSF), unconjugated gen, unconjugated EGF plus unconjugated gen, or G-CSF–gen, as previously described ***(66)***. To detect the DNA fragmentation in apoptotic cells, cells were harvested after treatment with EGF-gen and DNA was prepared from Triton-X-100 detergent lysates for analysis of fragmentation as previously described ***(66)***.

2.2.7. Clonogenic Assays

After treatment with EGF-gen, G-CSF–gen, unconjugated EGF, unconjugated gen, or PBS, cells were resuspended in clonogenic medium. Cells were cultured and cancer-cell colonies were enumerated on a grid using an inverted-phase microscope of high optical resolution. Results were expressed as the percent inhibition of clonogenic cells at a particular concentration of the test agent. Dose–survival curves were constructed using the percent control survival results for each drug concentration as the data points, and the IC_{50} values were calculated.

2.2.8. Crossreactivity of Human EGF and Antihuman EGFR Antibodies with Mouse EGFR

Livers and thymus of BALB/c mice were frozen in liquid nitrogen and 5 μm–thick tissue sections were prepared using a cryostat. The sections were processed for standard indirect immunofluorescence using a monoclonal antibody directed at the extracellular domain of human EGFR as the primary antibody and a goat antimouse IgG conjugated to FITC as the secondary antibody ***(2)***. In parallel, sections were also stained by direct immunofluorescence staining techniques with FITC-conjugated EGF.

2.2.9. Mouse Toxicity Studies

The toxicity profile of EGF-gen in BALB/c mice was examined as previously reported for other biotherapeutic agents ***(25,67)***. In single-dose toxicity studies, female BALB/c mice were administered an intraperitoneal bolus injection of EGF-gen in 0.2 mL PBS, or 0.2 mL PBS alone (control mice). In cumulative toxicity studies, mice received a total of 2800 μg (140 mg/kg) EGF-gen intraperitoneally over 28 consecutive days. Mice were monitored daily for mortality to determine the 30-d LD_{50} values ***(36)***.

2.2.10. Treatment of SCID Mouse Xenograft Model of Human Breast Cancer

The left hind legs of CB.17 SCID mice were inoculated subcutaneously with MDA-MB-231 breast cancer cells in 0.2 mL PBS. SCID mice inoculated with human breast cancer cells were treated with EGF-gen ***(36)***. Mice were monitored daily for health status and tumor growth. Primary endpoints of interest were tumor growth and tumor-free survival outcome. Estimation of life table outcome and comparisons of outcome between groups were done as previously reported ***(6,25,67)***. The efficacy of EGF-gen against established tumors was examined by treating SCID mice with subcutaneous MDA-MB-231 xenografts with EGF-gen on 10 consecutive days and determining the tumor diameter daily for 20 d from the start of therapy. Control mice were treated with 0.2 mL PBS for 10 consecutive days.

2.2.11. Pharmacokinetic Studies of SCID Mice Treated with EGF-Genistein

Tissue distribution studies in SCID mice were performed using EGF–^{125}I-gen and ^{125}I-gen as described previously ***(25)***. A flow-limited physiologic pharmacokinetic model was used to characterize the tissue disposition of EGF-gen in non–tumor-bearing as well as tumor bearing SCID mice ***(25,36,68)***.

3. Results

3.1. Structure-Based Design of Small-Molecule Inhibitors of EGFR

3.1.1. Predicted Binding of LFM-A12 with the EGFR Kinase Domain

Based on modeling studies of the kinase domain of EGFR, a binding mode was proposed for LFM analogs ***(1)***. The predicted binding mode allows LFM analogs to maintain close contact with the hinge region of EGFR. The inhibitor can fit into a space in the EGFR catalytic site defined by Leu^{694} and Val^{702} on one side, and Leu^{820} and Thr^{830} on the other. The nitrile nitrogen of LFM-A12 was predicted to interact with the amide of Met^{769} via hydrogen bonding. In

addition, the *para*-substituted OCF_3 group on LFM-A12 can form close contacts with residues Thr^{766} and Asp^{831}. Interaction scores, calculated K_i values, and measured IC_{50} data for several LFM analogs are listed in **Table 1**. Of the compounds predicted to interact most favorably with EGFR, LFM and LFM-A12 showed the most potent activity against EGFR in kinase assays, and LFM-A12 was the most cytotoxic against breast cancer cells.

3.1.2. Modeling Studies of 4-Anilinoquinazoline Derivatives with the EGFR Kinase Domain

Kinase inhibition properties have also been evaluated for derivatives of 4-anilinoquinazoline ***(4,5,47)***. In modeling studies aimed at identifying quinazoline derivatives with a high likelihood to bind favorably to the catalytic site of the EGFR, K_i values were estimated based on predicted binding interactions between the inhibitor and catalytic-site residues of the EGFR ***(47)***. The model of the EGFR binding pocket was used in combination with docking procedures to predict the favorable placement of chemical groups with defined sizes on a molecular template. These studies led to the design of six quinazoline derivatives, WHI-P97, WHI-P111, WHI-P131, WHI-P154, WHI-P180, and WHI-P197. The various docked positions of each quinazoline derivative were qualitatively evaluated in terms of an estimated K_i value and consequently compared with the IC_{50} values of the compounds in EGFR kinase inhibition assays. **Table 2** lists the interaction scores and estimated K_i values for the quinazoline derivatives. This most favorable docked position allowed the quinazoline inhibitor to maintain close contacts with the hinge region of EGFR. The quinazoline moiety in the molecule can align itself along the hinge region of EGFR, and the N1 nitrogen of the quinazoline group can form a hydrogen bond with the backbone carbonyl atom of the EGFR Met^{769} residue.

In the final docking mode, the 6,7-OCH_3 groups of the inhibitor faced the solvent accessible region, and the anilino ring was surrounded by residues Thr^{766}, Asp^{831}, Thr^{830}, and Val^{702}. This model of the anilinoquinazoline bound to the EGFR kinase domain is consistent with that reported by others ***(71)***. WHI-P97, WHI-P131, WHI-P154, WHI-P180, and WHI-P197 with 3' or 4'-OH substitutions on the anilino moiety can form an additional hydrogen bond with Asp^{831}. WHI-P79 was the least potent inhibitor in the series evaluated, followed by WHI-P111. The activity of these two compounds may be affected by the absence of 3' or 4'-OH substitutions that can form a second hydrogen bond with EGFR residues and enhance binding.

The crystal structures of the HCK–quercetin complex ***(48)*** and two FGFR–inhibitor complexes ***(50)*** revealed that PTK inhibitors can bind to the PTK catalytic (ATP-binding) site. When the catalytic sites of these PTK crystal

structures were superimposed, all atoms of the three PTK inhibitors present fell within the plane of a triangle defining the ATP-binding region, and each molecule was in close contact with the hinge region and a conserved Asp residue (Asp^{831} in EGFR). The inhibitors characteristically occupied only half of the binding site, closest to the hinge region. The fact that the inhibitors reside close to the hinge region seems to correlate with tighter binding and may be an important determinant for inhibitor binding. In the case of EGFR, the size and relatively planar shape of the catalytic site within the constructed EGFR kinase domain may contribute to its ability to form favorable interactions with molecules such as quinazoline derivatives and LFM analogs. This observation was in good agreement with conclusions derived from structure–activity relationships for pyrrolo- and pyrazoloquinazoline compounds ***(71)*** and was incorporated into the described modeling strategy for EGFR.

While most of the catalytic site residues of the EGFR kinase domain are conserved relative to other tyrosine kinases, a few specific variations are observed. In the EGFR modeling studies, the docked inhibitors were located between two regions of mostly hydrophobic residues. EGFR residues on one side of the docked inhibitor included Leu^{694}, Val^{702}, Lys^{721}, and Ala^{719}, which are conserved in EGFR, HCK, FGFR and IRK. EGFR residues on the other side of the docked inhibitor included Leu^{820} and Thr^{830}, which vary in FGFR (Leu, Ala) and IRK (Met, Gly). EGFR residues Asn^{818} and Asp^{831} (opposite the hinge) are conserved in all four PTKs. Residue Thr^{766} in the EGFR hinge region changes to Val in FGFR, and to Met in IRK. Residue Thr^{830} in EGFR changes to Ala in FGFR, and to Gly in IRK. One side of the binding pocket contains Cys^{773} in EGFR and is therefore considerably more hydrophobic than the corresponding residue of platelet derived growth factor (PDGF)R (Asp), FGFR (Asn), and IRK (Asn). These residue identity differences may provide the basis for designing selective inhibitors of the EGFR tyrosine kinase.

The catalytic site of EGFR may have specific features that can be advantageous for the design of inhibitors. Molecules that can fit into the triangular binding region of the EGFR catalytic site that can also form favorable contacts with the hinge region are likely to bind more strongly and inhibit EGFR more effectively. The docked position of LFM-A12 in the catalytic site of EGFR is shown in **Fig. 3**. It indicates that the molecule can maintain close contact with the hinge region of EGFR and can form a hydrogen bond between the nitrile nitrogen and the amide of Met^{769}.

The docked positions of several quinazoline derivatives in the EGFR catalytic site are shown in **Fig. 4**. Like LFM-A12, quinazolines can maintain close contacts with the hinge region of EGFR, and the N1 nitrogen of the quinazoline group can hydrogen bond with the backbone carbonyl atom of Met^{769}. WHI-P97, which can form the most favorable interactions with EGFR (two hydrogen

bonds and hydrophobic contacts), was the most potent of the quinazolines tested (EGFR IC_{50} = 2.5 μ*M*). However, in the EGFR model, the binding volume of the EGFR catalytic site is much larger than the volume occupied by WHI-P97 and LFM-A12. Increasing the size of the ligand by using larger ring systems might increase the contact area between the receptor and ligand and thus enhance binding. Interactions of the inhibitor with nonconserved residues such as Cys^{751} and Thr^{830} in the catalytic site of EGFR may also be utilized for the design of more potent and selective inhibitors of EGFR.

3.2. EGF-Gen Immunoconjugates

3.2.1. Biologic Activity of EGF-Gen Immunoconjugates

Treatment of EGFR with EGF-gen resulted in decreased tyrosine phosphorylation of the EGFR in a concentration-dependent fashion ***(2)***. Whereas EGF-gen exhibited marked PTK-inhibitory activity in MDR-MB-231 cells at concentrations as low as 0.1 μ*M* in the treatment medium, unconjugated gen did not significantly affect the EGFR tyrosine phosphorylation even at a 10 μ*M* concentration. The inhibitory effect of EGF-gen was blocked by preincubation of cells with excess EGF but not by excess G-CSF. Immune-complex kinase assays were used to assess the effects of EGF-gen on the enzymatic activities of EGFR-associated *Src* PTK in MBA-MB-231 cells. EGF-gen treatment inhibited the *Src* kinase. Unlike EGF-gen, a mixture of unconjugated gen and EGF or G-CSF–gen did not inhibit the *Src* kinase activity in MDA-MB-231 cells. Thus, EGF-gen is a potent inhibitor of both the EGFR tyrosine kinase as well as other PTKs that are associated with the EGFR.

Targeting gen to vital PTKs in leukemia cells results in apoptotic cell death ***(25,54)***. Furthermore, the examination of the morphologic features of EGF-gen treated BT-20 and MDA-MB-231 cells by immunocytochemistry suggested that these cells might be undergoing apoptosis. A quantitative flow-cytometric apoptosis detection assay was used to study whether EGF-gen could trigger apoptosis in breast cancer cells. MC540 binding and PI permeability of MDA-MB-231 breast cancer cells were simultaneously measured before and after treatment with 1 μg/mL EGF-gen (0.1 μ*M*), 10 μg/mL EGF (1 μ*M*) plus 10 μg/mL unconjugated Gen (37 μ*M*), or 1 μg/mL G-CSF–gen. Whereas less than 10% of MDA-MB-231 or BT-20 cells showed apoptotic changes after treatment with either EGF plus unconjugated gen or G-CSF–gen, a significant portion of cells underwent apoptosis within 24 h after EGF-gen treatment (95.1% = 57.9% $MC540^+$ early-stage apoptosis plus 37.2% $MC540^+/PI^+$ advanced-stage apoptosis at 24 h). Excess EGF (10 μg/mL) but not excess G-CSF (10 μg/mL) could prevent EGF-gen–induced apoptosis. Thus, EGF-gen causes apoptosis

in an EGFR-specific fashion, and this activity requires both its EGFR-binding growth factor moiety as well as its PTK inhibitory gen moiety.

DNA from Triton-X-100 lysates of EGF-gen–treated MDA-MB-231 or BT-20 breast-cancer cells showed a ladder-like and dose-dependent fragmentation pattern consistent with apoptosis. The EGF-gen–induced DNA fragmentation was EGFR-specific, as DNA from cells treated with G-CSF–gen showed no fragmentation. DNA fragmentation was dependent both on the PTK inhibitory function of gen and the targeting function of EGF, as cells treated with unconjugated gen plus unconjugated EGF did not show apoptotic DNA fragmentation.

3.2.2. Biodistribution and Toxicity of EGF-Gen in Mice

Tissue distribution studies were performed using EGF–^{125}I-gen and a flow-limited physiologic pharmacokinetic model was used to characterize the in vivo tissue disposition of EGF-gen in non–tumor-bearing as well as tumor-bearing SCID mice ***(2)***. When compared with unconjugated gen, a much greater amount of EGF-gen was partitioned to bone marrow, spleen, liver, kidney, and lungs. In both tumor-bearing and non–tumor-bearing mice, EGF-gen was most extensively partitioned to the liver, with tissue drug concentrations exceeding plasma concentrations more than seven times.

In toxicity studies, 28 female BALB/c mice were injected intraperitoneally with a single bolus dose of EGF-gen in 0.2 mL PBS from 2 μg (100 μg/kg) to 800 μg (40 mg/kg). Even at the highest doses of 400 μg or 800 μg (40 mg/kg), mice did not become weak or lethargic, lose weight, or develop diarrhea or scruffy skin. When mice were treated with multiple doses of EGF-gen at a total dose level of 2.8 mg (140 mg/kg) according to a 28 d, 100 μg/mouse/d (5 mg/kg/d) schedule, no significant toxicity was observed and none of the 10 mice died. No histopathologic lesions were found in any of the organs of EGF-gen–treated mice receiving a single dose or multiple doses of EGF-gen.

3.2.3. In Vivo Antitumor Activity of EGF-Gen in a SCID Mouse Xenograft Model of Human Breast Cancer

CB.17 SCID mice developed rapidly growing tumors after subcutaneous inoculation of 1×10^6 MDA-MB-231 cells. We examined the in vivo antitumor activity of EGF-gen in this SCID mouse xenograft model of human breast cancer. EGF-gen significantly improved tumor-free survival in a dose-dependent fashion when it was administered 24 h after inoculation of tumor cells. At a dose level of 100 μg/kg/d for 10 d (1 mg/kg total dose), which is >100-fold less than the highest tested and nontoxic cumulative dose (i.e., 140 mg/kg) in mice, EGF-gen was more effective than cyclophosphamide

(50 mg/kg/d for 2 d), adriamycin (2.5 mg/kg for 1 d) or methotrexate (0.5 mg/kg for 1 d), the most widely used standard chemotherapeutic drugs for breast cancer. None of the control mice treated with either PBS (n = 40), GCSF–gen (100 μg/kg/d; n = 10), or unconjugated gen (100 μg/kg/d; n = 10) remained tumor-free beyond 108 d (median tumor-free survival = 52 d). All of the 10 mice treated with EGF plus gen developed tumors within 45 d, with a median tumor-free survival of only 39 d. By comparison, 40 ± 16% of mice treated for 10 consecutive days with 10 μg/kg/d EGF-gen survived tumor-free beyond 3 mo and 20 ± 13% were still tumor-free at 7 mo. Remarkably, 60 ± 16% of mice treated for 10 consecutive days with 100 μg/kg/d EGF-gen remained free of detectable tumors for more than 7 mo. Tumors developing in EGF-gen–treated mice reached the 0.5 cm^3 tumor size much later than control mice (**Fig. 5**). Thus, EGF-gen elicited significant in vivo antitumor activity at nontoxic doses.

In contrast to EGF-gen, cyclophosphamide (50 mg/kg/d for 2 d; n = 5), adriamycin (2.5 mg/kg; n = 10), or methotrexate (0.5 mg/kg; n = 5) did not significantly affect tumor development in this SCID mouse model. Of the 20 mice treated with one of these chemotherapeutic drugs, only 10% remained tumor-free beyond 3 mo, indicating no improvement over the control group and a worse tumor-free survival outcome compared with the 2.0 μg/d EGF-gen group.

Furthermore, treating SCID mice with established subcutaneous human breast cancer xenografts of 0.5 cm in diameter with EGF-gen at this dose level resulted in eradication of the tumors in two of five mice and >50% shrinkage in three of five mice within 10 d. In contrast to the tumors in EGF-gen–treated mice, all of the control tumors in five PBS-treated mice as well as five mice treated with unconjugated gen showed a >200% increase in diameter within 10 d. These tumors continued their rapidly progressive growth and diameters at d 20 ranged from 1.8–2.6 cm in PBS-treated mice and from 1.9 to 2.4 in gen-treated mice.

EGF-gen treatment significantly reduced the growth rate of breast cancer xenografts of 1.0 cm diameter during the 20 d observation period, but unlike the case where tumors were 0.5 cm in diameter, it failed to cause shrinkage or disappearance of these larger tumors.

3.2.4. In Vivo Pharmacokinetic Features of EGF-Gen in SCID Mice

The therapeutic systemic exposure levels of EGF-gen were determined by examining its pharmacokinetics when administered at dose levels that were effective in the SCID mouse xenograft model of human breast cancer. EGF-gen was cleared rapidly from blood with an elimination half-life of 1.3–1.6 h. At the lower dose level, EGF-gen was cleared more rapidly from blood, had a larger central volume of distribution and lower measured maximum plasma concentration, and yielded a lower systemic exposure level in SCID mice with

human breast-cancer xenografts than in healthy SCID mice that were not inoculated with breast-cancer cells. The systemic exposure level, achieved by the therapeutically effective 10 μg/kg/d dose level of EGF-gen was 16.0 ± 1.5 μg · h/L in non–tumor-bearing healthy SCID mice and 7.6 ± 1.4 μg · h/L in SCID mice bearing 1 cm^3 MDA-MB-231 tumors, as measured by the area under the serum concentration–time curve (AUC). By comparison, treatment with 100 μg/kg/d EGF-gen over 10 d yielded an AUC of 2564 ± 231 μg · h/L in non–tumor-bearing mice and an AUC of 3125 ± 281 μg · h/L in tumor-bearing mice. Thus, the AUC showed a dramatic 160-fold (2564 μg · h/L vs 16 μg · h/L, $P < 0.001$) to 411-fold (3125 μg · h/L vs 7.6 μg · h/L, $P < 0.001$) increase as the dose of EGF-gen was increased 10-fold. This dramatic increase in AUC, which was accompanied by a dramatic 232-fold (11.6 ± 1.3) mL/g vs 0.05 ± 0.01 mL/g, $P < 0.001$) to 600-fold (30.0 ± 3.6 mL/g vs 0.05 ± 0.01 mL/g, $P < 0.001$) decrease of the volume of distribution is most likely due to saturable receptor-dependent binding and uptake of EGF-gen, reported to occur with unconjugated human EGF in rats at a dose level of 100 μg/kg ***(72)***. As a result of the increase in AUC, the clearance (i.e., dose/AUC) of EGF-gen significantly decreased with this dose escalation. The dose-dependent decrease in clearance was not associated with significant differences in t1/2β values (1.3 ± 0.2 vs 2.1 ± 0.3 for non–tumor-bearing mice, and 1.6 ± 0.4 vs 1.0 ± 0.1 for tumor-bearing mice), which is in accord with the published observations of Kim and associates ***(72,73)***. These results, taken together with previous reports regarding the pharmacokinetics of unconjugated EGF are consistent with the notion that the initial redistribution of EGF-gen from plasma to EGFR-positive cells in various tissues. These tissues determine that the t1/2α values are affected by factors influencing the binding of EGF-gen to EGFR-positive cells (e.g., affinity of the EGF-gen conjugate for EGFR, number of EGFR-positive targets in the extravascular compartments), while the later phase of removal from plasma determining the t1/2β values is likely affected by the EGFR turnover rates and dose-independent disassociation of EGF-gen from surface EGFR molecules.

3.2.5. Pharmacodynamic Features and Toxicity

EGF-gen was not toxic to healthy mice even at doses as high as 40 mg/kg given as a single dose or 140 mg/kg given in multiple doses, despite the crossreactivity of human EGF with murine EGFR. It was then proposed that similar systemic exposure levels could also be achieved in cynomolgus monkeys without excessive toxicity. The systemic exposure levels achieved in cynomolgus monkeys after treatment with 50 μg/kg/d over 10 d and 100 μg/kg/d for 10 d were tested.

The plasma concentration–time curves of EGF-gen in monkeys were also biphasic. The volume of distribution and clearance tended to decrease as the daily dose increased from 50 μg/kg to 100 μg/kg, similar to what was observed

in mice. Treatment with 100 μg/kg/d EGF-gen yielded an AUC of 1400 μg · h/L. This systemic exposure level was much higher than the target AUC of 16 μg · h/L, which was found to be effective in the SCID mouse model of human breast cancer.

Notably, no clinical or laboratory evidence of significant toxicity was observed, except for a transient alopecia in two of the monkeys. In particular, we observed no gastrointestinal or hepatic toxicity. No histopathologic lesions were found in the organs of EGF-gen–treated monkeys that were electively euthanized. Thus, EGF-gen concentrations higher than those required to elicit therapeutic efficacy in the SCID mouse xenograft model were achieved in cynomolgus monkeys without significant systemic toxicity.

4. Summary of Treatment Strategies for EGFR-Positive Malignancies

Recent studies have identified some promising EGFR inhibitors that may be useful for the treatment of cancer. These agents include small molecule kinase inhibitors such as quinazoline derivatives WHI-P97 (EGFR IC_{50} = 2.5 μ*M*; ***47***), and LFM-A12 (EGFR IC_{50} = 1.7 μ*M*; ***47***). LFM-A12 inhibited EGFR and killed human breast-cancer cells in vitro by triggering apoptosis ***(1)***. Both LFM-A12 and WHI-P97 inhibited the in vitro invasiveness of EGFR-positive human breast cancer cells at micromolar concentrations and induced apoptotic cell death. In addition, LFM-A12 inhibited the proliferation and in vitro invasiveness of EGFR-positive human breast cancer cells in a concentration-dependent fashion. Another promising anticancer agent is the protein–inhibitor conjugate EGF-gen. EGF-gen is a cytotoxic agent show to inhibit the EGFR tyrosine kinase in breast cancer cells with an IC_{50} value of 2.9 n*M* ***(2,36)*** and trigger rapid apoptotic cell death in MDA-MB-231 as well as BT-20 breast cancer cells at nanomolar concentrations. EGF-gen showed no toxicity in mice and significantly improved tumor-free survival in a SCID mouse xenograft model of human breast cancer. Administration of EGF-gen to cynomolgus monkeys did not result in any significant side effects. Both EGF-gen and LFM-A12 show potency against EGFR and specificity for EGFR, and may be useful for the treatment of breast cancer as well as other EGFR-positive malignancies.

References

1. Ghosh, S., Zheng, Y., Jun, X., Narla, R., Mahajan, S., Navara, C., et al. (1998) α-Cyano-β-hydroxy-β-methyl-*N*-[4-(trifluoromethoxy)phenyl]propenamide: An inhibitor of the EGF receptor tyrosine kinase with potent cytotoxic activity against breast cancer cells. *Clin. Cancer Res.* **4,** 2657–2668.
2. Uckun, F. M., Jun, X., Narla, R. K., Zeren, T., Venkatachalam, T., Waddick, K., et al. (1998) Cytotoxic activity of EGF-genistein against human breast cancer cells. *Clin. Cancer Res.* **4,** 901–912.

3. Traxler, P., Bold, G., Frei, J., Lang, M., Lydon, N., Mett, H., et al. (1997) Use of a pharmacophore model for the design of EGF-R tyrosine kinase inhibitors: 4-(phenylamino)pyrazolo[3,4-d]pyrimidines. *J. Med. Chem.* **40,** 3601–3616.
4. Fry, D. W., Kraker, A. J., McMichael, A., Ambroso, L. A., Nelson, J. M., Leopold, W. R., et al. (1994) A specific inhibitor of the epidermal growth factor receptor tyrosine kinase. *Science* **265,** 1093–1095.
5. Bridges, A. J., Zhou, H., Cody, D. R., Rewcastle, G. W., McMichael, A., Showalter, H. D., et al. (1996) Tyrosine kinase inhibitors. 8. An unusually steep structure–activity relationship for analogues of 4-(3-bromoanilino)-6,7-dimethoxyquinazoline (PD 153035), a potent inhibitor of the epidermal growth factor receptor. *Med. Chem.* **39,** 267–276.
6. Akiyama, T., Ishida, J., Nakagawa, S., Ogawara, H., Watanabe, S., Itoh, N., et al. (1987) Genistein, a specific inhibitor of tyrosine-specific protein kinases. *J. Biol. Chem.* **262,** 5592–5595.
7. Sudbeck, E. A., Liu, X.-P., Narla, R. K., Mahajan, S., Ghosh, S., Mao, C., et al. (1999) Structure-based design of specific inhibitors of Janus kinase 3 as apoptosis-inducing anti-leukemic agents. *Clin. Cancer Res.* **5,** 1569–1582.
8. Yamashita, N., Kazuo, S. Y., Kitamura, M., Wakao, H., Furihata, K., Furihata, K., et al. (1997) Cytovaricin B, a new inhibitor of JAK-STAT signal transduction produced by *Streptomyces torulosus. J. Antibiot. (Tokyo)* **50,** 440–442.
9. Wasik, M. A., Nowak, I., Zhang, Q., and Shaw, L. M. (1998) Suppression of proliferation and phosphorylation of Jak3 and STAT5 in malignant T-cell lymphoma cells by derivatives of octylamino-undecyl-dimethylxanthine. *Leuk. Lymphoma* **28,** 551–560.
10. Siemasko, K., Chong, A. S., Jack, H. M., Gong, H., Williams, J. W., and Finnegan, A. (1998) Inhibition of JAK3 and STAT6 tyrosine phosphorylation by the immunosuppressive drug leflunomide leads to a block in IgG1 production. *J. Immunol.* **160,** 1581–1588.
11. Fiorucci, G., Percario, Z. A., Marcolin, C., Coccia, E. M., Affabris, E., and Romeo, G. (1995) Inhibition of protein phosphorylation modulates expression of the Jak family protein tyrosine kinases. *J. Virol.* **69,** 5833–5837.
12. Meydan, N., Grunberger, T., Dadi, H., Shahar, M., Arpaia, E., Lapidot, Z., et al. (1996) Inhibition of acute lymphoblastic leukaemia by a Jak-2 inhibitor. *Nature* **379,** 645–648.
13. Wang, L. H., Kirken, R. A., Erwin, R. A., Yu, C. R., and Farrar, W. L. (1999) JAK3, STAT, and MAPK signaling pathways as novel molecular targets for the tyrphostin AG-490 regulation of IL-2–mediated T cell response. *J. Immunol.* **162,** 3897–3904.
14. Mahajan, S., Ghosh, S., Sudbeck, E. A., Zheng, Y., Downs, S., Hupke, M., et al. (1999) Rational design and synthesis of a novel anti-leukemic agent targeting Bruton's tyrosine kinase (BTK): LFM-A13 [α-cyano-β-hydroxy-β-methyl-*N*-(2,5-dibromophenyl)propenamide]. *J. Biol. Chem.* **274,** 9587–9599.
15. Ghosh, S. and Uckun, F. M. (1999) Alpha-cyano-N-(2,5-dibromophenyl)-beta-hydroxybut-2–enamide. *Acta Crystallogr. C* **55,** 1364–1365.
16. Kawakami, Y., Hartman, S. E., Kinoshita, E., Suzuki, H., Kitaura, J., Yao, L., et al. (1999) Terreic acid, a quinone epoxide inhibitor of Bruton's tyrosine kinase. *Proc. Natl. Acad. Sci. USA* **96,** 2227–2232.

17. Zaman, G. J., Vink, P. M., van den Doelen, A. A., Veeneman, G. H., and Theunissen, H. J. (1999) Tyrosine kinase activity of purified recombinant cytoplasmic domain of platelet-derived growth factor beta-receptor (beta-PDGFR) and discovery of a novel inhibitor of receptor tyrosine kinases. *Biochem. Pharmacol.* **57,** 57–64.
18. Teicher, B. A., Alvarez, E., Mendelsohn, L. G., Ara, G., Menon, K., and Ways, D. K. (1999) Enzymatic rationale and preclinical support for a potent protein kinase C beta inhibitor in cancer therapy. *Adv. Enzyme Regul.* **39,** 313–327.
19. Merritt, J. E., Sullivan, J. A., Drew, L., Khan, A., Wilson, K., et al. (1999) The bisindolylmaleimide protein kinase C inhibitor, Ro 32–2241, reverses multidrug resistance in KB tumour cells. *Cancer Chemother. Pharmacol.* **43,** 371–378.
20. Thavasu, P., Propper, D., McDonald, A., Dobbs, N., Ganesan, T., Talbot, D., et al. (1999) The protein kinase C inhibitor CGP41251 suppresses cytokine release and extracellular signal-regulated kinase 2 expression in cancer patients. *Cancer Res.* **59,** 3980–3984.
21. Begemann, M., Kashimawo, S. A., Choi, Y. A., Kim, S., Christiansen, K. M., Duigou, G., et al. (1996) Inhibition of the growth of glioblastomas by CGP 41**251,** an inhibitor of protein kinase C, and by a phorbol ester tumor promoter. *Clin. Cancer Res.* **2,** 1017–1030.
22. Schwartz, G. K., Ward, D., Saltz, L., Casper, E. S., Spiess, T., Mullen, E., et al. (1997) A pilot clinical/pharmacological study of the protein kinase C-specific inhibitor safingol alone and in combination with doxorubicin. *Clin. Cancer Res.* **3,** 537–543.
23. Kawamoto, S. and Hidaka, H. (1984) 1-(5-Isoquinolinesulfonyl)-2-methylpiperazine (H-7) is a selective inhibitor of protein kinase C in rabbit platelets. *Biochem. Biophys. Res. Commun.* **125,** 258–264.
24. Ido, M., Asao, T., Sakurai, M., Inagaki, M., Saito, M., and Hidaka, H. (1986) An inhibitor of protein kinase C, 1-(5-isoquinolinylsulfonyl)-2-methylpiperazine(H-7) inhibits TPA-induced reduction of vincristine uptake from P388 murine leukemic cell. *Leuk. Res.* **10,** 1063–1069.
25. Uckun, F. M., Evans, W. E., Forsyth, C. J., Waddick, K. G., Ahlgren, L. T., Chelstrom, L. M., et al. (1995) Biotherapy of B-cell precursor leukemia by targeting genistein to CD19-associated tyrosine kinases. *Science* **267,** 886–891.
26. Krystal, G. W., DeBerry, C. S., Linnekin, D., and Litz, J. (1998) Lck associates with and is activated by Kit in a small cell lung cancer cell line: Inhibition of SCF-mediated growth by the Src family kinase inhibitor PP1. *Cancer Res.* **58,** 4660–4666.
27. Miknyoczki, S. J., Chang, H., Klein-Szanto, A., Dionne, C. A., and Ruggeri, B. A. (1999) The Trk tyrosine kinase inhibitor CEP-701 (KT-5555) exhibits significant antitumor efficacy in preclinical xenograft models of human pancreatic ductal adenocarcinoma. *Clin. Cancer Res.* **5,** 2205–2212.
28. Miknyoczki, S. J., Dionne, C. A., Klein-Szanto, A. J., and Ruggeri, B. A. (1999) The novel Trk receptor tyrosine kinase inhibitor CEP-701 (KT-5555) exhibits

antitumor efficacy against human pancreatic carcinoma (Panc1) xenograft growth and in vivo invasiveness. *Ann. NY Acad. Sci.* **880,** 252–262.
29. Dionne, C. A., Camoratto, A. M., Jani, J. P., Emerson, E., Neff, N., Vaught, J. L., et al. (1998) Cell cycle-independent death of prostate adenocarcinoma is induced by the trk tyrosine kinase inhibitor CEP-751 (KT6587). *Clin. Cancer Res.* **4,** 1887–1898.
30. Tapley, P., Lamballe, F., and Barbacid, M. (1992) K252a is a selective inhibitor of the tyrosine protein kinase activity of the trk family of oncogenes and neurotrophin receptors. *Oncogene* **7,** 371–381.
31. Baselga, J., Norton, L., Albanell, J., Kim, Y. M., and Mendelsohn, J. (1998) Recombinant humanized anti-HER2 antibody (Herceptin) enhances the antitumor activity of paclitaxel and doxorubicin against HER2/neu overexpressing human breast cancer xenografts. *Cancer Res.* **58,** 2825–2831.
32. Pegram, M. D., Lipton, A., Hayes, D. F., Weber, B. L., Baselga, J. M., Tripathy, D., et al. (1998) Phase II study of receptor-enhanced chemosensitivity using recombinant humanized anti-p185HER2/neu monoclonal antibody plus cisplatin in patients with HER2/neu-overexpressing metastatic breast cancer refractory to chemotherapy treatment. *J. Clin. Oncol.* **16,** 2659–2671.
33. Baselga, J., Tripathy, D., Mendelsohn, J., Baughman, S., Benz, C. C., Dantis, L., et al. (1999) Phase II study of weekly intravenous trastuzumab (Herceptin) in patients with HER2/neu-overexpressing metastatic breast cancer. *Semin. Oncol.* **26,** 78–83.
34. Shak, S. (1999) Overview of the trastuzumab (Herceptin) anti-HER2 monoclonal antibody clinical program in HER2-overexpressing metastatic breast cancer. Herceptin Multinational Investigator Study Group. *Oncol.* **26,** 71–77.
35. Ross, J. S. and Fletcher, J. A. (1998) The HER-2/neu oncogene in breast cancer: prognostic factor, predictive factor, and target for therapy. *Oncologist* **3,** 237–252.
36. Uckun, F. M., Narla, R. K., Zeren, T., Yanishevski, Y., Myers, D. E., Waurzyniak, B., et al. (1998) In vivo toxicity, pharmacokinetics, and anticancer activity of Genistein linked to recombinant human epidermal growth factor. *Clin. Cancer Res.* **4,** 1125–1134.
37. Carpenter, G. and Cohen, S. (1990) Epidermal growth factor. *J. Biol. Chem.* **265,** 7709–7712.
38. George-Nascimento, C., Gyenes, A., Halloran, S. M., Merryweather, J., Valenzuela, P., Steimer, K. S., et al. (1988) Characterization of recombinant human epidermal growth factor produced in yeast. *Biochemistry* **27,** 797–802.
39. Khazaie, K., Schirrmacher, V., and Lichtner, R. (1993) EGF receptor in neoplasia and metastasis. *Cancer & Metasis Reviews* **12,** 255–274.
40. Mendelsohn, J. and Baselga, J. (1995) Antibodies to growth factors and receptors, *Biologic Therapy of Cancer: Principles & Practice,* J. B. Lippincott Co., Philadelphia, pp. 607–623.
41. Toi, M., Osaki, A., Yamada, H., and Toge, T. (1991) Epidermal growth factor receptor expression as a prognostic indicator of breast cancer. *European J. Cancer* **27,** 977–980.

42. Chrysogelos, S. and Dickson, R. (1994) EGF receptor expression, regulation, and function in breast cancer. *Breast Cancer Res. Treat.* **29,** 29–40.
43. Fox, S. B., Smith, K., Hollyer, J., Greenall, M., Hastrich, D., and Harris, A. L. (1994) The epidermal growth factor receptor as a prognostic marker: Results of 370 patients and review of 3009 patients. *Breast Cancer Res. Treat.* **29,** 41–49.
44. Fry, D. W., Bridges, A. J., Denny, W. A., Doherty, A., Greis, K. D., Hicks, J. L., et al. (1998) Specific, irreversible inactivation of the epidermal growth factor receptor and erbB2 by a new class of tyrosine kinase inhibitor. *Proc. Natl. Acad. Sci. USA* **95,** 12,022–12,027.
45. Moyer, J. D., Barbacci, E. G., Iwata, K. K., Arnold, L., Boman, B., Cunningham, A., et al. (1997) Induction of apoptosis and cell cycle arrest by CP-358,774, an inhibitor of epidermal growth factor receptor tyrosine kinase. *Cancer Res.* **57,** 4838–4848.
46. Ghosh, S., Zheng, Y., Jun, X., Mahajan, S., Mao, C., Sudbeck, E. A., et al. (1999) Specificity of alpha-cyano-beta-hydroxy-beta-methyl-*N*-[4-trifluoromethoxy)phenyl]-propenamide as an inhibitor of the EGF-receptor tyrosine kinase. *Clin. Cancer Res.* **5,** 4264–4272.
47. Ghosh, S., Narla, R. K., Zheng, Y., Liu, X.-P., Jun, X., Mao, C., et al. (1999) Structure-based design of potent inhibitors of EGF-receptor tyrosine kinase as anti-cancer agents. *Anticancer Drug Des.* **14,** 403–410.
48. Sicheri, F., Moarefi, I., and Kuriyan, J. (1997) Crystal structure of the *Src* family tyrosine kinase Hck. *Nature* **385,** 602–609.
49. Mohammadi, M., Schlessinger, J., and Hubbard, S. R. (1996) Structure of the FGF receptor tyrosine kinase domain reveals a novel autoinhibitory mechanism. *Cell* **86,** 577–587.
50. Mohammadi, M., McMahon, G., Sun, L., Tang, C., Hirth, P., Yeh, B. K., et al. (1997) Structures of the tyrosine kinase domain of fibroblast growth factor receptor in complex with inhibitors. *Science* **276,** 955–960.
51. Hubbard, S. R., Wei, L., Ellis, L., and Hendrickson, W. A. (1994) Crystal structure of the tyrosine kinase domain of the human insulin receptor. *Nature* **372,** 746–754.
52. Xu, X., Williams, J. W., Gong, H., Finnegan, A., and Chong, A. S. (1996) Two activities of the immunosuppressive metabolite of leflunomide, A77 1726. Inhibition of pyrimidine nucleotide synthesis and protein tyrosine phosphorylation. *Biochem. Pharmacol.* **52,** 527–534.
53. Mattar, T., Kochhar, K., Bartlett, R., Bremer, E. G., and Finnegan, A. (1993) Inhibition of the epidermal growth factor receptor tyrosine kinase activity by leflunomide. *FEBS Lett.* **334,** 161–164.
54. Myers, D. E., Jun, X., Waddick, K. G., Forsyth, C., Chelstrom, L. M., Gunther, R. L., et al. (1995) Membrane-associated CDl9-LYN complex is an endogenous p53-independent and bcl-2 independent regulator of apoptosis in human B-lineage lymphoma cells. *Proc. Natl. Acad. Sci. USA* **92,** 9575–9579.

55. Hubbard, S. R. (1997) Crystal structure of the activated insulin receptor tyrosine kinase in complex with peptide substrate and ATP analog. *EMBO J* **16,** 5572–5581.
56. Zheng, J., Trafny, E. A., Knighton, D. R., Xuong, N.-H., Taylor, S. S., Ten Eyck, L. F., et al. (1993) 2.2Å refined crystal structure of the catalytic subunit of cAMP-dependent protein kinase complexed with MnATP and a peptide inhibitor. *Acta Cryst.* **D49,** 362–365.
57. Narla, R. K., Liu, X.-P., Myers, D. E., and Uckun, F. M. (1998) 4-(3'-Bromo-4' hydroxylphenyl)-amino-6,7-dimethoxyquinazoline: A novel quinazoline derivative with potent cytotoxic activity against human glioblastoma cells. *Clin. Cancer Res.* **4,** 1405–1414.
58. Kuo, E. A., Hambleton, P. T., Kay, D. P., Evans, P. L., Matharu, S. S., Little, E., et al. (1996) Synthesis, structure-activity relationships, and pharmacokinetic properties of dihydroorotate dehydrogenase inhibitors: 2-Cyano-3-cyclopropyl-3-hydroxy-N-[3'-methyl-4'-(trifluoromethyl)phenyl] propenamide and related compounds. *J. Med. Chem.* **39,** 4608–4621.
59. Sjogren, E. R., Rider, M. A., Nelson, P. H., Bingham, S., Poulton, A. L., Emanuel, M. A., et al. (1991) Synthesis and biological activity of a series of diaryl-substituted alpha-cyano-beta-hydroxypropenamides, a new class of anthelmintic agents. *J. Med. Chem.* **34,** 3295–3301.
60. Nomoto, F., Obase, H., Takai, H., Hirata, T., Teranishi, M., Nakamura, J., et al. (1990) Studies on cardiotic agents. I. Synthesis of quinazoline derivatives. *Chem. Pharm. Bull.* **38,** 1591–1595.
61. Thomas, C. L. (1970) *Catalytic Processes and Proven Catalysts,* Academic Press, New York, NY, pp. 1–27.
62. Feng, R., Konishi, Y., and Bell, A. W. (1991) High accuracy molecular weight determination and variation, characterization of proteins up to 80 KU by ion spray mass spectrometry. *J. Am. Soc. Mass Spectrom.* **2,** 387–401.
63. Covey, T. R., Bonner, R. S., Shushan, B. I., and Henion, J. D. (1988) Determination of protein oligonucleotides and peptides molecular weights by ion spray mass spectrometry. *Rapid Comm. Mass Spectrom.* **2,** 249–256.
64. Uckun, F. M., Myers, D. E., Fauci, A. S., and Ambrus, J. L. (1989) Leukemic B-cell precursors constitutively express functional receptors for human interleukin-l. *Blood* **74,** 761–766.
65. Uckun, F. M., Burkhardt, A. L., Jarvis, L., Jun, X., Stealey, B., Dibirdik, I., et al. (1993) Signal transduction through the CDl9 receptor during discrete developmental stages of human B-cell ontogeny. *J. Biol. Chem.* **268,** 21,172–21,184.
66. Uckun, F. M., Waddick, K. G., Mahajan, S., Jun, X., Takata, M., Bolen, J., et al. (1996) Bruton's tyrosine kinase as a mediator of radiation-induced apoptosis in B-lineage lymphoid cells. *Science* **22,** 1096–1100.
67. Waurzyniak, B., Schneider, E. A., Tumer, N., Yanishevski, Y., Gunther, R., Chelstrom, L. M., et al. (1997) In vivo toxicity, pharmacokinetics, and antileuke-

mic activity of TXU (Anti-CD7)-pokeweed antiviral protein immunotoxin. *Clin. Cancer Res.* **3,** 881–890.
68. Gerlowski, L. E. and Jain, R. K. (1983) Physiologically based pharmacokinetic modelling: Principles and applications. *J. Pharm. Sci.* **72,** 1103–1126.
69. Connolly, M. L. (1983) Solvent-accessible surfaces of proteins and nucleic acids. *Science* **221,** 709–713.
70. Bohm, H. J. (1994) The development of a simple empirical scoring function to estimate the binding constant for a protein-ligand complex of known three-dimensional structure. *J. Comput. Aided Mol. Des.* **8,** 243–256.
71. Palmer, B. D., Fry, D. W., Nelson, J. M., Showalter, H. D., and Denny, W. A. (1997) Soluble analogs of pyrrolo- and pyrazoloquinazolines as epidermal growth factor receptor inhibitors: Synthesis, biological evaluation and modeling of the mode of binding. *J. Med. Chem.* **40,** 1519–1529.
72. Kim, D. C., Sugiyama, Y., Satoh, H., Fuwa, T., Iga, T., and Hanano, M. (1988) Kinetic analysis of in vivo receptor dependent binding of human epidermal growth factor by rat tissues. *J. Pharm. Sci.* **77,** 200–207.
73. Kim, D. C., Sugiyama, Y., Fuwa, T., Sakamoto, S., Iga, T., and Hanano, M. (1989) Kinetic analysis of the elimination process of human epidermal growth factor (hEGF) in rats. *Biochem. Pharmacol.* **38,** 241–249.

14

Targeting Tumor Vasculature Using VEGF-Toxin Conjugates

S. Ramakrishnan, Robert Wild, and Dana Nojima

1. Introduction

Tumor growth beyond a size of 1–2 mm^3 requires new blood supply to sustain the nutritional and oxygen demands of the proliferating cancer cells ***(1)***. Tumor neovascularization is a complex process involving endothelial cell proliferation, matrix degradation, endothelial cell migration and tube formation. Vascular endothelial growth factor (VEGF), also known as vascular permeability factor (VPF), is an important angiogenic mediator secreted by tumor cells ***(2)***. VEGF binds to receptor tyrosine kinases flt-1 and KDR/flk-1, which are expressed primarily on endothelial cells. Receptor expression is increased under hypoxia, and recent studies suggest that VEGF itself can upregulate their levels on endothelial cells. *In situ* hybridization and immunocytochemical analyses have identified that VEGF receptors are overexpressed on the endothelial cells of intratumoral and peritumoral blood vessels. In contrast, blood vessels in the adjoining normal tissues showed almost undetectable levels of VEGF receptors ***(2)***. These results suggest that VEGF can be used to target toxin polypeptides to tumor vascular endothelium to inhibit angiogenesis.

In this chapter, we will focus on VEGF-DT385 toxin conjugates prepared by chemical means, and we will describe methods to evaluate their biologic activity. Furthermore, a protocol is described to prepare VEGF–toxin fusion proteins.

1.1. Vascular Endothelial Growth Factor

VEGF is a homodimeric glycoprotein with multiple biologic functions relevant to tumor angiogenesis ***(2)***. At least four different types of VEGF have been identified, VEGF-A, -B, -C, and -D. VEGF-A and -B bind to the same receptor

From: *Methods in Molecular Biology, vol. 166: Immunotoxin Methods and Protocols*
Edited by: W. A. Hall © Humana Press Inc., Totowa, NJ

tyrosine kinases and play important roles in vasculogenesis; VEGF-C has been implicated in lymphatic development and binds to the flt-4 receptor tyrosine kinase. VEGF-D is not yet fully characterized but may be of special relevance for the vascularization of lung tissue during the last trimester of fetal development.

VEGF belongs to the cystine-knot family of proteins, with closest resemblance to platelet-derived growth factor (PDGF). There are six intrachain disulfide bonds and two interchain disulfide bonds, which keep the monomers linked together in an antiparallel configuration. There is a single glycosylation site in each subunit that does not play a critical role in its biologic activity. An N-terminal fragment of VEGF (residues 8–109) has been expressed in bacteria and analyzed by X-ray crystallography at the 1.93-Å level. Together with site-directed mutagenesis studies, two regions (or hot-spots) have been identified that are necessary for receptor binding. VEGF-A exists as five isoforms composed of either 206, 189, 165, 145, or 121 amino acids (**Fig. 1**). They are produced by means of alternative splicing. Although they are of different lengths, the biologic activities of these isoforms appear to be similar.

VEGF-A binds to flt-1 at a higher affinity (*K*d 50 n*M*) when compared to flk-1 (*K*d 250 n*M*). Flt-1 and flk-1 are receptor tyrosine kinases containing seven Ig-like domains. The ligand-binding domain has been mapped to the second and third Ig-like loops, which are necessary for high-affinity interaction with VEGF. However, the second domain alone can interact to the ligand, albeit with a 60-fold lower affinity.

1.2. Toxin Molecules

A number of toxin moieties have been used to prepare cytotoxic conjugates. In general, they fall into two groups: bacterial toxins, and plant-derived toxins, which include some of the toxin proteins secreted by fungi. Among the bacterial toxins, *Pseudomonas* exotoxin E (PE) and diphtheria toxin (DT) have been extensively studied for tumor-cell targeting. Both of these toxins are ADP-ribosylating enzymes and inactivate elongation factor (EF) 2 and thereby inhibit translation. Plant-derived toxins such as ricin are dual-chain toxins containing a catalytically active chain and a binding chain that targets the enzymatically active portion into cells. To prevent nonspecific toxicity, the binding domain of ricin is genetically deleted when used for preparing toxin conjugates. In addition to the dual-chain toxins, plants also produce single-chain ribosome inactivating proteins (RIP) that lack the cell-binding moiety and are functionally equal to the enzymatic subunit of ricin A-chain. Pokeweed antiviral protein is a good example of an RIP. Another type of toxin is produced by aspergillus that also inactivates ribosomes. Included in this class of toxins are α-sarcin, mitogillin, and restrictocin. Fungal RIPs are small (17 kDa) proteins that cleave a single phosphodiester bond on the 3' side of G4325 in eukaryotic

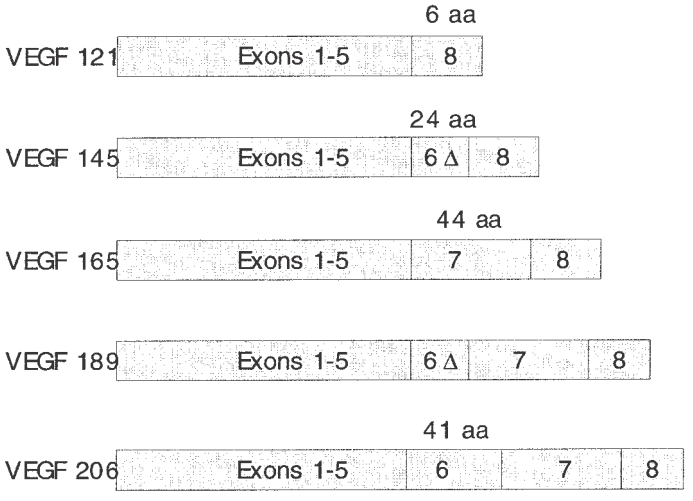

Fig. 1. Splice variants of VEGF-A.

28S rRNA. In contrast, plant toxins such as ricin A-chain cleave the *N*-glycosidic bond of A4324 of 28S rRNA. The cleavage site is embedded in a purine-rich single-stranded loop of 14 nucleotides called the sarcin/ricin loop, which is one of the most strongly conserved regions of the rRNA. Cleaved 28S rRNA is unable to participate in EF-1 dependent binding of aminoacyl tRNA and EF-2 catalyzed GTP hydrolysis and translocation during protein synthesis, leading to cell death ***(3)***. Although any one of these proteins can be selected for vascular targeting, we will describe here the use of a truncated DT (DT385) in preparing endothelial-specific cytotoxic conjugates.

1.3. Diphtheria Toxin

Diphtheria toxin is produced as a single chain and is nicked at a protease-sensitive site rich in arginine residues (**Fig. 2**). Detailed structure/function studies have been reviewed ***(4)***. The N-terminal 193 residues constitute the catalytic domain of DT (A-chain), which is disulfide linked to the B-chain. The B-chain consists of a translocation domain and a receptor-binding domain. The translocation domain contains four hydrophobic regions that are important for the transport of the catalytic domain into the cytoplasm. The receptor-binding domain is located at the C-terminus of DT. This region binds to an EGF-like molecule present on mammalian cells. CRM-107 is a mutant of DT that is not toxic to cells due to a point mutation in the receptor-binding domain. However, the catalytic and translocation domains are intact and functional. This mutant

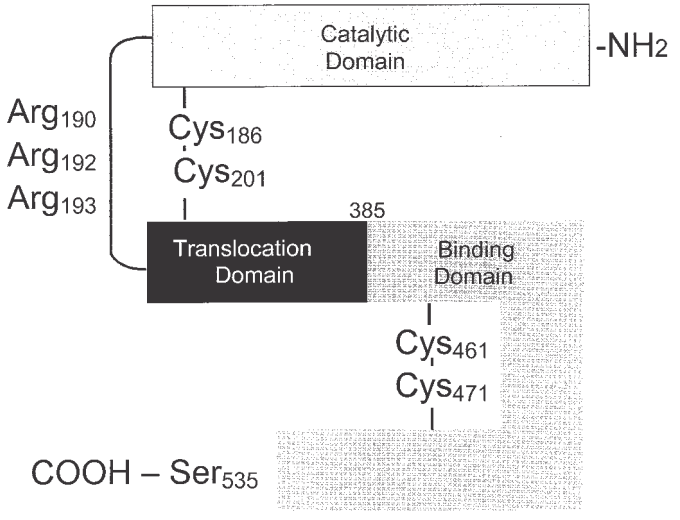

Fig. 2. Schematic diagram of full-length diphtheria toxin.

was the starting material for genetically engineering a toxin molecule suitable for VEGF targeting. DT (CRM-107) was truncated by site-directed mutagenesis to produce a 1–385 residue fragment of DT (DT385). This construct still contains the entire catalytic and translocation domains. Subsequently, a cysteine residue was introduced at the carboxy terminus to facilitate disulfide linkage to VEGF. The cysteine-modified DT385 (DT385cys+) was expressed in a His.Tag vector (pET17His) so that the engineered protein can be purified by affinity chromatography using a nickel column (Ni-NTA).

2. Materials

2.1. Chemical Derivatization and Conjugation of VEGF-Toxin Conjugates

1. Ni-NTA purified DT385cys+ toxin and heparin affinity-column–purified VEGF.
2. Dimethylsulfoxide (DMSO; Sigma, St. Louis, MO).
3. SPDP (Pierce Chemicals, Rockford, IL), 20-m*M* stock solution prepared in DMSO just before use.
4. Phosphate buffered saline (PBS): 20 m*M* phosphate buffer, 150 m*M* NaCl, 1 m*M* EDTA, pH 7.8.
5. Desalting columns such as G-25 sephadex (Sigma, St. Louis, MO).
6. Ultrafree concentrators (10,000 mol wt cutoff; Millipore, Bedford, MA).
7. Phenylmethylsulfonylfluoride (PMSF; Sigma).
8. Dithiothreitol (DTT; Sigma).
9. 2-iminothiolane (Traut's reagent; Pierce Chemicals).

2.2. Purification of VEGF-DT385 Conjugates

1. Ni-NTA affinity column (Qiagen, Valencia, CA).
2. Equilibration buffer: 50 m*M* sodium phosphate buffer, 300 m*M* NaCl, pH 7.8.
3. Imidazole (Sigma).
4. Ultrafree concentrators (10,000 and 50,000 mol wt cutoff; Millipore, Bedford, MA).
5. Superdex 75 gel filtration column, (Amersham Pharmacia Biotech, Piscataway, NJ).
6. PBS.
7. DTT (Sigma).
8. Antibodies to VEGF and DT385 for optional Western blot analysis (polyclonal IgG raised in rabbits are usually sufficient).

2.3. Endothelial Cell Proliferation Assays (Radioactive or Nonradioactive)

1. HUVEC (Clonetics, San Diego, CA).
2. Endothelial cell growth medium (EGM; Clonetics).
3. 96-Well, flat-bottom tissue culture-grade plate (Fisher Scientific, Pittsburgh, PA).
4. Gelatin (Sigma), dissolved at 0.2% in PBS, pH 7.8, and filter sterilized (0.2 μm).
5. [^{3}H]-Thymidine (for radioactive assay; Amersham, Arlington Heights, IL) or
6. MTT (3-[4,5-dimethylthiazol-2-yl]-2,5-diphenyltetrazolium bromide; Sigma). Dissolved at a concentration of 2.5 mg/mL in PBS, pH 7.8 (for nonradioactive method).
7. Hanks' balanced salt solution (HBSS) with Ca^{2+} and Mg^{2+} (Life Technologies, Grand Island, NY).
8. Sodium hydroxide (NaOH; Sigma).
9. DMSO (Dimethylsulfoxide; Sigma).

2.4. Chick Chorioallantoic Membrane Assay (CAM)

1. MDA-MB 435, LS174T, or other tumor cell line (ATCC, Rockville, MD).
2. RPMI 1640 medium (Life Technologies).
3. Gelfoam gelatin powder (Upjohn, Kalamazoo, MI).
4. Thermanox plastic coverslips, 13 mm diameter (Nunc, Naperville, IL).
5. Three-day old fertilized eggs (white leghorn; Spafas Inc., Preston, CT).
6. Tissue culture dish, 100 × 20 mm (Sarstedt, Newton, NC).
7. Camera (digital camera preferred for subsequent image analysis).
8. NIH Image, software (optional; available as freeware from NIH, Bethesda, MD).

2.5. Matrigel Assay (Mouse)

1. MDA-MB 435, LS174T or other tumor cell line (ATCC).
2. RPMI 1640 medium (Life Technologies).
3. Basement membrane matrix (ECM gel; Sigma).
4. Athymic nude mice (nu/nu), female, 8–10-wk old (Harlan Sprague Dawley, Indianapolis, IN).

5. 10% Neutral buffered formalin solution (Sigma).
6. Rabbit antimouse endothelial specific antibodies to von Willebrandt's factor (factor VIII) or CD-31 (PECAM-1; Pharmingen, San Diego, CA).
7. Antirabbit IgG peroxidase ABC kit (Vectastain, Burlingame, CA).
8. Hematoxylin (Sigma).

2.6. Expression of VEGF Fusion Proteins

1. LB-broth (1 L).
   10 g Bacto-tryptone (Difco, Detroit, MI).
   5 g Bacto-yeast extract (Difco).
   10 g NaCl (Sigma).
2. Ampicillin (Sigma).
3. IPTG (Boehringer Mannheim, GmbH, Germany).

2.7. Purification of VEGF Fusion Proteins

1. Buffers:
   A 6 *M* guanidine HCl, 0.1 *M* NaH_2PO_4, 0.01 *M* Tris-HCl (pH 8.0).
   B 8 *M* urea, 0.1 *M* NaH_2PO_4, 0.01 *M* Tris-HCl (pH 8.0).
   C 8 *M* urea, 0.1 *M* NaH_2PO_4, 0.01 *M* Tris-HCl (pH 6.3).
2. Ni-NTA resin (Qiagen).
3. Imidazole (Sigma).

2.8. Refolding of VEGF Fusion Proteins

1. Denaturing solution: 0.1 *M* Tris-HCl (pH 8), 6 *M* guanidine HCl , 2 m*M* EDTA, 0.3 *M* DTT.
2. Refolding solution: Tris-HCl (pH 8), 0.5 *M* L-arginine, 8 m*M* glutathione (oxidized, GSSG), 2 m*M* EDTA.
3. Dialysis buffer 1: 20 m*M* Tris-HCl, 100 m*M* urea, pH 7.4.
4. Dialysis buffer 2: 10 m*M* Tris-HCl (pH 7.4), 200 m*M* NaCl (all chemicals from Sigma).
5. Superdex 75 gel filtration column, (Amersham Pharmacia Biotech).
6. Complete protease inhibitor (Boehringer Mannheim, GmbH, Germany).

3. Methods

3.1. Chemical Derivatization and Conjugation of VEGF-Toxin Conjugates

A large number of protein crosslinkers have been developed that allow the chemical conjugation of proteins containing primary amines to secondary moieties with free sulfhydryl groups. These crosslinkers come in various configurations. Diverse spacer arm lengths allow proper conjugation reactions and circumvent problems associated with steric hindrance. In addition, certain crosslinkers are designed to form very stable, non-cleavable bonds, resulting

in increased in vivo stability. In short, there are numerous agents available to suit individual needs.

One of the most widely used crosslinkers is SPDP (*N*-succinimidyl 3-(2-pyridyldithio) propionate), a heterobifunctional, cleavable crosslinker. SPDP has been shown to be very effective in the preparation of immunotoxins ***(5)*** as well as growth factor–toxin conjugates ***(6,7)***. SPDP contains one *N*-hydroxysuccinimide (NHS) residue and one pyridyl disulfide residue. The 2-pyridyldisulfide moiety reacts with aliphatic thiols or free sulfhydryl groups to form disulfide bonds, whereas the NHS-ester group reacts with primary amines. As a consequence, SPDP crosslinkers can be used to conjugate amine-containing proteins with free sulfhydryl-containing proteins. In the case of preparing VEGF–DT385 conjugates, the amine-containing protein (VEGF) is first derivatized to the SPDP compound via the NHS-ester group. Next, the free sulfhydryl-containing protein (DT385cys+) is added to the 2-pyridyl disulfide–activated VEGF. In turn, a sulfhydryl exchange occurs between the two proteins, crosslinking the components together. VEGF was cloned and expressed in yeast and is readily purified from the culture medium with a heparin affinity column ***(8)***. The Diphtheria Toxin construct (DT385cys+) was genetically engineered to contain a free cysteine residue at its C-terminal end, which facilitates a more controlled linking of the two proteins. DT385cys+ was cloned into a bacterial expression vector containing a Histidine tag and therefore is easily purified via a Nickel-NTA (Ni-NTA) affinity column.

3.2. Conjugation of VEGF to DT385cys+

1. Add 5 *M* excess of freshly prepared SPDP stock solution (SPDP is dissolved in DMSO at approx 20 mg/mL) to 10 mg of VEGF in 1.0 mL of PBS (*see* **Note 1**).
2. Incubate for 30–60 min at room temperature, mixing contents gently every 10 min.
3. To remove unconjugated crosslinker, desalt the derivatized VEGF over a G-25 sephadex gel filtration column preequilibrated with PBS. Collect 1 mL fractions and pool protein peaks as determined by spectrophotometric absorbancy readings at 280 nm wavelength (*see* **Note 2**).
4. Add 10 mg of purified DT385cys+ to the derivatized VEGF and concentrate the mixture by ultrafiltration using a 10,000 mol wt cutoff membrane. Maintain the pH of the sample at 7.8 to facilitate disulfide bond formation (*see* **Note 3**).
5. Dialyze the conjugation mixture overnight at 4°C against PBS containing 0.5 m*M* PMSF.
6. Analyze an aliquot of the conjugate by 7.5% SDS-PAGE (nonreducing conditions) to determine efficiency of crosslinking. Unconjugated VEGF will migrate at an estimated molecular weight of 40 kDa, free DT385cys+ will run at approx 43 kDa, and VEGF–DT conjugates will appear as multiple bands of approx 83, 126, and 169 kDa.

3.3. Purification of VEGF-DT385 Conjugates

The chemical conjugates of VEGF–DT385 are purified using an Ni-NTA affinity column followed by size-separation chromatography. Both free DT385 toxin (unconjugated) and VEGF–DT385 conjugate bind tightly to the nickel column via the His.Tag region in the N-terminus of the toxin polypeptide and therefore elute at higher imidazole concentrations (100–150 m*M* imidazole). On the other hand, free VEGF has only a low affinity to the Ni-NTA resin. Consequently, this component can be efficiently removed during washing steps at low imidazole concentrations (10–50 m*M*). Finally, free DT385 toxin is separated from the conjugate by further purification over a size-separation column (Superdex 75).

1. Load crude conjugate onto an Ni-NTA column pre-equilibrated with equilibration buffer.
2. Wash the column with equilibration buffer until all nonspecific components are removed.
3. Elute low-affinity proteins from the Ni-NTA column using equilibration buffer containing 50 m*M* imidazole. This wash will remove free, unconjugated VEGF, which binds only very lightly to the affinity column. Monitor the elution by absorbance at 280 nm.
4. Elute high affinity components such as free DT385cys+ and VEGF-DT385 conjugate by using equilibration buffer containing 100–150 m*M* imidazole.
5. Pool peak fractions and concentrate mixture by ultrafiltration using a 10,000 molecular weight cutoff membrane to a volume suitable for subsequent gel filtration purification (typically 1–2 mL).
6. Isolate VEGF-DT385 conjugate from free, unconjugated toxin polypeptide by size-exclusion chromatography using a Superdex 75 column preequilibrated with PBS. The conjugate is eluted in the void volume and can be separated from free DT385cys+ because of its increased retention time (*see* **Note 4**).
7. Purified VEGF–DT385 fractions are then pooled and concentrated by ultrafiltration to approx 1–2 mg/mL (Ultrafree concentrators, 50,000 mol wt cutoff) and aliquoted for storage at –70°C.
8. Purity and identity of the chemical conjugate is assessed by 10% SDS-PAGE under both nonreducing and reducing (10 m*M* DTT) conditions. Treatment of the sample with DTT should give rise to free VEGF and DT385 monomers with estimated molecular weights of 20 and 43 kDa respectively (*see* **Note 5**).

3.4. Evaluation of the Biological Activity of VEGF-Toxin Conjugates with Endothelial Cell Proliferation Assays (Radioactive or Nonradioactive)

Several assay systems have been designed to assess the antiproliferative and antiangiogenic effects of VEGF–toxin conjugates. These tests can be applied to other agents intended to inhibit endothelial cell growth and angiogenesis.

In order to assess the cytotoxic ability of the VEGF–DT385 toxin conjugate on endothelial cells, a human umbilical-vein endothelial cell (HUVEC) proliferation assay is performed.

1. Seed 10,000 HUVEC in a volume of 180 μL EGM per well in a 96-well, flat-bottom, gelatin-coated plate.
2. Incubate overnight in a tissue culture incubator to allow cells to attach.
3. Dilute filter-sterilized (0.2 μm) VEGF–toxin conjugate in EGM and add samples in a volume of 20 μL to triplicate cultures.
4. Incubate for 48–72 h in a tissue culture incubator.
5. In order to determine the proliferative status of the endothelial cells, either pulse the cells with 1 μCi of [^{3}H]-thymidine per well for 18 h, or add 20 μL of MTT (2.5 mg/mL in PBS) per well for 3–4 h.
6. In case of the radioactive assay, wash cells twice with HBSS and lyse the cells with 100 μL of 1.5 *M* NaOH. Harvest the cell lysate and determine the radioactivity by scintillation counting.
7. In case of the nonradioactive assay, remove the medium and dissolve the Formosan crystals in 100 μL DMSO. Read the plate at 560 nm wavelength.
8. Calculate the inhibitory activity of the conjugate with the following formula:

$$\% \text{ Viability} = \frac{\text{mean radioactivity (or } A_{560}\text{) in experimental wells}}{\text{mean radioactivity (or } A_{560}\text{) in control wells}} \times 100$$

3.5. Inhibition of Tumor Cell-Induced Angiogenesis In Vivo

The objective of these experiments is to test for the ability of the toxin conjugate to inhibit angiogenesis in vivo. Two independent assay systems are shown here to test this hypothesis, the chick chorioallantoic membrane (CAM) assay, and a nude mouse matrigel assay. Both assay systems have been proven to be reliable test systems for in vivo angiogenesis experiments and utilize cancer cells as the angiogenic stimulus. Therefore, they are excellent tools to study the process of tumor cell-induced angiogenesis.

3.5.1. Chick Chorioallantoic Membrane Assay

1. Trypsinize confluent cultures of tumor cells and wash cells twice with serum-free RPMI 1640 medium (*see* **Note 6**).
2. Pellet cells by centrifugation and resuspend them at 2×10^7 cells/mL in serum-free medium containing 150 mg/mL Gelfoam in the absence or presence of VEGF-DT385.
3. Load 50 μL of the mixture onto sterile plastic coverslips and permit the sample to polymerize for 15–30 min in the tissue culture incubator.
4. Apply the discs to the CAMs of 10-d-old embryos in an area of relatively low blood vessel density (*see* **Note 7**).

5. After 72 h of incubation in a tissue culture incubator, observe and photograph the area of the CAM in which the test samples were applied. The process of angiogenesis will be assessed as the number of visible blood vessel branch points within the defined area of the coverslip, as well as the overall blood vessel density (*see* **Note 8**).

3.5.2. Matrigel Assay (Mouse)

1. Trypsinize confluent cultures of tumor cells (various cell lines are suitable, *see* **Subheading 2.4.**) and wash cells twice with serum-free RPMI 1640 medium.
2. Pellet cells by centrifugation and resuspend them at 2×10^7 cells/mL in a 10 mg/mL ECM gel solution.
3. Inject 500 μL of the mixture subcutaneously into the right flank of 10-wk-old female athymic nude mice and allow the sample to polymerize for 1–2 h (*see* **Note 9**).
4. Treat the animals for a 6 d period with VEGF-DT conjugate by daily intraperitoneal injections (20 μg in 0.1 mL/mouse/d).
5. Sacrifice animals on d 7 and remove matrigel plugs surgically.
6. Observe matrigels macroscopically for invasion of blood vessels into the matrix.
7. Fix matrigel plugs in 10% formalin and prepare paraffin-embedded tissue sections.
8. Immunohistochemical analysis of matrigel sections can be carried out by using antimouse-specific primary antibodies to endothelial cell markers such as von Willebrandt's factor (factor VIII) or CD-31 (PECAM-1). A secondary antibody–peroxidase conjugate can be used to develop areas of invading blood vessels, that can be identified after counterstaining the slides with hematoxylin (*see* **Note 10**).
9. Analyze the angiogenic response in your samples by counting the number of blood vessels per microscopic field (10–20× magnification). Express vascularity as the number of blood vessels per unit area.

3.6. Fusion Proteins

We described earlier the chemical linking of VEGF and truncated DT to produce a conjugate that was cytotoxic in vitro against HUVEC and inhibited tumor angiogenesis. However, chemical conjugates have some limitations, including:

1. The exact location and degree of derivatization cannot be controlled leading to a heterogeneous population of molecules;
2. Steric hindrance of the ligand and receptor can occur because of the random linking of the toxin to the ligand;
3. Large amounts of both proteins must be produced and purified before conjugation because of a low overall yield; and
4. Inherent batch-to-batch variability in conjugate preparation.

An alternative to chemical conjugation is the expression of both proteins as a single fusion protein. Fusion proteins composed of both the targeting and

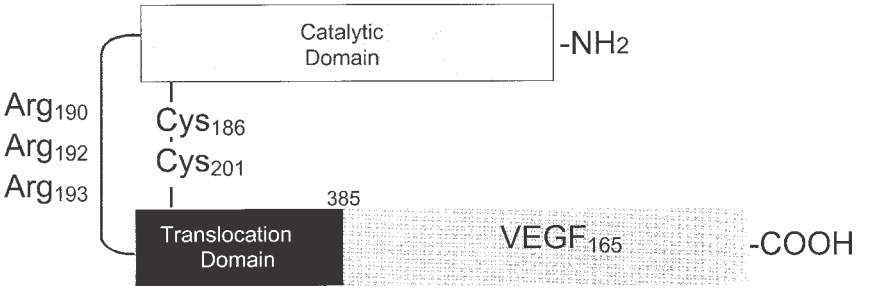

Fig. 3. DT_{385}–VEGF fusion protein.

toxin protein poses several advantages over constructs produced by chemical conjugation. Because fusion proteins are expressed as a single chain, the protein is homogeneous, with both the cell-binding region and toxin having a defined structure and stoichiometry. If the fusion of the toxin is engineered in a location that does not hinder ligand binding, the fusion protein is generally of higher affinity when compared to chemical conjugates. Finally, production is simplified, which significantly lowers the overall cost.

Fusion toxin constructs have extensively utilized bacterial toxins such as PE and DT. The method of cell entry and cellular intoxication for these toxins are well understood ***(4)***. In order to mimic the inate structure of these toxin molecules, it is suggested to replace the region of the native receptor-binding domain with the ligand of choice (i.e., VEGF). For instance, in the case of DT, the substitution is preferably carried out at the C-terminus. This provides a free N-terminal catalytic domain, which optimizes its cytotoxic activity (**Fig. 3**). To support this hypothesis, we have engineered constructs in both orientations (DT–VEGF and VEGF–DT) and have found that the DT–VEGF construct had superior biological activity.

3.7. Expression of VEGF Fusion Proteins

Currently, there exist a wide variety of commercially available recombinant protein expression systems for the production of proteins in bacteria, yeast, insect cells, and mammalian cells. The selection of the expression system is dependent on the nature of both the toxin and the ligand. Several systems have been developed to allow rapid and efficient purification of recombinant proteins in bacteria. We have used a modified pET17b and a pGEX vector for the expression of VEGF fusion proteins. The modified pET17bHis construct incorporates a poly-histidine tag at the N-terminus of the expressed protein. This modification allows for easy purification of the expressed protein. The poly-histidine tag does not interfere with the binding or toxicity of the expressed

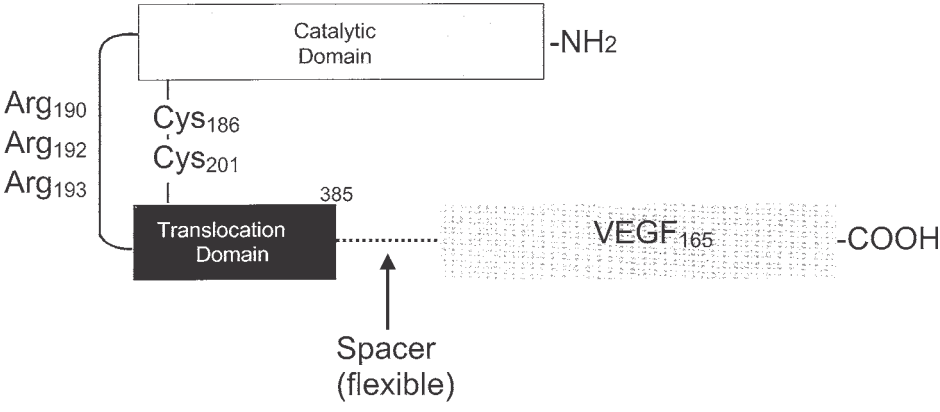

Fig. 4. Fusion protein with flexible linker (spacer).

proteins. The pGEX-GST proteins allow for the purification using a glutathione affinity column and easy cleavage of the GST molecule by thrombin. We and others ***(9)*** have utilized this construct for the expression and purification of DT-VEGF under native conditions by our group and others ***(9)***.

The expression of fusion proteins in bacteria often leads to the formation of inclusion bodies. Several methods that have been successful in increasing cytosolic expression of fusion proteins include:

1. Lowering the growth temperature during induction;
2. Changing the concentration of inducer from 1 m*M* to 0.1 m*M* isopropyl β-D-thiogalactopyranoside (IPTG) and increasing the period of induction from several hours to overnight;
3. Shortening the period of induction; and
4. Altering the timing of induction.

The exact conditions must be determined empirically for each fusion protein.

Bacterially expressed DT–$VEGF_{165}$ was almost exclusively found in inclusion bodies. Therefore, a denaturing/refolding protocol ***(10)*** was employed for the preparation of DT–$VEGF_{165}$.

1. Inoculate LB broth containing 100 μg/mL ampicillin with a single colony containing the expression plasmid. Grow overnight at 37°C with vigorous shaking.
2. Inoculate a large culture (LB broth, 100 μg/mL ampicillin) at a 1:50 dilution of the overnight culture.
3. Grow to an absorbance of 0.7–0.9 at 600 nm and then induce with 1.0 m*M* IPTG.

4. After 4 h of induction collect bacterial cells by centrifugation at 4000*g* for 10 min at 4°C.
5. Freeze pellets at –70°C.

3.8. Purification of VEGF Fusion Proteins

1. Thaw the cell pellet for 15 min and resuspend in buffer A at 5 mL/g wet weight.
2. Stir the cells for 15 min at room temperature.
3. Centrifuge the cell lysate at 10,000*g* for 30 min at room temperature and collect supernatant.
4. For every 4 mL of supernatant, add 0.5 mL of Ni-NTA resin that has been preequilibrated with buffer A.
5. Mix gently by rotating overnight at 4°C (*see* **Note 11**).
6. Load the resin into a column and wash with 10 column volumes of buffer A followed by 5 column volumes of buffer B.
7. Wash with buffer C until OD_{280} is <0.01 (*see* **Note 12**).
8. Elute with a gradient of imidazole from 25 m*M* to 250 m*M* prepared in buffer C. Follow elution of the protein peaks by monitoring absorbance at 280 nm (*see* **Note 13**).
9. If multiple peaks are eluted, verify the peak containing the fusion protein by SDS-PAGE analysis (*see* **Note 14**).

3.9. Refolding of VEGF Fusion Proteins

1. After isolation of the denatured protein, adjust the fusion protein to a concentration of 3 mg/mL in denaturing solution.
2. Incubate in denaturing solution for 2 h at room temperature.
3. Dilute denatured protein 1:100 into refolding buffer (10°C) with a final concentration of 30 µg/mL.
4. Concentrate (10-fold) by ultrafiltration, and dialyze overnight at 4°C against dialysis buffer 1.
5. Change to dialysis buffer 2 with two exchanges (1:100 ratio of sample to buffer).
6. Apply concentrated sample to a Superdex 75 gel filtration column (*see* **Note 15**).

A small amount of proteolytic cleavage (protease-sensitive loop) occurs during purification of DT fusion proteins. This will generate approx 20 kDa and approx 40 kDa fragments. Gel filtration is able to separate these fragments from the approx 60 kDa uncleaved protein. One can minimize proteolytic damage by adding protease inhibitors.

3.10. Biological Activity of VEGF Fusion Proteins

After purification, the biologic activity (toxin activity) of the fusion protein is analyzed in an in vitro translation assay (rabbit reticulocyte lysate kit; Promega, Madison, WI). Typically 50% inhibition of protein synthesis is observed at 0.1 n*M*. Receptor-mediated cytotoxicity of the fusion protein is determined by HUVEC cytotoxicity assay. Some of the controls necessary in this assay are

free DT, VEGF receptor-negative cell lines, and neutralization of the VEGF fusion protein with either anti-VEGF or anti-DT antibodies.

3.11. Monomers and Dimers of VEGF Fusion Proteins

We have found that the refolded DT–VEGF does not form dimers as determined by SDS-PAGE analysis. It has been observed that VEGF has a higher affinity to the VEGF receptor when the protein is expressed in its dimeric form ***(11)***.

3.12. Circularly Permuted Fusion Proteins

The genetic fusion of toxin polypeptides to targeting moieties has the potential to drastically reduce the affinity of the ligand to the receptor. Normally, fusion proteins are created by attaching the toxin to either the amino or carboxy terminus of the ligand. However, this strategy will not work if both the termini are necessary for the ligand to interact with its receptor. Therefore, circularly permuted recombinant proteins were designed by Kreitman et al. ***(12)***. In this case, the amino and carboxy termini of interleukin-4 were fused with a short spacer. A break was introduced between the central region of the protein (circularly permuted), which created new termini for fusion with the toxin. As a result, the toxin is now relocated away from the receptor-binding site. This strategy produced highly active interleukin-4–PE fusion toxins.

3.13. Fusion Proteins Joined by Peptide Linkers

Another method to spatially separate the toxin away from the location of the receptor-binding domain of the ligand is to introduce a linker sequence. (**Fig. 4**) For example, the inclusion of a flexible linker $(Gly_4Ser)_4$ between the toxin and the ligand increased the affinity of a growth factor–saporin fusion protein ***(13)***.

4. Notes

1. The molecular weight of VEGF is roughly 40 kDa. Therefore, a 10 mg/mL VEGF solution is approx 250 μ*M*, and 5 *M* excess of SPDP would correspond to 1.25 m*M* of SPDP. The molecular weight of SPDP is 312. Consequently, 390 μg/mL of SPDP are necessary for a functional derivatization of VEGF.
2. The amount of SPDP crosslinked to VEGF can be estimated by treatment of the sample with DTT. The reducing ability of DTT results in the release of pyridine-2-thione groups from the SPDP-derivatized protein. The concentration of the released pyridine-2-thione can be determined by measuring the absorbance at 343 nm (molar extinction coefficient = $8.08 \times 10^3/M^{-1} \cdot cm^{-1}$). To do this, take an aliquot of freshly desalted SPDP–VEGF and record the A_{280} reading. Estimate the amount of VEGF present in the sample using the approximate molecular weight of the protein. Next, add 50 μL of 10 m*M* DTT to the sample and record the ΔA_{343}. Divide the recorded number by the extinction coefficient of the released pyridine-2-thione, which will give you an estimate of SPDP derivatiza-

tions. Knowing the amount of VEGF present in the reducing reaction, you can now determine the ratio of VEGF vs SPDP derivatizations.

3. Toxin constructs without a free sulfhydryl group (free cysteine group) need to be activated first with 2-iminothiolane (Traut's reagent), which introduces a sulfhydryl group by derivatizing free amino groups. This process will not alter the overall charge of the protein.
4. Alternatively, crude conjugate can be purified on a heparin affinity column followed by the Superdex 75 size-exclusion column. The heparin column will retain the conjugate and free VEGF, whereas unconjugated DT385 will be removed. Subsequent application of the heparin column retentate will separate the crosslinked VEGF–DT385 from free VEGF.
5. A Western blot analysis can be added to verify the identity of the conjugate samples. This assay will require the additional materials of suitable antibodies to the VEGF and DT385 polypeptides.
6. A human ovarian carcinoma cell line (MA148) isolated in our lab has been shown to be very effective in this assay system. However, many other tumor cell lines as indicated under **Subheading 2.** are also suitable inducers of angiogenesis.
7. The CAMs are prepared previously by cracking 3-d-old fertilized eggs under sterile conditions into tissue culture-grade Petri dishes. The CAMs/embryos are then subsequently stored in a tissue culture incubator until d 10 of development. It is not uncommon that some of the CAM preparations will die and have to be discarded before the VEGF–toxin samples can be applied. Therefore, it is recommended to prepare a large enough quantity of CAMs to account for the potential loss of some of the specimens.
8. If the images are digitally recorded, they can be easily processed and analyzed using NIH image analysis software (available as free shareware from NIH for Macintosh computers; Scion Image is a PC version available from Scion Corp., Frederick, MD).
9. Athymic nude mice allow the use of human tumor xenografts. In contrast, Balb/c or C57Bl6 immunocompetent mice (which are usually more economical) require the use of syngeneic tumor cells and therefore limit their application.
10. Some antibodies may not be suitable for paraffin-embedded samples and may require the preparation of frozen tissue sections. Please refer to the instructions of the manufacturer of your antibodies to verify this fact.
11. Batch loading increases the binding of the expressed protein to the resin.
12. Extensive washing will greatly reduce the level of contamination and increase purity.
13. The elution in 8 *M* urea allows for SDS-PAGE analysis of the protein peaks. Elution with guanidine HCl will interfere with SDS-PAGE analysis.
14. VEGF fusion toxins elute at approx 100–150 m*M* imidazole.
15. For a good separation, restrict the sample loading volume to 1–3% of column volume.

References

1. Folkman, J. (1992) The role of angiogenesis in tumor growth. *Semin. Cancer Biol.* **3,** 65–71.

2. Ferrara, N. and Davis-Smyth, T. (1997) The biology of vascular endothelial growth factor. *Endocr. Rev.* **18,** 4–25.
3. Kao, R. and Davies, J. (1995) Fungal ribotoxins: a family of naturally engineered targeted toxins? *Biochem. Cell. Biol.* **73,** 1151–1159.
4. Collier, R. J. (1988) Structure-activity relationships in diphtheria toxin and Pseudomonas aeruginosa exotoxin A. *Cancer Treat. Res.* **37,** 25–35.
5. Cumber, A. J., Forrester, J. A., Foxwell, B. M., Ross, W. C., and Thorpe, P. E. (1985) Preparation of antibody-toxin conjugates. *Methods Enzymol.* **112,** 207–250.
6. Olson, T. A., Mohanraj, D., Roy, S., and Ramakrishnan, S. (1997) Targeting the tumor vasculature: inhibition of tumor growth by a vascular endothelial growth factor-toxin conjugate. *Int. J. Cancer* **73,** 865–870.
7. Ramakrishnan, S., Olson, T. A., Bautch, V. L., and Mohanraj, D. (1996) Vascular endothelial growth factor-toxin conjugate specifically inhibits KDR/flk-1–positive endothelial cell proliferation in vitro and angiogenesis in vivo. *Cancer Res.* **56,** 1324–1330.
8. Mohanraj, D., Olson, T., and Ramakrishnan, S. (1995) Expression of biologically active human vascular endothelial growth factor in yeast. *Growth Factors* **12,** 17–27.
9. Arora, N., Masood, R., Zheng, T., Cai, J., Smith, D. L., and Gill, P. S. (1999) Vascular endothelial growth factor chimeric toxin is highly active against endothelial cells. *Cancer Res.* **59,** 183–188.
10. Buchner, J., Pastan, I., and Brinkmann, U. (1992) A method for increasing the yield of properly folded recombinant fusion proteins: single-chain immunotoxins from renaturation of bacterial inclusion bodies. *Anal. Biochem.* **205,** 263–270.
11. Potgens, A. J., Lubsen, N. H., van Altena, M. C., Vermeulen, R., Bakker, A., Schoenmakers, J. G., Ruiter, D. J., et al. (1994) Covalent dimerization of vascular permeability factor/vascular endothelial growth factor is essential for its biological activity. Evidence from Cys to Ser mutations. *J. Biol. Chem.* **269,** 32,879–32,885.
12. Kreitman, R. J., Puri, R. K., and Pastan, I. (1994) A circularly permuted recombinant interleukin 4 toxin with increased activity. *Proc. Natl. Acad. Sci. USA* **91,** 6889–6893.
13. Chandler, L. A., Sosnowski, B. A., McDonald, J. R., Price, J. E., Aukerman, S. L., Baird, A., et al. (1998) Targeting tumor cells via EGF receptors: selective toxicity of an HBEGF-toxin fusion protein. *Int. J. Cancer* **78,** 106–111.

15

Gene Therapy With Immunotoxins

Daniel A. Vallera

1. Introduction

1.1. Retroviral Immunotoxins

The purpose of this chapter is to describe the method of treating lymphokine-activated killer (LAK) cells with retroviral immunotoxins (retIT) so that these cells can express and secrete immunotoxins (IT). The intent is to use LAK as a vehicle to deliver IT therapy directly to leukemia cells in vivo. This would reduce their systemic toxicity and thus solve a major problem that has limited the use of IT clinically.

1.2. Cancer Immunotherapy

There are two major approaches that have been explored for cancer immunotherapy: humoral therapy and cellular therapy. Humoral therapy has been limited by the low levels of injected agent that ultimately reach target tissue *(1)*. Clinical studies indicate that <0.001% of injected high-avidity antibody reaches tumor *(2–4)* and studies with IT have the same limitation. Cellular immunotherapy mostly involves stimulating immune lymphocytes in vitro and then administering them to cancer patients. One approach has been to use LAK cells in which patient lymphocytes are activated and expanded by interleukin-2 (IL-2) treatment *(5)*. These studies show that LAK cells have limited efficacy, but if they were somehow rendered more effective, they might more efficiently destroy the cancer cells.

1.3. Immunotoxins

Immunotoxins are made of antibodies or cytokines attached to catalytic toxins, which are enzymes having the unique advantage of displaying Michelis-Menton

From: *Methods in Molecular Biology, vol. 166: Immunotoxin Methods and Protocols*
Edited by: W. A. Hall © Humana Press Inc., Totowa, NJ

single-hit kinetics ***(6)***. The toxins belong to a special class of agents in which only a minute amount will destroy a cell by interference with protein synthesis at the ribosomal level. Only a limited number of toxins have been cloned for recombinant studies, but the most widely used in molecular studies include diphtheria toxin (DT). Intact DT contains two fragments, A and B. The A fragment catalyzes the ADP ribosylation of elongation factor 2 (EF-2), leading to protein synthesis inhibition and cell death ***(7,8)***. Although a single molecule of DT-A in the cytosol can be fatal to a cell, fragment A alone applied extracellularly is not highly toxic because the binding domain is located in fragment B.

1.4. Disadvantages of Immunotoxins

Although ITs were hailed as a new class of anticancer agent in the early 1980s, they have not measured up to their full potential ***(9)***. Several cytokine fusion toxins have been tested in clinical trials, some with surprising anticancer efficacy. For example, in one study of T-cell malignancies, a recombinant fusion toxin consisting of IL-2 combined with truncated DT resulted in a response rate of 37%, including 14% complete responses ***(10)***. However, despite some bright spots, response rates generally have been low, and ITs limited by their toxicity and narrow therapeutic window. We and others have shown that the major disadvantage of ITs is their toxicity to nontarget organs, which has limited progress in the field of IT research. Many still believe that these agents can be harnessed to deliver a potent killing signal to cancer cells. We believe that toxicity could be minimized if a means could be found to give the cytokines a chance to operate the way they are intended to operate (i.e., locally), so that they could deliver therapy to sites of cancer cells.

1.5. A Potential Solution

A solution may arise by somehow combining cellular therapy with humoral therapy. It has long been known that lymphocytes, particularly T-cells, are the most prominent cell types that penetrate, attack, and destroy tumors ***(11)***. They proliferate rapidly in vitro and recirculate to tumor sites after reinfusion ***(12–16)***. If these T-cells could be modified to deliver a toxic signal, we could take advantage of their availability to localize at the site of cancer. One approach is to transduce *IT* genes into LAK cells (which include expanded T-cells) using retrovirus, and use these to deliver ITs directly to cancer cells.

Chen et al. assembled a retrovirus vector containing an *IT* gene, in which the IT ligand was an sFv directed against the oncoprotein HER2 overexpressed on breast cancer cells ***(17)***. The toxin moiety, PE40, was truncated *Pseudomonas* exotoxin. Human LAK cells derived from peripheral blood mononuclear cells were transduced with the virus and injected into nude mice bearing subcutaneous HER2+ tumor xenografts. Mice given transduced cells all lived, while mice

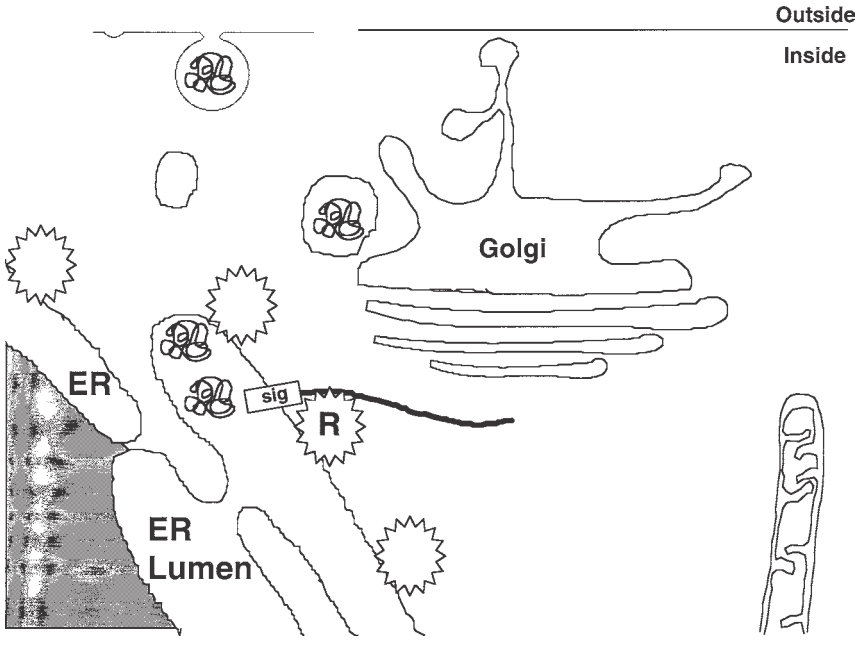

Fig. 1. Cotranslational protein transport. In cotranslational protein transport, IT is transported directly into the lumen of the endoplasmic reticulum (ER) without leakage into the cytosolic compartment. In the cytosol, the toxin would destroy the ribosome (*R*). This is an active process in which the signal sequence (*sig*) directs the IT through the ER membrane.

given mock-transduced or a comparable amount of systemic ITs died from the lethal effects of the tumor.

This is not the only case in which investigators have developed a retroviral immunotoxin. In a separate study, a retIT was assembled with the genes of the V_H and C_H domains of a MAb recognizing the CD4-binding site of HIV-1 gp120 and truncated PE. It was used to deliver the IT selectively to HIV-1 infected patient cells in vitro ***(18)***.

1.6. How Do RetIT Work?

How is this possible, since these toxins act in the cytosol and one would ordinarily expect that a mammalian cell expressing toxin would be killed by toxin leaking into the cytosolic compartment? In fact, cytosolic leak is a problem in yeast in posttranslational protein transport, where the ribosome plays no role ***(19)***.

However, cotranslational protein transport (**Fig. 1**) predominates in mammalian cells. In this case, polypeptide is transferred across the membrane while

it is being synthesized on a membrane-bound ribosome. Leader or signal sequences are responsible for the passage of proteins into or through membranes. In assembling retIT, a key modification of the ligand is the addition of its signal sequence. This permits recognition by the signal recognition particle (SRP) and translocation of IT polypeptide directly into the endoplasmic reticulum (ER) lumen, where it is sequestered away from the cytosol ***(20)***. The net result of cotranslational protein transport is that none of the packaged protein gains access to the cytosol compartment, and the fusion toxin is secreted.

The best choice of delivery vehicle is unknown. LAK cells might be considered for retIT delivery, since they are more easily obtained than antigen-specific cytotoxic T-cell (CTL) (*see* **Note 1**). Although these cells are expanded by IL-2 and are not generally considered antigen-specific (since humans they are generated by treating peripheral blood cells with IL-2), they can be transduced with *retIT* genes ***(17)***.

1.7. Myeloid Leukemia

If LAK cells are our delivery vehicle then what about our retIT and its target. Our target is the myeloid leukemia line C1498 (*see* **Note 2**). Myeloid leukemia is the most prevalent form of adult leukemia, with approx 10,000 new cases each year ***(21)***. Even with complete remission rates of 50–70% and effective consolidation and intensification regimens including allogeneic bone marrow transplantation, over 60% of patients will die from complications of the disease and its treatment ***(22)***. Radiochemotherapy-resistant blasts are a frequent cause of treatment failure in patients. Alternative therapies are needed.

Our laboratory has used the C1498 line extensively as a model for human myeloid leukemia for several reasons: It is spontaneously derived and targeted by T-cells in vivo ***(23,24)***; it expresses IL-4 receptors (IL-4R) as does the majority of myeloid leukemias. Also, like its human counterparts, studies performed by our laboratory confirm that the line expresses myeloid markers such as Mac-1, Mac-3, gran-1, and pan-hematopoietic determinants Ly5, and it does not express T-cell (Thy1), B-cell (B220), NK markers, or type II Fc receptor.

With respect to antigens potentially involved in immune recognition, C1498 expresses MHC class I and the adhesion molecule determinants ICAM-1 and ICAM-2, but does not express MHC class II antigens or B7-1 (CD80) or B7-2 (CD86) ligands, which can costimulate T-cell responses. It does not express p15 envelope expressed by most murine leukemia retroviruses ***(25)***, so that the putative tumor antigen and not retroviral antigen responses can be analyzed. This is desirable since most human AML arise due to translocations and mutations and not retroviral transformation.

Depending on cell dose, C1498 is uniformly lethal, killing injected mice, and it is on a C57BL/6 background. Numerous knockout, transgenic, and

congenic, mice are available on this background, which may be of use as our study progresses.

1.8. IL-4–DT Immunotoxin

Over 90% of acute myeloid leukemia (AML) cases express IL-4R ***(12)***. Other laboratories have made use of this observation to devise therapies targeting IL-4R (*see* **Note 3**) ***(13–15)***. Therefore, we felt it would be useful to synthesize retrovirus that could be used to transduce T-cells so that they could deliver IT in vivo. IL-4Rs have been reported on most myeloid leukemias ***(26)***, various lymphoid malignancies ***(27)***, and nonlymphoid tumors ***(28–30)***. IL-4 fusion toxins have been effective in curing cancer in animal models. Investigators have reported that a complete remission of human IL-4R-bearing carcinoma can be induced in nude mice by administering IL-4–IT ***(29)***. In our own hands, IL-4–DT fusion toxin induces regression of human colon carcinoma cells in nude mice ***(31)***. IL-4–DT is well tolerated in mice. Our comparisons revealed that DT–IL-4 has at least a higher maximum tolerated dose (MTD) than the other fusion toxins. Thus, it is better tolerated despite its broad expression on a variety of hematopoietic blood types.

Based on these facts, we have assembled a IL-4–retIT and will show for the first time that LAK cells can be transduced with retrovirus, and therefore express and secrete IL-4–IT that can selectively kill appropriate IL-4R$^+$ C1498 leukemia cells in vitro (**Fig. 2**).

2. Materials

C1498 is the IL-4R+ leukemia that is targeted using IT secreted by retrovirus-infected LAK cells. It is an IL-4R+ C57BL/6 myeloid leukemia that is lethal to mice in 20–30 d when injected at doses greater than 10^5 cells ***(32,33)***. To produce LAK cells, mouse splenic T-cells were enriched using commercial Cellect mouse T-cell columns (Cytovax Biotechnologies, Edmonton, AB, Canada). LAK cells were generated by incubating cells in RPMI 1640/10% fetal calf serum plus recombinant mIL-2 (1000 U/mL) (Cetus Corp., Emeryville CA) for 6 d. The retroviral IT used to infect the LAK cells was assembled by first constructing a single-chain cytokine gene encoding 423 bp, or 141 amino acids of the *IL-4* gene including the 20-amino-acid signal peptide, was fused using splice overlap extension (SOE) with a truncated *DT* gene encoding the first 389 amino acids and devoid of its native binding region that renders the toxin lethal to all eukaryotic cells ***(33)***. To determine whether mammalian LAK cells can be transduced with a *cytokine immunotoxin* gene, the target gene was ligated into a modified LNCX retroviral expression vector, in which a fragment encoding Neo marker was replaced with a gene fragment encoding human nerve growth factor receptor (NGFR; **Fig. 3**; ***34***). Successful

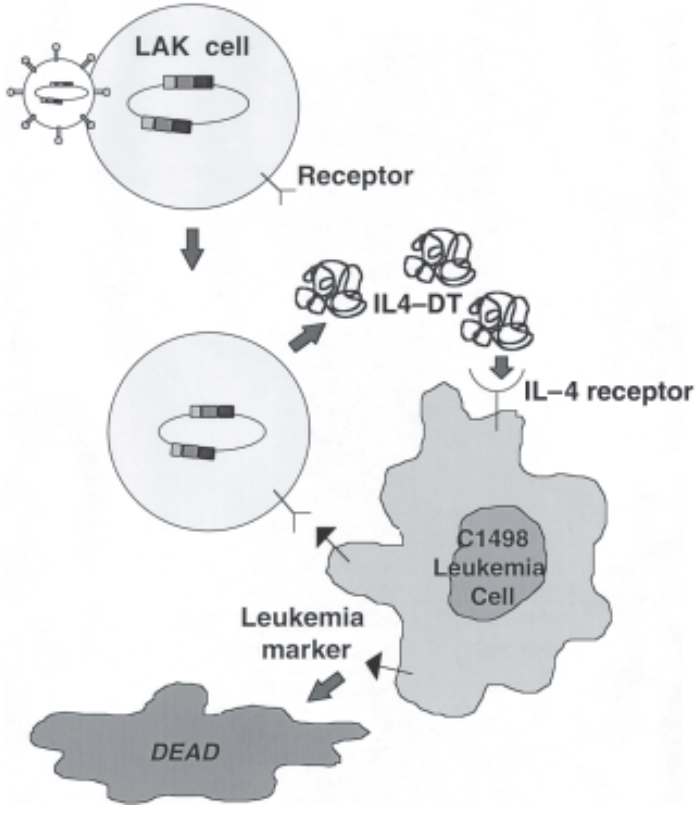

Fig. 2. LAK cell delivery of retIT. LAK cells are transduced with a retroviral vector encoding the IL-4–IT. LAK cells, which are capable of killing cancer cells and reaching cancer cells in vivo, serve as delivery vehicles to deliver IT therapy at the site of the cancer. The secreted IL-4–IT selectively binds and kills this IL-4R–expressing leukemia, but not cells that do not express the IL-4R.

integration of this retrovirus resulted in the expression of cell surface expression of NGFR, which could be used as a quantitative marker.

3. Method

3.1. Viral Supernatant

The first step was to use the retIT construct to transfect packaging cells so that we could generate viral supernatant. The embryo fibroblast PA317 (American Type Culture Collection, Rockville, MD) was used as a packaging cell line and transfected by electroporation using Gene Pulser II (Bio-Rad, Hercules, CA). Cells were resuspended in electroporation buffer (EB; 272 m*M* sucrose,

Fig. 3. Construct encoding the IL-4–DT_{390} fusion-toxin gene fragment used in these studies. Sig$IL4DT_{390}$ encodes the 1.7-kb gene fragment consisting of the IL-4 leader sequence (aa 1–19) followed by the murine *IL-4* gene (aa 20–140), a flexible EASGGPE linker, and a downstream fragment encoding DT_{390} (the first 389 aa of DT devoid of the native binding region). The SOE gene product was ligated into the retroviral vector LNCX.NGFR and then transfected into the PA317 packaging line to generate viral supernatant. LNCX.NGFR is identical to LNCX except *neo* was replaced with the gene encoding human NGFR to provide a selectable marker for assessing transduction levels and isolating stable transductants.

7 m*M* K_2HPO_4, 1 m*M* $MgCl_2$) at 10^7 cells/800 μL EB in an electroporation cuvette; 40 μg plasmid were added for 10 min on ice and then electroporated at 200 V, 950 microfarads, 200 Ω for 80 ms. The cells were plated in a 100 mm dish containing 10 mL DMEM/10% fetal calf serum and incubated overnight at 37°C. The viral supernatants were collected and centrifuged at 1300*g* for 10 min, filtered, and stored at –80°C.

3.2. Transduction of LAK Cells

The next step was to use the viral supernatant to transduce LAK cells, generated as described previously. Cytotoxicity was measured on a modified Jam assay in which target cell proliferation is assessed by thymidine incorporation ***(35)***. Briefly, 2×10^5 C1498 or EL4 target cells are pulsed for 3.5 h with 10 μCi tritiated thymidine (Amersham Corp., Arlington Heights, IL), washed, and then added to LAK cells in 96-well U-bottom Costar plates (Corning Inc., Corning, NY) at effector–target ratios of 100, 50, 25, 12.5, 6.2, 3.1, and 1.5 to 1. Plates were centrifuged and incubated for an additional 3.5 h in 5% CO_2/95% air at 37°C, and then harvested and counted by standard scintillation counting techniques. Cytotoxicity was calculated. **Figure 4** shows that LAK cells killed both C1498 and EL4 cells. Furthermore, the data show that the ability of LAK cells to kill C1498 or EL4 cancer cells was not impaired by the viral transduction procedure.

For transductions, LAK cells were transduced as follows: 1 mL supernatant was diluted in an equal volume of media and added to cells in 24-well plates plus 8 μg/mL polybrene, 100 U/mL murine IL-2. The mixture was centrifuged at 1300*g*, 32°C for 1.5 h, and then incubated at 32°C for 5 h. Cells were then transferred to a 100 mm dish and incubated in RPMI 1640/10% fetal calf serum

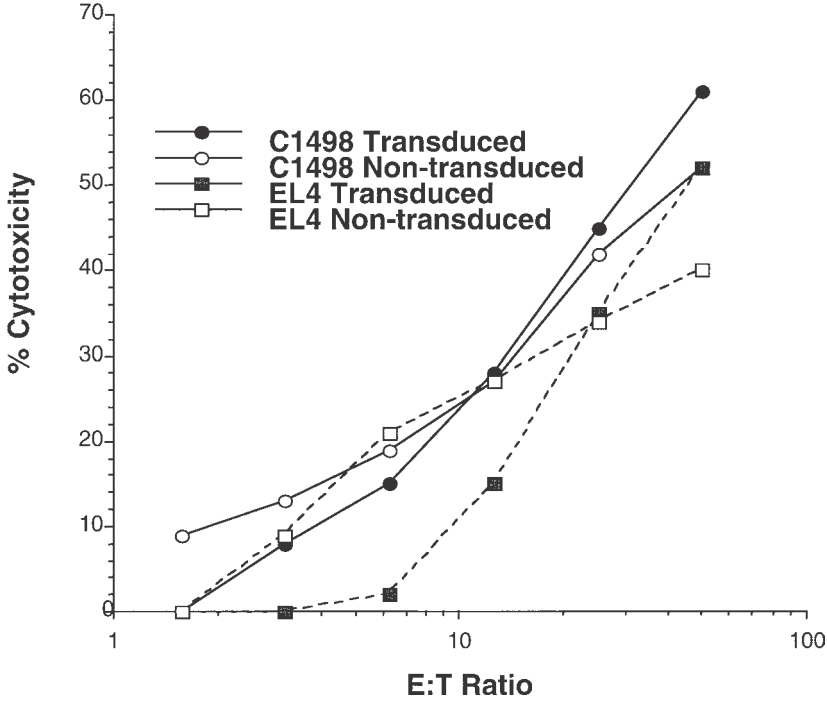

Fig. 4. LAK cells indescriminately kill both C1498 cells and EL4 cells. Cytotoxicity was measured against C1498 myeloid leukemia targets (solid lines) and EL4 targets (dashed lines) in triplicate wells. Data is plotted as % cytotoxicity vs effector–target ratio. Transduction had no effect on the ability of LAK cells to kill.

for 24–48 h. Transduction frequency was quantitated by the cytometric analysis of NGFR-expressing transduced cells. Thirty hours after transduction, there was an 18% increase in the level of NGFR expression in LAK cells measured by flow cytometry (data not shown).

3.3. Secretion of RetIT

The next step was to show that IL-4–IT could be secreted by retIT-transduced LAK cells. Supernatants were collected from transduced LAK cells, filtered, and then added to cultures of IL-4R$^+$ C1498 cells in viability assays designed to assess the killing of C1498 cells plated at 2×10^5/well in 24-well plates (Costar). One milliliter of filtered supernatant from cultured transfected or transduced T15 cells were added to each well. Wells were sampled at 24, 48, and 72 h, diluted in trypan blue dye/PBS solution, and the number of surviving cells determined. To assess selectivity, supernatants were simultaneously tested on IL-4R- EL4 cells (**Fig. 5**). LAK cells secreted functional fusion toxin, as

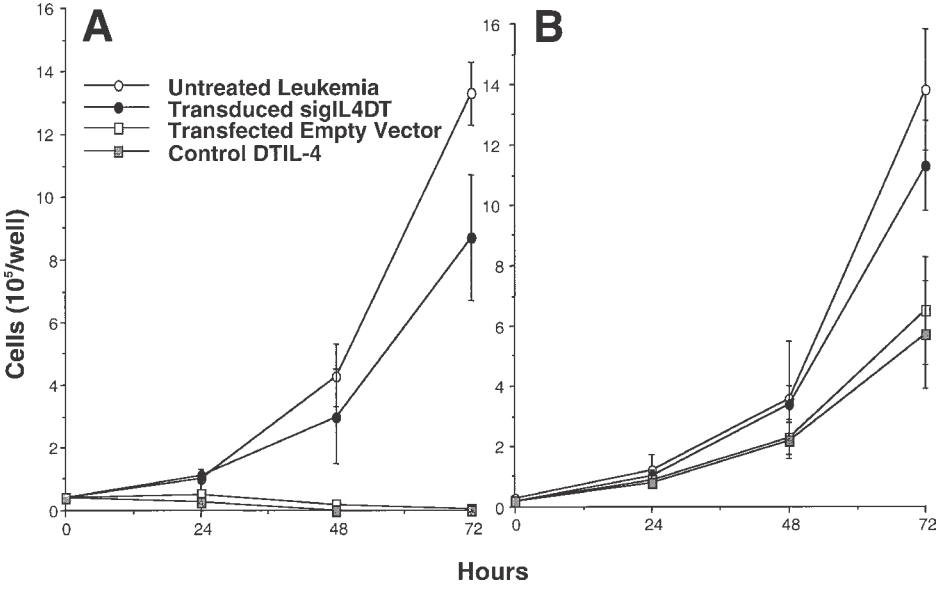

Fig. 5. Transduced LAK cells secrete IL-4 IT. **(A)** Supernatants were collected from cultured sigIL4DT$_{390}$/LNCX.NGFR–transduced LAK cells. Triplicate cultures of IL-4R+ C1498 leukemia cells were incubated with supernatants for 72 h and at 24 h intervals. Aliquots of cells from each well were stained with trypan blue and counted. **(B)** Control IL-4R- EL4 were also incubated with the same supernatants. Error bars represent standard error of the mean. Supernatant from transduced cells specifically killed C1498 cells.

supernatants selectively killed C1498 cells but not IL-4–EL4 cells. Control recombinant DT–IL-4 made in *E. coli* was selectively killed. Together, these studies show that transduced LAK cells can secrete IT that is selectively toxic to IL-4R–expressing leukemic target cells.

4. Notes

1. LAK cells are immune cells nonspecifically expanded using IL-2, and consist of T-cells and NK cells. Although LAK cells do mediate anticancer effects, it is generally agreed that antigen-specific T-cells instead of LAK cells would provide advantages in homing and selective recognition of cancer cells in vivo. However, antigen-specific T-cells represent an overall small proportion of the immune cell population, and selecting and expanding them for adoptive therapy in a timely and cost-effective manner for adoptive immunotherapy is problematic. To address these issues, we have shown that we can successfully transduce antigen-specific T-cells in the form of an MHC class I restricted, CD8-expressing CTL line called T15 ***(33)***. These transduced T-cells were capable of mediating a significant anti-C1498 effect in vivo.

2. It is clear that several questions will need to be addressed and obstacles overcome. We will need to determine if leukemia is the appropriate target disease for retIT therapy, since leukemia is bloodborne. If C1498 is administered intravenously, it will disseminate systemically with multiple growth sites. The production of retIT at multiple sites may enhance the risk of systemic toxicity.

   Another issue is the duration of secretion. Studies are in progress to measure retIT production in vitro and in vivo. Although it will be useful to establish a correlation between retIT levels and efficacy, it will be important to determine whether stable transductants can be generated in which provirus is stably integrated and retIT is secreted. Currently, cells must be transduced transiently prior to each injection, an approach that is neither labor efficient nor cost-effective. The further generation of stable transductants via Neo selection and flow cytometry sorting of $NGFR^+$ transductants may address this point.
3. One appealing aspect of the retIT approach is that T-cells could be recruited as vehicles to deliver any cytokine fusion toxin. Other cytokine fusion toxins might work better than IL-4–IT. For example, studies show that IL-3–IT, which has been limited by systemic toxic effects, are highly selective and capable of destroying IL-3R–expressing leukemias ***(36)***. Since these studies show that IL-3 kills committed but not uncommitted BM progenitor cells, and IL-3 receptor is expressed on greater than 90% of myeloid leukemias, it is also an excellent candidate for the retIT approach. IL-2 or any other cytokine with high-level receptor expression on T-cells are undesirable candidates for retIT, since secretion of IL-2 IT, for example, would immediately result in the suicide of T-cells expressing IL-2R. All of these issues can be addressed in animal models and studies are currently underway. Regardless of the number of issues that must be addressed, delivering IT using T-cells in this manner could overcome the unfavorable physiology, vascularization, and high tumor interstitial pressures that has limited the penetration of biologicals to cancer sites in vivo ***(1)***.

References

1. Jain, R. K. (1989) Delivery of novel therapeutic agents in tumors: physiological barriers and strategies. *J. Natl. Cancer Inst.* **81,** 570–576.
2. Shockley, T. R., Lin, K., Sun,g C., Nagy, J. A., Tompkins, R. G., Derick, R. L., et al. (1992) A quantitative analysis of tumor-specific monoclonal antibody uptake by human melanoma xenografts: effects of antibody immunological properties and tumor antigen expression levels. *Cancer Res.* **52,** 357–366.
3. Sung C., Shockley T. R., Morrison P. F., Dvorak H. F., Yarmush M. L., and Dedrick R. L. (1992) Predicted and observed effects of antibody affinity and antigen density on monoclonal antibody uptake in solid tumors. *Cancer Res.* **52,** 377–384.
4. Baxter, L. T., Yuan, F., and Jain, R. K. (1992) Pharmacokinetic analysis of the perivascular distribution of bifunctional antibodies and haptens: comparison with experimental data. *Cancer Res.* **52,** 5838–5844.
5. Rosenberg, S. A., Packard, B. S., Aebersold, P. M., Solomon, D., Topalian, S. L., Toy, S. T., et al. (1988) Use of tumor-infiltrating lymphocytes and interleukin-2

in the immunotherapy of patients with metastatic melanoma. *N. Engl. J. Med.* **319,** 1676–1680.
6. Frankel A., ed. (1992) *Genetically Engineered Toxins.* Marcel Dekker Inc., New York, pp. 3–115.
7. Honjo, T., Nishizuka, Y., Hataishi, O., and Kato, I. (1968) Diphtheria toxin-dependent adenosine diphosphate ribosylation of aminoacyl transferase II and inhibition of protein synthesis. *J. Biol. Chem.* **243,** 3553–55.
8. Collier, R. J. (1975) Diphtheria toxin: mode of action and structure. *Bact. Rev.* **39,** 54–85.
9. Vallera, D. A. (1994) Immunotoxins: will their clinical promise be fulfilled? *Blood* **83,** 309–17.
10. Foss, F. M., Borkowski, T. A., Gilliom, M., Stetler-Stevenson, M., Jaffe, E. S., Figg, W. D., et al. (1994) Chimeric fusion protein toxin DAB486IL-2 in advanced mycosis fungoides and the Sezary syndorme: correlation of activity and interleukin-2 receptor expression in a phase II study. *Blood* **84,** 1765–1774.
11. Lindauer, M., Stinisslawski, T., Haussler, A., Antunes, E., Huber, C., and Theobald, M. (1998) The molecular basis of cancer immunotherapy by cytotoxic T lymphocytes *J. Mol. Med.* **76,** 32–47.
12. Matsumura, T., Sussman, J. J., Krinock, R. A., Chang A. E., and Shu, S. (1994) Characteristics and in vivo homing of long-term T-cell lines and clones derived from tumor-draining lymph nodes. *Cancer Res.* **54,** 2744–2750.
13. Bolhuis, R. L. H., Strum, E., and Braakman, E. (1991) T-cell targeting in cancer therapy. *Cancer Immunol. Immunother.* **34,** 1–8
14. Eshhar, Z., Waks, T., Gross, G., and Schindler, D. (1993) Specific activation and targeting of cytotoxic lymphocytes through chimeric single chains consisting of antibody-binding domains and the gamma or zeta subunits of the immunoglobulin and T-cell receptors. *Proc. Natl. Acad. Sci. USA* **90,** 720–724
15. Gross, G., Waks, T., and Eshhar, Z. (1989) Expression of immunoglobulin-T-cell receptor chimeric molecules as functional receptors with antibody-type specificity. *Proc. Natl. Acad. Sci. USA* **86,** 10,024–10,028.
16. Topalian, S., Solomon, D., and Rosenberg, S. A. (1989) Tumor specific cytolysis by lymphocytes infiltrating human melanomas. *J. Immunol.* **142,** 3714–3725.
17. Chen, S-Y., Yang, A-G., Chen, J-D., Kute, T., King, R., Collers, J., et al. (1997) Potent antitumour activity of a new class of tumour-specific killer cells. *Nature* **385,** 78–80.
18. Yang, A. G. and Chen, S.-Y. (1997) A new class of antigen-specific killer cells. *Nat. Biotechnol.* **15,** 46–51.
19. Rapoport, T. A., Rolls, M., and Jungnickel, B. (1996) Approaching the mechanism of protein transport across the ER membrane. *Curr. Op. Cell Biol.* **8,** 499–504.
20. Walter, P. and Johnson, A. E. (1994) Signal sequence recognition and protein targeting to the endoplasmic reticulum membrane. *Annu. Rev. Cell Biol.* **10,** 87–119.
21. Parker, S., Tong, T., Bolden, S., and Wingo, P. (1997) Cancer statistics. *CA Cancer J. Clin.* **47,** 5–12.

22. Schiffer C. (1997) Acute myeloid leukemia in adults, in *Cancer Medicine* (Holland, J., Frei, E., Bast, R., Kufe, D., and Marton, D., eds.), Weichselbaum R. Lea, and Febiger, Philadelphia, pp. 2617–2633.
23. Durham, L. J. and Stewart, H. L. (1953) A survey of transplantable and transmissible animal tumors. *J. Natl. Canc. Inst.* **13,** 1299–1377.
24. Bradner, W. T. and Pindell, M. H. (1966) Myeloid leukemia C1498 as a screen for cancer chemotherapeutic agents. *Cancer Res. Cancer* **43,** 375–390.
25. Chesebro, B., Britt, W., Evans, K., Wehrly, K., Nishio, J., and Cloyd, M. (1983) Characterization of monoclonal antibodies reactive with murine leukemia viruses. *Virology* **127,** 134–148.
26. Wagteveld, A. J., van Zanten, A. K., Esselink, M. T., Halie, M. R., and Vellenga, E. (1991) Expression and regulation of IL-4 receptors on human monocytes and acute myeloblastic leukemic cells. *Leukemia* **5,** 782–788.
27. Ohara, J. and Paul, W. E. (1988) Up-regulation of interleukin 4/B-cell stimulatory factor 1 receptor expression. *Proc. Natl. Acad. Sci. USA* **85,** 8221–8227.
28. Lowenthal, J. W., Castle, B. E., Christian, J., Schreurs, J., Rennick, D., Arai, N., et al. (1988) Expression of high affinity receptors for murine interleukin-4 (BSF-1) on hematopoietic and nonhematopoietic cells. *J. Immunol.* **140,** 456–464.
29. Debinski, W., Puri, R. K., Kreitman, R. J., and Pastan, I. (1993) A wide range of human cancers express interleukin 4 (IL-4) receptors that can be targeted with chimeric toxin composed of IL-4 and *Pseudomonas* exotoxin. *J. Biol. Chem.* **268,** 14,065–14,070.
30. Puri, R. K., Hoon, D. S., Lelan, P., Snoy, P., Rand, R. W., Pastan, I., et al. (1996) Preclinical development of a recombinant toxin containing circularly permuted interleukin 4 and truncated Pseudomonas exotoxin for therapy of malignant astrocytoma. *Cancer Res.* **56,** 5631–5637.
31. Buchsbaum D. J., Laffoon K. Rogers B. E., Curiel D. T., Khazaeli M. B., McLean S., et al. (1997) Radiolabeled DT_{390}-mIL-4 fusion toxin binding and cytotoxicity to tumor cell induced to express mIL-4 receptor. *Cancer Gene Ther.* **4,** S41.
32. Boyer, M. W., Vallera, D. A., Taylor, P. A., Gray, G. S., Katsanis, E., Gorden, K., et al. (1997) The role of B7.1 by murine acute myeloid leukemia cells in the generation and function of a CD8+ T cell line with potent in vivo graft-versus-leukemia (GVL) properties. *Blood* **89,** 3477–3454.
33. Vallera D. A. , Jin N., Baldrica J., Panoskaltsis-Mortari A., Chen S.-Y., and Blazar BR. (2000). Retroviral immunotoxin gene therapy of acute myelogenous leukemia (AML) in mice using cytotoxic T cells (CTL) transduced with an IL-4/diphtheria toxin gene. *Cancer Res.* **60,** 976–984.
34. Chen, J. D., Bai, X., Yang, A. G., Cong, Y., and Chen, S. Y. (1997) Inactivation of HIV-1 chemokine co-receptor CXCR-4 by a novel intrakine strategy. *Nat. Med.* **10,** 1074, 1075.
35. Matzinger P. (1991) The JAM test: a simple assay for DNA fragmentation and cell death. *J. Immunol. Methods* **145,** 185–192.
36. Chan, C. H., Blazar, B. R., Eide, C. R., Greenfield, L., Krietman ,R. J., and Vallera, D. A. (1996) Reactivity of murine cytokine fusion toxin, DT_{390}-mIL-3, with bone marrow progenitor cells. *Blood* **88,** 1445–1451.

16

Effects of Selective Immunotoxic Lesions on Learning and Memory

Mark G. Baxter

1. Introduction

Immunotoxins provide the opportunity to make neurotoxic lesions of specific neurochemically-defined neuronal populations (*see* Chapter 17) by targeting cell-surface antigens that are uniquely expressed by the cells of interest. The greatest application of these toxins in the study of learning and memory has been through the use of one specific immunotoxin, 192 IgG-saporin, which kills neurons that express the low-affinity nerve growth factor (NGF) receptor ***(1,2)***. The low-affinity NGF receptor (sometimes referred to as the p75 neurotrophin receptor) within the central nervous system is expressed by neurons in the basal forebrain and by cerebellar Purkinje cells ***(3–5)***. Within the basal forebrain, this receptor is expressed only on cholinergic neurons ***(6)***. Therefore, when this toxin is injected into the basal forebrain, it produces selective lesions of cholinergic neurons, sparing noncholinergic neurons at the lesion site ***(7)***. This lesion method has been employed to create an animal model of the degeneration of basal forebrain cholinergic neurons seen in patients with Alzheimer's disease ***(8)***. Such a model has been impossible to achieve with other lesion methods that do not produce selective damage to basal forebrain cholinergic neurons, limiting the interpretation of behavioral deficits observed after such lesions.

This chapter begins with a brief review of the studies that have used immunotoxins to study learning and memory, consisting almost entirely of investigations of the basal forebrain cholinergic system. Subsequent sections will discuss practical issues encountered in working with immunotoxins. The overall goal of this chapter is to provide the necessary background for investigators

From: *Methods in Molecular Biology, vol. 166: Immunotoxin Methods and Protocols*
Edited by: W. A. Hall

experienced in stereotaxic neurosurgery and behavioral testing to use immunotoxins in their research programs.

1.1. Anatomy of the Basal Forebrain Cholinergic System

Anatomic and functional aspects of the basal forebrain cholinergic system have been treated extensively in recent reviews *(9,10)* and so will be discussed only briefly here. The basal forebrain cholinergic system can be divided into four groups of cells: the medial septum (MS), projecting primarily to the hippocampus; the vertical limb of the diagonal band of Broca (VDB), projecting to the hippocampus and cingulate cortex; the horizontal limb of the diagonal band of Broca (HDB), projecting to the olfactory bulb, piriform cortex, and entorhinal cortex; and the nucleus basalis magnocellularis (NBM) or substantia innominata (SI), projecting to the neocortex and amygdala *(11–22)*. The organization of the basal forebrain is similar in the primate and in the rat, although subdivisions of the nucleus basalis can be identified reliably in the primate but not in the rat *(18,19,22)*.

Cholinergic and noncholinergic neurons are interspersed in the basal forebrain *(23,24)*. Estimates of the proportion of cortically projecting basal forebrain neurons that are cholinergic vary somewhat from study to study *(19,24,25)*. Many noncholinergic neurons in the basal forebrain may be local circuit neurons, receiving cortical input and modulating activity of cortically projecting cholinergic and noncholinergic neurons *(26)*. **Figure 1** shows a comparison of immunostaining for ChAT in the basal forebrain of the rat with a Nissl-stained section at the same level. A casual comparison of cell density indicates that many neurons in the basal forebrain are noncholinergic, and that the cholinergic neurons are interspersed among the noncholinergic neurons. Hence, without a selective toxin for cholinergic neurons, experimental studies of the particular functions of this class of neurons are not possible.

1.2. Comparison of 192 IgG-Saporin with Other Neurotoxins

Experimental studies of the basal forebrain initially employed electrolytic or radiofrequency lesions to damage this region; such lesions damaged not only cell bodies in the basal forebrain (cholinergic and noncholinergic), but fibers of passage through the lesioned area as well. The use of excitatory amino acid analogs (excitotoxins) to produce axon-sparing lesions of cell bodies in the basal forebrain provided further advances, but it was not possible to establish a definitive relationship between damage to cholinergic basal forebrain neurons and memory impairment *(27–31)*. The general consensus from these studies was that damage to some other neuronal population within the basal forebrain was required to produce mnemonic deficits, and that damage to cholinergic neurons generally did not correlate with the severity of memory impair-

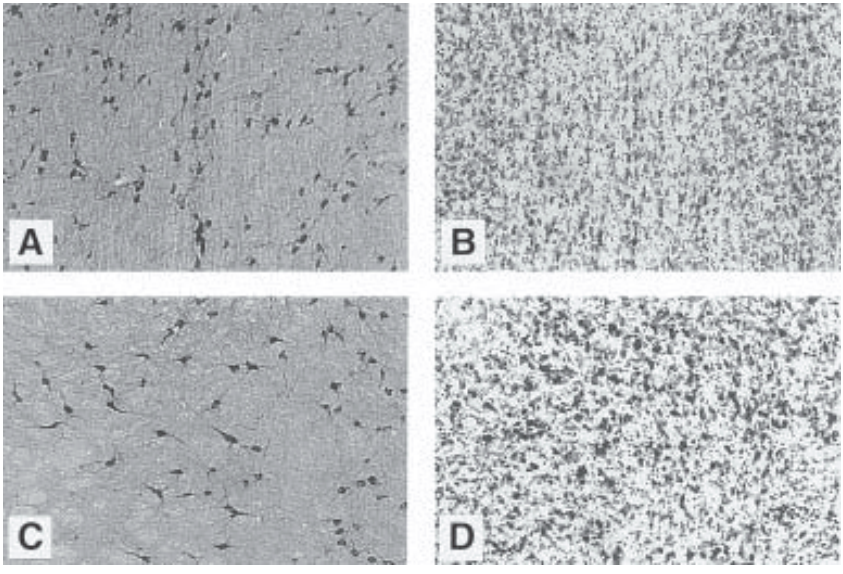

Fig. 1. Neurons in the basal forebrain of the rat at the level of the medial septum/vertical limb of the diagonal band (MS/VDB) (**A**,**B**) and nucleus basalis magnocellularis/substantia innominata (NBM/SI) (**C**, **D**). Immunohistochemistry for choline acetyltransferase demonstrates large cholinergic neurons in both regions (**A**, **C**). Thionin-stained sections (**B**, **D**) demonstrate the density of neurons in the region: Large numbers of noncholinergic neurons are interspersed within these regions. From Baxter, M. G. and Gallagher, M. Cognitive effects of selective loss of basal forebrain cholinergic neurons: Implications for cholinergic therapies of Alzeimer's disease, in *Pharmacological Treatment of Alzheimer's Disease: Molecular and Neurobiological Foundations* (Brioni, J. D. and Decker, M. W., eds.) Copyright © (1997) Reprinted by permission of Wiley-Liss, a division of John Wiley & Sons.

ment. The possibility that ethylcholine aziridinium ion (AF64A) might be a selective cholinergic toxin generated considerable excitement, but this toxin seems to produce nonspecific damage in addition to damaging cholinergic neurons ***(32–36)***.

192 IgG-saporin has proved to be the most selective agent to date for lesioning basal forebrain cholinergic neurons ***(1,2,7,37)***. Very high doses of 192 IgG-saporin administered into the cerebral ventricles produce alterations in brain catecholamine levels, but little or no change is seen with lower doses of the toxin (which are fully effective in producing nearly complete cholinergic depletion) or with administration of the toxin directly into the basal forebrain ***(38–41)***. Injection of 192 IgG-saporin into the cerebral ventricles destroys both basal forebrain cholinergic neurons and cerebellar Purkinje cells, which

also express the low-affinity NGF receptor *(7,39)*. Injection of 192 IgG-saporin into the basal forebrain produces selective damage to basal forebrain cholinergic neurons, without damaging noncholinergic neurons at the injection site or affecting other neurochemical systems within the basal forebrain, including catecholaminergic and peptidergic systems *(7,42)*.

1.3. Behavioral Effects of 192 IgG-Saporin Lesions

The results to date with this immunotoxin have indicated that the role of the basal forebrain cholinergic system in cognitive function is considerably more limited than was previously believed. For example, impairments in spatial learning and memory, which are commonly observed after basal forebrain lesions are produced with less selective methods, are generally not observed following selective immunotoxic lesions of basal forebrain cholinergic neurons. In contrast, these selective lesions do produce impairments in attentional processing that are similar to those observed following lesions of the basal forebrain that are not selective for cholinergic neurons *(9,10,43)*.

Despite the general consensus that behavioral deficits produced by 192 IgG-saporin lesions are more restricted than those produced by other lesion methods, several outstanding questions remain unresolved regarding the role of the basal forebrain cholinergic system in specific cognitive processes. Because these questions relate directly to the manner in which the immunotoxin is used, they will be discussed briefly here.

1.3.1. Extent of Cholinergic Loss Required to Produce Impairments in Learning and Memory

Tests of spatial learning and memory, commonly used to assess cognitive function in rats, are impaired by lesions of the basal forebrain that are not selective for cholinergic neurons *(44–48)*. The impairments following such lesions are frequently attributed to cholinergic loss despite the lack of selectivity of the lesion method.

Studies using intraparenchymal injections of 192 IgG-saporin to lesion specific nuclei in the basal forebrain (injections into specific nuclei in the basal forebrain) have generally failed to find an impairment in spatial learning tasks, primarily the Morris water maze task *(42,49–53)*. In contrast, studies in which 192 IgG-saporin is administered into the cerebral ventricles (damaging both basal forebrain cholinergic neurons and cerebellar Purkinje cells) have reported substantial impairments in spatial learning in the Morris water maze *(39,40,50,54,55)*. The depletion of cortical ChAT activity following intraventricular 192 IgG-saporin is generally slightly greater than that achieved following intraparenchymal injections of the toxin. This has led to the proposal *(56–58)* that extremely severe loss of cortical cholinergic input is required to produce deficits in learning and

memory; that is, the basal forebrain cholinergic system has a substantial reserve capacity, not unlike the nigrostriatal dopamine system in which 80–90% loss is required before motoric impairments become evident ***(59)***.

The interpretation of behavioral deficits following intraventricular administration of 192 IgG-saporin, however, is just as difficult as the interpretation of deficits following nonselective neurotoxic lesions of the basal forebrain, as a neuronal population other than cholinergic basal forebrain neurons is being damaged in each case. The destruction of cerebellar Purkinje cells by intraventricular administration of 192 IgG-saporin is well documented ***(7,39,60)***. Such damage results in impairments in a cued version of the Morris water maze in which spatial learning is not required, suggesting a sensory or motoric basic for the impairment in the spatial version of the task ***(39,50)***. Indeed, lesions restricted to cerebellar Purkinje cells can produce substantial deficits in spatial learning in the water maze ***(60)***. Deficits in other cognitive tasks (e.g., the operant delayed nonmatching-to-position task in rats) that are relatively mild after lesions limited to basal forebrain cholinergic neurons are much more severe after intraventricular 192 IgG-saporin lesions ***(52,61–63)***. The finding that lesions restricted to particular basal forebrain nuclei are capable of producing behavioral deficits in other settings (e.g., in tests of attentional processing ***(64–66)*** casts further doubt on the hypothesis that a substantial reserve capacity is responsible for the lack of effect of such lesions on spatial learning.

Of course, it remains a logical possibility that less extensive lesions of basal forebrain cholinergic neurons are capable of disrupting attentional processing but not spatial learning, and that extremely severe loss of basal forebrain cholinergic neurons (on the order of that produced by intraventricular lesions) would be sufficient to induce spatial learning deficits. Although this remains an open question, the relevance of such a finding to clinical conditions such as Alzheimer's disease, in which cortical ChAT depletion rarely reaches such extreme levels ***(67–69)*** is questionable.

1.3.2. Spatial Working Memory and Intraseptal Saporin: Specificity of Intraparechymal Injections

Damage to the MS/VDB, removing cholinergic projections to the hippocampus, has been associated with impairments in spatial working memory, commonly tested in rats on a radial arm maze in which an initial visit to each arm produces a food reinforcer, but return visits to arms do not ***(70,71)***. A version of this task in which a delay is interposed after several choices are made is used to test memory for spatial information: If memory for spatial information is specifically impaired, performance after short delays should be equivalent in lesioned and control rats, whereas performance at longer delays should be worse in lesioned rats than in controls (a delay-dependent deficit). Deficits that

do not vary with delay (delay-independent) are more difficult to interpret, as they may indicate impaired memory, impaired initial encoding of the information, or some perceptual or attentional deficit.

The effects of intraparenchymal injections on tests of spatial learning have been fairly consistent from study to study in that deficits have not been observed. However, the effects on tests of spatial working memory have been more variable: a delay-dependent deficit ***(41)***, a delay-independent deficit ***(49,72)***, or no deficit ***(53,73,74)***. In particular, based on their attempt to equalize behavioral procedures with studies that have found delay-dependent deficits in radial maze performance following 192 IgG-saporin lesions of the MS/VDB, Chappell et al. ***(74)*** suggest that the critical variable may be the surgical procedure used to inject 192 IgG-saporin into the MS/VDB. One published study noted a suppression of parvalbumin immunostaining after an injection into the midline of the MS, where these neurons are located ***(52)***. GAD immunostaining was intact, suggesting that the GABAergic neurons had not been destroyed but their function might have been compromised. (The lesions in this study produced no deficit in the water maze, but produced a mild delay-dependent impairment in an operant delayed nonmatching-to-position task.)

The two studies that used off-the-midline injections of 192 IgG-saporin into the MS/VDB achieved comparable depletion of hippocampal ChAT activity but failed to observe behavioral deficits in the radial arm maze ***(73,74)***, unlike the studies that tested radial maze performance following injections of 192 IgG-saporin on the midline ***(41,72)***. Importantly, the latter two studies provided no independent confirmation that GABAergic MS/VDB neurons were not compromised by their lesion technique. Therefore, unintended damage to these neurons may be responsible for the behavioral deficits observed in those studies.

It is worth noting that other explanations are possible. Indeed, a subsequent study by Walsh and colleagues demonstrated impairments in spatial working memory following 192 IgG-saporin injections into the hippocampus or cingulate cortex, which would remove cholinergic projections to those areas but would not be expected to damage noncholinergic basal forebrain neurons ***(75)***. The hippocampus and cingulate cortex did not display focal damage or necrosis as a consequence of the injections, suggesting that the behavioral impairments are due to loss of cholinergic input. Hence, it does appear that damage to MS/VDB cholinergic neurons is sufficient to induce spatial working memory impairments in some instances, although rats with these lesions can demonstrate intact spatial working memory ***(74)***. The possibility that other task variables may influence whether a memory impairment is seen (e.g., the nature of environmental cues available for use by the rats to navigate) remains open and invites parametric experimental studies.

1.4. Procedures Involved in Behavioral Experiments with Immunotoxic Lesions

Behavioral studies using immunotoxic lesions involve stereotaxic surgery to produce the lesions, behavioral testing to assess the effects of the lesions, and neurochemical or neurohistologic procedures to verify the effectiveness of the lesions. Although there is some generality in these procedures, the discussion in this chapter revolves around the use of 192 IgG-saporin in rats. Use of immunotoxins in other species (nonhuman primates; ***76–78***) is fraught with additional complications. For example, it is generally not feasible to pilot several different doses of the immunotoxin to establish optimal concentrations that produce selective damage to the neuronal population of interest. Nevertheless, it remains critical in all of these experiments to verify that the immunotoxin is in fact producing a selective lesion of the neuronal population of interest.

Many studies with 192 IgG-saporin have demonstrated specificity of the lesion for cholinergic basal forebrain neurons, without damage to other neuronal populations in the basal forebrain ***(7,42)***. Nonetheless, it is important for each investigator to independently establish that the toxin is selective with the particular preparation of toxin and surgical procedures used in their own laboratory (*see* **Subheading 3.1.**). As discussed in **Subheading 1.3.2.**, it is possible that particular injection procedures (or preparations of toxin) may result in nonspecific damage at the lesion site that compromises the interpretation of the results.

For experiments using 192 IgG-saporin, it is possible to assess the effectiveness of the lesion by immunohistochemistry for ChAT-immunoreactive neurons in the basal forebrain, or by in vitro determination of ChAT activity in the target areas of the particular basal forebrain region of interest. Immunohistochemistry has the advantage of providing good anatomical resolution, as well as the possibility of examining other neuronal populations to determine whether damage has occurred to noncholinergic neurons (e.g., GABAergic neurons). For example, immunohistochemistry for parvalbumin is commonly assessed in the MS/VDB when saporin injections target that area, as parvalbumin-immunoreactive septal neurons are GABAergic ***(79)*** and provide the other major component of the septohippocampal projection ***(25)***. Such damage would be difficult to visualize with general cell-body staining procedures (e.g., cresyl violet staining). In vitro neurochemical assays, on the other hand, provide a quantitative measure of the extent of the lesion, which is very difficult to achieve from immunohistochemical material.

It is probably good standard practice in each experiment to select a few of the subjects (two or three in each lesion group) to undergo immunohistochemi-

cal analysis at the end of the experiment to verify the selectivity of the lesions in that particular study. The remaining subjects could be processed for quantitative neurochemical assays. Alternatively, the method of lesion verification might be chosen depending on the particular behavioral results obtained. If a negative effect is obtained, it would be more informative to collect quantitative neurochemical information to ensure that the extent of the lesion was sufficient to produce a behavioral deficit if one was expected. On the other hand, if a behavioral deficit is seen, it might be more important to verify that the lesions selectively damaged basal forebrain cholinergic neurons, so immunohistochemical methods might be more appropriate.

2. Materials

2.1. Immunotoxin

The immunotoxin 192 IgG-saporin, along with several others targeted at different neuronal antigens, is commercially available from Chemicon (Temecula, CA) and Advanced Targeting Systems (San Diego, CA). 192 IgG-saporin should be stored at –70°C and appears to be stable under these conditions for at least 2 yr. As with any antibody, it is best to avoid repeated freeze–thaw cycles (*see* **Subheading 3.1.** for procedures on diluting and aliquoting the immunotoxin upon receipt). The storage conditions for immunotoxins made with different antibodies may vary—for example, certain antibodies are not stable when frozen. Such toxins should be kept at 4°C and used more quickly to avoid evaporation of the solution or degradation of the toxin.

2.2. Stereotaxic Surgery; Behavioral Testing; Lesion Verification

Specific materials for surgery, behavioral testing, and lesion verification will vary widely depending on the aims of the particular study, so discussion of these materials is beyond the scope of this chapter. General references for these topics include two recent laboratory manuals on neuroscience ***(80,81)***.

3. Methods

3.1. Immunotoxin

Even though toxins are designed to be selective for certain neuronal populations, it is essential to verify this with the particular preparation of immunotoxin, with each individual laboratory's particular surgical procedures. This can be relatively challenging, given the undesirability of repeatedly freezing and thawing the immunotoxin. At higher doses, 192 IgG-saporin will produce nonselective damage at the injection site, presumably because the toxin is taken up by nonspecific endocytosis by all cells in the region if it is present in high concentrations.

The following procedure for piloting doses of 192 IgG-saporin has been followed with success in my laboratory. To avoid repeatedly piloting optimal doses, it is advisable to obtain relatively large amounts of the toxin from a particular lot, to the extent that this is financially possible. Note that references to freezing the toxin should be modified if using an immunotoxin that is made with an antibody that cannot be frozen (*see* **Subheading 2.1.**).

1. Upon arrival, immediately remove a small amount of the toxin from the vial, perhaps slightly less than 10% of the total volume of the vial. (The toxin probably will not be frozen on arrival; if it is frozen, it can be thawed at this point.) For example, a vial of 250 μg 192 IgG-saporin at a concentration of 2 mg/mL will contain 125 μL of toxin, of which 10–20 μL might be removed for piloting.
2. Freeze the remainder of the toxin concentrate in the shipping vial (at –70°C) and dilute the amount removed to several lower concentrations by serial dilutions (*see* **Note 1**). (The initial concentration of the toxin will be noted on the packing information.) Using recent preparations of 192 IgG-saporin from Chemicon, a working concentration of 0.15–0.2 μg/μL has produced selective lesions of cholinergic neurons when infused into the basal forebrain, with no nonspecific damage at the lesion site. (Gliosis is not observed at the injection site, nor is the loss of parvalbumin-immunoreactive neurons.) Sterile phosphate-buffered saline (PBS) is used to dilute the toxin. For instance, the toxin concentrate might be initially diluted 1:1 with sterile PBS (to make it easier to work with), then several dilutions prepared at lower concentrations (e.g., 0.4 μg/μL, 0.2 μg/μL, 0.1 μg/μL) (*see* **Note 2**). Freeze these aliquots at –70°C until the pilot surgeries are performed. (0.5 mL microcentrifuge tubes are convenient for this purpose; with 8–10 μL in each vial, it is helpful to have at least 2 aliquots of each dilution.) Reserve the remainder of the toxin concentrate that was removed from the shipping vial in a separate vial in case a second series of pilot surgeries is required.
3. Perform surgeries with the different dilutions of the immunotoxin (*see* **Note 3**). Unilateral lesions with the toxin are probably best for this purpose if a nonmidline structure is being targeted (e.g., the nBM/SI) so that preparation of separate (unlesioned) brains for comparison will not be required (*see* **Notes 4** and **5**). After a 2–3 wk survival period, process the tissue for immunohistochemistry, including both ChAT and a marker for a noncholinergic cell population in the region of interest (e.g., parvalbumin, GAD, or GABA). Examine the tissue for damage to cholinergic neurons in the region of interest, as well as for the presence of nonspecific tissue disruption or damage to noncholinergic neurons (*see* **Note 5**). Commonly, concentrations that are too low will not remove all of the cholinergic neurons in the region of interest; concentrations that are too high will produce nonspecific damage.

   If none of the tested concentrations produce optimal lesions (i.e., they are all too high or too low), repeat **steps 2** and **3** with a different series of toxin dilutions, using either the remaining toxin concentrate that was removed from the shipment vial, or the aliquots of diluted toxin that have not been thawed yet, as appropriate.

4. Once an optimal concentration is established, thaw the entire quantity of toxin in the shipping vial, measure it carefully into a microcentrifuge tube or small vial (e.g., remove 10 μL at a time with a micropipeter), then dilute the toxin to the appropriate concentration with sterile PBS. Aliquot the toxin into 0.5 ml microcentrifuge tubes (10 μL in each vial). Wrap a small piece of parafilm around the lid of the tubes and freeze at –70°C. Each surgery usually requires 1–1.5 μL of toxin at most (generally one aliquot lasts for an entire day of surgery). The volume of each individual aliquot depends on the particular surgical procedures being used.

3.2. Surgical, Behavioral, Lesion Verification Methods

Again, specific methods for these procedures are highly variable and depend on the specific experiment, and so are beyond the scope of this chapter. The reader is again referred to general references for these topics ***(80,81***; *see also* **Note 6***)*.

4. Notes

1. The procedure outlined in **Subheading 3.1.** is designed to avoid repeated freezing and thawing of the toxin while permitting determination of the optimal concentration for a particular procedure. It is important to remember that it is always possible to dilute the toxin further if the initial concentration used is too high. In my experience, refreezing diluted toxin once has no effect on its activity in producing lesions; it can also be kept refrigerated at 4°C for several days. Specific procedures will depend on the particular surgical protocols being used. For example, highly diluted toxin is undesirable if intracerebroventricular (i.c.v.) lesions are being performed, because of the large dose required to produce an effective i.c.v. lesion (4 μg usually is injected i.c.v.).
2. Different applications of the toxin will require different dilutions. For example, intracortically injected saporin is very effective at removing cholinergic projections from the basal forebrain to specific cortical target areas ***(82–84)***. The concentration of immunotoxin required for effective damage following such infusions tends to be lower than that required for effective basal forebrain lesions (e.g., 0.01 μg/μL; ***82***). As with other applications of the immunotoxin, it is important to verify that the lesions produced are selective for cholinergic fibers and do not involve cortical cell bodies or other fibers of passage through the lesion site.
3. With regard to methods for infusing the toxin, I have used 28 gauge Hamilton syringes with flat tips (point style 3) held in a microsyringe holder mounted directly on the stereotaxic apparatus. When drawing up the toxin into the syringe, move the plunger back and forth very rapidly to expel all the air from the syringe—there should be no air bubbles in the barrel of the syringe. It is also critical to clear the syringe after each penetration into the brain—expel a small amount of toxin and wipe the tip with a cotton swab, then expel a bit more and make sure the flow is uninterrupted. Remove the toxin from the tip with something nonabsorbent (e.g., the wooden end of the swab) so that no toxin is wicked

out of the syringe needle. If several injections are being made in a single penetration, it is not necessary to withdraw the needle and clear it after each infusion, as repeated penetrations into the same needle track would cause unacceptable levels of tissue damage. It is better to make the deeper (more ventral) injections in each needle track first if multiple injections are being made.

4. The injections should be made at a slow flow rate (0.05–0.1 μL/min). Large bolus injections are associated with nonspecific damage at the injection site. The needle should be left in place for some period of time after the injection to limit diffusion up the needle track; this will vary depending on the volume infused, the rate of the infusion, and the depth of the structure being targeted. Usually, 1–1/2 times the time required to make the infusion is a good guideline (e.g., wait 6 min to remove the needle after a 4 min infusion).
5. The dosage of the toxin needed to produce selective lesions may be strain-dependent. In the laboratory, approx 2.5-fold lower concentration of toxin (0.06 μg/μL compared to 0.15 μg/μL) is required to produce selective lesions of the MS/VDB in Fischer-344 rats, compared to Long-Evans rats. Effective doses appear to be similar in Long-Evans and Sprague-Dawley rats. As noted previously, it is always good practice to perform extensive preliminary tests to ensure the specificity of the toxin.
6. The lesion is not complete for 3–5 d after toxin infusion ***(38)*** so behavioral testing should not begin until at least 1 wk after surgery (I routinely allow 2 wk for postoperative recovery). Anorexia is sometimes seen after these lesions, particularly after i.c.v. lesions ***(50,55)***. It is good general practice to monitor animals closely for several days after surgery, but particular caution should be taken with i.c.v. lesions. Seizure activity is not observed after these lesions.

References

1. Wiley, R. G., Oeltmann, T. N., and Lappi, D. A. (1991) Immunolesioning: Selective destruction of neurons using immunotoxin to rat NGF receptor. *Brain Res.* **562,** 149–153.
2. Book, A. A., Wiley, R. G., and Schweitzer, J. B. (1992) Specificity of 192 IgG-saporin for NGF receptor-positive cholinergic basal forebrain neurons in the rat. *Brain Res.* **590,** 350–355.
3. Pioro, E. P. and Cuello, A. C. (1990) Distribution of nerve growth factor receptor-like immunoreactivity in the adult rat central nervous system. Effect of colchicine and correlation with the cholinergic system—II. Brainstem, cerebellum, and spinal cord. *Neuroscience* **34,** 89–110.
4. Pioro, E. C. and Cuello, A. C. (1988) Purkinje cells of adult rat cerebellum express nerve growth factor immunoreactivity: Light microscopic observations. *Brain Res.* **455,** 182–186.
5. Pioro, E. P. and Cuello, A. C. (1990) Distribution of nerve growth factor receptor-like immunoreactivity in the adult rat central nervous system. Efect of colchicine and correlation with the cholinergic system—I. Forebrain. *Neuroscience* **34,** 57–87.
6. Batchelor, P. E., Armstrong, D. M., Blakler, S. N., and Gage, F. H. (1989) Nerve growth factor receptor and choline acetyltransferase colocalization in neurons

within the rat forebrain: Response to fimbria-fornix transection. *J. Comp. Neurol.* **284,** 187–204.
7. Heckers, S., Ohtake, T., Wiley, R. G., Lappi, D. A., Geula, C., and Mesulam, M.-M. (1994) Complete and selective cholinergic denervation of rat neocortex and hippocampus but not amygdala by an immunotoxin against the p75 NGF receptor. *J. Neurosci.* **14,** 1271–1289.
8. Whitehouse, P. J., Price, D. L., Clark, A. W., Coyle, J. T., and DeLong, M. R. (1981) Alzheimer disease: Evidence for selective loss of cholinergic neurons in the nucleus basalis. *Ann. Neurol.* **10,** 122–126.
9. Everitt, B. J. and Robbins, T. W. (1997) Central cholinergic systems and cognition. *Ann. Rev. Psychol.* **48,** 649–684.
10. Baxter, M. G. and Chiba, A. A. (1999) Cognitive functions of the basal forebrain. *Curr. Opin. Neurobiol.* **9,** 178–183.
11. Fibiger, H. C. (1982) The organization and some projections of cholinergic neurons of the mammalian forebrain. *Brain Res. Rev.* **4,** 327–388.
12. Bigl, V., Woolf, N. J., and Butcher, L. L. (1982) Cholinergic projections from the basal forebrain to frontal, parietal, temporal, occipital, and cingulate cortices: A combined fluorescent tracer and acetylcholinesterase analysis. *Brain Res. Bull.* **8,** 727–749.
13. Gaykema, R. P. A., van Weeghel, R., Hersh, L. B., and Luiten, P. G. M. (1991) Prefrontal cortical projections to the cholinergic neurons in the basal forebrain. *J. Comp. Neurol.* **303,** 563–583.
14. Gaykema, R. P. A., Luiten, P. G. M., Nyakas, C., and Traber, J. (1990) Cortical projection patterns of the medial septum-diagonal band complex. *J. Comp. Neurol.* **293,** 103–124.
15. Grove, E. A. (1988) Neural associations of the substantia innominata in the rat: Afferent connections. *J. Comp. Neurol.* **277,** 315–346.
16. Grove, E. A. (1988) Efferent connections of the substantia innominata in the rat. *J. Comp. Neurol.* **277,** 347–364.
17. Peterson, G. M. (1994) Diferential projections to the hippocampus by neurons of the medial septum and vertical limb of the diagonal band. *Brain Res.* **646,** 129–134.
18. Mesulam, M.-M., Mufson, E. J., Wainer, B. H., and Levey, A. I. (1983) Central cholinergic pathways in the rat: An overview based on an alternative nomenclature (Ch1-Ch6). *Neuroscience* **10,** 1185–1201.
19. Wainer, B. H. and Mesulam, M.-M. (1990) Ascending cholinergic pathways in the rat brain, in *Brain Cholinergic Systems* (Steriade, M. and Biesold, D., eds.), Oxford University Press, Oxford, pp. 65–119.
20. Koliatsos, V. E., Martin, L. J., and Price, D. L. (1990) Efferent organization of the mammalian basal forebrain, in *Brain Cholinergic Systems* (Steriade, M. and Biesold, D., eds.), Oxford University Press, Oxford, pp. 120–152.
21. Johnston, M. V., McKinney, M., and Coyle, J. T. (1981) Neocortical cholinergic innervation: A description of extrinsic and intrinsic components in the rat. *Exp. Brain Res.* **43,** 159–172.

22. Mesulam, M.-M., Mufson, E. J., Levey, A. I., and Wainer, B. H. (1983) Cholinergic innervation of cortex by the basal forebrain: Cytochemistry and cortical connections of the septal area, diagonal band nuclei, nucleus basalis (substantia innominata), and hypothalamus in the rhesus monkey. *J. Comp. Neurol.* **214,** 170–197.
23. Gritti, I., Mainville, L., Mancia, M., and Jones, B. E. (1997) GABAergic and other noncholinergic basal forebrain neurons, together with cholinergic neurons, project to the mesocortex and isocortex in the rat. *J. Comp. Neurol.* **383,** 163–177.
24. Rye, D. B., Wainer, B. H., Mesulam, M.-M., Mufson, E. J., and Saper, C. B. (1984) Cortical projections arising from the basal forebrain: A study of cholinergic and noncholinergic components employing combined retrograde tracing and immunohistochemical localization of choline acetyltransferase. *Neuroscience* **13,** 627–643.
25. Wainer, B. H., Levey, A. I., Rye, D. B., Mesulam, M.-M., and Mufson, E. J. (1985) Cholinergic and non-cholinergic septohippocampal pathways. *Neurosci. Lett.* **54,** 45–52.
26. Zaborszky, L., Gaykema, R. P., Swanson, D. J., and Cullinan, W. E. (1997) Cortical input to the basal forebrain. *Neurosci.* **79,** 1051–1078.
27. Markowska, A. L., Wenk, G. L., and Olton, D. S. (1990) Nucleus basalis magnocellularis and memory: Differential effects of two neurotoxins. *Behav. Neural Biol.* **54,** 13–26.
28. Dunnett, S. B., Whishaw, I. Q., Jones, G. H., and Bunch, S. T. (1987) Behavioural, biochemical and histochemical effects of different neurotoxic amino acids injected into nucleus basalis magnocellularis of rats. *Neuroscience* **20,** 653–669.
29. Page, K. J., Everitt, B. J., Robbins, T. W., Marston, H. M., and Wilkinson, L. S. (1991) Dissociable effects on spatial maze and passive avoidance acquisition and retention following AMPA- and ibotenic acid-induced excitotoxic lesions of the basal forebrain in rats: Differential dependence on cholinergic loss. *Neuroscience* **43,** 457–472.
30. Wenk, G. L., Harrington, C. A., Tucker, D. A., Rance, N. E., and Walker, L. C. (1992) Basal forebrain lesions and memory: A biochemical, histological, and behavioral study of differential vulnerability to ibotenate and quisqualate. *Behav. Neurosci.* **106,** 909–923.
31. Wenk, G. L., Markowska, A. L., and Olton, D. S. (1989) Basal forebrain lesions and memory: Alterations in neurotensin, not acetylcholine, may cause amnesia. *Behav. Neurosci.* **103,** 765–769.
32. Eva, C., Fabrazzo, M., and Costa, E. (1987) Changes of cholinergic, noradrenergic and serotonergic synaptic transmission indices elicited by ethylcholine aziridinium ion (AF64A) infused intraventricularly. *J. Pharmacol. Exp. Ther.* **241,** 181–186.
33. Chrobak, J. J., Hanin, I., Schmechel, D. E., and Walsh, T. J. (1988) AF64A-induced working memory impairment: behavioral, neurochemical and histological correlates. *Brain Res.* **463,** 107–117.
34. Jarrard, L. E., Kant, G. J., Meyerhoff, J. L., and Levy, A. (1984) Behavioral and neurochemical effects of intraventricular AF64A administration in rats. *Pharmacol. Biochem. Behav.* **21,** 273–280.

35. Nakamura, S., Tani, Y., Maezono, Y., Ishihara, T., and Ohno, T. (1992) Learning deficits after unilateral AF64A lesions in the rat basal forebrain: Role of cholinergic and noncholinergic systems. *Pharmacol. Biochem. Behav.* **42,** 119–130.
36. Walsh, T. J., Tilson, H. A., DeHaven, D. L., Mailman, R. B., Fisher, A., and Hanin, I. (1984) AF**64A,** a cholinergic neurotoxin, selectively depletes acetylcholine in hippocampus and cortex, and produces long-term passive avoidance and radial-arm maze deficits in the rat. *Brain Res.* **321,** 91–102.
37. Book, A. A., Wiley, R. G., and Schweitzer, J. B. (1994) 192 IgG-saporin: 1. Specific lethality for cholinergic neurons in the basal forebrain of the rat. *J. Neuropathol. Exp. Neurol.* **53,** 95–102.
38. Waite, J. J., Wardlow, M. L., Chen, A. C., Lappi, D. A., Wiley, R. G., and Thal, L. J. (1994) Time course of cholinergic and monoaminergic changes in rat brain after immunolesioning with 192 IgG-saporin. *Neurosci. Lett.* **169,** 154–158.
39. Waite, J. J., Chen, A. D., Wardlow, M. L., Wiley, R. G., Lappi, D. A., and Thal, L. J. (1995) 192 immunoglobulin G-saporin produces graded behavioral and biochemical changes accompanying the loss of cholinergic neurons of the basal forebrain and cerebellar Purkinje cells. *Neuroscience* **65,** 463–476.
40. Walsh, T. J., Kelly, R. M., Dougherty, K. D., Stackman, R. W., Wiley, R. G., and Kutscher, C. L. (1995) Behavioral and neurobiological alterations induced by the immunotoxin 192–IgG-saporin: Cholinergic and non-cholinergic effects following i.c.v. injection. *Brain Res.* **702,** 233–245.
41. Walsh, T. J., Herzog, C. D., Gandhi, C., Stackman, R. W., and Wiley, R. G. (1996) Injection of 192 IgG-saporin into the medial septum produces cholinergic hypofunction and dose-dependent working memory deficits. *Brain Res.* **726,** 69–79.
42. Wenk, G. L., Stoehr, J. D., Quintana, G., Mobley, S., and Wiley, R. G. (1994) Behavioral, biochemical, histological and electrophysiological effects of 192 IgG-saporin injections into the basal forebrain of rats. *J. Neurosci.* **14,** 5986–5995.
43. Baxter, M. G. and Gallagher, M. (1997) Cognitive effects of selective loss of basal forebrain cholinergic neurons: Implications for cholinergic therapies of Alzheimer's disease, in *Pharmacological Treatment of Alzheimer's Disease: Molecular and Neurobiological Foundations* (Brioni, J. D. and Decker, M. W., eds.), Wiley, New York, pp. 87–103.
44. Hagan, J. J., Salamone, J. D., Simpson, J., Iversen, S. D., and Morris, R. G. M. (1988) Place navigation in rats is impaired by lesions of medial septum and diagonal band but not nucleus basalis magnocellularis. *Behav. Brain Res.* **27,** 9–20.
45. Hepler, D. J., Olton, D. S., Wenk, G. L., and Coyle, J. T. (1985) Lesions in nucleus basalis magnocellularis and medial septal area of rats produce qualitatively similar memory impairments. *J. Neurosci.* **5,** 866–873.
46. Bartus, R. T., Flicker, C., Dean, R. L., III, Pontecorvo, M., Figueiredo, J. C., and Fisher, S. K. (1985) Selective memory loss following nucleus basalis lesions: Long term behavioral recovery despite persistent cholinergic deficiencies. *Pharmacol. Biochem. Behav.* **23,** 125–135.

47. Kesner, R. P., Adelstein, T., and Crutcher, K. A. (1987) Rats with nucleus basalis magnocellularis lesions mimic mnemonic symptomatology observed in patients with dementia of the Alzheimer's type. *Behav. Neurosci.* **101,** 451–456.
48. Winkler, J., Suhr, S. T., Gage, F. H., Thal, L. J., and Fisher, L. J. (1995) Essential role of neocortical acetylcholine in spatial memory. *Nature* **375,** 484–487.
49. Baxter, M. G., Bucci, D. J., Gorman, L. K., Wiley, R. G., and Gallagher, M. (1995) Selective immunotoxic lesions of basal forebrain cholinergic cells: Effects on learning and memory in rats. *Behav. Neurosci.* **109,** 714–722.
50. Berger-Sweeney, J., Heckers, S., Mesulam, M.-M., Wiley, R. G., Lappi, D. A., and Sharma, M. (1994) Differential effects on spatial navigation of immunotoxin-induced cholinergic lesions of the medial septal area and nucleus basalis magnocellularis. *J. Neurosci.* **14,** 4507–4519.
51. Baxter, M. G., Bucci, D. J., Sobel, T. J., Williams, M. J., Gorman, L. K., and Gallagher, M. (1996) Intact spatial learning following lesions of basal forebrain cholinergic neurons. *NeuroReport* **7,** 1417–1420.
52. Torres, E. M., Perry, T. A., Blokland, A., Wilkinson, L. S., Wiley, R. G., Lappi, D. A., et al. (1994) Behavioural, histochemical and biochemical consequences of selective immunolesions in discrete regions of the basal forebrain cholinergic system. *Neuroscience* **63,** 95–122.
53. Dornan, W. A., McCampbell, A. R., Tinkler, G. P., Hickman, L. J., Bannon, A. W., Decker, M. W., et al. (1996) Comparison of site-specific injections into the basal forebrain on water maze and radial arm maze performance in the male rat after immunolesioning with 192 IgG saporin. *Behav. Brain Res.* **82,** 93–101.
54. Leanza, G., Nilsson, O. G., Wiley, R. G., and Björklund, A. (1995) Selective lesioning of the basal forebrain cholinergic system by intraventricular 192 IgG-saporin: Behavioural, biochemical and stereological studies in the rat. *Eur. J. Neurosci.* **7,** 329–343.
55. Nilsson, O. G., Leanza, G., Rosenblad, C., Lappi, D. A., Wiley, R. G., and Björklund, A. (1992) Spatial learning impairments in rats with selective immunolesion of the forebrain cholinergic system. *NeuroReport* **3,** 1005–1008.
56. Leanza, G., Nilsson, O. G., Nikkhah, G., Wiley, R. G., and Björklund, A. (1996) Effects of neonatal lesions of the basal forebrain cholinergic system by 192 immunoglobulin G-saporin: Biochemical, behavioural and morphological characterization. *Neurosci.* **74,** 119–141.
57. Winkler, J., Thal, L. J., Gage, F. H., and Fisher, L. J. (1998) Cholinergic strategies for Alzheimer's disease. *J. Mol. Med.* **76,** 555–67.
58. Wrenn, C. C. and Wiley, R. G. (1998) The behavioral functions of the cholinergic basal forebrain: Lessons from 192 IgG-saporin. *Int. J. Dev. Neurosci.* **16,** 595–602.
59. Schultz, W., Studer, A., Romo, R., Sundstrom, E., Jonsson, G., and Scarnati, E. (1989) Deficits in reaction times and movement times as correlates of hypokinesia in monkeys with MPTP-induced striatal dopamine depletion. *J. Neurophysiol.* **61,** 651–668.
60. Waite, J. J., Wardlow, M. L., and Power, A. E. (1999) Deficit in selective and divided attention associated with cholinergic basal forebrain immunotoxic lesion

produced by 192-saporin; motoric/sensory deficit associated with Purkinje cell immunotoxic lesion produced by OX7-saporin. *Neurobiol. Learn. Mem.* **71,** 325–352.
61. Steckler, T., Keith, A. B., Wiley, R. G., and Sahgal, A. (1995) Cholinergic lesions by 192 IgG-saporin and short-term recognition memory: Role of the septohippocampal pathway. *Neuroscience* **66,** 101–114.
62. Leanza, G., Muir, J., Nilsson, O. G., Wiley, R. G., Dunnett, S. B., and Björklund, A. (1996) Selective immunolesioning of the basal forebrain cholinergic system disrupts short-term memory in rats. *Eur. J. Neurosci.* **8,** 1535–1544.
63. McDonald, M. P., Willard, L. B., Wenk, G. L., and Crawley, J. N. (1998) Coadministration of galanin antagonist M40 with a muscarinic M1 agonist improves delayed nonmatching to position choice accuracy in rats with cholinergic lesions. *J. Neurosci.* **18,** 5078–5085.
64. Baxter, M. G., Holland, P. C., and Gallagher, M. (1997) Disruption of decrements in conditioned stimulus processing by selective removal of hippocampal cholinergic input. *J. Neurosci.* **17,** 5230–5236.
65. Chiba, A. A., Bucci, D. J., Holland, P. C., and Gallagher, M. (1995) Basal forebrain cholinergic lesions disrupt increments but not decrements in conditioned stimulus processing. *J. Neurosci.* **15,** 7315–7322.
66. McGaughy, J., Kaiser, T., and Sarter, M. (1996) Behavioral vigilance following infusions of 192 IgG-saporin into the basal forebrain: Selectivity of the behavioral impairment and relation to cortical AChE-positive fiber density. *Behav. Neurosci.* **110,** 247–265.
67. Perry, E. K., Tomlinson, B. E., Blessed, G., Bergmann, K., Gibson, P. H., and Perry, R. H. (1978) Correlation of cholinergic abnormalities with senile plaques and mental test scores in senile dementia. *Brit. Med. J.* **2,** 1457–1459.
68. Etienne, P., Robitaille, Y., Wood, P., Gauthier, S., Nair, N. P. V., and Quirion, R. (1986) Nucleus basalis neuronal loss, neuritic plaques and choline acetyltransferase activity in advanced Alzheimer's disease. *Neuroscience* **19,** 1279–1291.
69. Bierer, L. M., Haroutunian, V., Gabriel, S., Knott, P. J., Carlin, L. S., Purohit, D. P., et al. (1995) Neurochemical correlates of dementia severity in Alzheimer's disease: Relative importance of the cholinergic deficits. *J. Neurochem.* **64,** 749–760.
70. Hepler, D. J., Wenk, G. L., Cribbs, B. L., Olton, D. S., and Coyle, J. T. (1985) Memory impairments following basal forebrain lesions. *Brain Res.* **346,** 8–14.
71. Janis, L. S., Bishop, T. W., and Dunbar, G. L. (1994) Medial septal lesions in rats produce permanent deficits for strategy selection in a spatial memory task. *Behav. Neurosci.* **108,** 892–898.
72. Shen, J., Barnes, C. A., Wenk, G. L., and McNaughton, B. L. (1996) Differential effects of selective immunotoxic lesions of medial septal cholinergic cells on spatial working and reference memory. *Behav. Neurosci.* **110,** 1181–1186.
73. McMahan, R. W., Sobel, T. J., and Baxter, M. G. (1997) Selective immunolesions of hippocampal cholinergic input fail to impair spatial working memory. *Hippocampus* **7,** 130–136.

74. Chappell, J., McMahan, R., Chiba, A., and Gallagher, M. (1998) A re-examination of the role of basal forebrain cholinergic neurons in spatial working memory. *Neuropharmacology* **37,** 481–487.
75. Dougherty, K. D., Turchin, P. I., and Walsh, T. J. (1998) Septocingulate and septohippocampal cholinergic pathways: Involvement in working/episodic memory. *Brain Res.* **810,** 59–71.
76. Fine, A., Hoyle, C., Maclean, C. J., Levatte, T. L., Baker, H. F., and Ridley, R. M. (1997) Learning impairments following injection of a selective cholinergic immunotoxin, ME20.4 IgG-saporin, into the basal nucleus of Meynert in monkeys. *Neuroscience* **81,** 331–343.
77. Mrzljak, L., Levey, A. I., Belcher, S., and Goldman-Rakic, P. S. (1998) Localization of the m2 muscarinic acetylcholine receptor protein and mRNA in cortical neurons of the normal and cholinergically deafferented rhesus monkey. *J. Comp. Neurol.* **390,** 112–32.
78. Ridley, R. M., Barefoot, H. C., Maclean, C. J., Pugh, P., and Baker, H. F. (1999) Different effects on learning ability after injection of the cholinergic immunotoxin ME20.4IgG-saporin into the diagonal band of Broca, basal nucleus of Meynert, or both in monkeys. *Behav. Neurosci.* **113,** 303–315.
79. Freund, T. F. (1989) GABAergic septohippocampal neurons contain parvalbumin. *Brain Res.* **478,** 375–381.
80. Paul, C. A., Beltz, B., and Berger-Sweeney, J., eds. (1997). *Discovering Neurons: The Experimental Basis of Neurosci.* Cold Spring Harbor Laboratory Press, Cold Spring Harbor, NY.
81. Crawley, J., Gerfen, C., McKay, R., Rogawski, M., Sibley, D., and Skolnick, P., eds. (1997–99). *Current Protocols in Neurosci.* John Wiley & Sons, New York.
82. Holley, L. A., Wiley, R. G., Lappi, D. A., and Sarter, M. (1994) Cortical cholinergic deafferentation following the intracortical infusion of 192 IgG-saporin: A quantitative histochemical study. *Brain Res.* **663,** 277–286.
83. McGaughy, J. and Sarter, M. (1998) Sustained attention performance in rats with intracortical infusions of 192 IgG-saporin-induced cortical cholinergic deafferentation: Effects of physostigmine and FG 7142. *Behav. Neurosci.* **112,** 1519–1525.
84. Bucci, D. J., Holland, P. C., and Gallagher, M. (1998) Removal of cholinergic input to rat posterior parietal cortex disrupts incremental processing of conditioned stimuli. *J. Neurosci.* **18,** 8038–8046.

17

Targeting Toxins to Neural Antigens and Receptors

Ronald G. Wiley

1. Introduction

This chapter describes the use of antineuronal immunotoxins to make selective neural lesions. The immunotoxin approach (immunolesioning) has significantly advanced the art of making neural lesions, combining the selectivity of monoclonal immunotoxins with various behavioral, neuroanatomic, neuropharmacologic, and neurophysiologic techniques to analyze the consequences of destroying highly selected neural populations ***(1,2)***. Assessing the effects of neural lesions is a time-honored and effective way to analyze structure–function relationships in the nervous system. Although only a few antineuronal immunotoxins have been described to date, it is clear that this is an analytically powerful improvement in the lesion-making art with great promise for bridging from molecular to systems neuroscience.

The first antineuronal immunotoxin to be developed was OX7–saporin which is directed at rat Thy 1, an abundant surface protein on all adult neurons. OX7–saporin injected subepineurally into the vagus nerve is taken up and axonally transported to the cell bodies of motor and sensory neurons that project through the injected nerve, resulting in selective destruction of just those neurons (suicide transport). Similarly, when injected into the striatum, OX7–saporin is taken up by terminals of nigrostriatal neurons and retrogradely transported to the perikarya in the pars compacta of the substantia nigra, where the saporin acts to kill just those neurons ***(3)***. Interestingly, intracerebroventricular injection of OX7–saporin preferentially destroys cerebellar Purkinje neurons, probably due to the high levels of Thy 1 expressed by these cells and the propensity of Purkinje cells to take up substances from the cerebrospinal fluid ***(4)***. Thus, OX7–saporin can be used to cause acute Purkinje cell degeneration. Some examples of suicide transport of OX7–saporin include a study of

From: *Methods in Molecular Biology, vol. 166: Immunotoxin Methods and Protocols*
Edited by: W. A. Hall © Humana Press Inc., Totowa, NJ

the cellular localization of dopamine receptors in the striatum ***(5)*** and selective destruction of the sensory innervation of the knee joint ***(6)***.

192 IgG–saporin was specifically made to model in rats a key feature of Alzheimer's disease. The monoclonal antibody 192 IgG recognizes p75, the low-affinity neurotrophin receptor ***(7)***. 192 IgG–ricin A-chain was reported to be active in vitro, but not in vivo ***(8)***. However, as previously described for OX7 ***(9)***, we found that saporin made an immunotoxin that was more effective than ricin A-chain in vivo. In the adult rat forebrain, the only neurons that express high levels of p75 are the cholinergic neurons of the basal forebrain, a special group of neurons that degenerate in Alzheimer's disease. Injection of 192 IgG into the lateral cerebral ventricles results in selective uptake and concentration of the antibody in the cholinergic basal forebrain (CBF) neurons ***(10,11)***. Intracerebroventricular (i.c.v.) injection of 192 IgG–saporin selectively destroys the CBF ***(12)***. Numerous studies have used rats treated with 192 IgG–saporin to analyze the effects of CBF lesions on behavior ***(13)*** and documented the extraordinary specificity of the lesions ***(14)***. The only caveat to date has been the destruction of some cerebellar Purkinje neurons with i.c.v. doses of 192 IgG–saporin sufficient to produce high-grade CBF lesions ***(15)***. Control experiments using i.c.v. OX7–saporin to produce comparable Purkinje cell loss have provided information on the contribution of the cerebellar damage to motor performance and behavioral deficits in various learning and memory paradigms ***(15,16)***. 192 IgG–saporin only works in rats, but recently, a similar immunotoxin using a different monoclonal antibody to the same antigen has been reported effective in primates ***(17,18)***, which should lead to even more revealing studies of CBF function.

Anti–dopamine β-hydroxylase–saporin (anti-DβH-saporin) was developed to selectively destroy neurons that express DβH, the enzyme that converts dopamine to norepinephrine (i.e., noradrenergic and adrenergic neurons). Systemic injection of anti–DβH-saporin produces widespread damage to the sympathetic nervous system ***(19–21)***, and i.c.v. injections very readily destroy pontine noradrenergic neurons ***(22)***. More recently, local injection of anti-DβH-saporin has been used to selectively ablate the noradrenergic innervation of the olfactory bulb ***(23)***, and spinal intrathecal injection of anti-DβH-saporin destroys the noradrenergic innervation of the spinal cord ***(24)***. In both cases, the immunotoxin is taken up by noradrenergic terminals that have DβH on the surface, and retrogradely transported to the cell bodies in the pons with destruction of just those neurons. Spinal injections promise to be of great interest in studies of pain perception. Anti–DβH-saporin is effective in a wide range of species.

Lastly, an immunotoxin to the dopamine transporter that is selectively expressed by midbrain dopaminergic neurons has been reported ***(25)***. Injection of this immunotoxin i.c.v. produces a lesion that closely resembles Parkinson's

disease (Wiley, Harrison, Levey, and Lappi, unpublished results). Species specificity of this immunotoxin has not been determined.

The general approach to the use of antineuronal immunotoxins is first to choose an immunotoxin with the appropriate specificity for the desired target neural population. Then, the route of administration (systemic, intrathecal, intraparenchymal, intraneural) and dose have to be carefully chosen to deliver adequate amounts of toxin in such a way as to achieve the desired anatomic distribution of cell loss. In general, systemically administered immunotoxins do not penetrate the central nervous system (CNS) sufficiently to produce significant cell loss, and conversely, the doses used for intraparenchymal and intrathecal injections do not produce detectable cell loss outside the CNS. Usually, pilot experiments are needed to determine the optimal dose, injection site, and volume of injection for the desired lesion (*see* **Note 1**). These choices are particularly critical if the goal is to completely destroy a target neural population without significant collateral damage to nontarget neurons. General considerations, regardless of the specific immunotoxin and target, include: careful handling to avoid microbial contamination which will cause loss of potency; precise control of dose and location of injections; awareness of the delay (2–7 d) to onset of failure of neuronal function and the delay to complete dissolution of target neurons (10–14 d); appreciation of the occurrence of secondary (transsynaptic) effects of the primary lesion (usually delayed); and the importance of anatomic confirmation of the extent of the lesion in each subject. Anatomic confirmation of the extent and specificity of the neural lesions typically requires the use of markers for both the target and nontarget neurons. Alternatively, neurchemical assays may be useful, particularly to document regional loss of specific neurotransmitters associated with the target neural population and sparing of nontarget neurotransmitter systems.

2. Materials

2.1 Immunotoxins

All of the immunotoxins currently available are from Advanced Targeting Systems (San Diego, CA). The technique used to construct the immunotoxins is previously described ***(26)***. The toxins are supplied in sterile frozen solutions of phosphate-buffered normal saline. Preservatives are not included because they are chemically incompatible with the immunotoxins. It is prudent to use sterile technique in handling toxin, to store the stock solution frozen in aliquots to minimize freezing and thawing cycles, and to keep working dilutions on ice. The precise shelf life of frozen immunotoxin is not known, but we have had success with immunotoxins stored for several years. We have experienced loss of activity of 192 IgG–saporin after 6–7 yr of frozen storage, but not after 3–4 yr.

2.2. Diluent

We routinely dilute the immunotoxins in sterile normal saline containing 1 mg/mL purified bovine serum albumin. For most uses, the diluent also contains 0.1% w/v Fast Green FCF dye. The albumin is included as a carrier protein for the dilute working solutions of toxin, and the dye permits visualization of exactly where the immunotoxin goes upon injection. The complete diluent solution is filter-sterilized and can be stored frozen for extended periods (years). The dye also facilitates seeing any spills. Starting with preservative-free sterile normal saline supplied for clinical use insures freedom from particulates and endotoxin contamination.

2.3. Injection Apparatus

For peripheral nerve injections, the best approach for delivering toxin is subepineurial in volumes of 200 nL–1 μL, depending on the size of the nerve.

For intraparenchymal CNS injections, the usual volumes are 100 nL–1 μL, and for intrathecal injections (intraventricular or spinal subarachnoid), 10 μL. Smaller i.c.v. volumes do not reliably yield uniform lesions.

A glass micropipet with the tip broken back to 25–50 μm diameter and connected to a water-filled Hamilton microsyringe by water-filled PE-10 tubing can be used for controlled volume injections. Mounting the pipet in a fully adjustable stereotactic electrode holder (David Kopf, Tujunga, CA) works well both for intracranial and peripheral nerve injections. Spinal intrathecal injections are typically made using stretched PE-10 tubing marked to the appropriate length and passed down the spinal subarachnoid space from an incision in the atlanto-occipital membrane. In all cases, the injection pipet or catheter is left in place for 10–15 min after toxin injection is complete.

3. Methods

3.1. Selection of Immunotoxin

This requires knowledge of the differential expression of a suitable target protein by the neural population of interest. Although only four immunotoxins are currently available, Advanced Targeting Systems also offers custom synthesis of new immunotoxins. The crucial considerations are:

1. The monoclonal targeting antibody must recognize an external surface epitope. Intracellular molecules or intracellular domains of surface molecules are not worthwhile targets.
2. The target of the antibody must be selectively expressed by the neural population of interest and not by adjacent neurons.
3. The site of injection must be selected with care. Restricted local injection of an immunotoxin to a peripheral nerve or intraparenchymal CNS site may result in a

localized lesion, in spite of the presence of other distant neurons that express the same target antigen. On the other hand, i.c.v. or spinal subarachnoid injection may result in extensive spread of the immunotoxin over the surfaces of the brain and spinal cord but not necessarily deep into the parenchyma.

3.2. Pretesting Animals

It is often desirable to pretest animals on functional or behavioral measures expected to be affected by the toxin-induced lesion. This can provide a basis for allocation of subjects to treatment groups and will enhance the sensitivity for detecting functional/behavioral changes after toxin injection. A good example is studies with 192 IgG–saporin that require extensive training on a radial maze task. Rats were first trained to stable performance then ranked by quartiles; equal numbers of rats from each quartile were allocated to each of four treatment groups. After toxin or vehicle injection, the animals were again tested until they reached stable performance levels.

3.3. Toxin Injection

The immunotoxins always require dilution before intracranial or peripheral nerve injections. We routinely make the working dilution the day of injection and keep it on ice until all injections are completed and then dispose of any remaining. The stability of very dilute immunotoxins has not been thoroughly characterized. We have encountered loss of potency with dilute neuropeptide–saporin conjugates that were reused after frozen storage. We have reused dilute immunotoxins, but prudent lab practice would favor making working dilutions fresh each day.

Toxin injections generally need to be accurately located with precise control over volume of the injections. For this purpose, 10 μL–25 μL Hamilton microsyringes serve well. These syringes can be mounted directly into a stereotactic electrode holder or attached by thin polyethylene tubing to glass micropipets drawn from volumetric capillary pipet tubing. The polyethylene tubing is glued to the glass pipet with epoxy, and the tip is broken back to 25 μm–50 μm diameter. The dye in the toxin solution permits ready visualization of the progress of the injection, and with peripheral nerve injections, visualization of spread of the toxin solution at the injection site.

3.4. Posttoxin Testing

Neuronal failure after toxin injection evolves over 2–7 d. Therefore, functional performance measures during the first week after toxin injection may not reflect the full effect of the lesion. Primary (direct) functional, anatomic, neurochemical, and neuropharmacologic effects of the lesion of the target population need to be distinguished from secondary (transsynaptic) effects on

nontarget populations (*see* **Note 2**). Typically, the secondary effects occur later than primary effects *(27)*. The initial approach to separating primary and secondary effects is to make assessments repeatedly over time beginning 2–3 d after toxin injection and continuing for as much as six months, depending on the experimental goals.

"Collateral" damage to nontarget populations can occur if the extracellular saporin concentration is too high, or if the nontarget population expresses the target antigen. The problem of excessive saporin concentration most often is a concern with intraparenchymal injections. Reducing the concentration of immunotoxin, reducing the dose at each injection site, and using multiple small, low-dose injections spread throughout the target can reduce the problem of nonspecific toxicity from excessive saporin concentration. Obviously, if collateral damage is due to binding of the immunotoxin to nontarget neurons, then changing immunotoxin is the first solution to consider. Selectively inhibiting binding or endocytosis of immunotoxin by nontarget neurons is theoretically possible but has not been reported.

3.5. Lesion Assessment

In order to determine the extent of target neuron loss, specific anatomic or biochemical markers are needed for the target neurons (*see* **Note 3**). Obviously, the monoclonal antibody used in the immunotoxin can be used for immunohistochemical staining of any surviving target neurons (*see* **Note 4**). This strategy should not be applied in less than 2 wk after toxin injection to permit complete dissolution of poisoned target neurons. Surrogate markers (i.e., substances known to be selectively localized to the target neurons) can also be used for immunohistochemical or neurochemical studies.

Similarly, specific binding of a radioactive ligand to target neurons can be used to estimate the extent of lesion. An example of this last strategy is the use of ^{3}H-mazindol binding to striatal sections of rats injected i.c.v. with various doses of anti–DAT-saporin. Mazindol binds to the dopamine transporter, which is the target molecule of the immunotoxin. Autoradiographs of striatal tissue sections incubated with ^{3}H-mazindol give quantitative estimates of the loss of dopaminergic terminals from the striatum, because the nigrostriatal dopaminergic neurons were destroyed by the immunotoxin (Wiley, Harrison, Levey, and Lappi, unpublished results).

Evaluation of nontarget neurons can be an unending task. Anatomic assessment must use markers not expressed by the target population. Neurochemical studies can assay neurotransmitter systems specifically expressed by nontarget neurons but not the target population. Obviously, there can be a very large number of options in any particular situation. Care is necessary in choosing which nontarget neurons to evaluate. Most often, it is appropriate to evaluate at

least some adjacent neural populations close to the target or intermingled with target neurons, but other choices typically depend on the specifics of the experiment and the target neurons.

4. Notes

1. It is essential to perform a series of pilot studies to determine the optimal range of doses and routes of administration for particular target neurons. Obviously, the goals of the experiment will have important bearing on the final choices of dose and administration route. Skipping this step can result in considerable wasted effort.
2. Sometimes, secondary (transsynaptic) plastic changes are the principal dependent variables, but in all cases, they need to be taken into consideration. Collecting multiple data points before and at various intervals after toxin injection may reveal the evolution of secondary changes that typically come after the primary effects of the lesion. Another important consideration is the need for a control lesion. In some situations, it is not enough to do sham surgery or inject vehicle or prereduced immunotoxin that contains both antibody and saporin not coupled to one another, because none of these includes selective loss of neurons. Thus, it may be important to produce a lesion using another approach, such as a different immunotoxin, excitotoxin, or surgical lesion, that will cause loss of a different neural population. Also, using more than one dose of immunotoxin (experimental or control) can be valuable.
3. Confirming the extent of target neuron loss in each individual animal is an essential and powerful experimental design component when using antineuronal immunotoxins. The most commonly used quantitative approaches include counting labeled neurons and neurochemical assays relevant to the target neurons, such as assays for neurotransmitter levels or enzyme activities. Correlations between the extent of target neuron loss and functional changes over a range of immunotoxin doses can strengthen conclusions regarding causality much as dose–response relationships do in pharmacology. Sometimes such correlations reveal unexpected relationships that extend beyond the original aim of the experiment ***(28)***.
4. There are two alternatives in cases where no appropriate monoclonal antibody exists to target a particular neural population. Lectins, ricin, abrin, modeccin, and volkensin can be used without modification to produce anatomically restricted lesions by retrograde axonal transport of toxin from an injection site (suicide transport) ***(1,2)***. Also, neuropeptides have recently been shown effective in targeting saporin to cells that express receptors for a specific neuropeptide, such as substance P ***(29,30)***.

Acknowledgments

This work was supported by the Department of Veterans Affairs, Research Service. The authors wish to acknowledge the skilled technical assistance of Brenda Evans.

References

1. Wiley, R. G. (1992) Neural lesioning with ribosome-inactivating proteins: suicide transport and immunolesioning. *Trends Neurosci.* **15,** 285–290.
2. Wiley, R. G. and Lappi, D. A. (1994) *Suicide Transport and Immunolesioning.* R. G. Landes, Austin, TX.
3. Wiley, R. G., Stirpe, F., Thorpe, P., and Oeltmann, T. N. (1989) Neuronotoxic effects of monoclonal anti-Thy 1 antibody (OX7) coupled to the ribosome inactivating protein, saporin, as studied by suicide transport experiments in the rat. *Brain Res.* **505,** 44–54.
4. Davis, T. L. and Wiley, R. G. (1989) Anti-Thy 1 immunotoxin, OX7-saporin, destroys cerebellar Purkinje cells after intraventricular injection. *Brain Res.* **504,** 216–222.
5. Harrison, M. B., Wiley, R. G., and Wooten, G. F. (1992) Changes in D2 but not D1 receptor binding in the striatum following a selective lesion of striatopallidal neurons. *Brain Res.* **590,** 305–310.
6. Salo, P. T., Theriault, E., and Wiley, R. G. (1997) Selective ablation of rat knee joint innervation with injected immunotoxin: a potential new model for the study of neuropathic arthritis. *J. Orthop. Res.* **15,** 622–628.
7. Chandler, C. E., Parsons, L. M., Hosang, M., and Shooter, E. M. (1984) A monoclonal antibody modulates the interaction of nerve growth factor with PC12 cells. *J. Biol. Chem.* **259,** 6882–6889.
8. DiStefano, P. S., Schweitzer, J. B., Taniuchi, M., and Johnson, E. M. J. (1985) Selective destruction of nerve growth factor receptor-bearing cells in vitro using a hybrid toxin composed of ricin A chain and a monoclonal antibody against the nerve growth factor receptor. *J. Cell Biol.* **101,** 1107–1114.
9. Thorpe, P. E., Brown, A. N. F., Bremner, J. A. G., Foxwell, B. M. J., and Stirpe, F. (1985) An immunotoxin composed of monoclonal anti-Thy 1.1 antibody and a ribosome-inactivating protein from *Saponaria officinalis:* potent antitumor effects in vitro and in vivo. *J. Nat. Canc. Inst.* **75,** 151–159.
10. Schweitzer, J. B. (1987) Nerve growth factor receptor-mediated transport from cerebrospinal fluid to basal forebrain neurons. *Brain Res.* **423,** 309–317.
11. Schweitzer, J. B. (1989) Nerve growth factor receptor-mediated transport from CSF labels cholinergic neurons: direct demonstration by a double-labeling study. *Brain Res.* **490,** 390–396.
12. Wiley, R. G., Oeltmann, T. N., and Lappi, D. A. (1991) Immunolesioning: selective destruction of neurons using immunotoxin to rat NGF receptor. *Brain Res.* **562,** 149–153.
13. Wrenn, C. C. and Wiley, R. G. (1998) The behavioral functions of the cholinergic basal forebrain: lessons from 192 IgG-SAPORIN. *Int. J. Dev. Neurosci.* **16,** 595–602.
14. Wiley, R. G. (1997) Findings about the cholinergic basal forebrain using immunotoxin to the nerve growth factor receptor. *Ann. NY Acad. Sci.* **835,** 20–29.
15. Waite, J. J., Chen, A. D., Wardlow, M. L., Wiley, R. G., Lappi, D. A., and Thal, L. J. (1995) 192 immunoglobulin G-saporin produces graded behavioral and

biochemical changes accompanying the loss of cholinergic neurons of the basal forebrain and cerebellar Purkinje cells. *Neuroscience* **65,** 463–476.
16. Wiley, R. G., Berbos, T. G., Deckwerth, T. L., Johnson, E. M. J., and Lappi, D. A. (1995) Destruction of the cholinergic basal forebrain using immunotoxin to rat NGF receptor: modeling the cholinergic degeneration of Alzheimer's disease. *J. Neurol. Sci.* **128,** 157–166.
17. Ridley, R. M., Barefoot, H. C., Maclean, C. J., Pugh, P., and Baker, H. F. (1999) Different effects on learning ability after injection of the cholinergic immunotoxin ME20.4IgG-saporin into the diagonal band of Broca, basal nucleus of Meynert, or both in monkeys. *Behav. Neurosci.* **113,** 303–315.
18. Fine, A., Hoyle, C., Maclean, C. J., Levatte, T. L., Baker, H. F., and Ridley, R. M. (1997) Learning impairments following injection of a selective cholinergic immunotoxin, ME20.4 IgG-saporin, into the basal nucleus of Meynert in monkeys. *Neuroscience* **81,** 331–343.
19. Picklo, M. J., Wiley, R. G., Lappi, D. A., and Robertson, D. A. (1995) Noradrenergic lesioning using an immunotoxin against dopamine beta-hydroxylase. *Brain Res.* **666,** 195–200.
20. Picklo, M. J., Wiley, R. G., Lonce, S., Lappi, D. A., and Robertson, D. (1995) Anti-dopamine b-hydroxylase immunotoxin-induced sympathectomy in adult rats. *J. Pharmacol. Exp. Therap.* **275,** 1003–1010.
21. Picklo, M. J., Wiley, R. G., Lappi, D. A., and Robertson, D. (1994) Noradrenergic lesioning with an anti-dopamine beta-hydroxylase immunotoxin. *Brain Res.* **666,** 195–200.
22. Wrenn, C. C., Picklo, M. J., Lappi, D. A., Robertson, D., and Wiley, R. G. (1996) Central noradrenergic lesioning using anti-DBH-saporin: anatomical findings. *Brain Res.* **740,** 175–184.
23. Blessing, W. W., Lappi, D. A., and Wiley, R. G. (1998) Destruction of locus coeruleus neuronal perikarya after injection of anti-dopamine-β-hydroxylase immunotoxin into the olfactory bulb of the rat. *Neurosci. Lett.* **243,** 85–88.
24. Martin, W. J., Gupta, N. K., Loo, C. M., Rohde, D. S., and Basbaum, A. I. (1999) Differential effects of neurotoxic destruction of descending noradrenergic pathways on acute and persistent nociceptive processing. *Pain* **80** 57–65.
25. Wiley, R. G., Brown, J., Levey, A. I., and Lappi, D. A. (1996) Destruction of midbrain dopaminergic neurons using immunotoxin to the dopamine transporter. *Abs. Soc. Neurosci.* **21,** 1732.
26. Wiley, R. G. and Lappi, D. A. Preparation of anti-neuronal immunotoxins for selective neural immunolesioning. *Neurosci. Protocols* **93–020,** 1–11.
27. Harrison, M. B., Roberts, R. C., and Wiley, R. G. (1993) A selective lesion of striatonigral neurons decreases presynaptic binding of [3H]hemicholinium-3 to striatal interneurons. *Brain Res.* **630,** 169–177.
28. Zhang, Z. J., Berbos, T. G., Wrenn, C. C., and Wiley, R. G. (1996) Loss of nucleus basalis magnocellularis, but not septal, cholinergic neurons correlates with passive avoidance impairment in rats treated with 192–saporin. *Neurosci. Lett.* **203,** 214–218.

29. Wiley, R. G. and Lappi, D. A. (1997) Destruction of neurokinin-1 receptor expressing cells in vitro and in vivo using substance P-saporin. *Neurosci. Lett.* **230,** 97–100.
30. Mantyh, P. W., Rogers, S. D., Honore, P., Allen, B. J., Ghilerdi, J. R., Li, J., et al. (1997) Ablation of lamina I spinal neurons expressing the substance P receptor profoundly inhibits hyperalgesia. *Science* **278,** 239–240.

18

In Vivo Testing of Anti-HIV Immunotoxins

Seth H. Pincus, Tamera K. Marcotte, Brent M. Forsyth, and Hua Fang

1. Introduction

The past several years have seen great optimism resulting from the deployment of highly active antiretroviral therapies for the treatment of HIV infection. Combinations of reverse transcriptase and protease inhibitors can induce suppression of viremia, reversal of immunodeficiency state, and remission from AIDS-associated illnesses. However, long-term compliance with these drug regimens is difficult because of complicated dosing schedules, cost, and drug toxicities. The development of drug-resistant HIV has also limited the effectiveness of antiviral therapies. The evolution of drug-resistant HIV is enhanced when patient compliance drops and HIV replicates in the presence of moderate concentrations of antiviral agents. Even in patients in whom there has been complete suppression of HIV replication for several years, there are persistent reservoirs of HIV-infected cells. Cessation of therapy, or even modification of the intensive drug regimens, results in the prompt reestablishment of HIV replication. Thus, despite the great improvements made in the treatment of AIDS, there is still a need for the development of new antiviral agents, particularly ones that have different modes of action than existing antivirals.

Anti-HIV immunotoxins have proven to be among the most effective anti-HIV therapies when tested in vitro ***(1–4)***, with a therapeutic index of >10,000 and reports of the elimination of HIV-infection from tissue cultures ***(5)***. The goal of immunotoxin therapy is to eliminate those cells in which HIV is actively replicating and thus remove the nidus of infection. The immunotoxins are directed to HIV-infected cells either by targeting the viral envelope protein that is expressed on the surface of HIV-infected cells ***(1–9)***, or by delivering the immunotoxin to those subsets of cells in which HIV replicates, most notably

From: *Methods in Molecular Biology, vol. 166: Immunotoxin Methods and Protocols*
Edited by: W. A. Hall © Humana Press Inc., Totowa, NJ

activated T-cells expressing the IL-2 receptor ***(10–13)***. The HIV-envelope proteins gp120 (extracellular), gp41 (transmembrane), and gp160 (precursor) may be targeted with either antienvelope monoclonal antibodies ***(1–4)*** or with soluble forms of the viral receptor CD4 ***(5–9)***.

Despite the impressive in vitro activity of anti-HIV immunotoxins, there has been little acceptance of this approach in the clinical arena, in large part due to a human trial with CD4-PE40, a chimeric fusion protein of CD4 and *Pseudomonas* exotoxin. This molecule was found to be highly toxic, and no therapeutic effect was seen at the low doses that were tolerated ***(14,15)***. We have argued that three key factors unique to CD4-PE40 played a role in its failure in clinical trials, and that the therapeutic utility of anti-HIV immunotoxins has not been fully explored ***(4)***. These factors are: 1) the high toxicity of this molecule compared to other immunotoxins used to treat cancer and autoimmunity (15 μg/kg vs >250 μg/kg for other toxins); 2) the short serum half-life of this molecule (60 min) vs antibody-targeted immunotoxins (hours to days); and 3) the target molecule (gp120 vs gp41), since the activity of anti-gp41 but not anti-gp120 immunotoxins may be enhanced as much as 100-fold by the addition of soluble CD4 without any increase in nonspecific toxicity ***(2)***. To prove our hypothesis, it will be necessary to demonstrate in an animal model that therapeutic effects may be seen with antibody-targeted anti-HIV immunotoxins and not with CD4-PE40.

The development of animal models of HIV infection has been, and continues to be, problematic. Since immunotoxins are based on anti-HIV antibodies, the animal model must be based on HIV and not other retroviruses. The model must also allow testing of many different immunotoxins, combinations, doses, and replicates in each experimental group. To accomplish this, it must be relatively inexpensive, and a reasonable number of animals must be available for study, thus ruling out simian models as an initial in vivo assay. A variety of SCID mouse models have been developed to study different aspects of HIV infection ***(16)***. Different sources of human tissue have been used, including fetal liver and thymus, peripheral blood mononuclear cells from both HIV-infected and uninfected donors, and human T-cell lymphomas. To varying degrees, these models reflect physiologic events that occur in human AIDS, including the depletion of thymic and CD4+ T-cells ***(17,18)***.

To test the activity of antiviral drugs, the SCID mouse model has proven to be less useful than was originally hoped. This is particularly true in the models with greatest physiologic relevance, where it is difficult to obtain adequate numbers of reproducibly infected mice because there is either insufficient starting material (e.g., fetal liver) or unreliable induction of infection (different donors yield different results in terms of engraftment and susceptibility to infection, and it is impossible to remove sufficient blood from a single patient to do

all the necessary studies). Ideally, animals should be followed serially to study the therapeutic effects, rather than having to sacrifice an animal to obtain a data point (i.e., parameters of HIV secretion should be measurable in the peripheral blood, which is not always possible with standard SCID models).

In developing an animal model suitable for testing immunotoxins, we have turned to a technique that is well established in testing the efficacy of immunologic therapies in neoplastic disease, xenografting human tumors into SCID mice ***(19–22)***. This approach has been used in preclinical testing to demonstrate the efficacy of a number of immunotoxins. On the basis of such studies, several of the immunotoxins were entered into clinical trials and have been shown to be efficacious in phase I and II trials ***(23,24)***.

In our model, the tumor is an HIV-infected T-cell lymphoma (H9 cells infected with the molecularly cloned HIV NL4-3). After many years in serial culture, this cell line maintains a high degree of infection (>99% positive by FACS for gp120/gp41) and all cells secrete infectious virus ***(25)***. We have clearly demonstrated that H9/NL4-3 cells are exquisitely sensitive to immunotoxins in vitro. Immunotoxin-resistant variants arise at a frequency of 10^{-3}–10^{-4} ***(26,27)***. Thus H9/NL4-3 cells represent an excellent source of reproducibly HIV-infected cells that can be injected into SCID mice.

It is extremely unlikely that this model will reflect the underlying pathogenesis of HIV infection. However, this model will allow for the evaluation of anti-HIV immunotoxins, and possibly other therapies, in the presence of in vivo and viral factors that can influence therapeutic efficacy. In vivo factors include toxicity, body distribution of drug, serum half-life ($T_{1/2}$), and other pharmacokinetic parameters. Viral factors include the production of free infectious virus by cells that might interfere with the accessibility of therapeutic agent to the target cell or otherwise compete for pharmacologic effect. We also expect that this model will be relatively inexpensive, highly reproducible, and will allow for serial study of individual animals.

In the subheadings that follow, we will describe two sets of procedures. The first are the in vitro assays that we have developed to quantify HIV production in experimental animals. These assays may also be used to test the in vitro activity of anti-HIV immunotoxins, although for this purpose they are described elsewhere in greater detail ***(1,3,28)***. The second procedure described is the actual mouse model used for testing anti-HIV immunotoxins.

2. Materials

All of the assays described below involve the use of infectious HIV. Scientists wishing to perform these protocols should be thoroughly familiar with procedures for working with HIV. These are described in detail in HHS Publication No. (CDC) 93–8395: “Biosafety in Microbiological and Biomedical

Laboratories," and HHS Publication No. (CDC) 93–8395 "Biosafety in Microbiological and Biomedical Laboratories," which may be accessed online at http://www.cdc.gov/od/ohs/biosfty/bmbl/bmbl-1.htm.

2.1. In Vitro Assays

A number of different in vitro assays have been developed to measure HIV replication in tissue culture, experimental animals, and in patients. We have used two of these assays for following the production of HIV in mice injected with HIV-infected H9/NL4-3 cells. The first assay measures the production of a specific HIV protein, p24. Detection of p24 is via a highly sensitive antigen-capture enzyme-linked immunoassay (ELISA) capable of detecting <5 pg/mL. Plasma p24 levels can be measured serially in mice. The second assay, termed a focal infectivity assay (FIA), measures the production of infectious HIV ***(29,30)***. It is highly sensitive and quantitative. Although it can detect cell-free virus, it is most sensitive for the detection of cells secreting infectious HIV, capable of detecting one infected cell among 10^6 uninfected cells. In conjunction with the animal model, we have used this assay to measure the metastasis of H9/NL4-3 cells from their primary site to distant locations. With these two assays, we are thus able to monitor the production of HIV and the spread of the tumor.

2.1.1. P24 Antigen Capture

1. P24 antigen capture ELISA kits may be purchased from any one of several suppliers (e.g., Cellular Products, Buffalo, NY). However, the kits are expensive ($3–4 per microtiter well) and we have found our "homemade" assay to be as sensitive and as easy to perform.
2. Immulon-2 microtiter plates (96 wells, U-bottom, are obtained from Dynex (Chantilly, VA). Wells are coated with the capture anti-p24 monoclonal antibody 183-H12-5C. Cells secreting this antibody may be obtained from the AIDS Reagent Program, McKessonHBOC BioServices, Rockville, MD 20850, Telephone: (301) 340–0245 http://www.aidsreagent.org/ (hereafter referred to as the AIDS Reagent Program). Plates are blocked and the detecting antibodies are diluted in blotto (phosphate buffered saline [PBS] containing 10% nonfat dry milk, 0.2% Tween-20, and 0.01% thiomersal).
3. Samples to be tested for p24 are dissociated and disinfected in lysis buffer (1% Triton X-100 in PBS with 0.004% trypan blue [GIBCO, Grand Island, NY]).
4. Recombinant p24 antigen for use as a standard may be obtained from the AIDS Reagent Program. The detecting antibody is HIV immune globulin (HIVIG, available from the AIDS Reagent Program), which is biotinylated with sulfo-NHS-LC-biotin (Pierce Chemical, Rockford, IL) at a molecular ratio of 20:1.
5. To detect the biotinylated antibody, we utilize AMDex streptavidin-horseradish peroxidase (HRP) (Amersham Pharmacia, Piscataway, NJ). This product has multiple HRP molecules conjugated to streptavidin and is extremely sensitive.

6. The enzyme substrate is tetramethyl benzidine (TMB, Sigma, St. Louis, MO). The TMB is stored at 4 mg/mL in DMSO. At the time of use, substrate solution is made up as follows: To 1 mL of 0.1 *M* sodium acetate (pH 5), add 30 µL of TMB solution and 0.5 µL of 30% H_2O_2. The substrate reaction is stopped by adding 2 *M* H_2SO_4.

2.1.2. Focal Infectivity Assay (FIA)

1. The FIA detects HIV infection of monolayer cells that express HIV receptors and coreceptors ***(29,30)***. Several different cell lines are available for these purposes. The AIDS Reagent Program can provide a number of different HeLa cell lines expressing the HIV receptor CD4. Of those available from this source, we have found HeLa 1022 the most effective ***(31)***. However, even better is the cell line H1-J.C53, which is sensitive to infection with clinical isolates of HIV and with macrophage-tropic HIV ***(32)*** (*see* **Note 1**). This cell line is only available directly from its creator, David Kabat (Oregon Health Sciences University, Portland, OR, kabat@ohsu.edu). Cells are grown in standard tissue culture plasticware. We have found 48-well plates (Costar, Cambridge, MA) best for performing the assays.
2. Cells are grown in RPMI 1640 medium (GIBCO) supplemented with 10% fetal calf serum and antibiotics (RPMI complete medium). All cell growth is done in a 37°C, humidified, 5% CO_2 incubator.
3. If the monolayer cells are to be infected with cell-free virus, the cells are first treated with DEAE-dextran (Sigma) diluted to 8 µg/mL in serum-free RPMI 1640 medium. Following infection and growth, monolayer cells are fixed with 95% ethanol.
4. Foci of HIV infection are detected with HIV immune globulin, followed by HRP-conjugated antihuman IgG (Cappel Organon-Teknica, Durham, NC).
5. Staining of foci is done with the insoluble HRP substrate aminoethyl carbazol (AEC, Sigma). AEC is stored in solution in dimethyl formamide at 4 mg/mL at –10°C. AEC is highly carcinogenic and is light sensitive.
6. Substrate solution is prepared immediately prior to use. To 1 mL of 0.05 *M* sodium acetate (pH 5), add 50 µL of AEC solution and 0.5 µL 30% H_2O_2. Foci are counted using a dissecting microscope with 40–80× magnification.

2.2. Studies in Mice

1. NOD/LtSz-scid mice (*see* **Note 2**), which in addition to the SCID mutation have defects in natural killer (NK) cells and complement activity ***(33)***, may be ordered from Jackson Labs (Bar Harbour, ME).
2. Mice are irradiated on a Varian 2100C 6MV linear accelerator, although any alternative irradiation source may be used (*see* **Note 3**).
3. We utilize the persistently infected cell line H9/NL4-3 for our studies; these cells may be obtained from S. Pincus by direct request. The AIDS Reagent Program also has several persistently-infected H9 cell lines available; however, these differ significantly from H9/NL4-3 in that they must be mixed with uninfected H9 cells every 2–3 wk, or the infection will "burn out" (*see* **Note 4**). We have not investigated the in vivo behavior of any cell lines other than H9/NL4-3.

4. Cells are injected into mice in a 40% mixture of Matrigel (Becton Dickinson Labware, Franklin Lakes, NJ). To obtain plasma from mice, they are bled into heparinized "Natelson" capillary tubes (Fischer Scientific, Los Angeles, CA). Because of the danger of accidental HIV infection of the technician, we avoid the use of any sharp objects (e.g., needles, scalpel blades) in bleeding the mice.

3. Methods

We have developed an animal model to test the comparative efficacy of anti-HIV immunotoxins. Although this model does not reflect the underlying pathogenesis of HIV, it does allow us to test the in vivo effects of immunotoxins in a well-established model for testing immunotoxins and other immune therapies. This model is inexpensive, reproducible, and allows the testing of a sufficient number of animals to compare the efficacy of different immunotoxin preparations. At the same time immunotoxin efficacy is compared, toxicity and pharmacokinetics can be evaluated. If immunotoxins that have greater efficacy than the failed immunotoxin CD4-PE40 are identified, then we may proceed to studies of macaques infected with the chimeric human/simian immunodeficiency virus.

3.1. In Vitro Assays

The in vitro assays described below are used to monitor the production of virus by HIV-infected cells implanted into mice. The p24 antigen-capture assay may be used to monitor mice serially through evaluation of plasma p24 levels. The FIA is used to detect the presence of HIV-secreting cells in different tissues. Although the H9/NL4-3 cells occasionally enter the blood stream in a leukemic form, we utilize the FIA after sacrificing mice to detect metastatic cells in the spleen. Although there are many other assays to detect the presence of HIV-infection, we have found that the combined use of these two assays gives us information on the total body burden of H9/NL4-3 cells (plasma p24), as well as their presence at distant sites (FIA). By monitoring these parameters, we can assess the efficacy of anti-HIV immunotoxins.

3.1.1. P24 Antigen Capture

P24 is the capsid protein of HIV and is secreted by HIV-infected cells as part of intact virions, in incomplete virions that are rendered noninfectious by virtue of lacking key viral components, and possibly as free protein. Approximately 20% of AIDS patients have detectable p24 antigenemia, and until the advent of more sensitive nucleic acid-based measures of viral load, this test will be used to monitor viral burden in patients. A number of commercial p24 antigen-capture assays have been developed, but because they are still used for clinical purposes, the kits are expensive. We have developed an experimental

alternative that has the same level of sensitivity and reproducibility that we have obtained with the commercial kits.

1. Microtiter wells are coated with 100 μL of the capture antibody 183-H12–5C at 30 μg/mL in PBS for 18 h at 4°C. We utilize antibody that has been purified from hybridoma supernatant using protein G. We do not use the wells located on the outer edges of the microtiter plate; only the internal 60 wells of the 96 well plate are coated.
2. Following the coating, the plates are flicked out and 200 μL blotto is added to each well. The blotto remains in the wells for at least 4 h or up to several days, when the plates are then used for the assay.
3. Samples to be tested are mixed with a 10% vol of lysis buffer and incubated at 37° for 30 min. Mouse plasma samples are tested at a 1:10 dilution. This releases any p24 within virions and also decontaminates the material.
4. In every experiment, we run a full range of p24 0–240 pg/mL standards utilizing recombinant p24.
5. Samples or standards are added to microtiter wells in a volume of 100 μL and incubated in the wells overnight at 4°C. The wells are washed six times in PBS/0.1% Tween-20. The detecting antibody, biotinylated HIV immune globulin diluted to 0.5–1.0 μg/mL in blotto, is then added to the wells to a total volume of 100 μL and incubated for 4 h at room temperature.
6. Following another wash, 100 μL HRP-conjugated streptavidin (1:10,000 dilution in blotto) is added and incubated for 45 min at 37°. Wells are washed a final time, and 100 μL of freshly prepared TMB substrate solution is added.
7. Plates are incubated at room temperature for 20 min and 50 μL of 2 *M* H_2SO_4 is added. Absorbance at 450 nm is determined using a microplate ELISA reader.

Figure 1 shows a linear regression analysis of the results obtained with recombinant p24. The data demonstrate that this assay is sensitive to <7.5 pg/mL, and that the results are linear in the range shown. A curve and plateau begin to develop at approx 120 pg/mL. These results are similar to standard curves obtained with commercial assays.

3.1.2. Focal Infectivity Assay

The FIA measures infectious HIV by its ability to infect sensitive monolayer cells. Thus, it measures a very different parameter than the p24 antigen-capture assay, which detects the presence of a protein that may be either associated with infectious virus or pseudovirions, or may even be secreted in its free form by HIV-infected cells. The FIA detects both cell-free virus and infected cells that are producing infectious HIV (infectious centers, ICs), although the sensitivity is highest for ICs. The FIA has been used to study the presence of ICs in the peripheral blood of AIDS patients ***(31)***, and we are currently adapting it to serve as a phenotypic drug-resistance assay to guide clinicians in the choice of appropriate antiviral therapy.

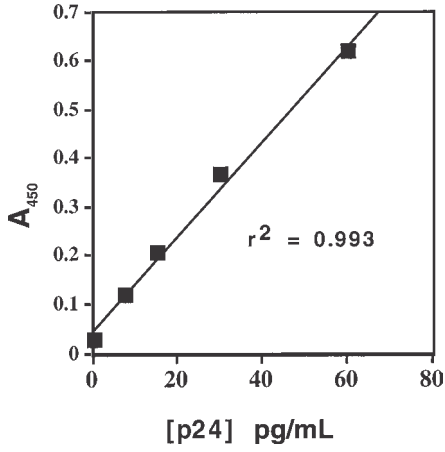

Fig. 1. Linear regression analysis of standard curve in p24 antigen-capture ELISA. Replicate samples of recombinant p24 antigen and different concentrations, ranging from 0–60 pg/mL, was tested in the assay. The A_{450} was plotted against the concentration of antigen and is indicated by the points. A linear regression was performed and is shown by the line.

1. The sensitivity of the FIA and its ability to detect different HIV isolates with different tropisms is highly dependent upon the indicator cell line used. We use H1-J.C53, which are HeLa cells transduced to express high levels of CD4 and CCR5; they naturally express CXCR4. These cells are highly susceptible to infection with laboratory-associated as well as primary clinical isolates of all known tropisms and clades ***(32)***. They are of equal or greater sensitivity than the gold standard for HIV-culture: peripheral blood mononuclear cells activated with phytohemagglutinin and maintained with IL-2 ***(29,31,32,34)***.
2. The sensitivity of some cell lines (especially HeLa 1022) is dependent upon cell density. We have found optimal results in all cell lines when the monolayers are 75–80% confluent on the day they are harvested, either in the FIA or during cell maintenance. Thus it will be important for each investigator to monitor the growth of the cell line they are utilizing and to determine the optimal concentration of cells to place in each tissue culture well, so that the monolayer will have reached appropriate confluence 4 d later. We utilize 48 well tissue culture plates for our assays because this optimizes visual examination of the wells for viral foci with a dissecting microscope. In a 48 well plate, we add 4×10^4 cells per mL in 0.5 mL of RPMI-1640 medium with 10% fetal calf serum (FCS).
3. One day after the indicator monolayers are established, the cells or virus preparation to be tested is added to the well. Different protocols are applied for cell-free virus and for ICs. To detect cell-free virus, the monolayer is washed once in serum free-RPMI and then DEAE-dextran (8 μg/mL in serum-free medium) is added for 20 min. Serial dilutions of the virus preparation (again, in serum-free

medium) are added to the wells in a minimum volume: 100 μL per well of a 48 well plate. The tissue culture plates are maintained for 3–4 h in an incubator and then washed three times with tissue culture medium before the addition of RPMI complete medium. The cells are then incubated for 3 d prior to harvesting.

4. To detect ICs, serial dilutions of the cells to be tested are added to the wells in RPMI complete medium and incubated for 1 d. The wells are then washed and incubated for two more days. Three days after infection, the monolayers are harvested and stained. Care should be taken never to allow the wells to dry until the staining is complete. Tissue culture medium is removed from the monolayers by flicking out the plate or by aspiration. The cells are then fixed in 95% ethanol for 20 min and then incubated for at least 2 h in PBS with 1% bovine serum albumin, 0.01% thiomersal (PBS/BSA). Plates may be stored in this solution for up to one week prior to staining. Immunoperoxidase staining is performed using HIV immune globulin (30 μg/mL in PBS/BSA) as the primary antibody. In 48 well plates we add 100 μL/ well. Plates are incubated at room temperature with slow rotation (20 rpm) for 1 h, washed three times in PBS/0.1% Tween-20, and then HRP-conjugated goat antihuman IgG (diluted 1:800 in PBS/BSA) is added. The plates are incubated as before and washed. Freshly prepared AEC substrate solution is then added. Because the substrate is light sensitive, the culture plates are wrapped in aluminum foil. The substrate is carcinogenic, so gloves should be worn at all times, and the substrate solution should be discarded properly following use. The substrate solution is incubated on the plates for 20–30 min and then aspirated. The plates are thoroughly rinsed in tap water and allowed to air-dry.
5. To detect and enumerate foci, the monolayers are visualized on a dissecting microscope under 40–80× magnification. HIV-specific foci are identified by the red immunoperoxidase staining as well as by the characteristic morphology of the foci: red cytoplasm, unstained nuclei, and the presence of multinucleated giant cells (**Fig. 2**). Different HIV strains may produce very different focal morphology, some having very little cell-to-cell fusion, while others produce huge foci with >100 nuclei per giant cell. Despite variations in size, each focus represents a single infectious event. In enumerating foci, it is important that the density of foci be sufficiently low and that they are spatially separated from each other (if they are actually touching, two distinct foci cannot be distinguished from cell-to-cell spread of virus from a single event). We have found that 100 foci/well is the greatest density that we can accurately count on 48 well plates.

3.2. Studies in Mice

By injecting HIV-infected human tumor cells into immunodeficient mice, we are using a model that is well established for studying the efficacy of immunotoxins that are used in the treatment of cancer. However, in this case, the target antigens are derived from HIV. Because these cells are secreting HIV, we can use extremely sensitive assays for following tumor progression and spread. While this model does not reflect the disease processes seen in

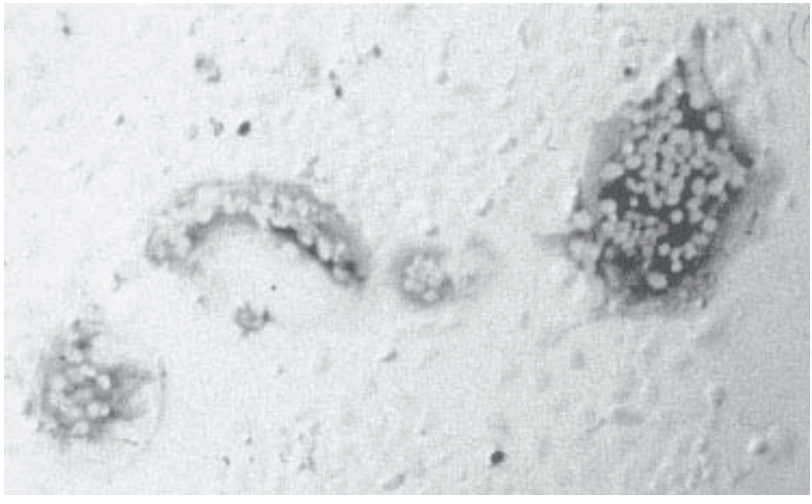

Fig. 2. Viral foci. Immunoperoxidase-stained foci are detected both by their staining as well as their characteristic morphology. Although multinucleated giant cells predominate in this figure, viral foci may consist of a single cell with stained cytoplasm and an unstained nucleus.

AIDS, it does allow us to test the ability of immunotoxins to kill HIV-infected cells in vivo.

1. We utilize NOD/LtSz-SCID mice at 6–10 wk of age. All food, water, and caging of mice is sterilized prior to use. Mice are maintained in filtered cages and have trimethoprim-sulfamethoxazole added to their drinking water 3 d/wk. One day prior to injection, the mice receive 300 rads of total body irradiation.
2. HIV-infected H9/NL4-3 cells are injected as follows. The cells are washed once in cold PBS and then counted. Matrigel is stored frozen. One day prior to use, it is thawed at 4°C. This cell matrix material is designed to remain a liquid while cold but will form a gel at body temperature, thus encapsulating the tumor cells in vivo. The cell suspension and Matrigel are mixed in a 3:2 ratio, with sufficient cells and volume so that each mouse will receive 10^7 cells in 0.2 mL total volume. The mice are injected intraperitoneally through a 22 gauge needle. The cell suspension/Matrigel mixture and the syringes are kept on ice until the time of injection.
3. Mice are maintained in an appropriately designed isolation room. Mice are bled at various intervals for monitoring of plasma p24. Blood is obtained from the retro-orbital plexus using heparinized Natelson capillary tubes. At the final time point, mice are bled via subclavian cutdown and then dissected, removing organs and/or tumor for study by FIA.

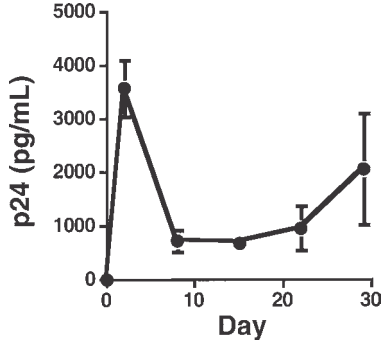

Fig. 3. P24 measured as a function of time. Four mice were injected with H9/NL4-3 cells on d 0 and then bled serially at the indicated time points. Plasma p24 antigenemia was measured. Each time point is the mean and standard error of the mean (SEM).

4. Single cell suspensions of tissues are made in RPMI complete medium either by teasing the tissue apart using 18 gauge needles, by squashing the tissue with a glass stopper, or both.

We have followed mice for up to 10 wk following injection of the tumor. Interestingly, if mice receive a similar injection of uninfected H9 cells they succumb to the tumor approx 2 wk following injection. Thus, it seems that the HIV-infected H9/NL4-3 cells have decreased tumorigenicity. Whether this is due to HIV infection or due to other factors is difficult to ascertain, since the cells have been maintained separately for over 10 yr.

Prior to testing the efficacy of immunotoxins, we performed a series of experiments to determine the time course of p24 production and the appearance of tumor cells in the spleens of mice. **Figure 3** shows the results of a serial determination of p24 levels during the first month following injection of tumor cells. There is an initial burst of plasma detectable 3 d following injection. This most likely represents acute anoxic death of cells prior to the vascularization of the tumor. By 7 d, p24 levels dropped and then climbed steadily over the remainder of the observation period. We then followed p24 for a total of 10 wk (data not shown) and found that the level of p24 continues to increase throughout this time interval. **Figure 4** shows FIA and p24 values obtained in individual mice sacrificed 7–14 d postinjection.

This model was used to determine the in vivo activity of two different immunotoxins targeted at the same molecule: HIV gp120. The first immunotoxin consists of a monoclonal antibody conjugated to the ricin A-chain and is designated 924-RAC ***(1,3)***. The second immunotoxin is CD4-PE40, which uses

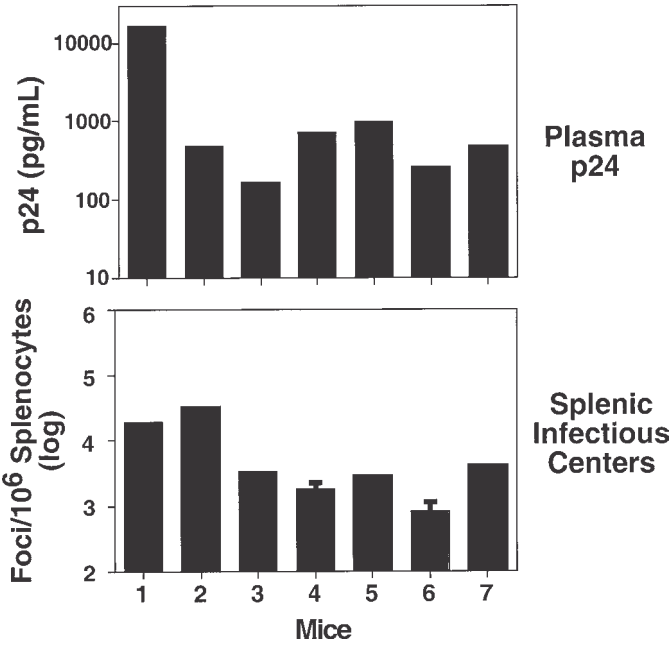

Fig. 4. Plasma p24 and HIV-secreting cells in mice bearing tumors of H9/NL4-3 cells. Individual mice were injected with H9/NL4-3 tumor cells and then sacrificed 7–14 d later. For each mouse, the plasma p24 level (pg/mL) and the proportion of HIV-secreting cells (log foci per 10^6 splenocytes) is shown.

the gp120-CD4 interaction to target *Pseudomonas* exotoxin A to HIV-infected cells ***(35)***. These two immunotoxins have comparable in vitro cytotoxicity on H9/NL4-3 cells ***(3)***.

The in vivo toxicity of these immunotoxins in irradiated, NOD/LtSz-SCID mice bearing the tumors with H9/NL4-3 also have been tested. We have determined that the maximum tolerable dose (MTD) is 3 μg/mouse for CD4-PE40 and >150 μg/mouse for 924-RAC. The relative toxicity of these immunotoxins in mice is comparable to that observed in humans for CD4-PE40 and for ricin immunotoxins used to treat cancer ***(4)***. In the first experiment, we tested the ability of 924-RAC to suppress an already established tumor (**Fig. 5**). The results show that saline-treated mice had an increase in p24 during the treatment period, while those receiving 924-RAC had a marked drop in p24 levels. At sacrifice, saline-treated mice had large numbers of HIV-infected cells in their spleens, which were virtually absent in 924-RAC–treated mice. In the second experiment, 924-RAC and CD4-PE40 were compared for their ability to inhibit the establishment of tumors (**Fig. 6**). Immunotoxins were tested at

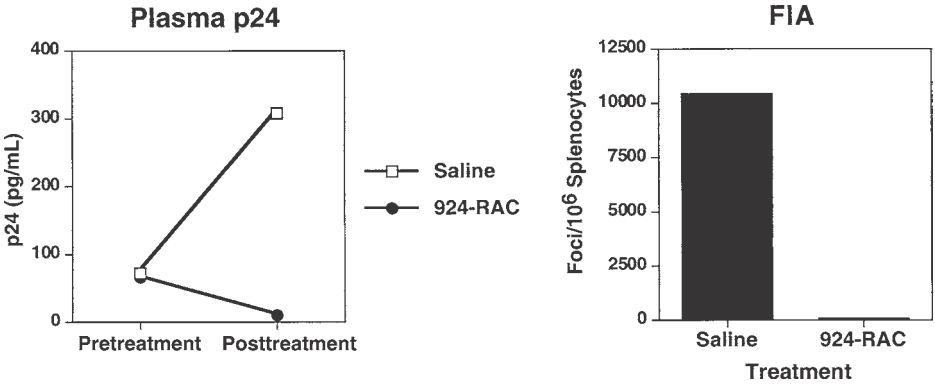

Fig. 5. Effect of immunotoxin treatment on established tumors. Irradiated SCID/NOD mice were injected with tumors on d 0. They were bled on d 9 and treated with either saline or 924-RAC (150 μg/mouse) on d 9 and 13. Mice were sacrificed on d 15. Plasma p24 levels were determined on blood samples from d 9 and 15; splenic infectious centers were also determined on d 15. Results shown are the mean of each group of mice (four treated with saline, three with 924-RAC).

their MTDs. The results demonstrate that 924-RAC was effective, while CD4-PE40 was not. There was some experimental variability indicating the need for larger experimental groups.

In summary, the data presented here suggest that the model described will offer a suitable alternative for the early in vivo testing of anti-HIV immunotoxins. Moreover, they confirm the high degree of nonspecific toxicity of CD4-PE40 when compared with antibody-targeted immunotoxins utilizing other toxic moieties. The data, although highly preliminary, suggest that when used at MTD, 924-RAC can kill HIV-infected cells in vivo, while CD4-PE40 does not. These data support our contention that CD4-PE40 is a flawed immunotoxin, and that its failure in clinical trials does not invalidate the concept of using anti-HIV immunotoxins to treat AIDS.

4. Notes

1. The susceptibility of cells to infection with HIV is dependent upon many factors, not all of which have been defined. Obviously critical is that the cells express the HIV receptor CD4 and the coreceptors CXCR4 and/or CCR5. Particularly for clinical isolates of HIV, susceptibility to infection may be dependent upon the level of CD4 expression ***(34)***. In the presence of high levels of CD4 expression, the amount of coreceptor expressed may be less important once it is above a certain threshold value ***(32)***. However, in the presence of lower levels of CD4, the degree of coreceptor expression may also play a critical role. In certain indicator cell lines, the level of expression of CD4 decreases with increasing cell

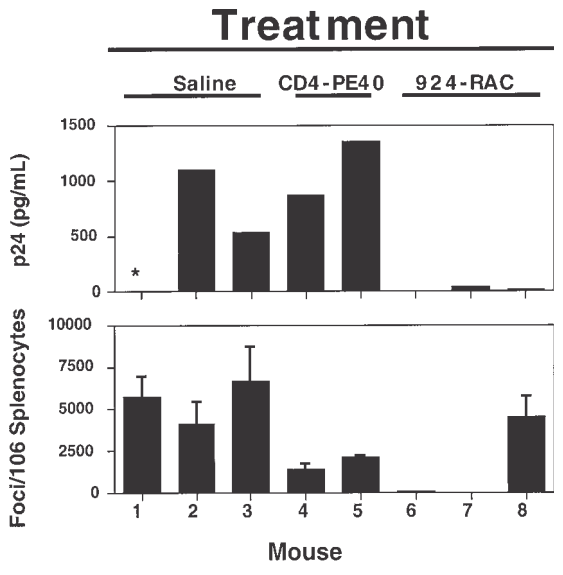

Fig. 6. Effect of immunotoxin treatment on mice injected with H9/NL4-3 cells. Irradiated mice were injected with H9/NL4-3 cells on d 1, treated on d 2 and 6, and sacrificed on d 7. Treatments consisted of intraperitoneal injections of saline (mice 1–3), CD4-PE40 (mice 4–5), or 924-RAC (mice 6–8). Plasma p24 antigenemia and the proportion of splenocytes secreting HIV on d 7 are shown.

density ***(31)***. Many different CD4-transfected HeLa cell lines are available from the AIDS Reagent Program, and several of them are adequate for detecting foci with H9/NL4-3 cells, which does not require a high degree of sensitivity. However, we have found that the H1-J.C53 or H1-J.C37 cell lines produced by David Kabat are most useful. These cell lines have been retrovirally transduced to express CD4 and CCR5. They express high levels of CD4 and coreceptors in an extremely stable manner that is not density dependent. They are susceptible to infection with all isolates of HIV that we have tested.

2. Mice with the SCID mutation have profound defects in their adaptive immune response because they are unable to rearrange immunoglobulin and T-cell receptor genes. A number of other mutations have been bred onto the SCID background. Among them are Bg (beige), which encodes a defect in natural killer cells, and *NOD* (nonobese diabetic), which encodes defects in both complement and natural killer cells ***(33)***. Comparative studies have been performed on the relative susceptibility of different SCID strains to HIV infection of xenografted human peripheral blood mononuclear cells. Mice carrying both the SCID and NOD mutation developed the highest level of viremia ***(36)***. Similarly, we have compared SCID, SCID/Bg, and SCID/NOD in our model and have found that SCID/NOD mice produce the highest level of HIV activity and the most reproducibly "infected" mice.

3. The need for irradiation may seem superfluous in mice with profound immune defects, such as the NOD/LtSz-SCID strain. Nevertheless, we have found that without total body irradiation, the number of mice with measurable levels of HIV activity is markedly decreased. Others have also noted that sublethal irradiation can enhance the establishment of tumors in genetically immunodeficient mice *(22)*. The mechanism of this is not well understood, but it may involve the temporary depletion of cells from lymphoid organs, allowing for a physiological space that can be occupied by the invading tumor cells.
4. The maintenance of persistent HIV infection in cell lines has been the matter of much investigation. In most cell lines permissive for HIV infection, the result of acute infection is cytopathicity and cell death within 48–96 h. Eventually, small numbers of persistently infected cells will grow out. However, to maintain infection in most of these cell lines, it is necessary to add uninfected cells every 1–2 wk, following which the infection flares up, all of the uninfected cells become infected, and the majority of these cells then die until another population of cells grows out. During this process, variant cells that are no longer susceptible to HIV infection emerge and may even become dominant. Thus the majority of cells in such a culture are not actively producing HIV, except for the short period of acute infection following the addition of uninfected cells and prior to the death of the majority of these cells.

   The H9/NL4-3 cell line is significantly different from other persistently infected cell lines in this regard. These cells maintain a very high degree of infection without the need for replenishment. Studies of immunotoxin-resistant variants indicate that >99.9% of these cells are consistently producing infectious HIV *(26,27)*. We have investigated the molecular basis of the stability of infection in these cells and have determined that the cells have a mutation that cripples the vpr gene *(27)*.

Acknowledgments

We would like to thank the staff of the Animal Resources Center at Montana State University, especially Leta Eng, Tammy Jacques, and its director, Warren Frost, DVM, for their excellent and compassionate care of the research animals and their willingness to work with HIV. We greatly appreciate the staff at Bozeman Deaconess Cancer Center, in particular Nancy Judd, Tim Stack, and Dr. Simeon Cantril, for being willing to irradiate mice in a clinical facility. Chun Liu performed important technical procedures. This work was supported by USPHS grant CA74690.

References

1. Pincus, S. H., Cole, R. L., Hersh, E. M., Lake, D., Masuho, Y., Durda, P. J., and McClure, J. (1991) In vitro efficacy of anti-HIV immunotoxins targeted by various antibodies to the envelope protein. *J. Immunol.* **146,** 4315–4324.

2. Pincus, S. H. and McClure, J. (1993) Soluble CD4 enhances the efficacy of immunotoxins directed against gp41 of the human immunodeficiency virus. *Proc. Natl. Acad. Sci. USA* **90,** 332–336.
3. Pincus, S. H., Wehrly, K., Cole, R., Fang, H., Lewis, G. K., McClure, J., et al. (1996) In vitro effects of anti-HIV immunotoxins directed against multiple epitopes on the HIV-1 envelope glycoprotein gp160. *AIDS Res. Hum. Retrovirus* **12,** 1041–1051.
4. Pincus, S. H. (1996) Therapeutic potential of anti-HIV immunotoxins. *Antiviral Res.* **33,** 1–9.
5. Ashorn, P., Moss, B., Weinstein, J. N., Chaudhary, V. K., FitzGerald, D. J., Pastan, I., et al. (1990) Elimination of infectious human immunodeficiency virus from human T-cell cultures by synergistic action of CD4-*Pseudomonas* exotoxin and reverse transcriptase inhibitors. *Proc. Natl. Acad. Sci. USA* **87,** 8889–8893.
6. Chaudhary, V. K., Mizukami, T., Fuerst, T. R., FitzGerald, D. J., Moss, B., Pastan, I., et al. (1988) Selective killing of HIV-infected cells by recombinant human CD4-Pseudomonas exotoxin hybrid protein. *Nature* **335,** 369–372.
7. Berger, E. A., Clouse, K. A., Chaudhary, V. K., Chakrabarti, S., FitzGerald, D. J., Pastan, I., et al. (1989) CD4-*Pseudomonas* exotoxin hybrid protein blocks the spread of human immunodeficiency virus infection in vitro and is active against cells expressing the envelope glycoproteins from diverse primate immunodeficiency retroviruses. *Proc. Natl. Acad. Sci. USA* **86,** 9539–9543.
8. Ashorn, P., Englund, G., Martin, M. A., Moss, B., and Berger, E. A. (1991) Anti-HIV activity of CD4-*Pseudomonas* exotoxin on infected primary human lymphocytes and monocyte/macrophages. *J. Infect. Dis.* **163,** 703–709.
9. Berger, E. A., Moss, B., and Pastan, I. (1998) Reconsidering targeted toxins to eliminate HIV infection: you gotta have HAART. *Proc. Natl. Acad. Sci. USA* **95,** 11,511–11,513.
10. Finberg, R. W., Wahl, S. M., Allen, J. B., Soman, G., Strom, T. B., Murphy, J. R., et al. (1991) Selective elimination of HIV-1-infected cells with an interleukin-2 receptor-specific cytotoxin. *Science* **252,** 1703–1705.
11. Bell, K. D., Ramilo, O., and Vitetta, E. S. (1993) Combined use of an immunotoxin and cyclosporine to prevent both activated and quiescent peripheral blood T cells from producing type 1 human immunodeficiency virus. *Proc. Natl. Acad. Sci. USA* **90,** 1411–1415.
12. Ramilo, O., Bell, K. D., Uhr, J. W., and Vitetta, E. S. (1993) Role of CD25+ and CD25–T cells in acute HIV infection in vitro. *J. Immunol.* **150,** 5202–5208.
13. Borvak, J., Chou, C.-S., Bell, K., G. Van Dyke, Zola, H., Ramilio, O., et al. (1995) Expression of CD25 defines peripheral blood mononuclear cells with productive versus latent HIV infection. *J. Immunol.* **155,** 3196–3204.
14. Davey, R. T., Boenning, C. M., Herpin, B. R., Batts, D. H., Metcalf, J. A., Wathen, L., et al. (1994) Recombinant soluble CD4-*Pseudomonas* exotoxin, a novel immunotoxin, in the treatment of individuals infected with HIV. *J. Infect. Dis.* **170,** 1180–1188.

15. Ramachandran, R. V., Katzenstein, D. A., Wood, R., Batts, D. H., and Merigan, T. C. (1994) Failure of short-term CD4–PE40 infusions to reduce viral load in HIV infected individuals. *J. Infect. Dis.* **170,** 1009–1013.
16. Mosier, D. E. (1996) Small animal models for AIDS research. *Lab. Animal Sci.* **46,** 257–265.
17. Bonyhadi, M. L., Rabin, L., Salimi, S., Brown, D. A., Kosek, J., McCune, J. M., et al. (1993) HIV induces thymus depletion in vivo. *Nature* **363,** 728–732.
18. Mosier, D. E., Gulizia, R. J., MacIsaac, P. D., Torbett, B. E., and Levy, J. A. (1993) Rapid loss of CD4+ T cells in human-PBL-SCID mice by noncytopathic HIV isolates. *Science* **260,** 689–691.
19. Pai, L. H., Batra, J. K., FitzGerald, D. J., Willingham, M. C., and Pastan, I. (1992) Antitumor effects of B3–PE and B3-LysPE40 in a nude mouse model of human breast cancer and the evaluation of B3-PE toxicity in monkeys. *Cancer Res.* **52,** 3189–3193.
20. Trail, P. A., Willner, D., Lash, S. J., Henderson, A. J., Hofstead, S., Casazza, A. M., et al. (1993) Cure of xenografted human carcinomas by BR96-doxorubicin immunoconjugates. *Science* **261,** 212–215.
21. Jansen, B., Vallera, D. A., Jaszcz, W. B., Nguyen, D., and Kersey, J. H. (1992) Successful treatment of human acute T-cell leukemia in SCID mice using the anti-CD7-deglycosylated ricin A-chain immunotoxin DA7. *Cancer Res.* **52,** 1314–1321.
22. Ghetie, M. A., Gordon, B. E., Podar, E. M., and Vitetta, E. S. (1996) Effect of sublethal irradiation of SCID mice on growth of B-cell lymphoma xenografts and on efficacy of chemotherapy and/or immunotoxin. *Lab. Animal Sci.* **46,** 305–309.
23. Frankel, A. E., Fitzgerald, D., Siegall, C., and Press, O. W. (1996) Advances in immunotoxin biology and therapy. *Cancer Res.* **56,** 926–932.
24. Thrush, G. R., Lark, L. R., Clinchy, B. C., and Vitetta, E. S. (1996) Immunotoxins: an update. *Ann. Rev. Immunol.* **14,** 49–71.
25. Pincus, S. H. and Wehrly, K. (1990) AZT demonstrates anti-HIV-1 activity in persistently infected cell lines: implications for combination chemotherapy and immunotherapy. *J. Infect. Dis.* **162,** 1233–1238.
26. Fang, H. and Pincus, S. H. (1995) Unique insertion sequence and pattern of CD4 expression in variants selected with immunotoxins from human immunodeficiency virus type 1-infected T cells. *J. Virol.* **69,** 75–81.
27. Duensing, T. D., Fang, H., Dorward, D. W., and Pincus, S. H. (1995) Processing of the envelope glycoprotein gp160 in immunotoxin-resistant cell lines chronically infected with HIV-1. *J. Virol.* **69,** 7122–7131.
28. Pincus, S. H. (1999) Targeting drugs to HIV-infected cells, in *Drug Targeting*, Methods in Molecular Medicine, vol. 11. (Francis, G. E., ed.), Humana Press, Totowa, NJ, pp. 193–214.
29. Pincus, S. H., Wehrly, K., and Chesebro, B. (1991) Use of a focal infectivity assay for testing susceptibility of HIV to antiviral agents. *BioTechniques* **10,** 336–342.

30. Chesebro, B. and Wehrly, K. (1988) Development of a sensitive quantitative focal assay for human immunodeficiency virus infectivity. *J. Virol.* **62,** 3779–3788.
31. Chesebro, B., Wehrly, K., Metcalf, J., and Griffin, D. E. (1991) Use of a new CD4-positive HeLa cell clone for direct quantitation of infectious human immunodeficiency virus from blood cells of AIDS patients. *J. Infect. Dis.* **163,** 64–70.
32. Platt, E. J., Wehrly, K., Kuhmann, S. R., Chesebro, B., and Kabat, D. (1998) Effects of CCR5 and CD4 cell surface concentrations on infections by macrophage-tropic isolates of HIV-1. *J. Virol.* **72,** 2855–2864.
33. Shultz, L. D., Schweitzer, P. A., Christianson, S. W., Gott, B., Schweitzer, I. B., Tennent, B., et al. (1995) Multiple defects in innate and adaptive immunologic function in NOD/LtSz-scid mice. *J. Immunol.* **154,** 180–191.
34. Kabat, D., Kozak, S. L., Wehrly, K., and Chesebro, B. (1994) Differences in CD4 dependence for infectivity of laboratory-adapted and primary patient isolates of HIV. *J. Virol.* **68,** 2570–2577.
35. Berger, E. A., Fuerst, T. R., and Moss, B. (1988) A soluble recombinant polypeptide comprising the amino-terminal half of the extracellular region of the CD4 molecule contains an active binding site for human immunodeficiency virus. *Proc. Natl. Acad. Sci. USA* **85,** 2357–2361.
36. Koyanagi, Y., Tanaka, Y., Kira, J., Ito, M., Hioki, K., Misawa, N., et al. (1997) Primary human immunodeficiency virus type 1 viremia and central nervous system invasion in a novel hu-PBL-immunodeficient mouse strain. *J. Virol.* **71,** 2417–2424.